THE UNIVERSITY *of* EDINBURGH

Aspects of Modelling Plain and Reinforced Concrete at Elevated Temperatures

Joanne J. Knox

Doctor *of* Philosophy

The University *of* Edinburgh

2012

Declaration

The writing of this thesis, and the research herein was conducted solely by Joanne Knox under the supervision of Dr Pankaj Pankaj and Prof. Asif Usmani.

Where other sources are quoted, references are given in full.

Joanne Knox, 2012

Abstract

Extreme events such as the Mont Blanc Tunnel fire in 1999 (Bettelini et al. 2001) or the Windsor Tower fire in 2005 (Calavera et al. 2005) have shown how concrete failure at elevated temperatures can be hazardous to the safety of members of the public. Generally, there is an absence of understanding of the mechanical behaviour of both plain and reinforced concrete at elevated temperatures, which is essential for computational modelling. Since fire is an extreme event, a certain amount of damage within the structure would be seen to be permissible within its performance objectives. This necessitates analysis in the post-peak regime. As a material, concrete has a very low value of thermal conductivity. This means that large thermal gradients often occur within concrete, causing differential expansion of the material. This, coupled with the change in mechanical properties at elevated temperatures, further complicates analytical analysis procedures.

This study investigates issues associated with computational modelling of plain and reinforced concrete at elevated temperatures and its residual behaviour (behaviour when tested after the material has been heated, for example in a fire, and then cooled). In order to achieve this, first the constitutive material properties of both plain and reinforced concrete at ambient and elevated temperatures were investigated. The study showed that mesh sensitivity and localisation of strain softening occurs in plain concrete under both tensile and compressive loading. Path dependency of the stress-strain behaviour of plain concrete was also demonstrated, when it was subjected to loading and heating.

Tension stiffening was included in the reinforced concrete material model, to represent the interaction between concrete and reinforcing steel. Complex behaviours were seen for simple reinforced concrete benchmark tests, due to changing material properties at elevated temperatures and differential thermal expansion of steel and concrete. Non-linear load-displacement relationships

were seen as a result of complex load-sharing between concrete and reinforcement.

A hypothesis was proposed – that variation of temperatures during heating and cooling of a specimen will cause damage, and hence material degradation, in plain and reinforced concrete. On investigation, it was seen that damage due to differential thermal expansion plays a small part in the reduction of elastic load-displacement slope and peak strength seen in experimental data on residual tests, indicating that other factors identified in previous research also affect the residual behaviour of plain and reinforced concrete. Indeed, in reinforced concrete, when tension stiffening was included, it was found that damage due to differential thermal expansion and contraction had a negligible effect on the residual response in the pre-peak regime.

The study also found that for a simply supported beam pure thermal expansion caused a localised response, while pure thermal gradient gave distributed yield. When both were present, in this study, distributed yield with no mesh sensitivity was seen. Realistic heating of a restrained reinforced concrete plane strain model caused compressive stresses accompanied by tensile longitudinal total strains and tensile longitudinal plastic strains throughout the depth of the slab, with the largest values occurring near to the model supports. Damage and recovery variables were found to have no effect on the response of the model.

When a portal frame was exposed to heating, plastic strains were distributed throughout the beam, with column rotation limiting downward thermal bowing due to a uniformly distributed load or thermal gradient present. Application of displacement loading causing plastic damage changed the behaviour of the structure under heating – instead of symmetrical compressive plastic strains being induced, areas of varying tensile and compressive strain were caused within the beam.

Throughout, simple, easily reproducible simulations were used so that single parameters could be altered and considered. This was important, so that the important parameters to computational modelling could be identified. These can

be used to guide experimental series to ensure that they are investigated, in order to improve computational material models. Not all variations of parameters were investigated in this study, but it is clear where further repetition would be beneficial (e.g. in varying thermal expansion and thermal gradient ratios in heating regimes). This study looks to address experimentalists and people working in structural analysis, who would be interested in the parameters investigated, as well as practitioners who may want to use these results.

Bettelini, M., L. Glarey, et al. (2001). The new Mont Blanc Tunnel - A milestone in tunnel safety. International conference International tunnel forum. Basel, 4-6 December.

Calavera, J., E. Gonzalez-Valle, et al. (2005). Fire in the Windsor building, Madrid. Survey of the fire resistance and residual bearing capacity of the structure after the fire. Instituto Technico De Materiales Y Constructiones (INTEMAC).

Acknowledgements

I would like to thank my supervisor Dr Pankaj for all his help and support throughout this project. His unstinting enthusiasm was of great encouragement to me, and he was always there to assist and to advise. Also, to Prof. Asif Usmani, my second supervisor for all his help.

Thank you to my sponsors, the EPSRC.

Thank you to everyone who lived in John Muir throughout my stay – for a long or short time. The tea drinking, Monday Morning Munching and cake club has been excellent.

To friends at home who put up with me reading concrete papers on holiday on the bus or by the pool, friends in Guiding who have helped me with logistical nightmares and spreadsheets when I got in too deep, 'homies' who kept encouraging me with peanut butter cookies, asking whether I had a question yet, the people of St Peter's who shared their bring-and-share lunches a whole lot more times than I brought (and shared), and flatmates who were always entertaining and great to live with.

Lastly, to my parents and sister – thank you for the support, comfort, sympathy and interest in late night phone calls and random graphs, and their understanding when I couldn't get back home as often as I should.

Table of Contents

Table of Figures

thermal stresses caused by expansion not being permitted due to the boundary condition. (2) The element is heated to 200°C with free expansion permitted and then loaded under tension at elevated temperature. This model shows initial tensile stress and strain on heating, due to compromise between the differing thermal expansions of concrete and reinforcement – reinforcing steel has a higher coefficient of thermal expansion and expands more than concrete, forcing the concrete into tension. On loading the model follows the shape of concrete's 200°C material properties curve. (3) The element is heated to 200°C, strains due to thermal expansion are removed, and then the element is loaded under tension. This model follows the 200°C material properties with less of an offset than was seen previously, but does not follow the curve exactly due to the strains which are removed at the end of the heating phase being a mix of thermal and mechanical (caused by the compromise in expansion between concrete and reinforcement on heating), and not being pure thermal strains. ..120

Figure 4-21: Stress-strain for reinforcement in a one-element RC model, with thermal expansion and tension stiffening included, under tension, compared with steel material properties, with (1) The element loaded in tension using a displacement-controlled boundary condition and then heated to 200°C. The model follows the ambient material properties curve during loading, while on being heated the tensile stress decreases as the elastic modulus of steel reduces with increasing temperature and thermal stresses occur due to expansion not being permitted by the boundary condition. Note that the reinforcement remains in the elastic regime throughout the analysis. (2) The element is heated to 200°C with free expansion permitted and then loaded under tension at elevated temperature. This model shows initial compressive stress and tensile strain on heating due to compromise between the differing thermal expansions of concrete and reinforcement – concrete has a lower coefficient of thermal expansion and expands less than reinforcing steel, forcing the reinforcement into compression. On loading the model follows the gradient of the loading branch of steel's 200°C material properties curve. (3) The element is heated to 200°C, strains due to thermal expansion are removed, and then the element is loaded

Table of Tables

Nomenclature

α	coefficient of thermal expansion
α_c	coefficient of thermal expansion for concrete
α_s	coefficient of thermal expansion for steel
ΔT	change in temperature T
ε	strain
ε_y	yield strain
ε_{cm}	strain at peak stress at temperature T
ε_{cmo}	strain at peak stress at ambient temperature
ε_{cu}	ultimate strain at temperature T
ε_{cuo}	ultimate strain at ambient temperature
$\varepsilon_{c1,\theta}$	thermal strain
$\varepsilon_{cu1,\theta}$	ultimate strain at zero stress
$\tilde{\varepsilon}_c^{pl}$	compressive equivalent plastic strain
$\tilde{\varepsilon}_t^{pl}$	tensile equivalent plastic strain
θ	temperature OR angle of localization band from the horizontal
κ_C	an internal damage parameter
κ_e	equivalent strain at maximum compressive strength
κ_{E_i}	aggregate and test type dependent coefficient for elastic modulus
$\kappa_{f_{mi}}$	aggregate and test type dependent coefficient for peak strength

$\kappa_{\varepsilon_{mi}}$ aggregate and test type dependent coefficient for strain at peak stress

$\kappa_{\varepsilon_{iu}}$ aggregate and test type dependent coefficient for ultimate strain

κ_u maximum equivalent strain

λ material parameter used in post-peak softening behaviour; 1.01 for concrete

ρ reinforcement ratio in reinforced concrete

σ uniaxial stress

σ_c concrete compressive strength

σ_{b0} initial equibiaxial compressive yield stress

σ_{c0} initial uniaxial compressive yield stress

σ_s reinforcing steel strength

σ_t concrete tensile strength

σ_y yield stress

$\hat{\sigma}_{\max}$ maximum principal stress

$\overline{\sigma}$ effective stress tensor

$\overline{\sigma}_c$ effective compressive stress

$\overline{\sigma}_t$ effective tensile stress

$\hat{\overline{\sigma}}_{\max}$ algebraically maximum eigenvalue of $\overline{\sigma}$ (or maximum principal effective stress)

υ Poisson's ratio

ϕ diameter

$\mathbf{A}$ acoustic tensor

d depth

d_c damage variable in compression

d_t damage variable in tension

$\mathbf{D}^{\mathbf{ep}}$ elasto-plastic tensor

e_{nn}^{ck} cracking strain

E Young's modulus

E_c concrete compressive elastic modulus

E_{co_ACI} elastic modulus at ambient temperature, from ACI

E_s elastic modulus of steel at ambient temperature

$E_{s,\theta}$ elastic modulus of steel at temperature θ

f_c uniaxial compressive strength

$f_{c,\theta}$ compressive strength of concrete at temperature θ

$f_{ck,t}$ peak tensile strength at ambient temperature

$f_{ck,t}(\theta)$ tensile strength of concrete at temperature θ

f_{cm} compressive strength

f_{cmo} mean compressive strength at ambient temperature

$f_{sp,\theta}$ tensile strength at temperature θ for reinforcing steel

f_t uniaxial tensile strength

f_t' tensile splitting strength of concrete

f_y tensile strength of reinforcing steel

f_{yk} tensile strength at ambient temperature for reinforcing steel

F yield function

G_c compressive fracture energy

G_f tensile fracture energy

G_f^o fracture energy G_f at temperature T_0

h element characteristic length

H softening modulus

$\mathbf{I}$ identity matrix

k material parameter used in post-peak softening behaviour

K_c parameter used in determining the shape of the yield surface; ratio of the second stress invariant on the tensile median to that on the compressive median at initial yield for any given value of the pressure invariant, p, such that the maximum principal stress is negative, $\hat{\sigma}_{\max} < 0$

$k_{c,t}(\theta)$ coefficient related to the reduction of characteristic tensile strength of concrete

L span of beam or slab

n an exponent determined by measuring the rate of growth of the crack length at various load values OR ratio of steel elastic modulus to concrete elastic modulus

$\mathbf{n}$ unit vector satisfying the acoustic tensor equation

$\bar{p}$ effective hydrostatic pressure

$\bar{q}$ Mises equivalent effective stress

R universal gas constant

$\bar{\mathbf{S}}$ deviatoric part of the effective stress tensor $\bar{\sigma}$

T absolute temperature

T_0 reference temperature (normally 298 K)

u_n^{ck} cracking displacement

U activation energy of bond rupture

w crack width OR dimension width

w_c compression stiffness recovery variable

w_t tension stiffness recovery variable

1

Introduction

1.1 Introduction

Concrete has been used in construction for hundreds of years, right from Roman times to the present day. It can be used in its plain form, or reinforced with steel bars to improve its properties. Many tests have been conducted on concrete to determine its material properties so that adequate design of structures can be carried out, however much of this work focuses on the material properties at ambient temperature. With increasing recognition of the need to understand

how structures behave in extreme circumstances such as a fire, the determination of material properties at elevated temperatures has become increasingly important in analysis and design. This is especially relevant as detailed computer simulation of structures becomes more commonplace.

Extreme events such as the Mont Blanc Tunnel fire in 1999 (Bettelini et al. 2001) or the Windsor Tower fire in 2005 (Calavera et al. 2005) have shown how concrete failure at elevated temperatures can be hazardous to the safety of members of the public and economy of the region. Some full-scale tests of structures in fires were carried out in the 1990s and 2000s (Lamont et al. 2004; Rein et al. 2007), and these helped engineers to find out about the global response of reinforced concrete structures to elevated temperatures. This knowledge has led to performance-based design of structures (CIB 1982), where they are designed to exceed particular performance standards, rather than to obey specific rules. This often involves complex modelling of structures, for which a comprehensive knowledge of the behaviour of materials is necessary. Generally, there is an absence of understanding of the mechanical behaviour of both plain and reinforced concrete, which is essential for computational modelling.

Unlike steel, there is no agreement on the constitutive model for concrete, even at ambient temperatures. Many different models have been proposed, from the well used Mohr-Coulomb and Drucker-Prager criterions, to more recent criteria proposed by various other authors (Ottosen 1977; Hoek and Brown 1980; Lin et al. 1987; Lubliner et al. 1989; Bicanic et al. 1993; Menetrey and Willam 1995; Feenstra and de Borst 1996; Lee and Fenves 1998). Material models used must account for the pressure sensitivity of concrete, its lower tensile strength than compressive strength, localised cracking and crushing, and issues to do with mesh sensitivity.

The situation becomes even more complicated when reinforcement is included, as not only do the individual material models for concrete and reinforcing steel

need to be characterised, the interaction between the two materials and issues to do with the bond between concrete and reinforcement must be considered.

Since fire is an extreme event, a certain amount of damage within the structure would be seen to be permissible within its performance objectives, while collapse needs to be avoided. If only minor damage occurs to the structure then strengthening and retro-fitting may permit reuse of the structure. This necessitates analysis within the post-peak regime.

As a material, concrete has a very low value of thermal conductivity. This means that large thermal gradients often occur within concrete, especially in deep specimens. Large thermal gradients cause differential expansion of the material, and this can cause convergence problems in finite element modelling. It may also cause damage within the material itself during experimental heating. Concrete and steel have different values of thermal expansion. If reinforced concrete is heated, then the different thermal expansion of the two materials can cause large plastic deformation adjacent to the reinforcement. Again, this may be a cause of damage in heated concrete. This, coupled with the change in mechanical properties at elevated temperatures, further complicates analytical analysis procedures trying to replicate these actual experiments.

The aim of this study is to examine the effect of constitutive modelling on the response of plain and reinforced concrete systems at elevated temperatures.

1.2 Scope and layout of the thesis

As stated previously, the main aim of this thesis is to investigate issues associated with computational modelling of plain and reinforced concrete at elevated temperatures and in residual testing (when it has been heated, for example in a fire, and then cooled). It is expected that this study will help identify issues associated with computational modelling of reinforced concrete at elevated temperatures, in particular parameters that are important and need to be carefully provided to the models. It is apparent that there is a dearth of

experimental data at elevated temperatures. High temperature triaxial testing is practically non-existent. It is hoped that this study will help design experiments which may be conducted in the future. The outline of the remaining chapters of this thesis is as follows:

- Chapter 2 looks at plain concrete in tension. It includes a study of the basic tensile parameters at ambient and elevated temperature, including the use of fracture energy. Benchmark finite element analyses are carried out to examine the effect of changing material parameters at elevated temperatures on the response.
- Chapter 3 studies plain concrete in compression. There have been more compressive experimental tests on concrete, and so a brief review of this data is included. Again, compressive material parameters are discussed and their evolution at elevated temperatures proposed. Simple finite element analyses are carried out to test this material model.
- Chapter 4 discusses the finite element modelling of reinforced concrete in tension and compression. This includes a discussion of reinforcement material properties, tension stiffening, and how to incorporate steel and concrete properties to give an appropriate material model of the composite material. Simple benchmark tests are carried out on one-element reinforced concrete FE models.
- Chapter 5 investigates the residual properties of concrete specimens after they have been heated and cooled – both plain concrete and reinforced. Material models proposed in the previous chapters are used, and experimental data from a test series carried out at IIT, Roorkee is used in the FE analyses carried out. A hypothesis is proposed about the cause of degradation in material properties on residual testing, and this is investigated.
- Chapter 6 considers some more real world analyses. It includes investigation of a plain concrete beam under temperature increase and

thermal gradient, as well as a reinforced concrete slab that is subjected to both thermal expansion and gradients.

- Chapter 7 looks at a simple reinforced concrete portal frame. It is subjected to displacement at its top, in simplified simulation of damage caused by earthquakes to concrete structures. After this the frame is heated to consider the behaviour of damaged structures in fire.
- Chapter 8 includes both some conclusions on this work, and some suggestions for further work that might be carried out.

1.3 References

Bettelini, M., L. Glarey, et al. (2001). The new Mont Blanc Tunnel - A milestone in tunnel safety. International conference International tunnel forum. Basel, 4-6 December.

Bicanic, N., R. de Borst, et al. (1993). Computational Aspects of Finite Element Analysis of Reinforced Concrete Structures (Topic 7). Structural Engineering and Structural Mechanics Research Series, CU/SR-93/3, Department of Civil Engineering and Architectural Engineering, University of Colorado, Boulder.

Calavera, J., E. Gonzalez-Valle, et al. (2005). Fire in the Windsor building, Madrid. Survey of the fire resistance and residual bearing capacity of the structure after the fire. Instituto Technico De Materiales Y Constructiones (INTEMAC).

CIB (1982). Working with the performance approach to building. Report of Working Commission W60, Publication 64**:** 30p.

Feenstra, P. H. and R. de Borst (1996). "A composite plasticity model for concrete." International Journal of Solids and Structures **33**: 707-730.

Hoek, E. and E. T. Brown (1980). "Empirical strength criterion for rock masses." Journal of the Geotechnical Engineering Division, ASCE **106**: 1013-1035.

Lamont, S., A. S. Usmani, et al. (2004). "Behaviour of a small composite steel frame structure in a 'long-cool' and 'short-hot' fire." Fire Safety Journal.

Lee, J. H. and G. L. Fenves (1998). "Plastic-damage model for cyclic loading of concrete structures." Journal of Engineering Mechanics-Asce **124**(8): 892-900.

Lin, F. B., Z. P. Bazant, et al. (1987). "Concrete model with normality and sequential identification." Computers and Structures **26**: 1011-1025.

Lubliner, J., J. Oliver, et al. (1989). "A Plastic-Damage Model for Concrete." International Journal of Solids and Structures **25**(3): 299-326.

Menetrey, P. and K. J. Willam (1995). "A triaxial failure criterion for concrete and its generalization." ACI Structural Journal **92**: 311-318.

Ottosen, N. S. (1977). "A failure criterion for concrete." Journal of Engineering Mechanics, ASCE **103**: 527-535.

Rein, G., C. Abecassis-Empis, et al., Eds. (2007). The Dalmarnock Fire Tests: Experiments and Modelling, The University of Edinburgh.

2

Concrete in tension

2.1 Introduction

Concrete has been used in construction for hundreds of years, and considerable research has been carried out to understand its behaviour.

Generally, concrete at ambient temperature is classified by its compressive strength, based on the characteristic cylinder strength determined at 28 days (EN1992-1-1 2004). Concrete commonly used in the construction industry has a

compressive strength in the range 30 to 50 MPa, though concrete with much higher strengths is also being used. Concrete is much stronger in compression than in tension (EN1992-1-1 2004) – typically concrete's tensile strength is approximately one tenth of its compressive strength. In design of reinforced concrete structural components the tensile load carrying capability of concrete is generally neglected. However, understanding its behaviour in tension is important for the evaluation of the post-peak response under extreme loads (e.g. fire, earthquake).

Experimental data suggests that the elastic modulus of concrete is the same for both tension and compression (Teller 1956; Neville 1963). Although concrete is a quasi-brittle material its mechanical response to loads is often modelled using the theory of plasticity. After yield, concrete starts to crack, with the cracking localising in small areas which become weakened. This is represented by a reduction in stress as the strain on the material continues increasing, shown on the stress-strain curve as a descending branch. This occurs both in tension and in compression. As design codes ignore concrete's contribution in tension, its post-linear behaviour is not specified. For example in the concrete design Eurocode (EN1992-1-1 2004) the material parameters typically specified include secant modulus of elasticity, strain at peak stress, and ultimate compressive strain for different concrete strengths. For instance, for a concrete with compressive strength of 30 MPa, the specified values are: elastic modulus of 33 GPa; strain at peak compressive stress of 0.0022 and ultimate compressive strain of 0.0035 (EN1992-1-1 2004). These values can be used together to give material stress-strain curves, also provided in codes, for computational modelling. However this data is not sufficient for the full triaxial loading that concrete may experience during its lifetime. Modelling of concrete as a continuum requires constitutive models which are left to the discretion of the designer. These are discussed first in this chapter and followed by discussion on modelling concrete at elevated temperatures.

2.2 Constitutive Models for Concrete

Before discussing the behaviour of plain concrete in tension it is important to consider constitutive models for concrete. Numerous constitutive models have been proposed for concrete with the Mohr-Coulomb and Drucker-Prager criterion being often used. More recent criteria include those due to Ottosen (1977), Hoek and Brown (1980), Lin et al. (1987), Lubliner et al. (1989), Bicanic et al. (1993), Menetrey and Willam (1995), Feenstra and de Borst (1996), and Lee and Fenves (1998). Concrete is a pressure sensitive material which implies that its yield strength is dependent on hydrostatic stress. This feature also means that it has a much lower tensile strength in comparison to compressive strength. Tensile cracking is typically normal to the direction of maximum principal stress which can be reasonably well described using a Rankine type maximum principal stress criterion. In tension, 'yielding' is concurrently followed by localised cracking. It is now recognised that in numerical modelling, using theories of plasticity, one needs to use non-local laws to prevent mesh sensitivity (Bazant and Oh 1983; Rots et al. 1985; Pramono 1988; Pankaj 1990) (to be discussed). It is also important to note that concrete fracture force was previously modelled using two distinct approaches: the smeared crack approach (Rashid 1968) and the discrete crack approach (Ngo and Scordelis 1967). However in recent years, the gap between these two approaches has been bridged (de Borst et al. 2004).

In this study, the concrete damage – plasticity model proposed by Lubliner et al. (1989) and Lee and Fenves (1998) is examined and employed. The choice of this model is based on its availability in Abaqus (Abaqus 2008), the commercial FE package used in this study, and the fact that it can model all the key features of concrete discussed above.

2.2.1 Concrete damage – plasticity

In concrete damage – plasticity the yield function, F, used to describe the evolution of the yield surface, is given by (Abaqus 2008):

$$F\left(\bar{\sigma},\tilde{\varepsilon}^{pl}\right)=\frac{1}{1-\alpha}\left(\bar{q}-3\alpha\bar{p}+\beta\left(\tilde{\varepsilon}^{pl}\right)\left\langle\hat{\bar{\sigma}}_{\max}\right\rangle-\gamma\left\langle-\hat{\bar{\sigma}}_{\max}\right\rangle-\bar{\sigma}_c\left(\tilde{\varepsilon}_c^{pl}\right)\right)\leq 0 \qquad (2.1)$$

where:

$$\alpha=\frac{\left(\sigma_{b0}/\sigma_{c0}\right)-1}{2\left(\sigma_{b0}/\sigma_{c0}\right)-1};\ 0\leq\alpha\leq 0.5 \qquad (2.2)$$

$$\beta=\frac{\bar{\sigma}_c\left(\tilde{\varepsilon}_c^{pl}\right)}{\bar{\sigma}_t\left(\tilde{\varepsilon}_t^{pl}\right)}\left(1-\alpha\right)-\left(1+\alpha\right) \qquad (2.3)$$

$$\gamma=\frac{3\left(1-K_c\right)}{2K_c-1} \qquad (2.4)$$

$\bar{\sigma}_c$ and $\bar{\sigma}_t$ are the effective compressive and tensile cohesion stresses, respectively, $\tilde{\varepsilon}_t^{pl}$ and $\tilde{\varepsilon}_c^{pl}$ are tensile and compressive equivalent plastic strains and σ_{b0}/σ_{c0} is the ratio of initial equibiaxial compressive yield stress to initial uniaxial compressive yield stress;

$$\bar{p}=-\frac{1}{3}\bar{\sigma}:\mathbf{I} \qquad (2.5)$$

is the effective hydrostatic pressure;

$$\bar{q}=\sqrt{\frac{3}{2}\bar{\mathbf{S}}:\bar{\mathbf{S}}} \qquad (2.6)$$

is the Mises equivalent effective stress;

$$\bar{\mathbf{S}}=\bar{p}\mathbf{I}+\bar{\sigma} \qquad (2.7)$$

is the deviatoric part of the effective stress tensor $\bar{\sigma}$; and $\hat{\bar{\sigma}}_{\max}$ is the algebraically maximum eigenvalue of $\bar{\sigma}$ (or maximum principal effective stress).

The parameter K_c is used in determining the shape of the yield surface, as it is related to γ and β.

$$K_c = \frac{\beta + 3}{2\beta + 3} \tag{2.8}$$

K_c is the ratio of the second stress invariant on the tensile median to that on the compressive median at initial yield for any given value of the pressure invariant, p, such that the maximum principal stress is negative, $\hat{\sigma}_{\max} < 0$. The value of K_c must be between 0.5 and 1.0, with the default value in Abaqus being $K_c = 2/3$.

The above equations indicate that the specification of the initial yield surface requires the compressive and tensile yield strengths of the material ($\overline{\sigma}_c$ and $\overline{\sigma}_t$), the ratio K_c and the ratio σ_{b0}/σ_{c0}. While the effective strength parameters $\overline{\sigma}_c$ and $\overline{\sigma}_t$ can be estimated with some degree of confidence, other parameters have a greater degree of uncertainty associated with them. Uncertainty with respect to the evolution of the yield surface after first yield is even higher. There exist a large number of tests defining the post-yield behaviour of concrete in compression, but the rest of the parameters needed to define yield surface evolution are generally based on approximations and common sense. For example, the model uses a non-associated flow rule and requires the specification of the dilation angle. There is little data to specify this with any degree of accuracy. However, it has been recognised that the dilation angle needs to be half or less of the friction angle; the use of the associated flow rule (dilation angle = friction angle) leads to excessive dilation. Further, the concrete damage – plasticity model also permits stiffness degradation in tension and compression through its tension and compression damage variables. Once again there is little data to support the specification of these parameters. Unloading or reversal of loading can lead to some crack closing within the material – this then provides some recovery of load-carrying ability and stiffness, called damage

recovery. While the model permits this recovery, data to support its specification is not readily available.

A typical yield surface for plane stress is shown in Figure 2-1. This has been plotted for $\overline{\sigma}_c$ = 30 MPa, $\overline{\sigma}_t$ = 3 MPa, K_c = 1 and σ_{b0}/σ_{c0} = 1.16. The uniaxial tensile and compressive points are marked in Figure 2-1. A full 3D representation of the criterion in principal stress space is shown in Figure 2-2.

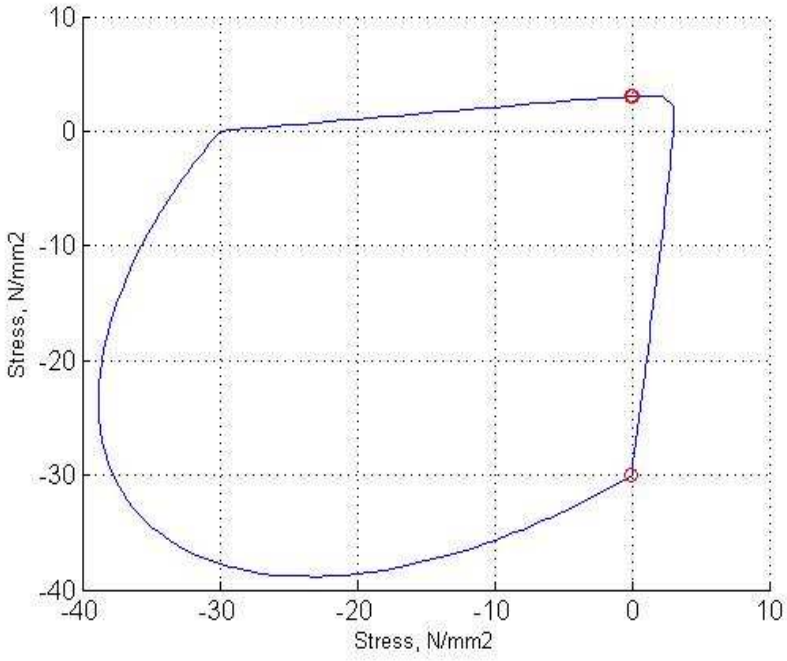

Figure 2-1: Plane stress 2D yield surface using concrete damage – plasticity with uniaxial tension and compression points marked

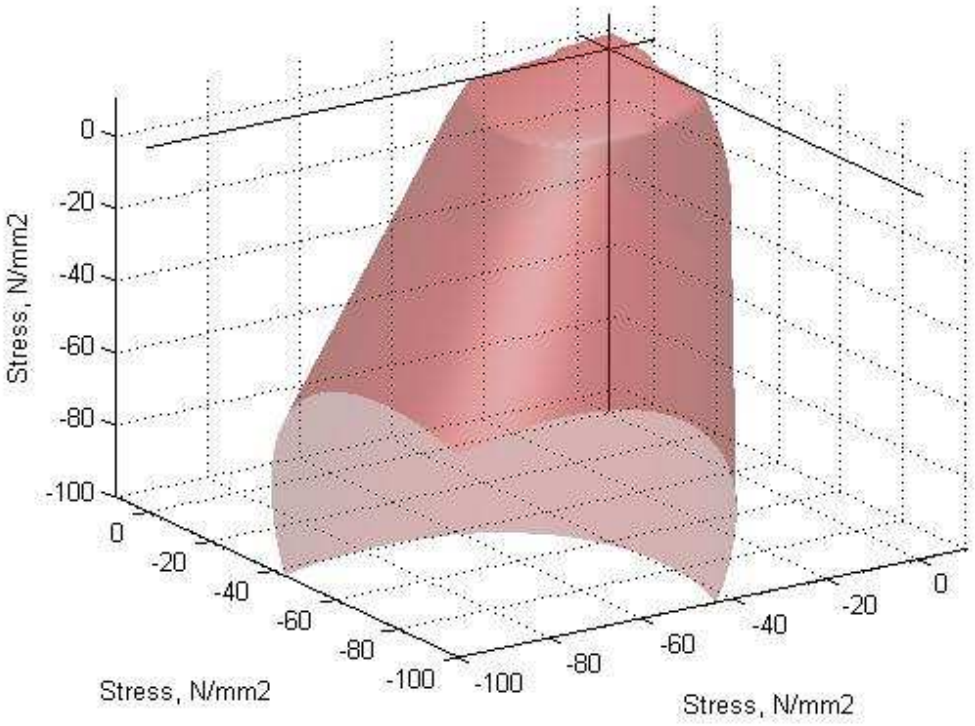

Figure 2-2: 3D yield surface for concrete damage – plasticity in principal stress space

2.3 Modelling at Ambient Temperatures

2.3.1 Strain Softening and mesh sensitivity

Strain softening has been described using a linear descending branch (Hillerborg et al. 1976), as bilinear descending branches (Roelfstra and Wittmann 1986), a power curve (Du et al. 1990) and as an exponential descending branch (Gopalaratnam and Shah 1985). A linear descending branch and exponential curve (Gopalaratnam and Shah 1985) offer simplicity and will therefore be used in this study.

Strain softening of concrete is due to strain localisation and is therefore not a material property. This has implications for finite element modelling, as the slope of the softening branch must be dependent on the element sizes used, otherwise mesh sensitivity occurs with analysis results changing according to

the element size used. Fracture energy is defined as the total energy dissipated in cracking a unit area of concrete (Bazant and Prat 1988) and is a material property. The value of fracture energy can be visualised as the area under the curve when stress is plotted against cracking displacement.

To examine issues associated with mesh sensitivity, a cylindrical concrete specimen was subjected to uniaxial tension (see Figure 2-3). The cylinder had a height of 500mm and a diameter of 160mm. The analysis was conducted with models having elements of different sizes. As uniaxial tension results in a homogenous stress state, a weakened central row of elements was introduced to induce localisation. The concrete damage – plasticity model was used for analysis with uniaxial tensile strength f_t = 3.3 MPa, Young's modulus E = 28.4 GPa and Poisson's ratio υ = 0.25 for normal elements. The weakened elements have the same properties, but uniaxial tensile strength f_t = 3.0 MPa. A linear softening branch with a fracture energy G_f = 100 N/m was used for all elements.

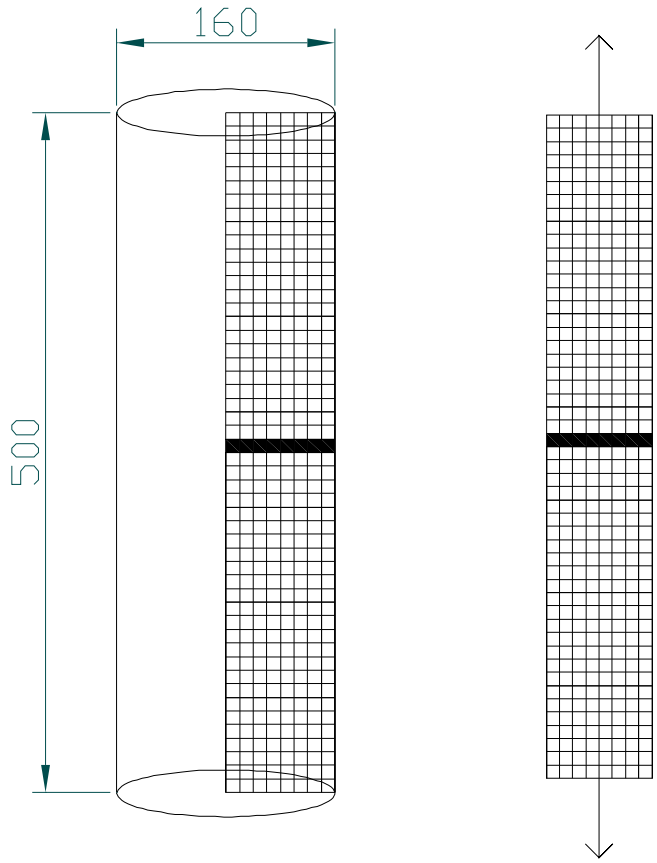

Figure 2-3: The cylinder modelled, with 10x10mm mesh using axisymmetric elements. Weakened elements are shaded, and dimensions given in mm.

The post-peak softening properties were provided to Abaqus in three different ways:

a) As post-peak stress versus direct cracking strain

b) As post-peak stress versus direct cracking displacement

c) The fracture energy value

For a) above, the values input need to be adjusted according to element size; in this case the element size is along the axis of the cylinder and in the direction of loading. Abaqus converts these three types of input into stress – cracking strain

values which are then used in the analysis. Hence the three methods have an equivalence based on the element size and shape used in the model.

Two meshes with square elements of 20x20mm (a 25x4 element mesh) and 10x10mm (a 50x8 element mesh) were analysed. The load-displacement plot is shown in Figure 2-4 and shows that the models are not mesh sensitive, and all material input methodologies work equally well. The finer mesh gives slightly higher load values at yield due to a smaller area of material yielding at first.

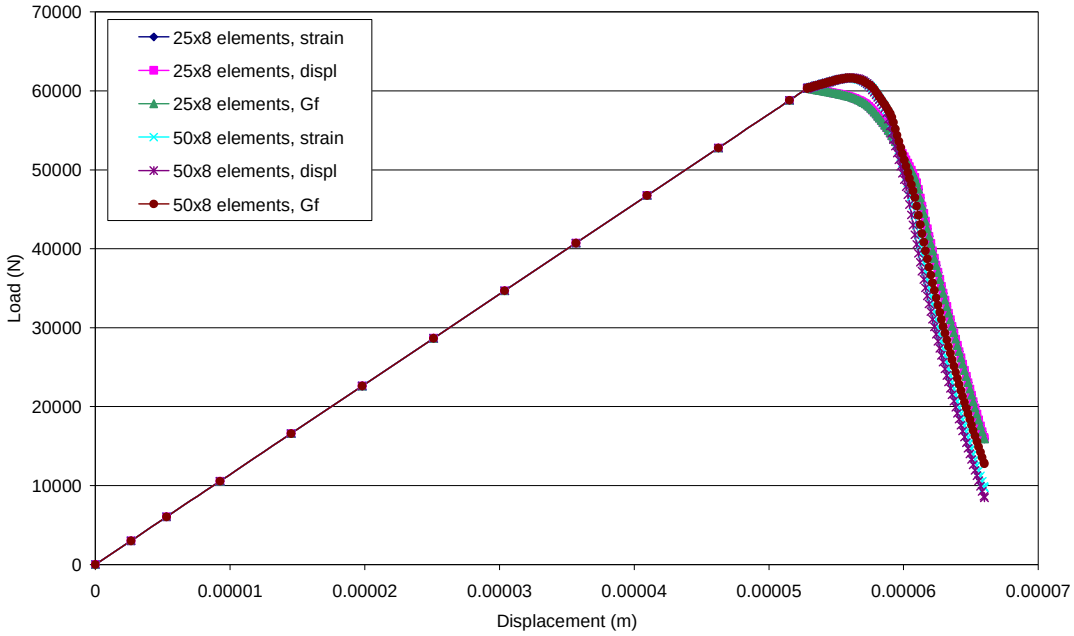

Figure 2-4: Plot of tensile load versus tensile displacement for a cylinder with square elements used throughout its mesh. Two different mesh sizes and three different methods of input are shown.

It is important to note that there is no ambiguity with regard to element size in these models as the dimensions of each element are identical in the two directions. For general analysis it is not feasible to maintain element size aspect ratio as unity at all times. It is therefore important to examine the response when elements used are not square.

The cylinder was modelled using elements of dimension 50x10mm (a 10x8 element mesh) with the central row of elements weakened slightly under uniaxial tension (as before the normal elements have a uniaxial tensile strength f_t = 3.3 MPa, while the weakened elements have a uniaxial tensile strength f_t = 3.0 MPa) (see Figure 2-5), and the results were compared with the model with square elements. The load-deformation plot is shown in Figure 2-6.

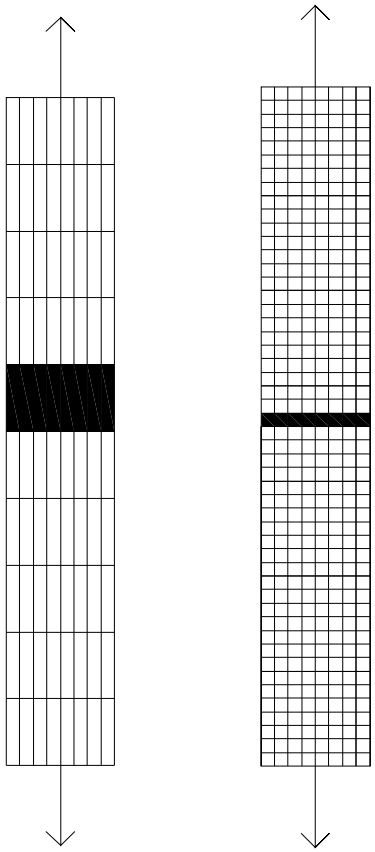

Figure 2-5: Cylinders modelled using non-square elements, again the weakened elements are shaded.

It can be seen that the descending branches of the load-displacement curves are not similar. The response with rectangular elements matches up with the response from square elements in the lower part of the descending branch, when stress versus direct cracking strain input is provided. The response of rectangular elements with stress versus cracking displacement input and with

fracture energy input is similar, but significantly different from the response for square elements.

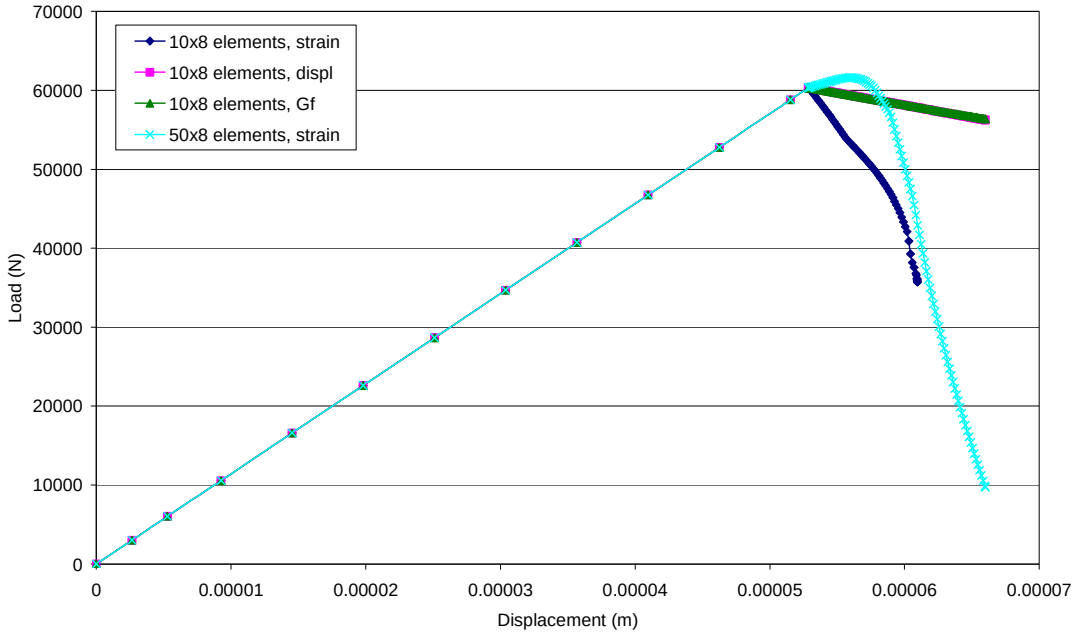

Figure 2-6: Plot of tensile load versus tensile displacement for cylinders modelled with 10 or 50 elements along their length, and 3 different methods of material property input.

When fracture energy or stress-cracking displacement data is provided, finite element codes generally convert this to stress-cracking strain data using a characteristic length. One of the commonly used techniques is to obtain the characteristic length using the square root of element area (sometimes area enclosed by integration points).

Abaqus uses a characteristic length h to convert cracking displacements into cracking strains (and a similar method to calculate cracking strains from fracture energies) (Abaqus 2008), as seen in the equation given below, where u_n^{ck} is the cracking displacement and e_{nn}^{ck} is the cracking strain.

$$u_n^{ck} = e_{nn}^{ck} h \tag{2.9}$$

The characteristic length (Oliver 1989) is based on element geometry, with it being the typical length of a line across an element for a first-order element. This can cause problems when elements have a large aspect ratio, as is apparent from this example, and can cause mesh sensitivity. When the material property cracking strain values are adjusted according to element length (with the strain values being 5 times less when the element is 5 times longer) the analysis results do match up. The characteristic length in this case is along the direction of loading and the results show that mesh sensitivity can be manually removed in simple examples such as this by specifying appropriate material properties. When displacement or fracture energy is used to determine the softening material properties, the results show mesh sensitivity due to the material properties being adjusted automatically by Abaqus on the basis of the evaluated characteristic length.

These results demonstrate that the mere use of non-square elements can lead to mesh insensitivity in the post-peak response. It is apparent that additional problems will ensue if the cracking directions are not parallel to element sides. For general problems, it is impossible to have square elements all the time and to have an *a priori* estimate of loading directions. Therefore some element of mesh sensitivity can always be expected. The recent development of techniques based on the partition of unity (Dolbow et al. 2001) in conjunction with plasticity (for triaxial loading states) may be able to overcome some of these issues in the future.

2.3.2 Localisation Directions

As discussed previously, localisation can be modelled as the growth and interaction of microcracks, which eventually join to form a macroscopic surface of rupture (Pankaj 1990). However, an alternative method is available by considering localisation as instability in the macroscopic constitutive description of the inelastic deformation of the material. Modelling the instability in this way

allows the deformation of an initially uniform material to lead to a bifurcation point, where non-uniform deformation occurs in a planar band under equilibrium conditions of continuing deformation outside the localisation zone (i.e. a cracking band is formed).

Localisation conditions occur when the following condition is satisfied (Pankaj 1990):

$$\det(A(n)) = \det\left(n_i D^{ep}_{ijkl} n_l\right) = 0 \qquad (2.10)$$

where $\mathbf{D^{ep}}$ is the elasto-plastic tensor for the material and **n** is the unit vector satisfying the above equation. **A** is called the acoustic tensor.

Equation 2.10 was used with damage – plasticity and material properties specified for the cylinder discussed earlier. A uniaxial stress state in the vertical direction was applied. The direction of unit vector **n** was varied from -90^o to +90^o from the horizontal and the determinant of the acoustic tensor evaluated in each case. The results are shown in Figure 2-7.

If the graph's minimum approaches zero or negative values, this suggests that localisation will occur. The θ angle at which the minimum values occur gives the direction of the crack band. The graph below shows that under uniaxial tension in the vertical direction, cracking and localisation will be in a horizontal band (i.e. at 0^o to the horizontal plane). These results show that the concrete damage – plasticity model behaves as a Rankine criterion in tension.

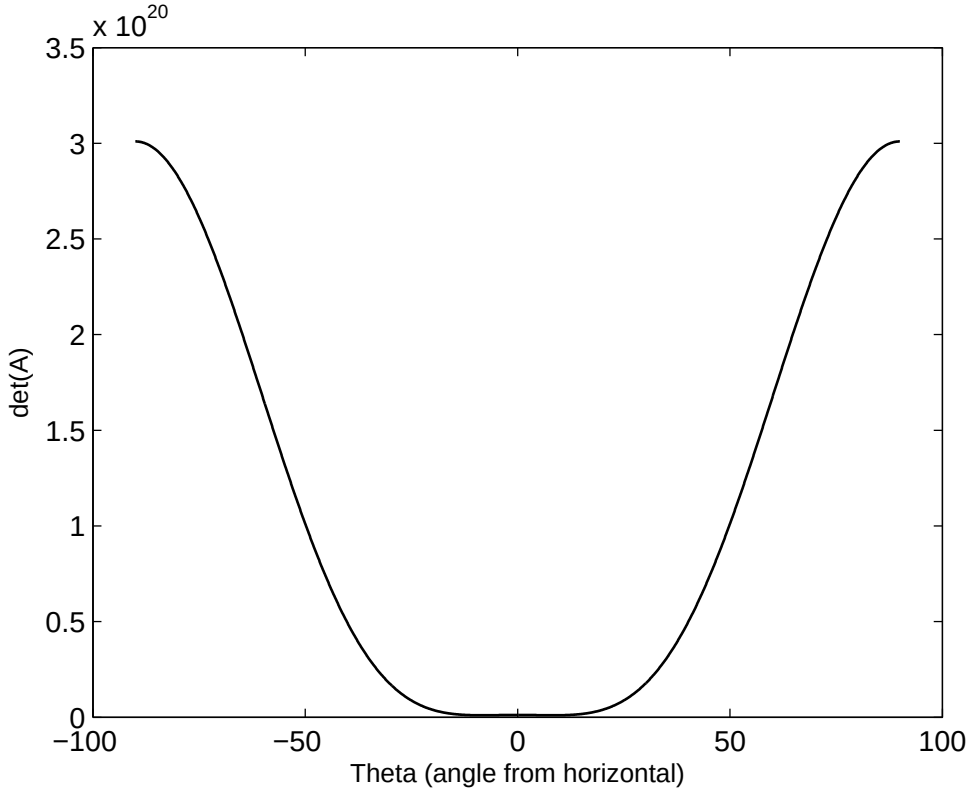

Figure 2-7: θ (angle from the horizontal) versus the determinant of the acoustic tensor for uniaxial tension in the vertical direction.

2.4 Modelling at Elevated Temperatures

Few experimental tests have been carried out on concrete at elevated temperatures, so information as to its behaviour and hence material properties at elevated temperatures is limited. However a few sets of data are available (Bazant and Prat 1988; Nielsen and Bicanic 2003; Zhang and Bicanic 2006), and Schneider (1988) has collated several others to evaluate the various material properties of concrete.

2.4.1 Change in properties with temperature

The structural fire design Eurocode (EN1992-1-2 2004) and previous studies (Bazant and Prat 1988; Schneider 1988) give some guidance on how the material properties of concrete alter at high temperatures. The key features of material behaviour of concrete at elevated temperatures are:

- Reduction in peak strength, which is detailed in the Eurocode and is also supported by experimental tests. As per the Eurocode concrete's tensile strength decreases linearly as its temperature increases beyond 100°C. The reduction of characteristic tensile strength of concrete is allowed for by the coefficient $k_{c,t}(\theta)$ as

$$f_{ck,t}(\theta) = k_{c,t}(\theta) f_{ck,t} \tag{2.11}$$

  where $f_{ck,t}$ is the peak tensile strength at ambient temperature and $f_{ck,t}(\theta)$ is the tensile strength at temperature θ.

  The variation of $k_{c,t}(\theta)$ with temperature is shown in Figure 2-8.

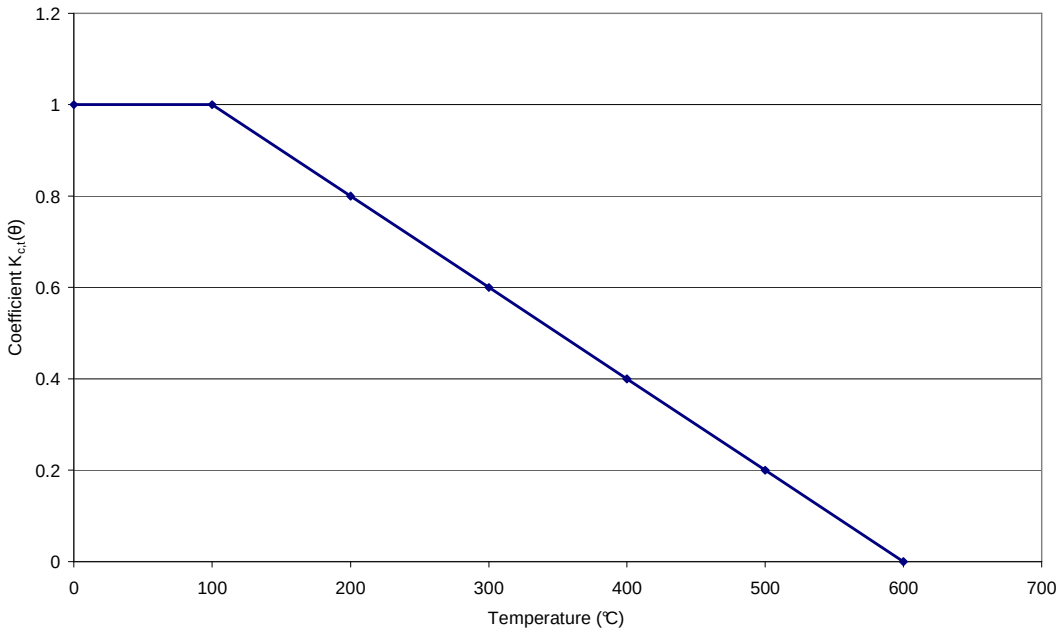

Figure 2-8: Coefficient $k_{c,t}(\theta)$ with temperature (redrawn from Eurocode EN1992-1-2 2004)

- Reduction in elastic modulus. Although the elastic modulus is not given explicity in the Eurocode a stress-strain graph has been provided for compression which permits evaluation of the elastic moduli at various temperatures. The variation of stress with strain is expressed by

$$\sigma(\theta) = \frac{3\varepsilon f_{c,\theta}}{\varepsilon_{c1,\theta}\left(2 + \left(\frac{\varepsilon}{\varepsilon_{c1,\theta}}\right)^3\right)} \tag{2.12}$$

where ε is strain, $f_{c,\theta}$ is the compressive strength of concrete at temperature θ for a specified strain, and $\varepsilon_{c1,\theta}$ is the thermal strain of concrete. The above equation holds for $\varepsilon \le \varepsilon_{c1,\theta}$. Differentiating the above equation the elastic modulus $E(\theta)$ can be obtained as

$$E(\theta) = \frac{3 f_{c,\theta}}{2\varepsilon_{c1,\theta}} \tag{2.13}$$

- Post-peak softening branch behaviour in tension is not defined in Eurocodes. It is unclear how fracture energy varies with temperature. In the sections that follow we consider the softening behaviour of concrete at elevated temperatures based on the limited available information. As discussed previously Murthy et al. (2009) list some of the most commonly used curves for post-peak softening behaviour. The two shapes considered here are linear and an exponential curve (Gopalaratnam and Shah 1985), defined by

$$\sigma = f_t \exp\left(kw^{\lambda}\right) \tag{2.14}$$

where σ is uniaxial stress, f_t is tensile strength, w is crack width, $\lambda = 1.01$ for concrete and k is a material parameter.

The fracture energy at different temperatures can be altered by varying the material parameter k.

2.4.2 Effect on fracture energy

Bazant and Prat (1988) determined the fracture energy of concrete at temperatures ranging from 20°C to 200°C. The three-point bending test and an eccentric compression loading test were carried out on both dry and wet (saturated) specimens. The two different tests gave approximately the same fracture energy for the material, while the influence of moisture on the fracture energy was found to be small at ambient temperature and more significant at temperatures around 100°C. They were then able to derive a simple formula relating fracture energy and temperature based on the activation energy theory. This was verified by the test results. The fracture energy G_f was given by

$$G_f = G_f^o \exp\left(\gamma/T - \gamma/T_0\right) \tag{2.15}$$

where

$$\gamma = 2U/nR \tag{2.16}$$

and G_f^o is the value of fracture energy G_f at T_0, T is the absolute temperature, T_0 is the chosen reference temperature (normally 298 K), U is the activation energy of bond rupture, R is the universal gas constant and n is an exponent determined by measuring the rate of growth of the crack length at various load values.

The test results of Bazant and Prat (1988) are shown in Table 2-1, and Figure 2-9. Fracture energy is seen to decrease as the temperature increases.

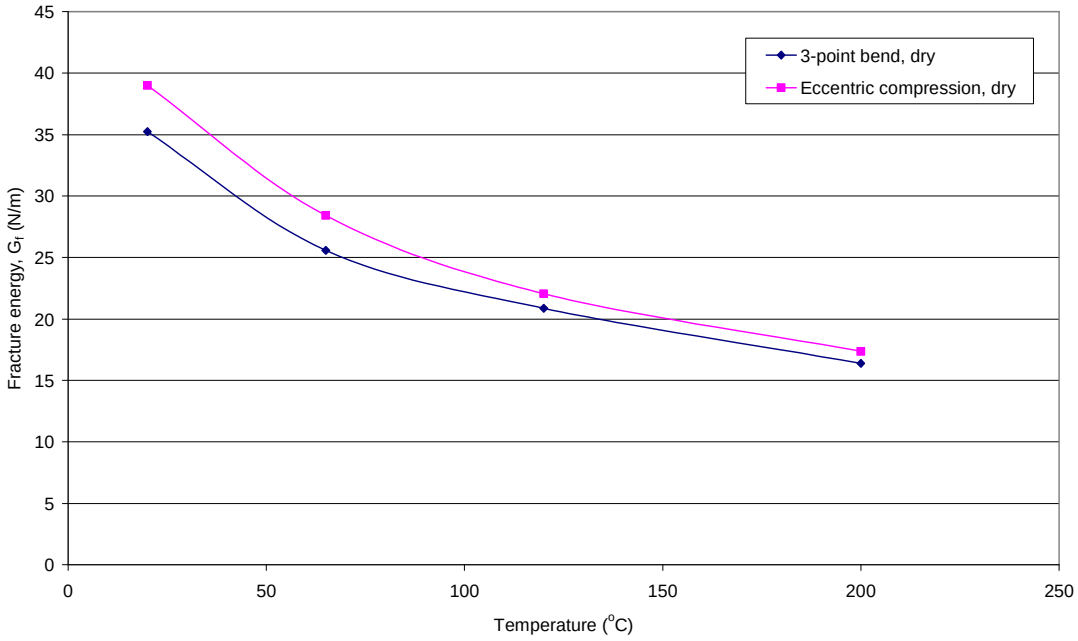

Figure 2-9: Experimental results for the effect of temperature on fracture energy for dry specimens (redrawn from Bazant and Prat 1998)

Table 2-1: Fracture energy values obtained from tests (N/m) (Bazant and Prat 1988)

	Temperature (°C)			
Test	20	65	120	200

3-point bend, dry	35.24	25.58	20.87	16.39
Eccentric compression, dry	39.01	28.42	22.06	17.36

In order to examine what the stress crack width graphs would look like at elevated temperatures the fracture energy data from Bazant and Prat (1988) was extrapolated and normalised with fracture energy at ambient temperature, as shown in Figure 2-10.

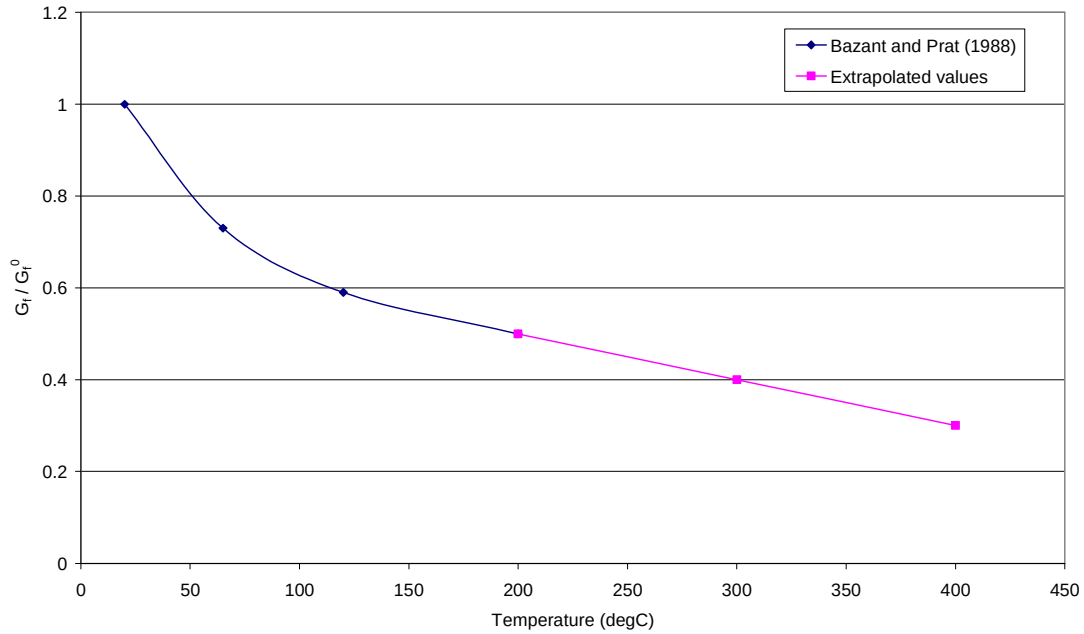

Figure 2-10: Relationship between fracture energy at ambient and elevated temperatures, with increasing temperature (extrapolated from data in Bazant and Prat (1988))

The values of fracture energy determined in the study by Bazant and Prat (1988) appear to be much lower than those found in more recent studies (Zhang et al. 2000; Wittmann 2002; Duan et al. 2007; Cedolin and Cusatis 2008) wherein values in the range of 60 – 150 N/m have been proposed for different aggregate sizes. Here a value of G_f = 100 N/m is taken for the fracture energy at ambient

temperatures. This is also a lower bound value from experimental tests conducted by Zhang and Bicanic (2006). When the reducing fracture energy ratios from Figure 2-10 are used in conjunction with ambient fracture energy of 100 N/m and the exponential curve of equation 2.14, the stress-crack width graph obtained is as shown in Figure 2-11. It should be noted that the peak stress is based on the Eurocode values.

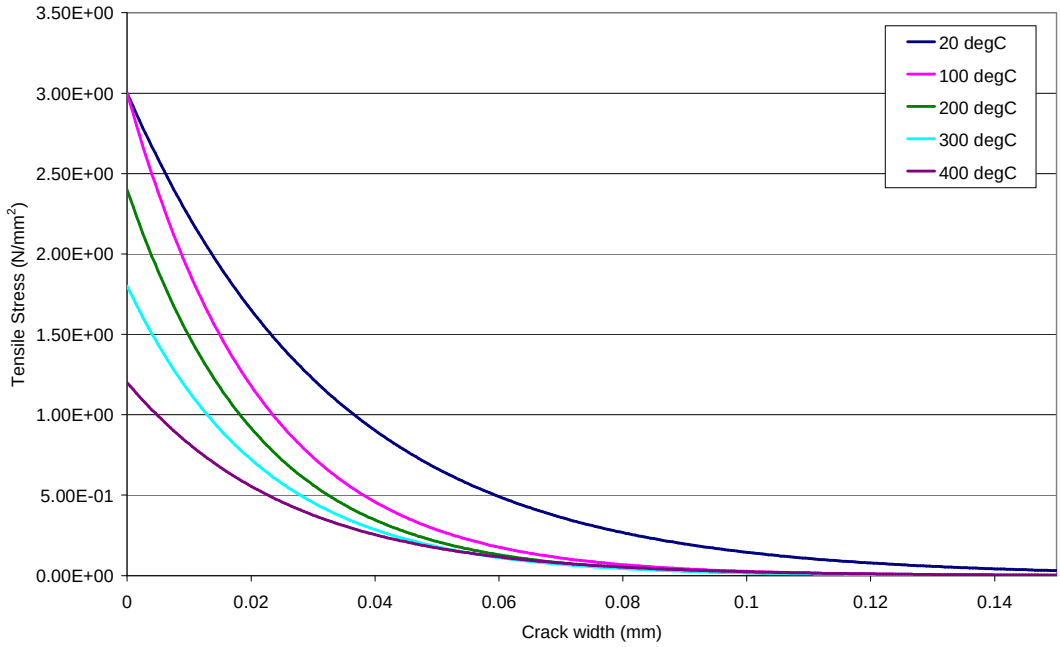

Figure 2-11: Strain softening descending branches plotted for increasing temperatures, when fracture energy decreases with increasing temperature

If the fracture energies of Figure 2-10 are used with a linear softening branch the stress-crack width variation obtained is as shown in Figure 2-12.

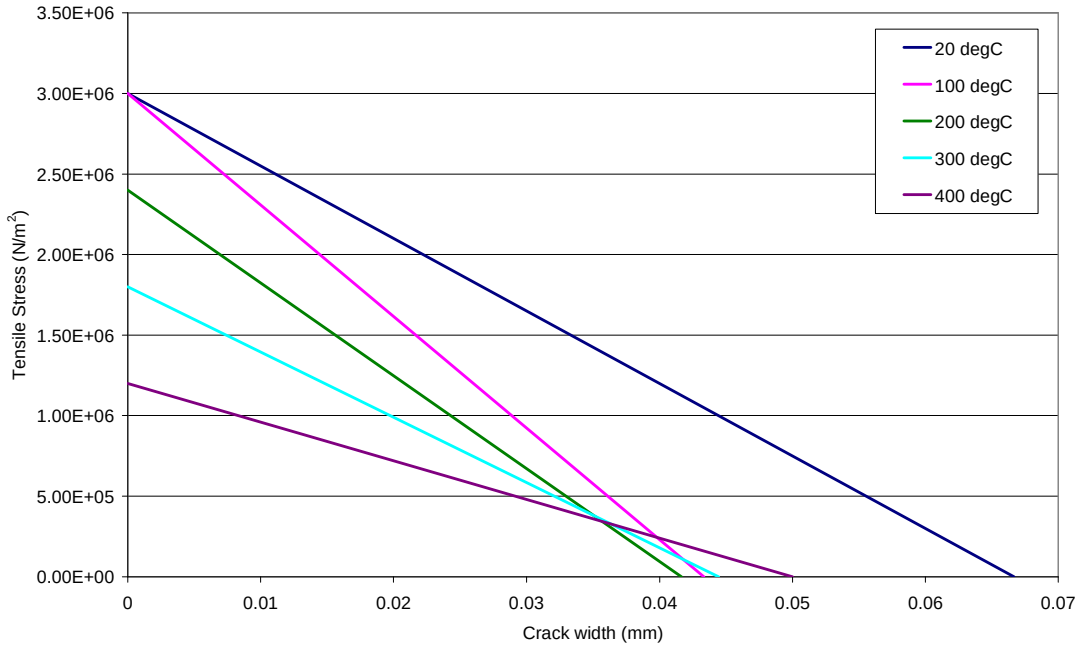

Figure 2-12: Linear strain softening behaviour at increasing temperatures when fracture energy decreases as temperature increases

Figures 2-11 and 2-12 show that cracking displacement for different temperatures corresponding to total loss of strength is very similar, particularly for the exponential curves. This behaviour is distinctly different to the known behaviour of concrete in compression at elevated temperatures wherein the crushing strain corresponding to zero stress increases with temperature. In the absence of significant experimental data at elevated temperatures, it can be hypothesised that the increase of ductility with temperature in compression may also occur in tension. In order to maintain simplicity and transparency, a constant fracture energy at varying temperatures was considered. Here a constant value of G_f = 100 N/m is used for all temperatures. The resulting crack width versus stress graphs are shown in Figures 2-13 and 2-14 for exponential and linear softening assumptions respectively.

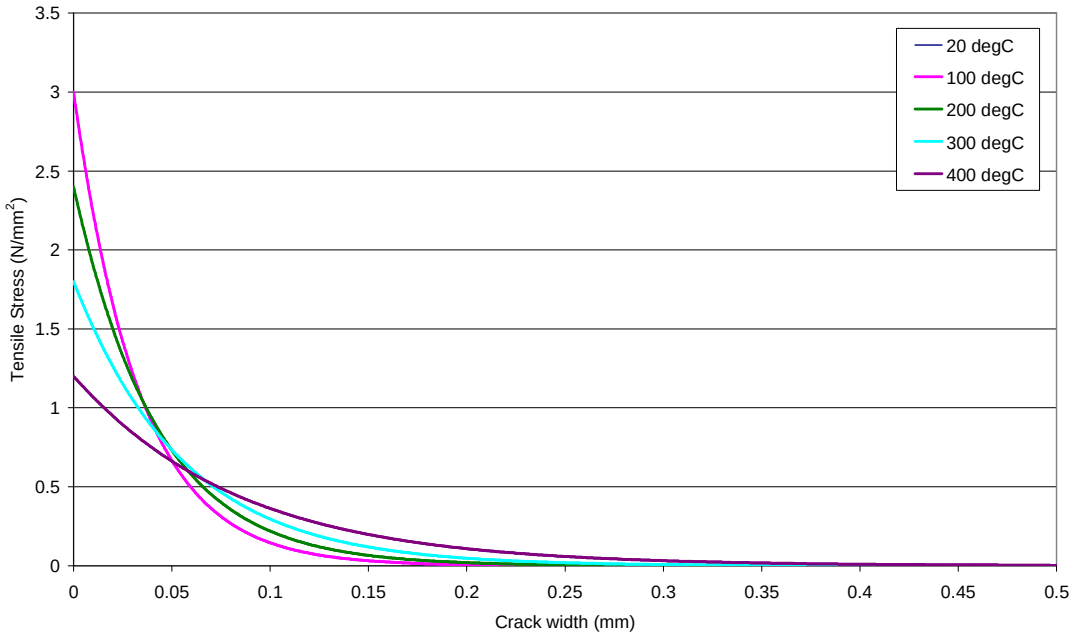

Figure 2-13: Strain softening descending branches plotted for increasing temperatures, when fracture energy remains constant

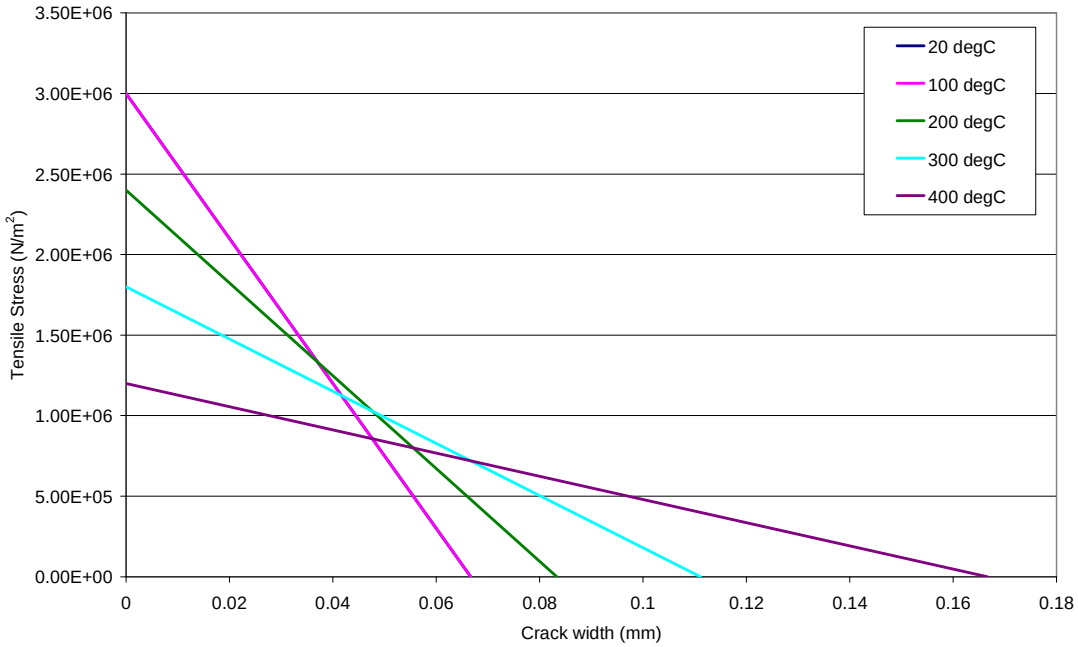

Figure 2-14: Post-peak softening behaviour of concrete in tension, assuming a constant fracture energy of 100 N/m

It can be seen that as the temperature increases, so does the strain at which tensile strength is zero; hence the gradient of the softening branch becomes less steep with increasing temperature.

The properties in Figure 2-14 will be used in the modelling work discussed below.

2.5 Constitutive behaviour in tension

Based on the three key variations at elevated temperatures – reduction of elastic modulus, reduction in tensile strength, and a constant fracture energy – a number of example problems were conducted. In these a one-element plane stress element, shown in Figure 2-15, was subjected to various tensile loading and heating patterns to check its behaviour. The first scenario involved the element being loaded using a displacement-controlled boundary condition, and then, with the boundary condition still in place, heated by applying an increase of temperature directly to the nodes of the element. In the second scenario the element is heated first, with expansion permitted both horizontally and vertically, before being loaded using a displacement-controlled boundary condition. In both scenarios the temperature is applied to the nodes of the element gradually, increasing over one timestep from ambient to the maximum temperature applied. Hence expansion and gradual change of the material properties present is permitted, but no thermal conduction or heat transfer is present.

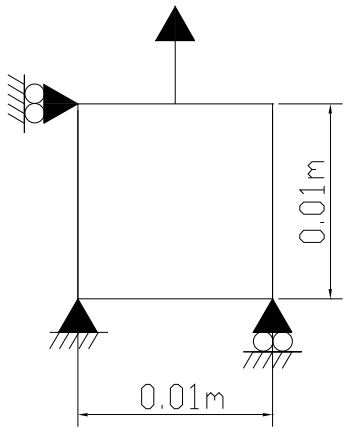

Figure 2-15: A one-element, plane stress model

2.5.1 Example 1

In this example two tests were conducted. In the first, the element is subjected to a tensile strain of 0.002 using a displacement-controlled boundary condition. It is then heated to 200^{o}C uniformly, while the boundary condition is still present. In the second test it is first heated while free to expand, and then subjected to mechanical strain. In each case the stress and strain found within the element throughout the tests is computed. To prevent thermal stresses and strains the element is given a thermal expansion coefficient of zero.

Figure 2-16 shows the material constitutive model curves at different temperatures along with the results of the two tests discussed above. It can be seen that in the first test, loading followed by heating, the element follows the ambient material properties curve well through the loading step. As the element is heated, the stress decreases as the strain is maintained at its constant value. In the absence of thermal expansion, which would have reduced the mechanical strain and thereby the stress, the cause for reduction in stress is not immediately apparent. However, since the stress in the post-elastic regime is given by the elastic modulus times the elastic strain, the decrease in stress is clearly due to the low elastic modulus at 200^{o}C.

In the second test, initial heating produces no stresses (since the thermal expansion has been set to zero), and subsequent loading makes the stress-strain response follow the 200°C material property curve.

These tests indicate that the stress-strain behaviour, even under monotonic loading and temperature increase, is strongly path dependent.

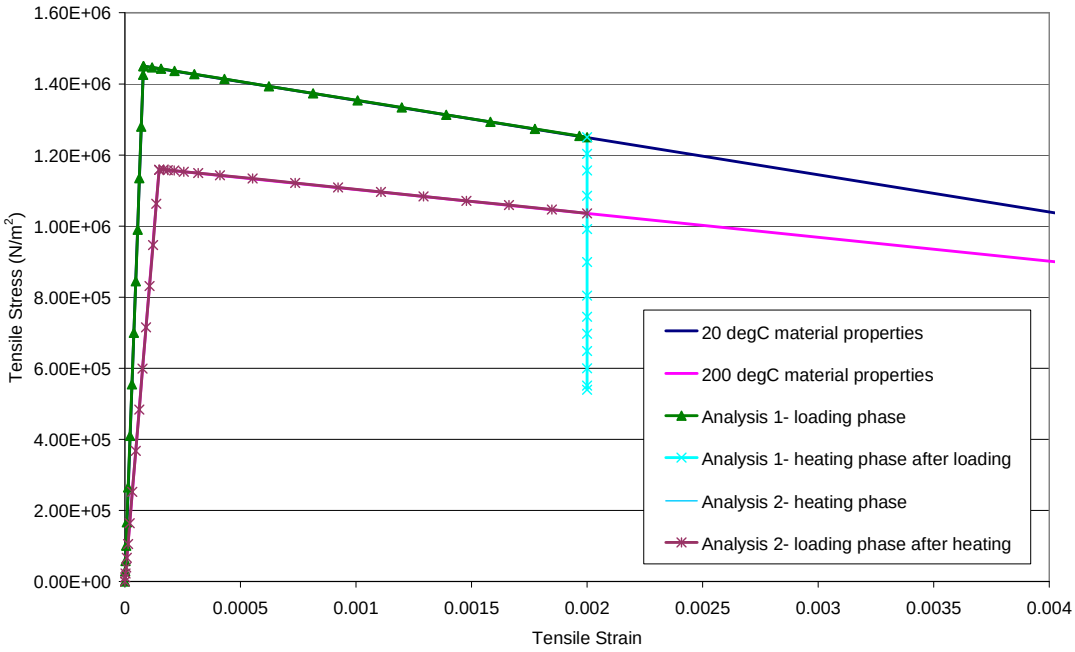

Figure 2-16: Stress-strain of a one-element plane stress model when the thermal expansion coefficient is zero: 1. The element is loaded by a displacement-controlled boundary condition and then heated to 200°C. The model follows the ambient material properties curve on loading, while the stress present reduces on heating due to the reduction in the elastic modulus at higher temperatures. 2. The element is heated to 200°C and then loaded using a displacement-controlled boundary condition. The model shows no expansion on heating but follows the 200°C material properties curve during the loading phase.

2.5.2 Example 2

From Figure 2-14 it can be seen that the post-peak softening branch lines for different temperatures intersect each other. In the previous example the strain

value considered was small, i.e. lower than any of the intersection strain values. This example considers the response at large strains. Once again the thermal expansion is set to zero. Again two tests are conducted, as in the previous example, but a strain of 0.012 is applied. The response along with the material property curves is shown in Figure 2-17.

Once again, the results are similar to the previous example. For the loading followed by heating test, the stress follows the ambient temperature curve and drops upon heating. In the heating followed by loading test, the response follows the material property curve at 200°C.

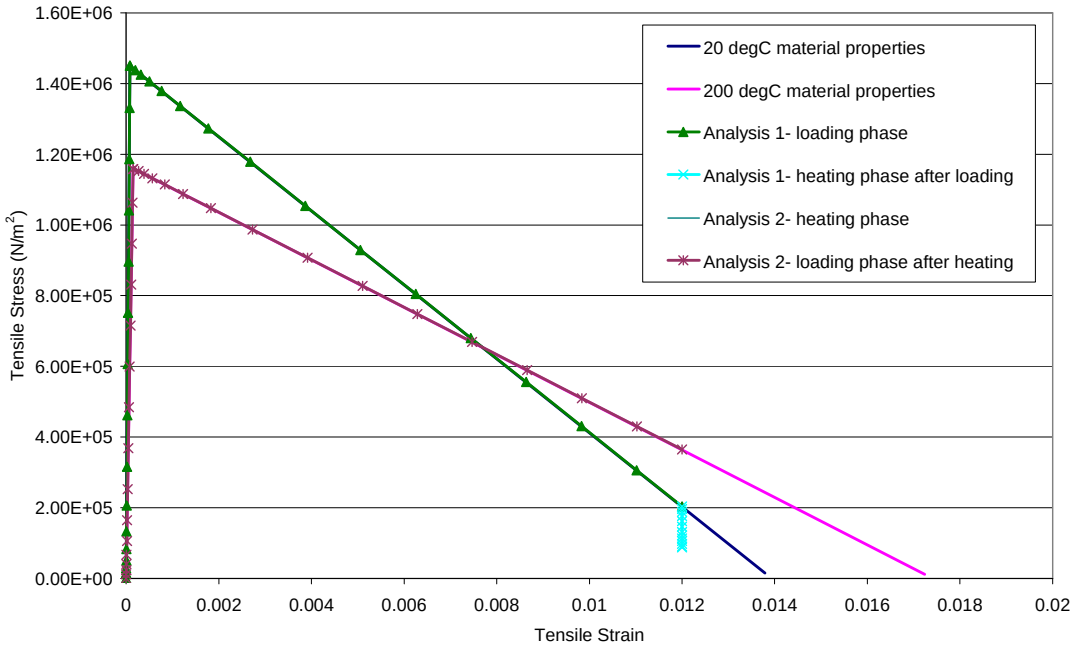

Figure 2-17: Stress-strain of a one-element plane stress model when the thermal expansion coefficient is zero, and the loading applied is much greater than in Figure 2-16: 1. The element is loaded by a displacement-controlled boundary condition and then heated to 200°C. The model follows the ambient material properties curve on loading, while the stress present reduces on heating due to the reduction in the elastic modulus at higher temperatures. 2. The element is heated to 200°C and then loaded using a displacement-controlled boundary condition. The model shows no expansion on heating but follows the 200°C material properties curve during the loading phase.

2.5.3 Example 3

Lastly, the same element is modelled, but this time the thermal expansion coefficient (α = 0.000009288 /^{o}C) is included, so thermal strains are now present on heating.

The element is first loaded in tension to a strain of 0.002, using a displacement-controlled boundary condition; it is then heated to 200^{o}C. The results are shown in Figure 2-18. The element again follows the ambient material properties through the loading step, as expected. As the element is heated, the total strain (elastic, plastic and thermal) stays the same while the stress decreases much more rapidly in comparison to previous examples in which thermal expansion was ignored. In fact, the stress ends up being significantly negative (or compressive) as the thermal strains overcome the initially applied tensile mechanical strain. The displacement boundary condition is fixed at the maximum loading value throughout the heating step. The stress decreases as the thermal expansion coefficient causes the material to expand on heating, forcing the element into compression from tension eventually.

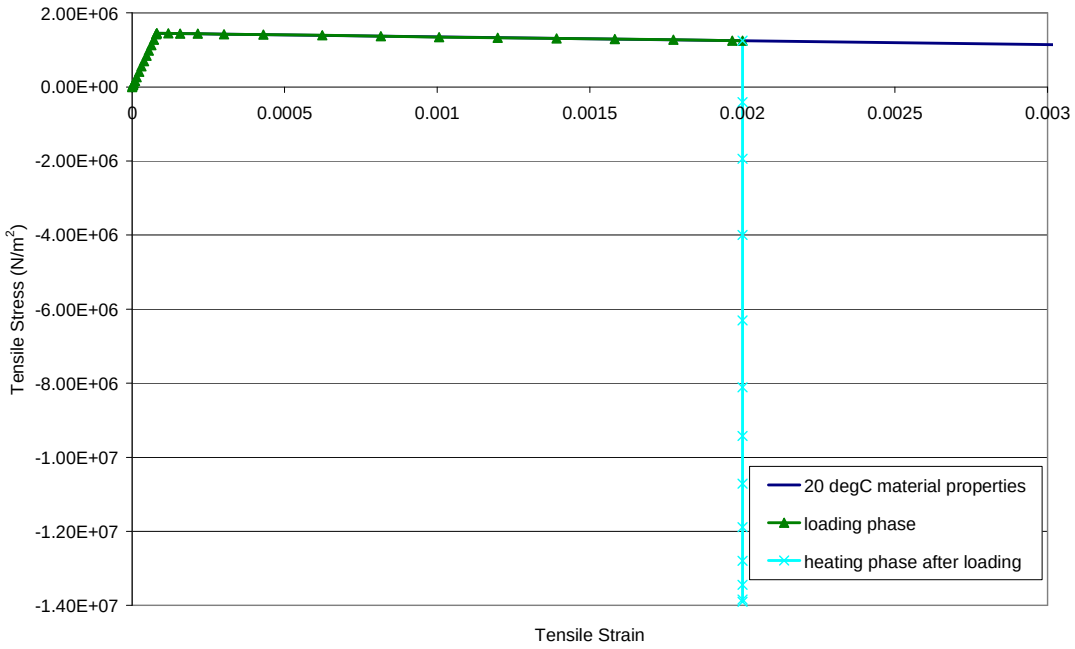

Figure 2-18: Stress-strain of a one-element plane stress model when thermal expansion is present: The element is loaded using a displacement-controlled boundary condition and then heated to 200°C. In this model the stress present decreases much more rapidly on heating in comparison to previous examples, due to the combined effect of the reduction in elastic modulus and the increase in thermal strains present.

In the second test the element is heated to 200°C while free to expand, before being strained in tension. It is shown in Figure 2-19 that the strain in the element increases during the heating step while the stress stays zero. This is thermal strain, caused by the thermal expansion coefficient. Once loading begins the stresses and strains follow the basic shape of the 200°C material properties curve; however they are offset from it due to the strain present in the element after the heating step.

If the thermal strains are removed from the total strains, leaving only the mechanical strains it can be seen that the stress-mechanical strain curve follows the 200°C material properties exactly, as expected.

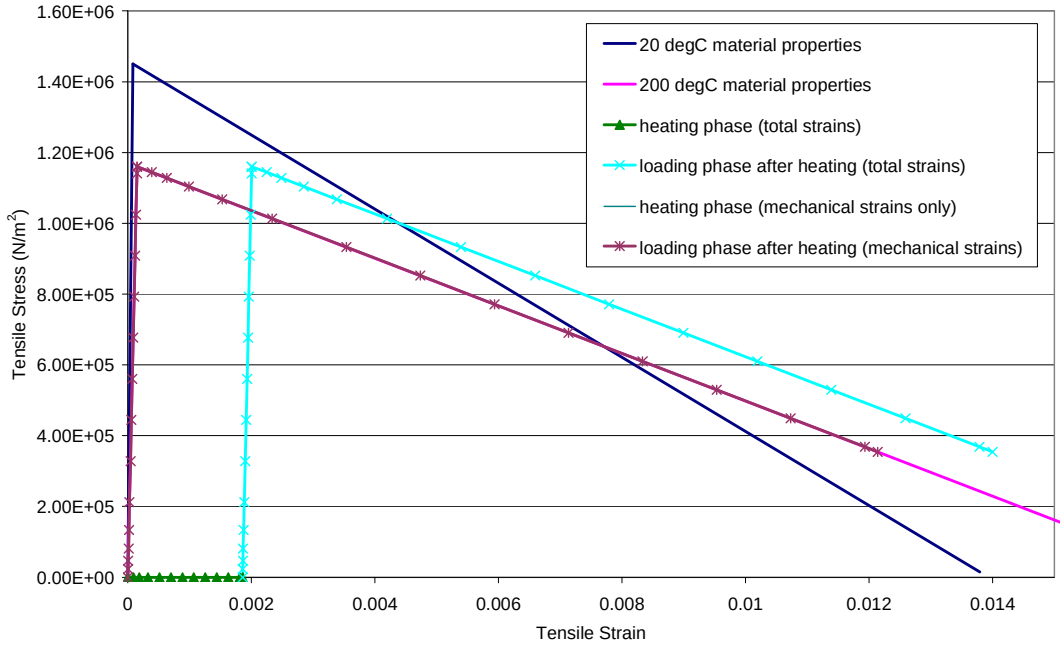

Figure 2-19: Stress-strain of a one-element plane stress model when thermal expansion is present: The element is heated to 200°C and then loaded using a displacement-controlled boundary condition. The stress-strain behaviour follows the material properties curve at 200°C, however it is offset by the value of thermal strains present. If thermal strains are removed and only mechanical strains are plotted, then the model behaviour matches the material properties curve exactly.

2.5.4 Cylinder example

The cylinder discussed earlier (Figure 2-3) for ambient temperature analyses, was subjected to elevated temperature situations. It was modelled using square elements, with an element size of 20mm. Again one central row of elements was weakened slightly (the normal elements have a uniaxial tensile strength f_t = 3.3 MPa, while the weakened elements have a uniaxial tensile strength f_t = 3.0 MPa). The cylinder was loaded in tension, and stress and strain values for both normal and weak elements within the cylinder are computed.

Figure 2-20 shows the stress-strain response in the weakened layer as well as in the elements outside this layer. Once yield occurs in the weakened elements, and tensile loading continues, the strain in the weaker elements continues increasing while the stress decreases (following the material properties of the element). Meanwhile the normal elements unload, with strain reducing with decrease in stress, following the elastic part of their material property curve at all times. In other words, localisation in the weakened layer is accompanied by unloading in other regions. The cylinder is behaving as expected under these conditions.

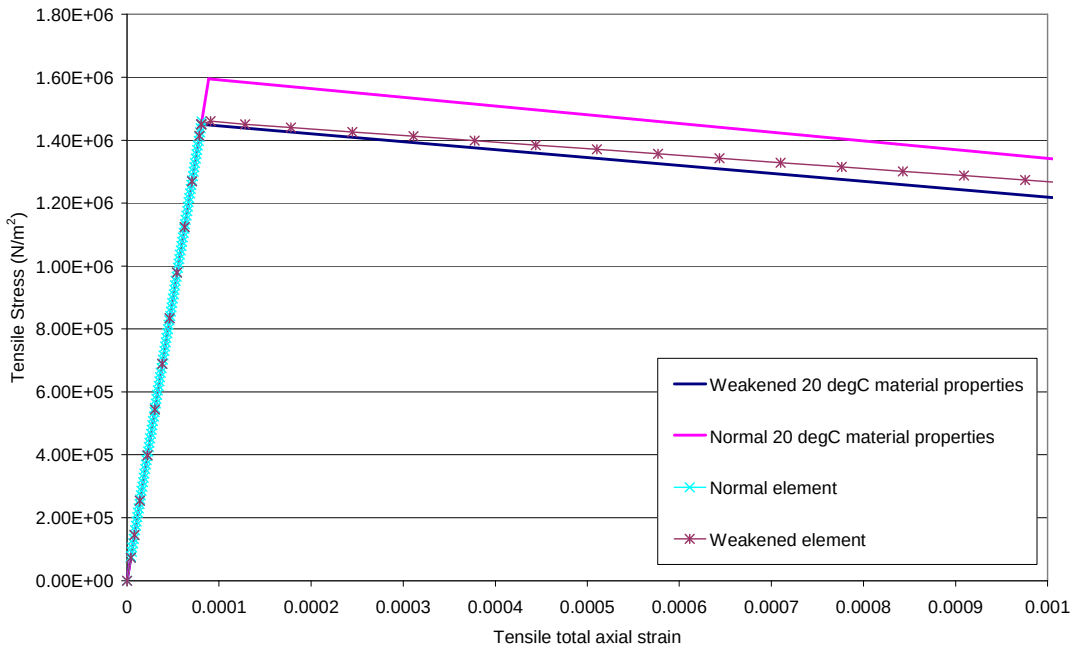

Figure 2-20: Stress-strain for the cylinder at ambient temperature, with tensile loading applied only (to test behaviour with material properties). When yield occurs in the weakened elements, and tensile loading continues, the strain in the weakened elements continues increasing while the stress decreases. The normal elements unload, following the elastic part of their material properties curve.

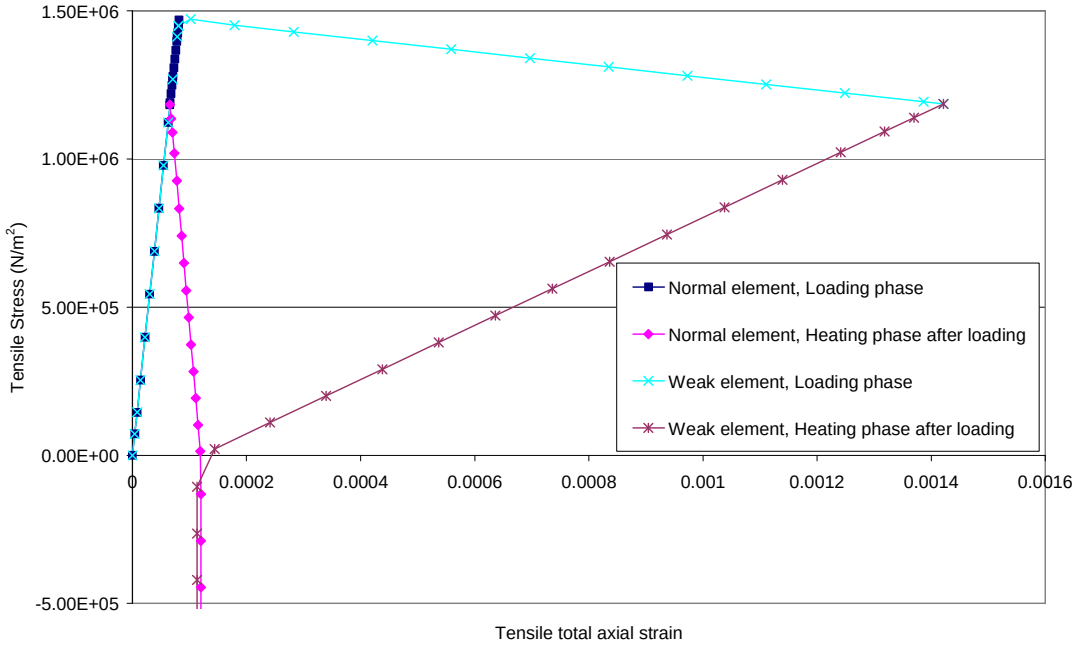

Figure 2-21: Stress-strain for the cylinder when it is first loaded using a displacement-controlled boundary condition and then heated to 100°C. Behaviour in the loading phase is as seen in Figure 2-20, while during heating the concrete expands. This increases the total strain in the normal elements and decreases the strain in the weakened elements – the weakened layer is being squeezed as the normal elements expand.

Next the cylinder was subjected to a tensile displacement followed by heating to 100°C while maintaining the displacement as constant (Figure 2-21). On heating the concrete expands, increasing the total strain in the normal elements, while decreasing the total strain in the weakened elements, i.e. the weakened layer is being squeezed as the normal elements expand. The stress in all elements decreases as expected, as the initially applied tensile load is reduced due to thermal expansion. The total strain at zero stress is found to be the same for both normal and weak elements, and subsequent heating results in an identical compressive stress response.

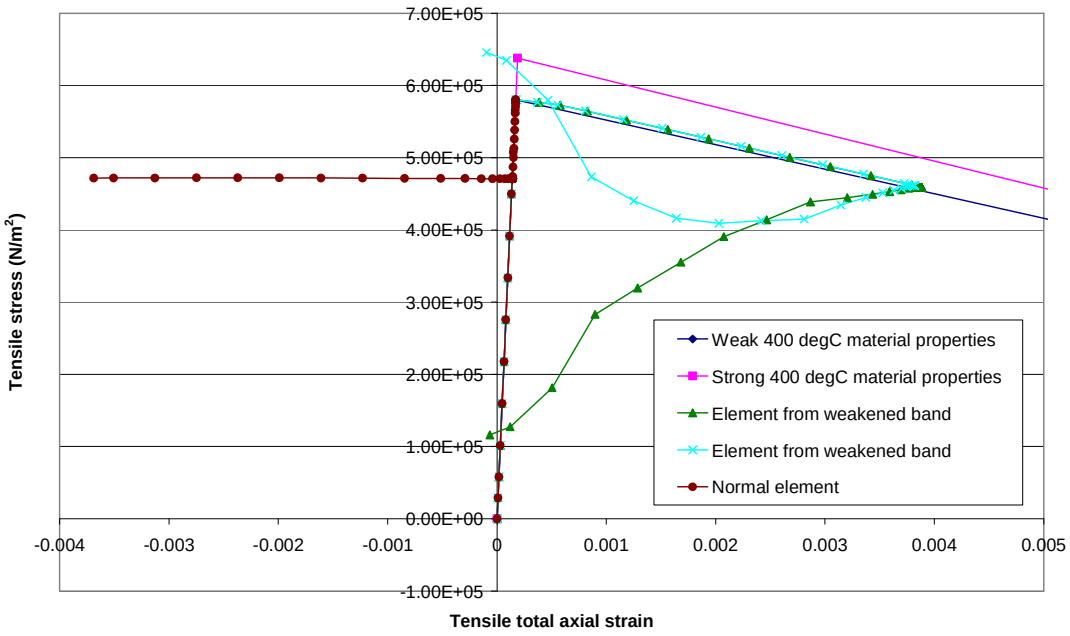

Figure 2-22: Stress-strain for a cylinder where it is heated to 400°C, then a prescribed tensile displacement is applied, the equivalent tensile load is applied, the displacement boundary is released, and the cylinder is cooled. The tensile load applied keeps the normal strength elements at a constant stress value as the total strain decreases due to contraction of the cylinder on cooling. The strain present in the weakened elements also decreases, however different stress values are seen with the stress in some elements increasing and in some decreasing on cooling.

Lastly, the cylinder is heated before being loaded (Figure 2-22). While free to expand it is heated up to 400°C, and while at 400°C a tensile displacement is applied. At this stage it can be seen that the weakened layer follows the 400°C softening slope, while the normal elements unload. The equivalent tensile load to this displacement is then applied to the cylinder and the displacement boundary released (to allow contraction of the cylinder under cooling). The stress and strain remain constant throughout these steps. The cylinder is then cooled back to ambient temperature.

If one were to maintain displacements and cool this cylinder it is apparent that the weakened layer would undergo additional strain localisation while the normal elements contract.

In this example, however, the tensile load corresponding to the applied displacement keeps the normal elements at a constant stress value; and as the material is cooled it contracts, causing the strain present to decrease. A decrease in strain is also seen in the weak elements; however they do not remain at a constant stress throughout cooling. Different stress values are seen in the weak elements, with some increasing in stress throughout cooling and some decreasing. As the stress in some elements in the weakened band increases, and decreases in others, the total load carried by the weakened band should stay constant throughout cooling. This is shown in Figure 2-22.

2.6 References

Abaqus (2008). Abaqus Analysis User's Manual. Providence, Dassault Systemes Simulia Corp.

Bazant, Z. P. and B. H. Oh (1983). "Crack band theory for fracture of concrete." Materials and Structures: Research and Testing (RILEM, Paris) **16**: 155-177.

Bazant, Z. P. and P. C. Prat (1988). "Effect of Temperature and Humidity on Fracture Energy of Concrete." Aci Materials Journal **85**(4): 262-271.

Bicanic, N., R. de Borst, et al. (1993). Computational Aspects of Finite Element Analysis of Reinforced Concrete Structures (Topic 7). Structural Engineering and Structural Mechanics Research Series, CU/SR-93/3, Department of Civil Engineering and Architectural Engineering, University of Colorado, Boulder.

Cedolin, L. and G. Cusatis (2008). "Identification of concrete fracture parameters through size effect experiments." Cement and Concrete Composites **30**(9): 788-797.

de Borst, R., J. J. C. Remmers, et al. (2004). "Discrete vs smeared crack models for concrete fracture: bridging the gap." International Journal for Numerical and Analytical Methods in Geomechanics **28**: 583-607.

Dolbow, J., N. Moes, et al. (2001). "An extended finite element method for modeling crack growth with frictional contact." Computer Methods in Applied Mechanics and Engineering **190**(51-52): 6825-6846.

Du, J., J. H. Yon, et al. (1990). Analysis of the Fracture Process Zone of a Propagating Concrete Crack Using Moire Interferometry. Micromechanics of Failure of Quasi-Brittle Materials. S. P. Shah, S. E. Swartz and M. L. Wang. Barking Essex, Elsevier Appl Sci Publ Ltd**:** 146-155.

Duan, K., X. Hu, et al. (2007). "Size effect on specific fracture energy of concrete." Engineering Fracture Mechanics **74**(1–2): 87-96.

EN1992-1-1 (2004). Eurocode 2: Design of Concrete Structures - Part 1-1: General Rules and Rules for Buildings.

EN1992-1-2 (2004). Eurocode2: Design of Concrete Structures - Part 1-2: General Rules - Structural Fire Design.

Feenstra, P. H. and R. de Borst (1996). "A composite plasticity model for concrete." International Journal of Solids and Structures **33**: 707-730.

Gopalaratnam, V. S. and S. P. Shah (1985). "Softening Response of Plain Concrete in Direct Tension." American Concrete Institute Journal **May-June 1985**: 310-323.

Hillerborg, A., M. Modeer, et al. (1976). "Analysis of crack formation and crack growth in concrete by means of fracture mechanics and finite elements." Cement and Concrete Research **6**: 773-782.

Hoek, E. and E. T. Brown (1980). "Empirical strength criterion for rock masses." Journal of the Geotechnical Engineering Division, ASCE **106**: 1013-1035.

Lee, J. H. and G. L. Fenves (1998). "Plastic-damage model for cyclic loading of concrete structures." Journal of Engineering Mechanics-Asce **124**(8): 892-900.

Lin, F. B., Z. P. Bazant, et al. (1987). "Concrete model with normality and sequential identification." Computers and Structures **26**: 1011-1025.

Lubliner, J., J. Oliver, et al. (1989). "A Plastic-Damage Model for Concrete." International Journal of Solids and Structures **25**(3): 299-326.

Menetrey, P. and K. J. Willam (1995). "A triaxial failure criterion for concrete and its generalization." ACI Structural Journal **92**: 311-318.

Murthy, A. R. C., G. S. Palani, et al. (2009). "State-of-the-art review on fracture analysis of concrete structural components." Sadhana-Academy Proceedings in Engineering Sciences **34**(2): 345-367.

Neville, A. M. (1963). Properties of concrete. London, Sir Isaac Pitman & Sons Ltd.

Ngo, D. and A. C. Scordelis (1967). "Finite element analysis of reinforced concrete beams." Journal of the American Concrete Institute **64**: 152-163.

Nielsen, C. V. and N. Bicanic (2003). "Residual fracture energy of high-performance and normal concrete subject to high temperatures." Materials and Structures **36**(262): 515-521.

Oliver, J. (1989). "A consistent characteristic length for smeared cracking models." International Journal for Numerical Methods in Engineering **28**: 461-474.

Ottosen, N. S. (1977). "A failure criterion for concrete." Journal of Engineering Mechanics, ASCE **103**: 527-535.

Pankaj, P. (1990). Finite Element Analysis in Strain Softening and Localisation Problems, University of Wales. **PhD thesis**.

Pramono, E. (1988). Numerical Simulation of Distributed and Localized Failure in Concrete. Boulder, University of Colorado.

Rashid, Y. R. (1968). "Analysis of prestressed concrete pressure vessels." Nuclear Engineering and Design **7**(334-344).

Roelfstra, R. E. and F. H. Wittmann (1986). A Numerical Method to Link Strain Softening with Fracture in Concrete, Fracture Toughness and Fracture Energy in Concrete. Amsterdam, Elsevier Science.

Rots, J. G., P. Nauta, et al. (1985). "Smeared crack approach and fracture localisation in concrete." Heron **30**(1).

Schneider, U. (1988). "Concrete at High Temperatures - A General Review." Fire Safety Journal **13**: 55-68.

Teller, L. W. (1956). Elastic Properties. Significance of Tests and Properties of Concrete and Concrete Aggregates. **169:** 94-103.

Wittmann, F. H. (2002). "Crack formation and fracture energy of normal and high strength concrete." Sadhana **27**(4): 413-423.

Zhang, B. and N. Bicanic (2006). "Fracture energy of high-performance concrete at high temperatures up to 450 degrees C: the effects of heating temperatures and testing conditions (hot and cold)." Magazine of Concrete Research **58**(5): 277-288.

Zhang, B., N. Bicanic, et al. (2000). "Residual fracture properties of normal- and high-strength concrete subject to elevated temperatures." Magazine of Concrete Research **52**(2): 123-136.

3

Concrete in compression

3.1 Introduction

Many more experiments have been carried out on concrete in compression than have been done under tension, so more data and a better idea of concrete's compressive behaviour is available. A brief introduction to the basic properties of concrete has already been given in Chapter 2, outlining how concrete is much stronger in compression than in tension, how concrete is generally classified by its compressive strength at ambient temperatures, its elastic behaviour until

yield and then its softening behaviour in the plastic region of the stress-strain curve, and the fact that concrete is pressure sensitive. A unique single yield point and post-yield behaviour are difficult to define for concrete in compression in spite of the large amount of data available.

The Eurocodes (EN1992-1-1 2004) give generalised values for material parameters including secant modulus of elasticity, strain at peak stress, and ultimate compressive strain, at different concrete strengths. A typical stress-strain relationship for 30 MPa strength siliceous concrete at ambient temperatures is shown below in Figures 3-1 and 3-2, as per Figure 3.1 found in the structural fire design Eurocode (EN1992-1-2 2004). The definition of the stress-strain curve as per the concrete design Eurocode (EN1992-1-1 2004) appears to be a bit different to the one in the structural fire design Eurocode (EN1992-1-2 2004). A comparison at ambient temperature is seen in Figures 3-3 and 3-4. The concrete design Eurocode gives a higher elastic modulus value and so shows a steeper loading curve. It also only defines the descending branch to a value of around 60% of the compressive stress, assuming that failure occurs at a higher stress and that the material will not unload to almost zero stress. This could be due to the fact that the concrete design Eurocode is used as a design document and it is better to take a conservative value for concrete's ultimate strain, whereas the structural fire design Eurocode is more often used for analysis at varying temperatures, and so a more complete stress-strain curve is more appropriate.

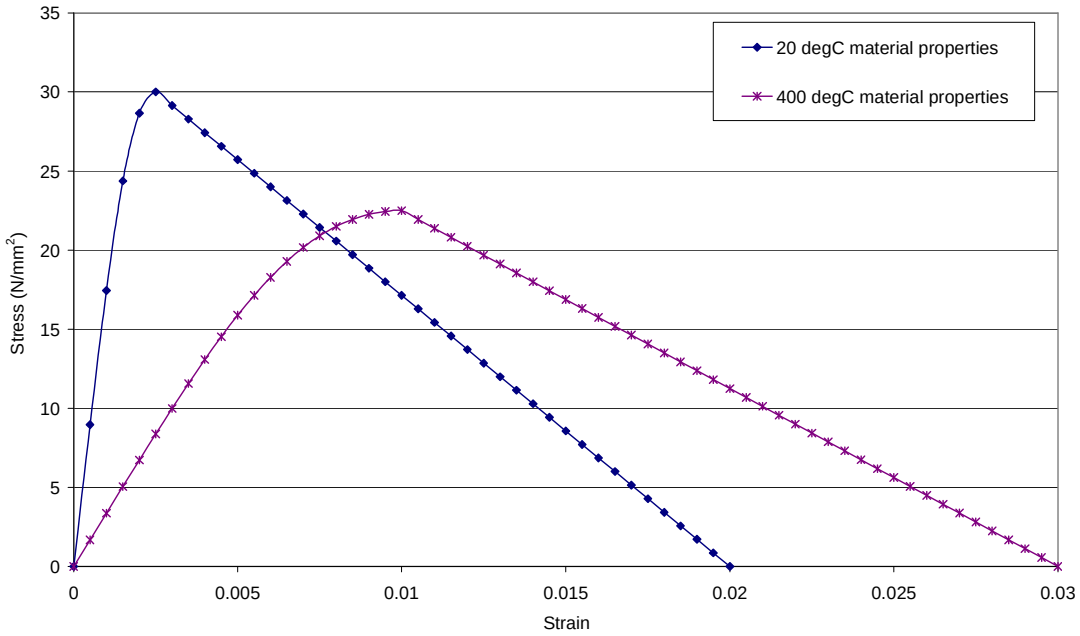

Figure 3-1: Typical concrete compressive stress-strain curves at 20°C and 400°C taken from the structural fire design Eurocode (EN1992-1-2 2004)

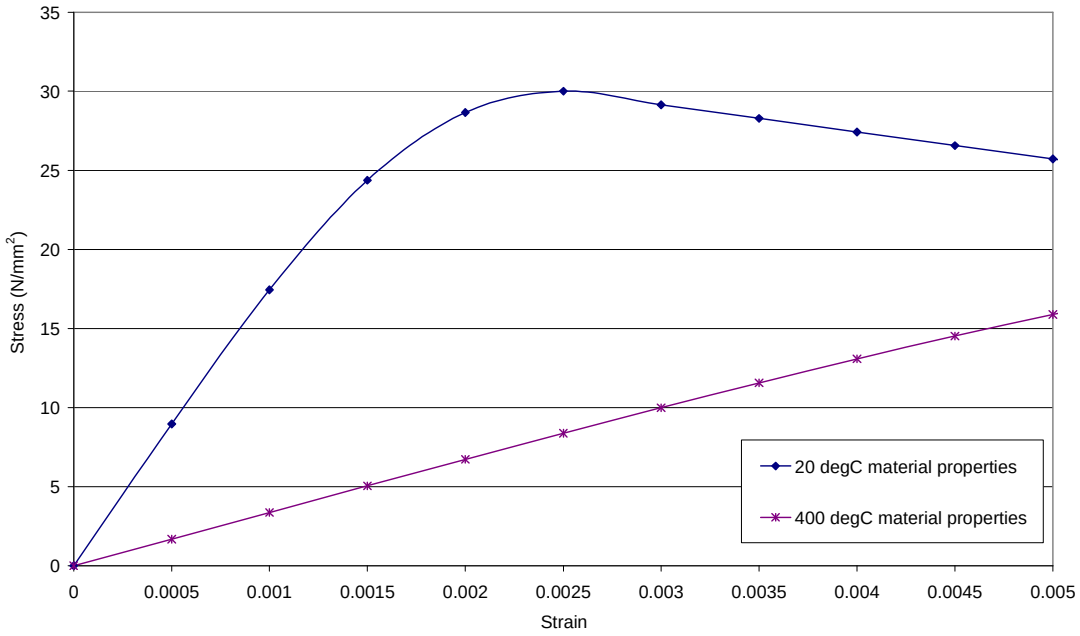

Figure 3-2: Magnification of the loading branch of compressive stress-strain curves taken from the structural fire design Eurocode (EN1992-1-2 2004)

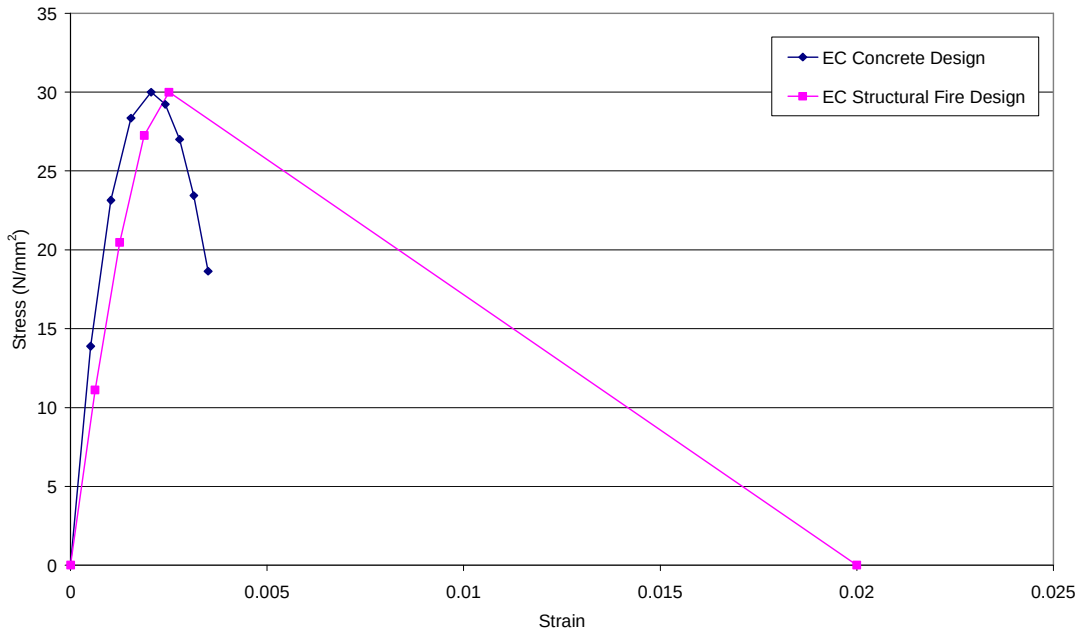

Figure 3-3: Comparison of a typical concrete compressive stress-strain curve at ambient temperature, for a compressive strength of 30 MPa, according to the concrete design Eurocode (EN1992-1-1 2004) and the structural fire design Eurocode (EN1992-1-2 2004)

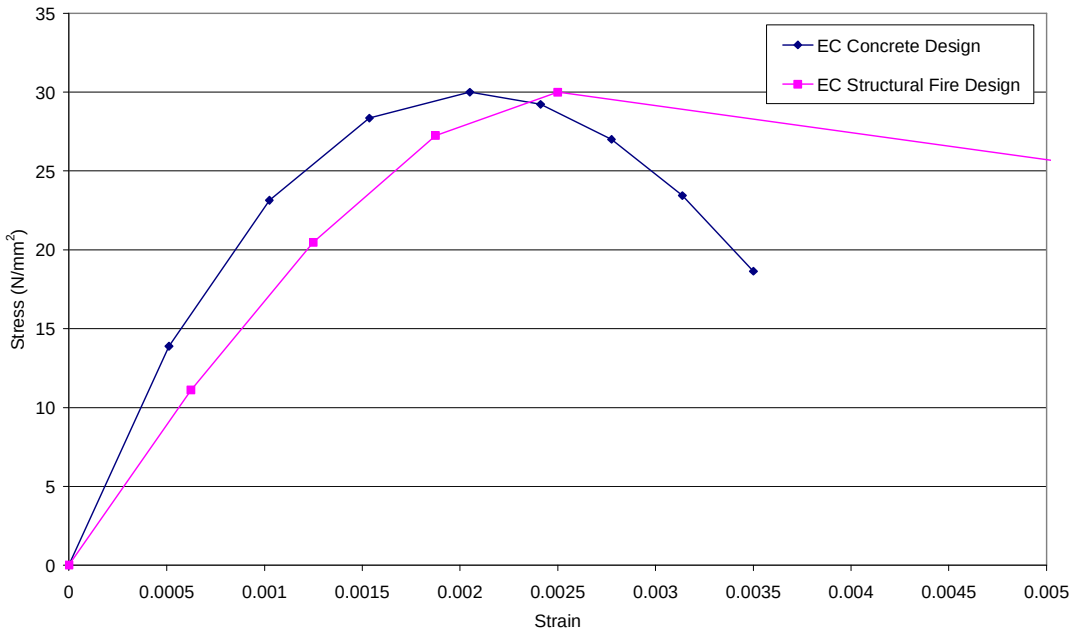

Figure 3-4: Magnification of the loading branches of the compressive stress-strain curve at ambient temperature, according to the concrete design Eurocode (EN1992-1-1 2004) and the structural fire design Eurocode (EN1992-1-2 2004)

This chapter considers issues associated with modelling plain concrete in compression at ambient and elevated temperatures. Of particular interest is the post-peak response of concrete.

3.2 Modelling at ambient temperature

3.2.1 Strain softening and fracture energy

In compression concrete undergoes crushing rather than cracking. Concrete exhibits strain softening under crushing, which is treated as a local material property in commercial FE codes such as Abaqus. While the concept of fracture energy is well recognised for tension, equivalent models for compression are generally not included (Cartensen 2011).

Compressive fracture energy based models are rarely used in modelling, and few authors have investigated the compressive fracture energy G_c. Vonk (1992)

considered compressive fracture energy and suggested that there are two parts to it – a local part and a continuum part. The local fracture energy is assumed to be a constant, with the continuum taking account of the size of the specimen or mesh being modelled. Thus, according to Vonk, fracture energy in compression is not a material property but depends on the specimen size.

Nakamura and Higai (2001) also carried out experiments, and used their data to state that concrete's compressive fracture energy was independent of the size and shape of the test specimens if the aggregate used was the same. This fracture energy can be considered a material property. They developed an empirical relation for the compressive fracture energy in terms of the compressive strength of the concrete.

$$G_c = 8.8\sqrt{f_{cm}} \tag{3.1}$$

where G_c is the compressive fracture energy and f_{cm} is the compressive strength in MPa.

They also suggest that the compressive and tensile fracture energies are related through:

$$G_c = 250 G_f \tag{3.2}$$

The differences in the value of G_c evaluated from these different methods are easily illustrated. For example, for concrete with G_f = 100 N/m and f_{cm} = 30 MPa, the compressive fracture energy for two different element sizes will be as shown in Table 3-1.

Table 3-1: Fracture energy, G_c, in N/mm, calculated using various different methods.

Element Length (mm)	Vonk	Nakamura and Higai (3.1)	Nakamura and Higai (3.2)
10	10	48.2	25
50	12	48.2	25

Nakamura and Higai also suggest a model for concrete's behaviour under compression. They use a parabola for the elastic behaviour of the material up to peak stress, and then a linear relationship between stress and strain in the post-peak section of the curve. As the compressive fracture energy is considered to be the area under the stress-plastic displacement curve, this value can be used to determine the ultimate strain of the material. A generalised curve for this model is shown in Figure 3-5.

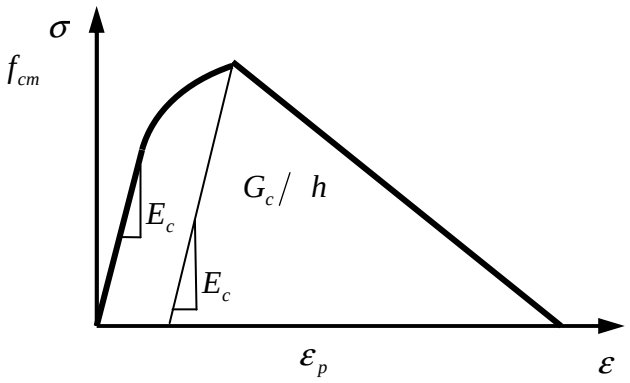

Figure 3-5: The stress-strain relationship for the compression model by Nakamura and Higai (2001). E_c is the compressive elastic modulus and h is the element size.

It can be seen that the descending branch of the stress-strain curve is element size dependent for compression, as it is in the case of tension. As the element size increases, the descending branch becomes steeper. Use of larger and larger

elements will cause the branch to become vertical and subsequently double back on itself – a behaviour called 'snap back.' Snap back causes huge computational problems and so the element sizes used with this model need to be limited. However the element size restriction in compression is generally less restrictive than that for tension.

Feenstra and de Borst (1995) use an energy based formulation to define the compressive softening behaviour of concrete. In this the stress-equivalent strain variation is given by

$$\bar{\sigma}_C(\kappa_C) = \frac{f_{cm}}{3}\left(1 + 4\frac{\kappa_C}{\kappa_e} - 2\frac{\kappa_C^2}{\kappa_e^2}\right), \text{ if } \kappa_C < \kappa_e \tag{3.3}$$

$$\bar{\sigma}_C(\kappa_C) = f_{cm}\left[1 - \frac{(\kappa_C - \kappa_e)^2}{(\kappa_{uC} - \kappa_e)^2}\right], \text{ if } \kappa_e \le \kappa_C < \kappa_{uC} \tag{3.4}$$

where κ_C is an internal damage parameter and κ_e is the equivalent strain at maximum compressive strength and is given by

$$\kappa_e = \frac{4 f_{cm}}{3E_c} \tag{3.5}$$

The maximum equivalent strain κ_u is related to compressive fracture energy G_c and element size h as

$$\kappa_{uC} = 1.5\frac{G_c}{h f_{cm}} \tag{3.6}$$

Note that the ultimate strain value is dependent on the compressive fracture energy, and hence the fracture energy value has a significant effect on the overall shape of the stress-strain relationship.

Most commercial finite element programmes such as Abaqus (2008) do not have a provision for providing energy based softening behaviour. Compressive post-peak stress-strain behaviour is defined in Abaqus by providing the compressive stress and inelastic crushing strain at various points on material properties curve. Energy based softening behaviour can only be included by calculating the compressive crushing energy from the material curves and altering the post-peak values to fit. The structural fire design Eurocode (EN1992-1-2 2004) provides a stress-strain relationship for plain concrete which does not incorporate energy concepts.

A comparison of the two models – the Eurocode model and that due to Feenstra and de Borst – is shown in Figures 3-6 and 3-7. In this G_c = 25000 N/m is used. The stress-plastic strain relationship for the Feenstra and de Borst model is evaluated for two different element sizes.

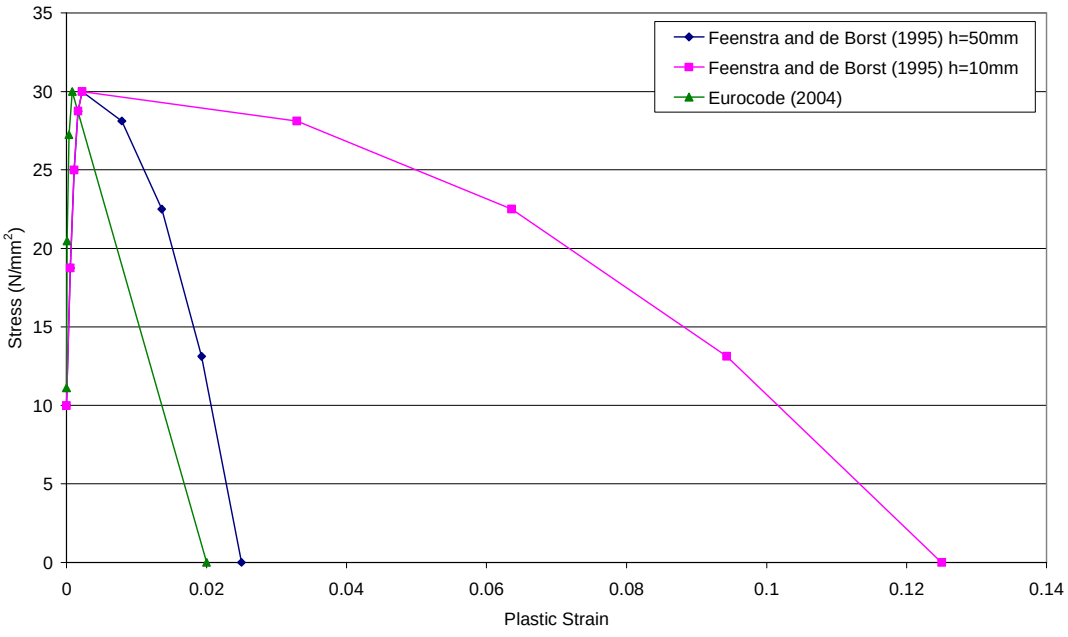

Figure 3-6: Comparison of the stress-plastic strain curves for the Eurocode model and the Feenstra and de Borst model at ambient temperatures when using en element length of 50mm and 10mm (Feenstra and de Borst 1995; EN1992-1-2 2004)

The two models are similar when small element sizes are used. However, as the Feenstra and de Borst model's ultimate strain is element size dependent, at larger element sizes the descending branch of the two models differ significantly. In the rest of this work, the Eurocode model from the structural fire design code (EN1992-1-2 2004) will be used, as it is element size independent.

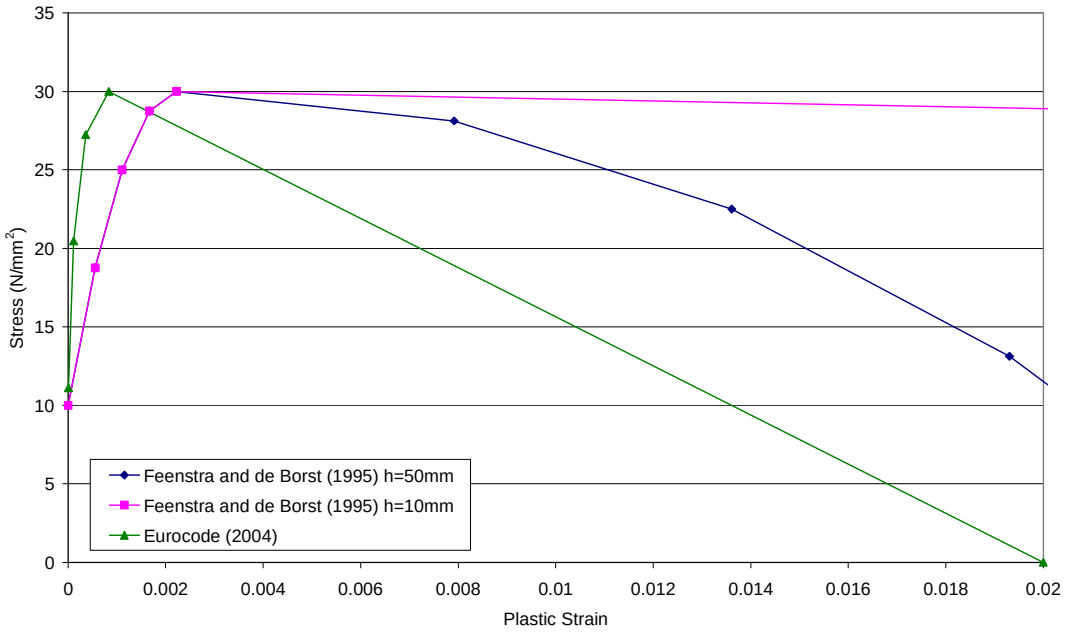

Figure 3-7: Magnification to show the loading branch of the stress-plastic strain curves for the Eurocode model and the Feenstra and de Borst model at ambient temperatures when using en element length of 50mm and 10mm (Feenstra and de Borst 1995; EN1992-1-2 2004)

3.2.2 Localisation Directions

The concept of localisation directions based on acoustic tensor was discussed in the last chapter. It was seen that with the concrete damaged plasticity model, in uniaxial tension, the acoustic tensor predicts a crack band orthogonal to the maximum principal stress direction.

The cylinder discussed in the previous chapter is subjected to uniaxial compression in the vertical direction. Use of the acoustic tensor provides the direction in which the localisation bands will occur should yield not be distributed throughout the material, as shown in Figure 3-8. If the graph's minimum approaches zero or negative values, this suggests that localisation will occur. The angle at which the minimum values occur gives the direction of the crack band.

Figure 3-8 shows that under uniaxial compression using the concrete damaged plasticity model, cracking and localisation will be in a band at 47° from the horizontal. It is important to note that the determinant of the acoustic tensor at 47° is negative, i.e. the softening modulus used in this problem results in instantaneous localisation.

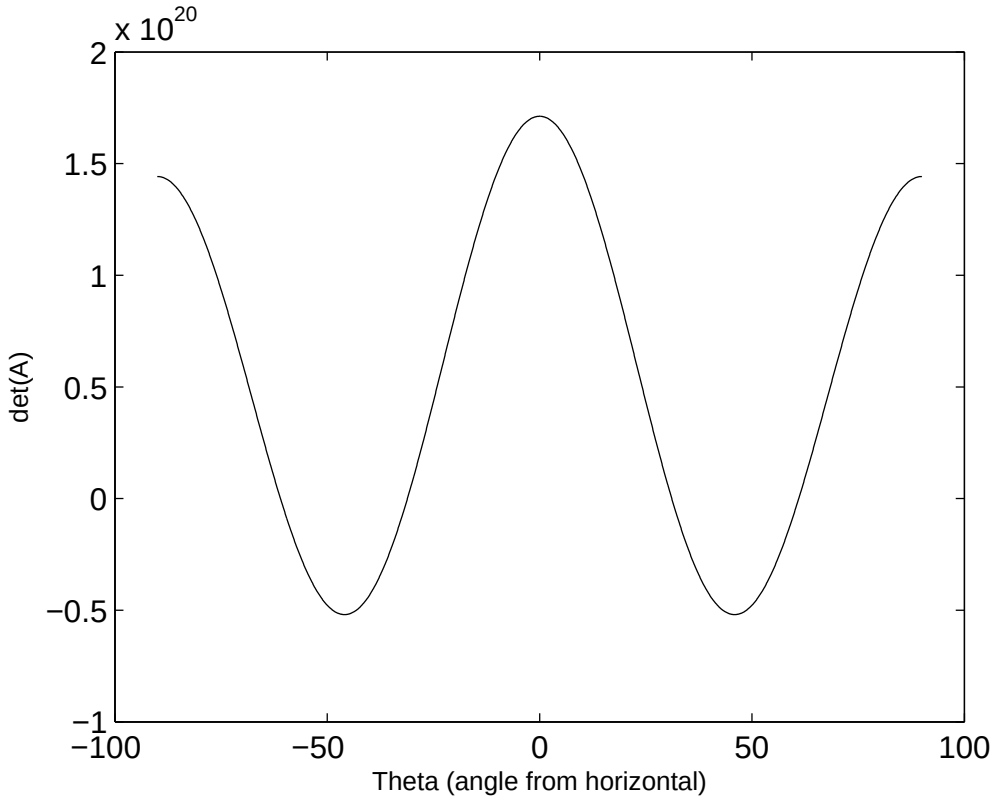

Figure 3-8: θ (angle from the horizontal) versus the determinant of the acoustic tensor for uniaxial compression in the vertical direction using the Concrete Damaged Plasticity

model. Values less than zero indicate localisation, while the theta value at the minimums (47^{o}) indicates the direction of cracking.

A uniaxial compression analysis of the cylinder was conducted with a single weakened element in the centre as shown in Figure 3-9 to induce localisation through this element. Figure 3-9 shows the developed plastic strain in two directions, each at approximately 47^{o} from the horizontal.

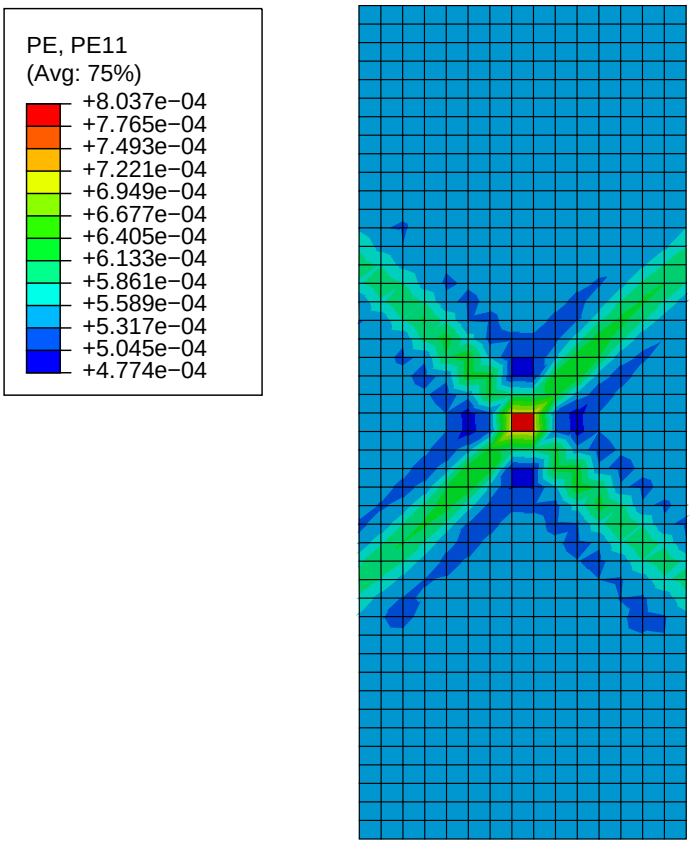

Figure 3-9: A concrete damaged plasticity cylinder model with weakened central element, showing localised bands of cracking at an angle of 47^{o} from the horizontal.

3.3 Modelling at Elevated Temperatures

As with concrete's tensile behaviour, there are several key compressive material properties that change as concrete is heated. A literature review and study of most available experimental data of plain concrete under compression was carried out by Knaack et al. (2009). They used information on compressive strength, modulus of elasticity, strain at peak stress and ultimate strain at varying temperatures to develop temperature-dependent compressive stress-strain properties. This was done by performing statistical regression analyses on existing experimental data for each of the main parameters. Independent material properties were used as variables in the regression analysis, and a Student's t-test was used to determine whether each variable had a significant effect on the model. It should be noted that most of the experiments considered were carried out in electric furnaces, which may not accurately simulate the heat transfer of a real fire. Aggregate type in concrete has a huge effect on temperature-dependent behaviour, and this should be noted when considering the results. Also results for high strength concrete were not considered in this work. Each parameter was considered in turn and this report's findings compared with other information available, for example existing models as described by Kodur et al. (2008), Hertz (2005), Li and Purkiss (2005), Shi et al. (2002) and existing building codes such as the Eurocodes (EN1992-1-2 2004) and ASCE code (1992).

It is important to note that when loaded concrete elements are heated load induced thermal strains (LITS) are introduced to the structure (Khoury et al. 1985). Load induced thermal strain (LITS) is a term which covers a number of different strain components in heated concrete including the transient thermal creep, the drying creep and the transient strain. LITS has been defined as the difference between the free thermal expansion of concrete when it is heated, and the net thermal expansion when the same concrete is heated under a level of pre-stress (Law and Gillie 2008). Most LITS components are non-recoverable on

cooling, so the effects are only seen on first heating. Several authors have created models to incorporate LITS including Terro (1998) and Anderberg and Thelandersson (1976). Li and Purkiss (2005) provide a simplification of the model due to Anderberg and Thelandersson.

These models show a difference between the 'actual' and the 'apparent' elastic modulus when using constitutive curves. When LITS is included the strains seen are higher, making the stress-strain curve less steep, and giving a lower apparent elastic modulus. The structural fire design Eurocode does not distinguish between strain components and suggests that it includes transient effects to some extent.

For simplicity this study chose not to include LITS explicitly in the models. It was assumed that some of its effects are included via the properties defined in the Eurocode.

Generally the following behaviour is observed at elevated temperatures:

3.3.1 Reduction in peak strength

Reduction of peak compressive strength is characterised in the Eurocode (EN1992-1-2 2004). It is shown as decreasing with increasing temperature up to 1200^{o}C, when concrete is shown to have no compressive strength. Separate values are given for siliceous and calcareous aggregates and these are shown in Figure 3-10 and Table 3-2 (alongside other main parameters which will be discussed in the following sections).

Table 3-2: Values for ratio of peak strength at elevated temperature to peak strength at ambient temperature ratio ($f_{c,\theta}/f_{ck}$), strain at peak stress ($\varepsilon_{c1,\theta}$) and ultimate strain at zero stress ($\varepsilon_{cu1,\theta}$) for normal strength concrete at elevated temperatures (EN1992-1-2 2004)

Concrete temp. θ	Siliceous aggregates			Calcareous aggregates		
	$f_{c,\theta}/f_{ck}$	$\varepsilon_{c1,\theta}$	$\varepsilon_{cu1,\theta}$	$f_{c,\theta}/f_{ck}$	$\varepsilon_{c1,\theta}$	$\varepsilon_{cu1,\theta}$
°C						
20	1.00	0.0025	0.0200	1.00	0.0025	0.0200
100	1.00	0.0040	0.0225	1.00	0.0040	0.0225
200	0.95	0.0055	0.0250	0.97	0.0055	0.0250
300	0.85	0.0070	0.0275	0.91	0.0070	0.0275
400	0.75	0.0100	0.0300	0.85	0.0100	0.0300
500	0.60	0.0150	0.0325	0.74	0.0150	0.0325
600	0.45	0.0250	0.0350	0.60	0.0250	0.0350
700	0.30	0.0250	0.0375	0.43	0.0250	0.0375
800	0.15	0.0250	0.0400	0.27	0.0250	0.0400
900	0.08	0.0250	0.0425	0.15	0.0250	0.0425
1000	0.04	0.0250	0.0450	0.06	0.0250	0.0450
1100	0.01	0.0250	0.0475	0.02	0.0250	0.0475
1200	0.00	-	-	0.00	-	-

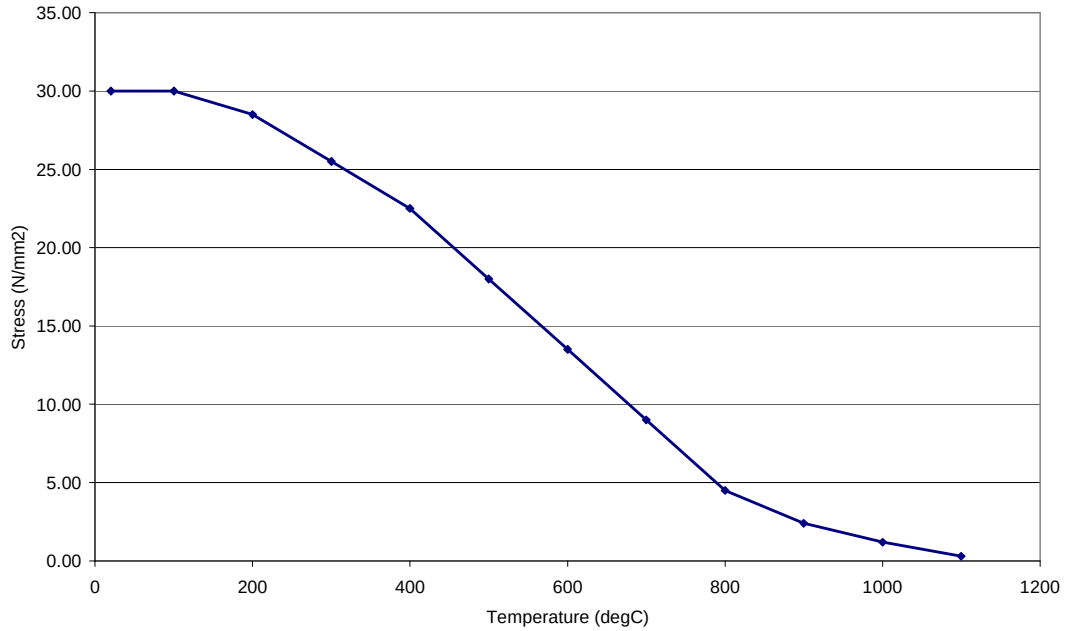

Figure 3-10: Peak compressive stress varying with increasing temperature according to Eurocode (EN1992-1-2 2004)

Knaack et al. (2009) agree that concrete's compressive strength decreases as its temperature increases. The studies considered (Harmathy and Berndt 1966; Abrams 1971; Castillo and Durani 1990; Cheng et al. 2004) tested residual (tested after a heating and cooling cycle), stressed (tested at elevated temperature, having been heating under preload) and unstressed (tested at elevated temperature with sample unloaded during heating) cylinders, and they found that the stressed cylinders retained most strength with the residual ones retaining least. They found that varying the loading applied prior to the tests or the initial compressive strength of the concrete (i.e. concrete type) did not have a significant effect on the results. Some tests (Abrams 1971) showed a very small initial increase in compressive strength at low temperatures of around 200^{o}C, but this was not considered to be significant. Calcareous concrete was found to retain more strength than siliceous, and there were often relatively large

variations in the compressive strength, even of samples using the same concrete mix and environmental conditions.

Knaack et al. (2009) proposed the following relationship for the compressive strength loss model (values throughout are normalised against those at ambient temperatures):

$$f_{cm} / f_{cmo} = \kappa_{f_{mo}} + \kappa_{f_{m1}} T + \kappa_{f_{m2}} T^2 + \kappa_{f_{m3}} T^3 \qquad (3.7)$$

where:

f_{cm} / f_{cmo} is the ratio of mean compressive strength at temperature T to mean compressive strength at ambient temperature; $\kappa_{f_{mi}}$ is the aggregate and test type dependent coefficient, see Table 3-3; and T is the temperature in degrees Fahrenheit.

Table 3-3: Compressive strength relationship regression coefficients (Knaack et al. 2009) for residual (tested after a heating and cooling cycle), stressed (tested at elevated temperature, having been heating under preload) and unstressed (tested at elevated temperature with sample unloaded during heating) samples. Also the acceptable ranges of ambient strength, f_{cmo}, and test temperature, T, to be used, and the coefficient of determination, R^2, which indicates how well the equation fits the data (R^2=1 indicates a perfect fit to data, while R^2=0 indicates a total lack of fit).

	NSC: normal-strength concrete					
	Siliceous			Calcareous		
	Residual	Stressed	Unstressed	Residual	Stressed	Unstressed
$\kappa_{f_{m0}}$	0.963	0.995	0.953	0.997	1.023	0.981
$\kappa_{f_{m1}}$ ($^oF^{-1}$)	6.44E-04	8.421E-05	7.887E-04	6.514E-05	-4.001E-04	3.109E-04
$\kappa_{f_{m2}}$ ($^oF^{-2}$)	-1.643E-06	-9.024E-08	-1.645E-06	-3.125E-07	1.106E-06	-5.413E-07
$\kappa_{f_{m3}}$ ($^oF^{-3}$)	5.459E-10	-1.894E-10	5.280E-10	-6.748E-11	-6.99E-10	1.760E-11
T range (^{o}F)	[70,1472]	[70,1503]	[70,1600]	[70,1472]	[70,1504]	[70,1600]
f_{cmo} range (psi)	[3900,5500]	[3900,5500]	[3900,5500]	[3542,6000]	[3900,5600]	[1149,6000]
R^2	0.90	0.92	0.93	0.86	0.61	0.69

It was noted that the relative humidity of the samples may also have had a significant effect which was not considered here as there was not sufficient data.

A comparison of the relationship by Knaack et al. for siliceous, normal-strength, stressed concrete, with the Eurocode one under similar conditions is shown in Figure 3-11. It can be seen that while the shapes of the two lines are distinctly different, the reduction of strength at elevated temperatures is not significantly different. The shape and reductions proposed by Eurocode will be used in simulations conducted in this study.

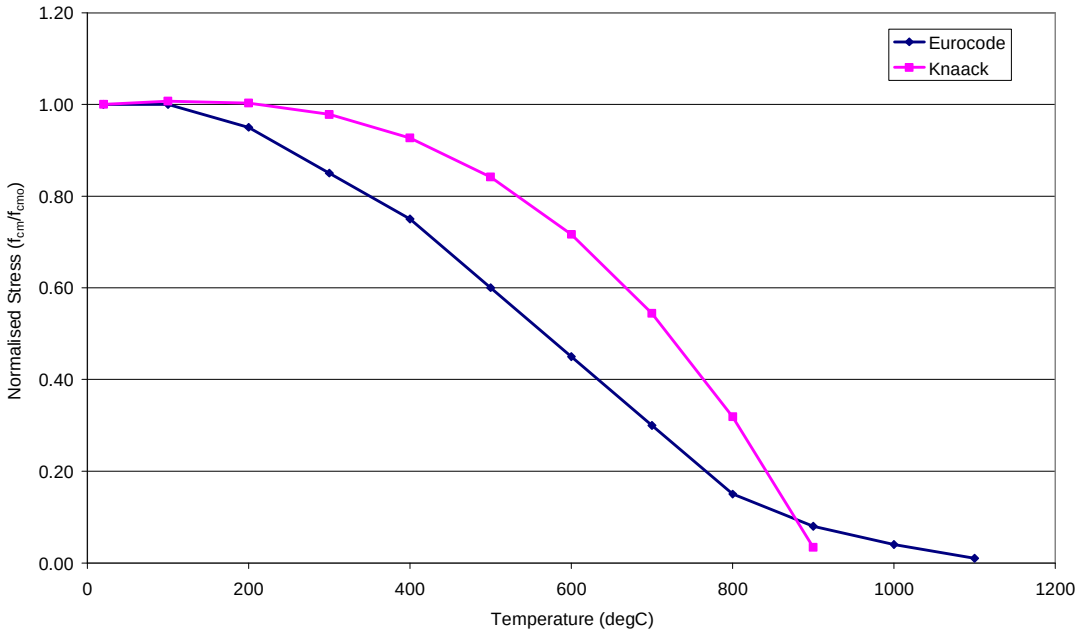

Figure 3-11: Normalised peak compressive strength plotted against temperature, values taken from expressions by Knaack et al. (2009), and compared with the Eurocode relationship for siliceous, normal-strength, stressed concrete.

3.3.2 Reduction in elastic modulus

The static modulus of elasticity is defined as the slope of the compressive stress-strain curve either as a tangential slope at the origin or as the secant slope between the origin and a point on the stress-strain curve at approximately 30% of the peak stress; and its reduction with increasing temperature characterizes concrete's loss of stiffness with heating.

As discussed previously, the Eurocodes (EN1992-1-2 2004) give values for compressive strength and strain at peak stress, and from these and the definition given above for the secant slope, the elastic modulus at increasing temperatures can be calculated. The variation for 30 MPa strength concrete is shown in Figure 3-12. The Eurocode stress-strain relationship can also be differentiated to gain a value for the modulus of elasticity, as described in the previous chapter, and again this variation can be seen in Figure 3-12. However when this value is used it should be noted that it implicitly includes creep strains.

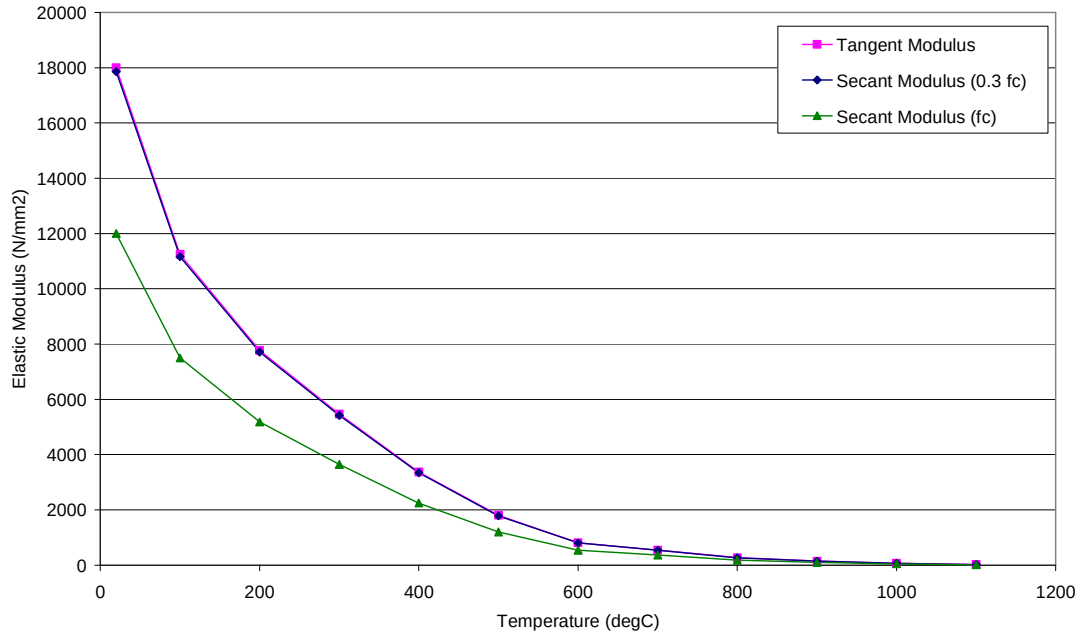

Figure 3-12: Elastic modulus varying with temperature according to EC2, using the secant modulus (taken to either peak stress f_c or $0.3 f_c$) or the tangent modulus at zero strain

Elastic moduli at elevated temperatures have also been provided by ACI (2007) and ASCE (1992). The models due to ASCE and Kodur et al. (2008) include creep strains and hence contain larger strain values than the ACI model. The general trend seen throughout is for concrete to lose its stiffness, starting immediately on heating.

Knaack et al. (2009) looked at data from residual, stressed and unstressed, normal strength and high strength concrete tests (Harmathy and Berndt 1966; Castillo and Durani 1990; Cheng et al. 2004). They also concluded that generally as the temperature increases, elastic modulus decreases, with the rate of decay being greater after 260°C. Harmathy and Berndt (1966) considered the exposure time of the samples to heat and found that as the heating duration increases so the stiffness of concrete decreases.

Knaack et al. combined static and dynamic test results to obtain a larger number of data points for statistical analysis. To carry out the regression analysis, the measured modulus of elasticity, E_c was normalised with respect to the ACI modulus at ambient temperatures E_{co_ACI}, where:

$$E_{co\_ACI} = 57000\sqrt{f_{cmo}} \text{ in psi} \tag{3.8}$$

The final form of the model for the elastic modulus developed by Knaack et al. was:

$$E_c / E_{co\_ACI} = \kappa_{E_o} + \kappa_{E_1} T + \kappa_{E_2} T^2 \tag{3.9}$$

where κ_{E_i} is the aggregate and test type dependent coefficient, T is the maximum exposure temperature (°F), and coefficients are given in Table 3-4.

Table 3-4: Modulus of Elasticity relationship regression coefficients (Knaack et al. 2009) for residual (tested after a heating and cooling cycle), stressed (tested at elevated temperature, having been heating under preload) and unstressed (tested at elevated temperature with sample unloaded during heating) samples. Also the acceptable ranges of ambient strength, f_{cmo}, and test temperature, T, to be used, and the coefficient of determination, R^2, which indicates how well the equation fits the data (R^2=1 indicates a perfect fit to data, while R^2=0 indicates a total lack of fit).

	NSC		HSC		
	Calcareous	Light-weight	Calcareous		
	Unstressed	Unstressed	Residual	Stressed	Unstressed
κ_{E_0}	1.292	0.738	1.351	1.058	1.055
κ_{E_1} ($^oF^{-1}$)	-1.271E-03	-5.916E-04	-2.037E-03	-1.168E-03	-1.146E-03
κ_{E_2} ($^oF^{-2}$)	4.163E-07	1.308E-07	9.671E-07	3.180E-07	4.654E-07
T range (^oF)	[75, 1400]	[74, 1412]	[73, 1112]	[77, 1112]	[75, 1400]
f_{cmo} range (psi)	[1149, 5443]	[2716, 3893]	[6440, 13982]	[7102, 14707]	[6316, 14707]
R^2 on E_c	0.64	0.72	0.73	0.97	0.91

Comparison between the Eurocode model and that due to Knaack et al.'s proposed model is shown in Figure 3-13. Information for siliceous concrete

cannot be shown due to lack of data. Generally there is reasonable correlation and the Eurocode model will be used in future work.

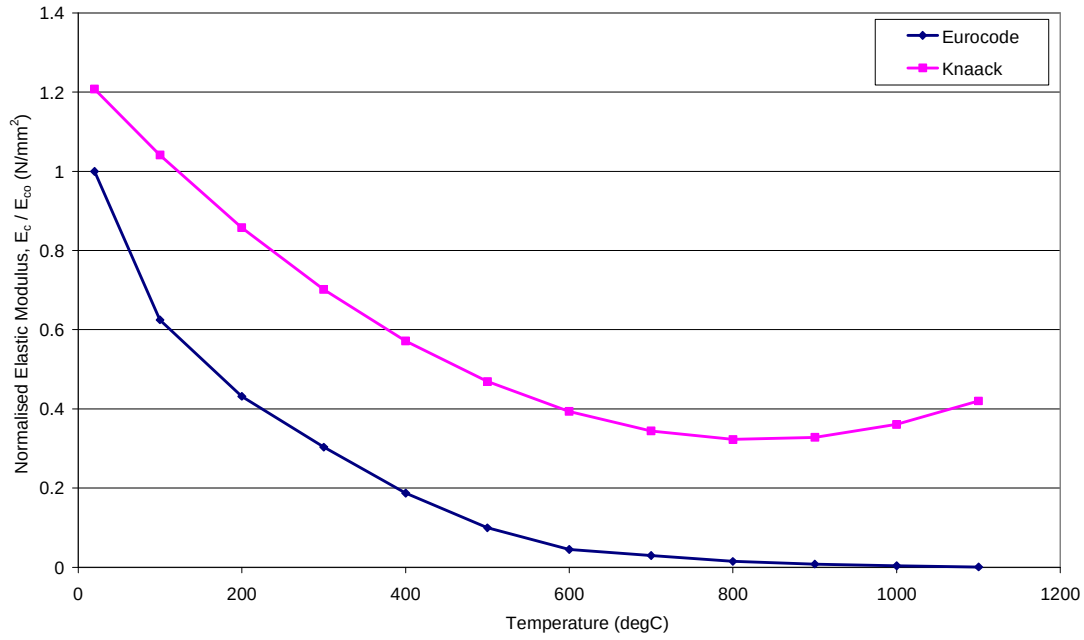

Figure 3-13: Elastic modulus plotted against temperature, with values taken from Knaack et al. (2009) and compared with the Eurocode relationship for calcareous, normal-strength, unstressed concrete.

3.3.3 Increase in strain at peak stress

Fewer experiments have been carried out where strain has been measured at elevated temperatures, and hence there is less data available to researchers. Castillo and Durani (1990) and Cheng et al. (2004) showed that for low temperatures (up to 200°C) the strain at peak stress did not vary significantly. The strain at peak stress increased slightly between 300 and 400°C, and at temperatures above 400°C the strain increased much more significantly.

Previously used models have given values of strain at peak stress in different ways – ASCE (1992) use explicit equations of temperature, Kodur et al. (2008) use equations containing temperature and ambient compressive strength, and

the Eurocode (EN1992-1-2 2004) gives individual values based on temperatures in a tablular form. Note that the Eurocode does not differentiate between aggregate type or strength classification of concrete even though these use different stress-strain relationships in other sections.

When Knaack et al. carried out their statistical analysis on the data from experiments mentioned previously (2009), it was apparent that due to lack of data, any differences that aggregate type cause in high strength concrete could not be identified, so these cases were combined. The final equation proposed was:

$$\varepsilon_{cm} \left/ \varepsilon_{cmo} = \kappa_{\varepsilon_{mo}} + \kappa_{\varepsilon_{m1}} T + \kappa_{\varepsilon_{m2}} T^2 \right. \tag{3.10}$$

where:

$\varepsilon_{cm}/\varepsilon_{cmo}$ is the ratio of strain at peak stress at temperature T, to the strain at peak stress at ambient temperature; $\kappa_{\varepsilon_{mi}}$ is the aggregate and test type dependent coefficient; T is the maximum exposure temperature (°F); and coefficients are given in Table 3-5.

Table 3-5: Strain at peak stress relationship regression coefficients (Knaack et al. 2009) for stressed (tested at elevated temperature, having been heating under preload) and unstressed (tested at elevated temperature with sample unloaded during heating) samples. Also the acceptable ranges of ambient strength, f_{cmo}, and test temperature, T, to be used, and the coefficient of determination, R^2, which indicates how well the equation fits the data (R^2=1 indicates a perfect fit to data, while R^2=0 indicates a total lack of fit).

	NSC	HSC
	Calcareous	Siliceous and Calcareous
	Unstressed	Unstressed
$\kappa_{\varepsilon_{m0}}$	0.981	0.896
$\kappa_{\varepsilon_{m1}}$ ($^oF^{-1}$)	2.181E-04	1.431E-03
$\kappa_{\varepsilon_{m2}}$ ($^oF^{-2}$)	6.426E-07	8.772E-08
T range (^oF)	[73, 1472]	[73, 1472]
f_{cmo} range (psi)	[4504, 4666]	[9102, 11458]
R^2	0.93	0.74

The equation:

$$\varepsilon_{cmo} = 0.0016 + \left(1.189 \times 10^{-7}\right) f_{cmo} \tag{3.11}$$

is used to estimate the strain at which peak compressive stress occurs.

The normalised strains from equation 3.10 are compared with those from the Eurocode in Figure 3.14. It can be seen that the normalised strains from the

Eurocode at elevated temperatures are much higher in comparison to those compiled in the study by Knaack et al. Whereas Knaack et al. suggest that the strain at peak stress at 1100°C is four times the value at ambient temperatures the Eurocode puts this ratio at 10. The reason for the difference between the two models is unclear. It may be due to the implicit inclusion of creep strains in the models of Kodur (2008), ASCE (1992) and the Eurocodes (EN1992-1-2 2004). This comparison shows the need for further research in this area, particularly for a time and temperature-dependent explicit total strain relationship including creep effects.

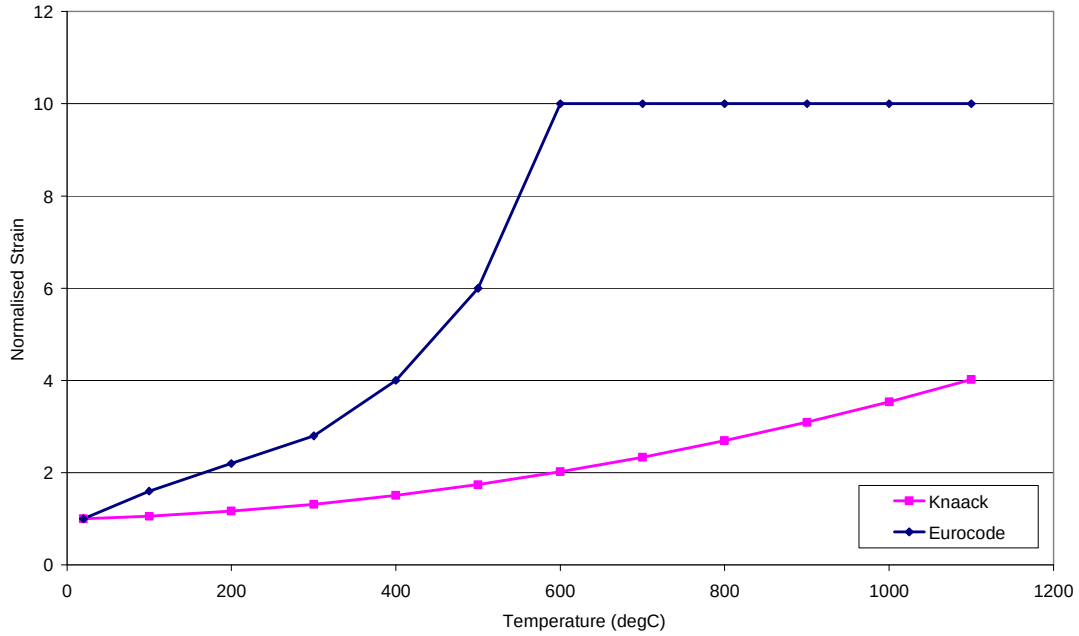

Figure 3-14: A comparison of the Eurocode relationship for strains at peak stress with that taken from Knaack et al. for calcareous, normal-strength, unstressed concrete.

3.3.4 Post-peak softening and fracture energy

It has been discussed in section 3.2.1 that concrete's softening behaviour in compression is not a material property, but is rather a non-local or structural one. It was also discussed that the compressive 'fracture energy' can be

calculated from the ultimate crushing displacement by calculating the area under the post-peak stress-displacement curve. Therefore ultimate displacement is an important parameter for the post-peak behaviour of concrete in compression. Most studies on concrete in compression at elevated temperatures treat its post-peak behaviour as a material property wherein ultimate strain rather than ultimate displacement is defined.

Ultimate strain is defined as the maximum strain reached by a specimen before failure occurs. Knaack et al. (2009) comment on three studies that measured ultimate strains in their tests; Castillo and Durani (1990), Chang et al. (2004) and Harmathy and Berndt (1966). For comparison purposes, Knaack et al. consider ultimate strain to be the strain present when 85% of the peak stress is present in the post-peak regime. Generally it was found that the ultimate strain increases as the temperature increases.

As with the strain at peak stress, the Eurocode (EN1992-1-2 2004) defines the ultimate strain at a series of temperatures in tabular form. Ultimate strain has also been provided as stress-strain relationships in ASCE (1992) and Kodur et al. (2008). The Eurocode gives higher values of ultimate strain at ambient temperature than the other sources. This could be due to the implicit inclusion of creep strains in its values, or it could be due to the Eurocode's definition of the stress at which the ultimate strain occurs – if this is smaller than 0.85 of the peak stress then that may explain the larger strain values, as more of the descending branch is present before failure occurs.

When analysis of experimental data available was carried out by Knaack et al., it was found that there was not enough data to accurately differentiate between the different aggregate types, so only one proposed model was created for normal strength concrete. They propose that the ultimate strain of concrete at high temperatures be modelled by:

$$\varepsilon_{cu} / \varepsilon_{cuo} = \kappa_{\varepsilon_{U0}} + \kappa_{\varepsilon_{U1}} T + \kappa_{\varepsilon_{U2}} T^2 + \kappa_{\varepsilon_{U3}} T^3 \qquad (3.12)$$

where:

$\varepsilon_{cu}/\varepsilon_{cuo}$ is the ratio of ultimate strain at temperature T to the ultimate strain at ambient temperature; $\kappa_{\varepsilon_{iu}}$ is the aggregate and test type dependent coefficient; and T is the maximum exposure temperature (°F).

Coefficients are given in Table 3-6.

Table 3-6: Ultimate strain relationship regression coefficients (Knaack et al. 2009) for stressed (tested at elevated temperature, having been heating under preload) and unstressed (tested at elevated temperature with sample unloaded during heating) samples. Also the acceptable ranges of ambient strength, f_{cmo}, and test temperature, T, to be used, and the coefficient of determination, R^2, which indicates how well the equation fits the data (R^2=1 indicates a perfect fit to data, while R^2=0 indicates a total lack of fit).

	NSC	HSC
	Light-weight and Calcareous	Siliceous and Calcareous
	Unstressed	Unstressed
$\kappa_{\varepsilon_{U0}}$	0.979	0.991
$\kappa_{\varepsilon_{U1}}$ ($^oF^{-1}$)	3.377E-04	-7.689E-05
$\kappa_{\varepsilon_{U2}}$ ($^oF^{-2}$)	-7.561E-07	2.803E-06
$\kappa_{\varepsilon_{U3}}$ ($^oF^{-3}$)	1.186E-09	-1.035E-09
T range (^{o}F)	[73, 1472]	[73, 1472]
f_{cmo} range (psi)	[2716, 4667]	[9102, 11458]
R^2	0.86	0.83

The value of the ultimate strain at ambient temperature is recommended always to be ε_{cuo} = 0.003. It should be noted that ε_{cu} must be greater or equal to ε_{cm}, as otherwise 'snapback' may occur, creating material properties which cause problems in computational modelling.

A comparison of ultimate strain values from Knaack et al. (2009) and the Eurocode (EN1992-1-2 2004) is shown in Figure 3-15. It can be seen that the Eurocode values are significantly higher in comparison than those suggested by Knaack et al. It is, however, important to note that the ultimate strain as per Knaack et al. is at 85% of the peak stress value.

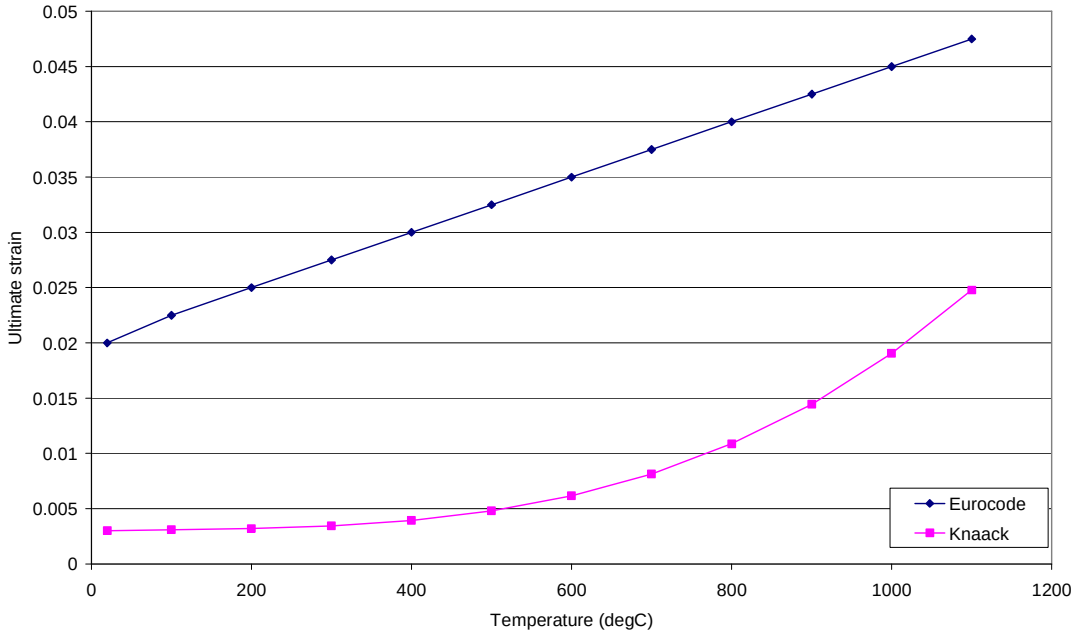

Figure 3-15: A comparison of the Eurocode relationship for ultimate strain with that taken from Knaack et al. for calcareous, normal-strength, unstressed concrete

These values can be used to define the slope of the softening branch of the stress-strain curve. The Eurocode states that any form of linear or non-linear descending branch can be used, and several different forms have been proposed by various authors. These vary from a simple linear graph (Nakamura and Higai 2001), to non-linear curves (Feenstra and de Borst 1995).

If a linear compression softening branch is used, with the Eurocode parameters outlined, as shown in Figure 3-16, then the crushing energy for concrete can be said generally to decrease with increasing temperature. Values for these are

plotted in Figure 3-17, in which a characteristic length of 250mm (typical height of cylinder tested) has been assumed.

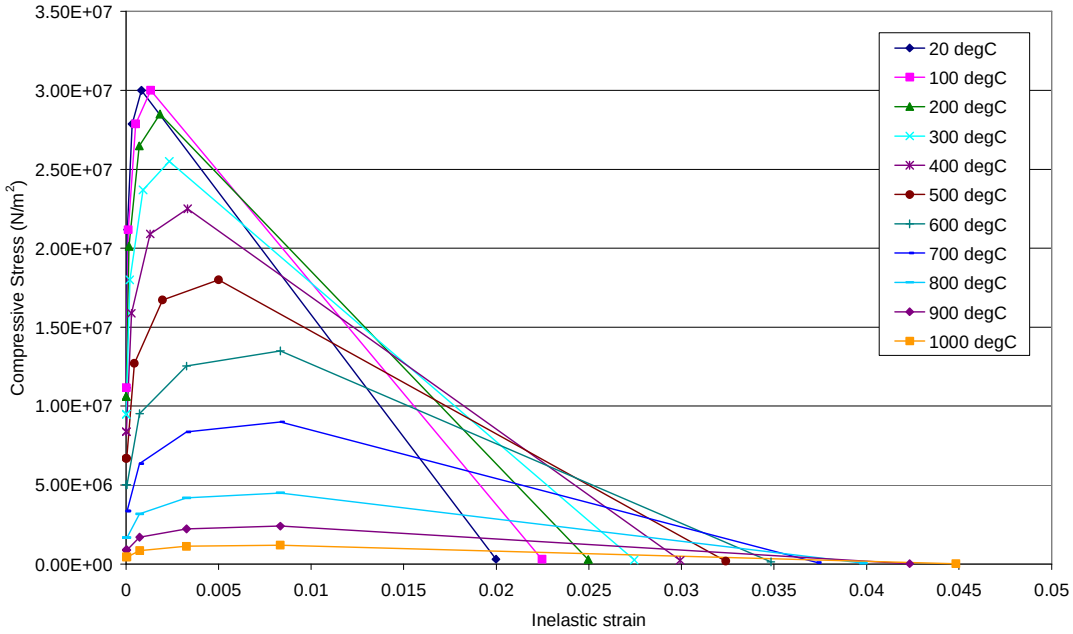

Figure 3-16: Compressive material properties based on the Eurocodes, when plotting plastic strain against stress with increasing temperature

When all four of these main parameters are combined, complete stress-strain relationships can be plotted. A typical variation based on the Eurocode (EN1992-1-2 2004) for 30 MPa, siliceous, normal-strength concrete at elevated temperatures is shown in Figure 3-18.

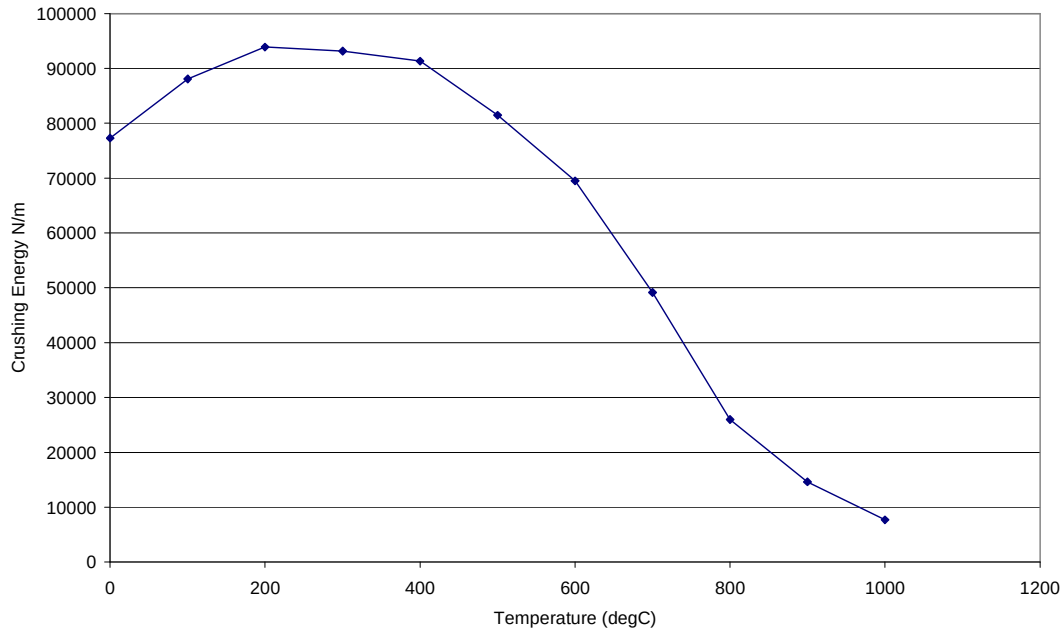

Figure 3-17: Compressive crushing energy as it varies with increasing temperature, calculated from stress-plastic strain properties based on the Eurocodes

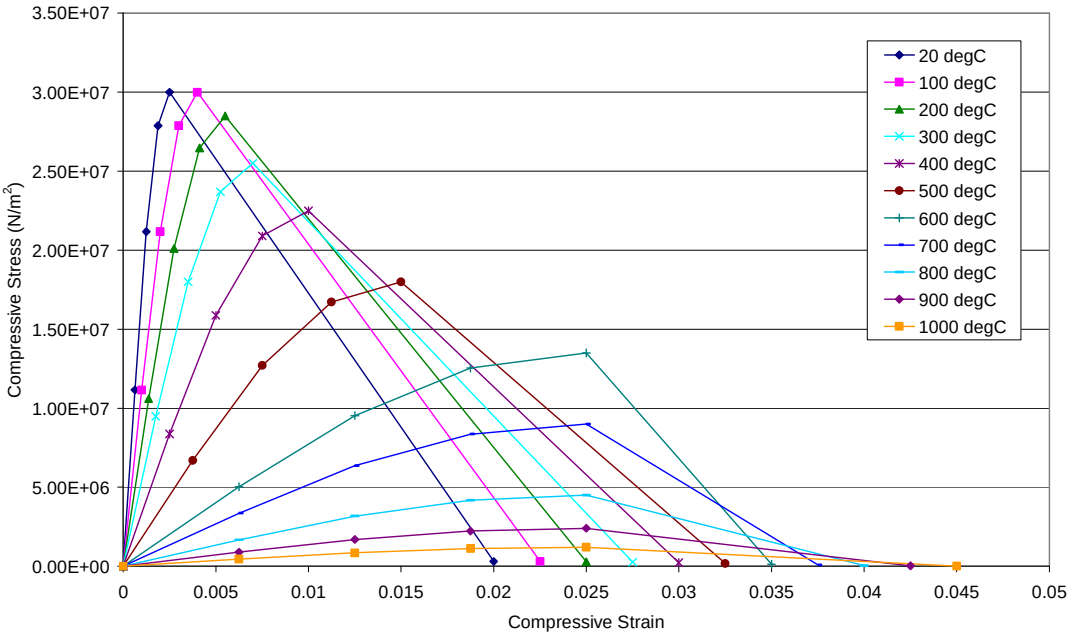

Figure 3-18: Compressive stress-strain curves based on parameters from the Eurocodes at elevated temperatures

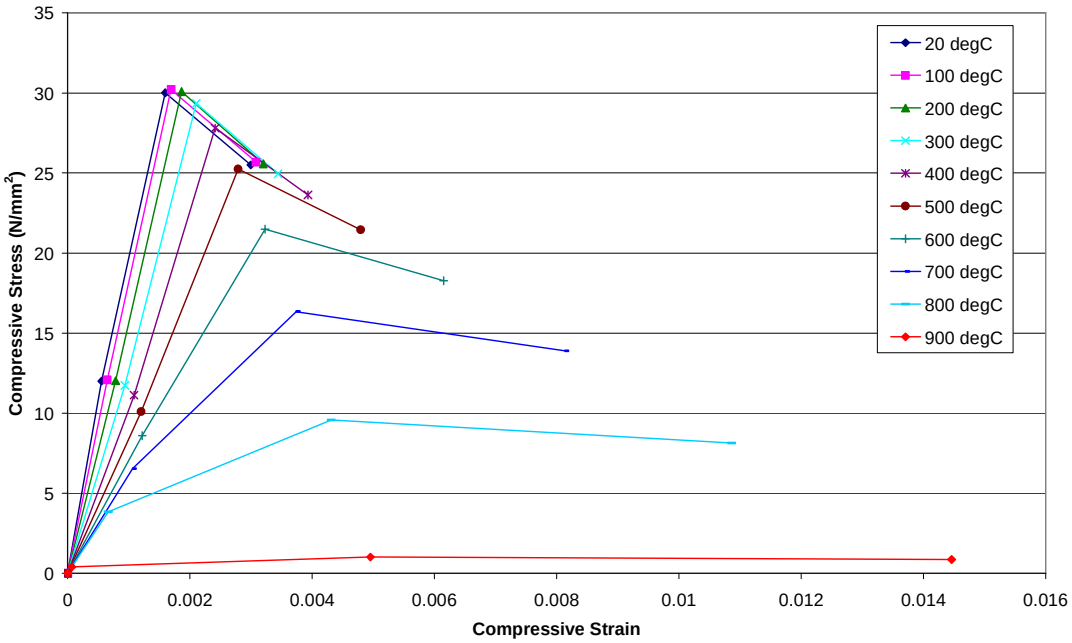

Figure 3-19: Compressive stress-strain curves, plotted using parameters proposed by Knaack et al. (2009) for a standard 30 MPa strength concrete

Similar curves from Knaack et al. (2009) are shown in Figure 3-19. The large difference in the post-peak response is apparent. The lower elastic modulus and higher strains, both ultimate and at peak stress, in the Eurocode values could be due to the implicit inclusion of creep strains.

3.4 Behaviour of concrete in compression

A number of example problems were considered to examine the behaviour of concrete at ambient and elevated temperatures in uniaxial compression. In the first set of examples a simple one-element, plane stress element (seen in Figure 3-20) was modelled and analysed under various combinations of compressive loading and heating. In the second set of examples, a cylinder was subjected to compressive loading to examine formation of localisation bands.

The concrete damaged plasticity model was used for analysis with uniaxial compressive strength f_c = 30 MPa, Young's modulus E = 18 GPa and Poisson's ratio υ = 0.25. The softening behaviour as per Eurocodes was adopted.

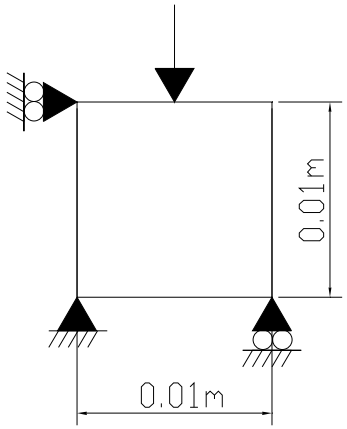

Figure 3-20: A one-element, plane stress element to be analysed under compression loading and heating.

3.4.1 Constitutive behaviour – Example 1

In this example two tests were conducted. In the first, the element is subjected to a compressive strain of 0.015 using a displacement-controlled boundary condition. It is then heated to 200^{o}C uniformly, while the boundary condition is still present. In the second test, it is first heated while free to expand, and then subjected to mechanical strain. In each case the stress and strain found within the element throughout the tests is computed. To prevent thermal stresses and strains the element is given a thermal expansion coefficient of zero.

Figure 3-21 shows the material constitutive model curves at different temperatures (based on the Eurocode (EN1992-1-2 2004)) along with the results of the two tests discussed above. It can be seen that the behaviour in compression is similar to that seen for tension in the last chapter. Once again the

tests indicate that the stress-strain behaviour under loading and temperature increase is strongly path dependent.

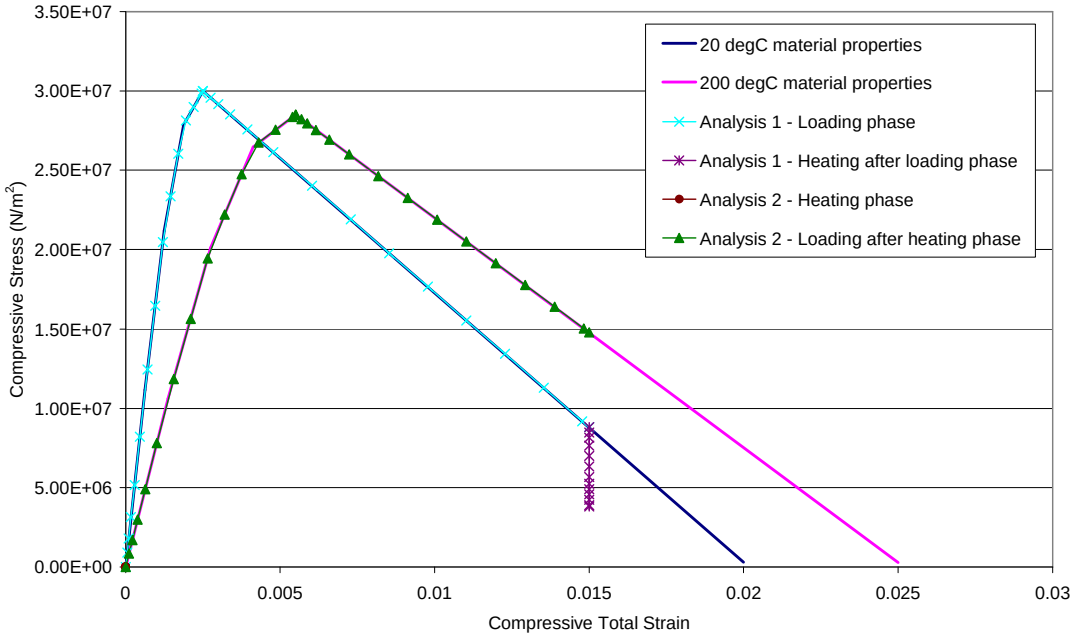

Figure 3-21: Stress-strain of a one-element plane stress model when the thermal expansion coefficient is zero: 1. The element is loaded using a displacement-controlled boundary condition and then heated to 200°C. The model follows the ambient material properties curve during loading, while during heating the stress present reduces as the strain remains constant – this is due to the elastic modulus being lower at elevated temperatures. 2. The element is heated to 200°C and then loaded in compression using a displacement-controlled boundary condition. As no thermal expansion occurs there is no change in stress or strain during heating, however on loading the model follows the 200°C material properties curve as expected.

3.4.2 Constitutive behaviour – Example 2

Example 1 was re-analysed after the inclusion of the thermal expansion coefficient. Once again two tests, loading followed by heating and heating followed by loading, were conducted. The results are shown in Figure 3-22.

The element is loaded first, again to a strain of 0.015, and then heated to 200°C. As the element is loaded it behaves exactly the same as in example 1, with the stress-strain curve following the ambient material properties curve, see Figure 3-22. When heating starts, the stress within the element starts to increase. This is due to thermal expansion not being permitted by the displacement controlled boundary condition.

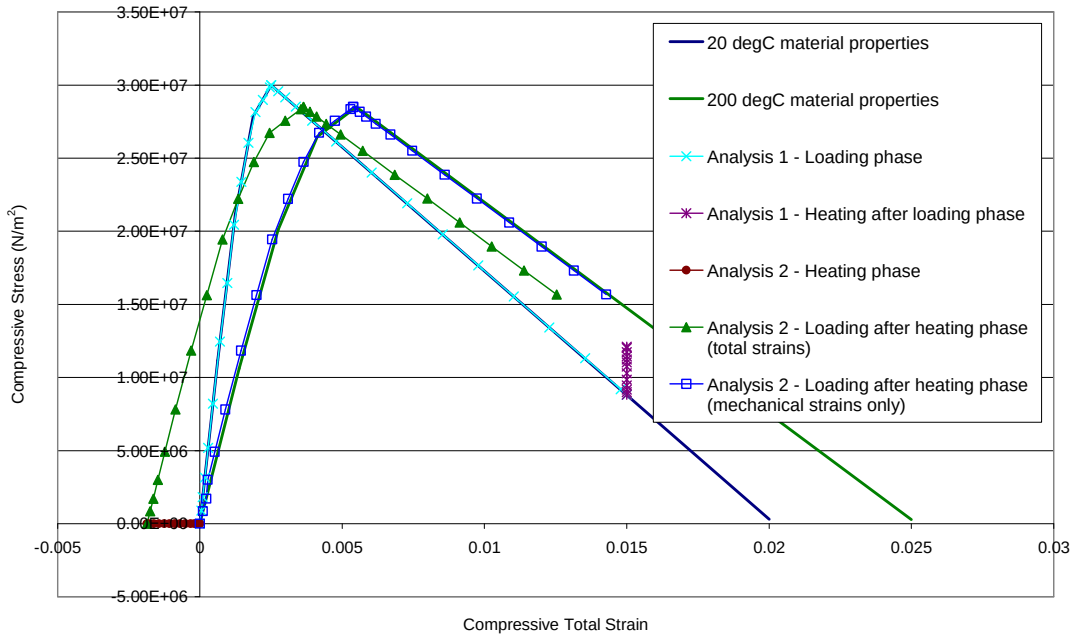

Figure 3-22: Stress-strain of a one-element plane stress model when the thermal expansion coefficient is non-zero and thermal stresses and strains occur: 1. The element is loaded using a displacement-controlled boundary condition and then heated to 200°C. The model follows the ambient material properties curve during loading, while during heating the stress present increases as the strain remains constant – this is due to the thermal stresses induced by expansion not being permitted due to the displacement-controlled boundary condition. 2. The element is heated to 200°C with expansion freely permitted and then loaded in compression using a displacement-controlled boundary condition. On loading the model follows the shape of the 200°C material properties curve, however it is offset by the value of thermal strain caused in the heating phase – if thermal strains are removed and only mechanical strains plotted then this model follows the 200°C material properties curve exactly.

In the second test the element is heated to 200°C first, with thermal expansion permitted, and then it is loaded under compression. Figure 3-22 shows that the total strain in the element becomes tensile (the element expands) on heating, while the stress remains zero. When loading begins, and when total strains are plotted, the stress-strain curve of the element follows the shape of the 200°C material properties curve, however it is offset negatively (in tension) due to the thermal strains present. Once the thermal strains are removed, and only the mechanical strains are plotted, it is seen that the model follows the 200°C material properties curve exactly as expected.

3.4.3 Localisation under compression – Example 3

Next, a cylinder is modelled and subjected to uniaxial compression. The cylinder was of height 500 mm and diameter 160 mm, and the analysis was carried out using axisymmetric elements. Concrete damaged plasticity was used, with uniaxial compressive strength f_c = 30 MPa, Young's modulus E = 18 GPa and Poisson's ratio υ = 0.25. A linear softening branch was used for all elements.

First, two meshes with square elements of 20 x 20 mm and 10 x 10 mm were analysed. The material properties used were altered according to element size, with the smaller elements having a less steep softening slope. The load-displacement plot is shown in Figure 3-23, and it shows that because no localisation occurs, and all the material in the cylinder yields at the same time, the descending branch is material model dependent. The fracture energy/crushing energy concept leads to mesh insensitive answers only when localisation occurs. Furthermore, if the localisation band is diffused, i.e. it is several elements thick; mesh sensitivity may still be encountered. It is noted that the two models are identical in the elastic range, up to approximately 30% of the compressive strength.

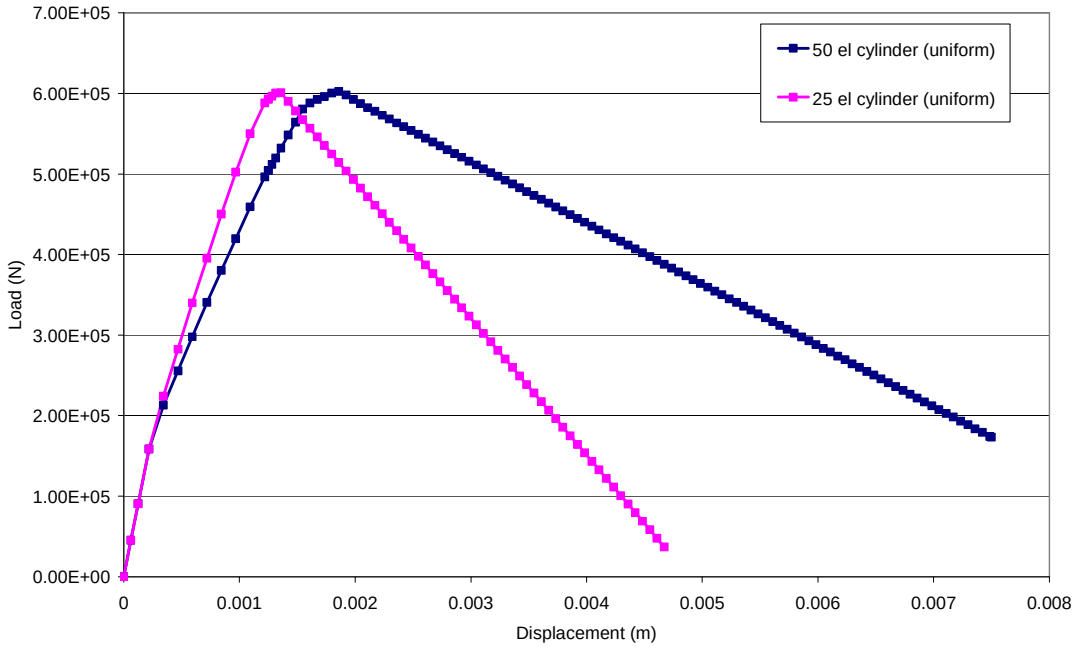

Figure 3-23: Compressive load-compressive displacement showing the different responses of the cylinder under uniaxial compression with element sizes of 10 mm and 20 mm

3.4.4 Localisation under compression – Example 4

To induce localisation in the cylinder a weakened element was introduced, at one corner of the base of the cylinder. Again, the model was subjected to uniaxial compression in the form of prescribed downward displacement at the top. Vertical plastic strain evolution at a post-peak instant is shown in Figure 3-24. The plastic strain initiates in the weak element, and propagates diagonally upwards. A complete localised band was not obtained due to lack of convergence caused by excessive distortion of the yielded elements, especially the weakened element. The vertical normal stress versus the equivalent plastic strain was plotted for the weak element, for a normal element outside the band that developed, and for a normal element within the band. These are shown in Figure 3-25. It can be seen that the weak element exhibits softening behaviour,

and the element outside the band shows elastic unloading (i.e. no plastic strains are developed and the vertical normal stress reduces). Interestingly, in a normal strength element within the band, initial increase in equivalent plastic strain is followed by it becoming almost constant, indicating elastic unloading. The vertical load versus vertical displacement plot is shown in Figure 3-26. In this the initial softening response is followed by an almost brittle behaviour.

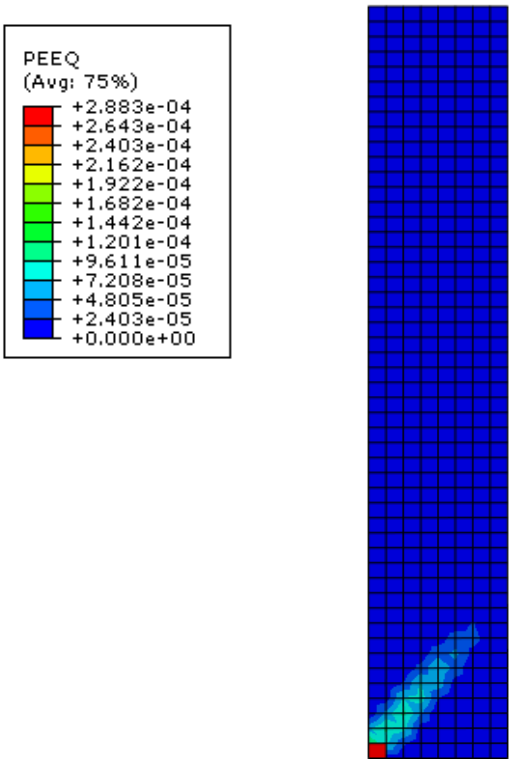

Figure 3-24: Cylinder under uniaxial compression when one element (at the base) is weakened – plastic yield is confined to a diagonal band extending from the weak element

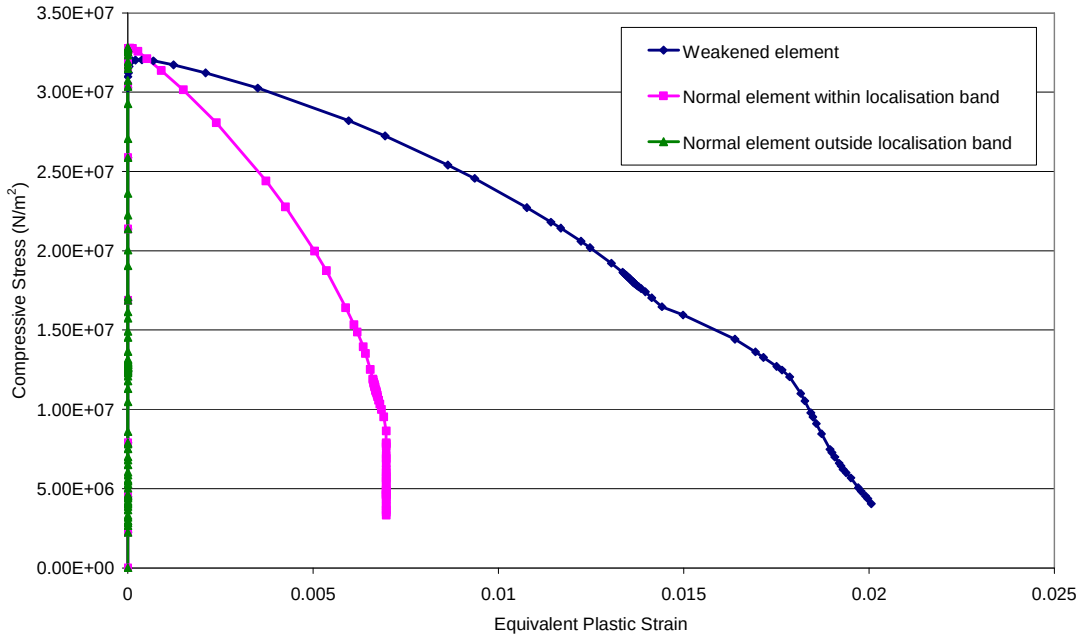

Figure 3-25: Vertical compressive stress–Equivalent plastic strain for the weak element, a normal element within the localisation band and a normal element outwith the localisation band, in a cylinder under uniaxial compression. The weakened element shows softening behaviour, while the element not within the localisation band shows elastic unloading (no yield), and the normal strength element within the developing localisation band shows initial strain softening behaviour followed by elastic unloading.

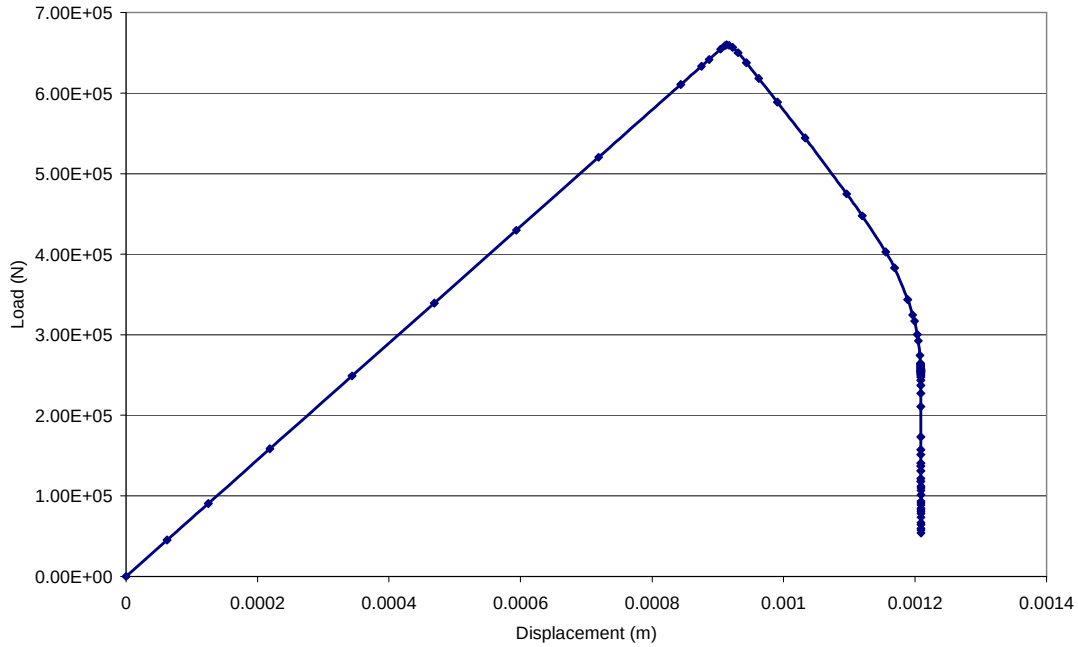

Figure 3-26: Vertical load-vertical displacement for a cylinder under uniaxial compression with one weakened element at its base – the initial softening response is followed by an almost brittle behaviour as the load carried decreases at a constant displacement.

3.4.5 Localisation under compression – Example 5

Previously the localised band of yielding did not develop fully as the weakened element and other elements in that area deformed too much. In an attempt to prevent excessive distortion a layer of elastic elements with a very low Young's modulus (E = 3.6E09 for the overlay elements, as opposed to E = 3.6E10 for the normal elements) were overlaid, prior to subjecting the cylinder to uniaxial compression. As these elements are elastic, they can distort without yielding, while the low Young's modulus value will prevent the overlay elements from restricting the behaviour of the normal elements, while preventing the convergence issues seen previously. Further, symmetry was assumed and only half the cylinder modelled using axisymmetric elements. The element size used was 5mm. An analysis was conducted with an element on the left side of the mesh, near the base, made weaker. The localisation band was found to

propagate diagonally and was diffused (Figure 3-27). The vertical load versus vertical displacement plot is shown in Figure 3-28. In this figure lines for the load carried by the cylinder with and without the presence of overlay elements have been plotted. It can be seen that the response for the two different locations of weak elements is significantly different. Use of overlay elements appears to provide a simple methodology to avoid convergence problems. However, issues related to diffused bands and thereby mesh sensitivity persist. Unlike the previous example, the post-peak load-displacement response is relatively flat, in spite of the band being able to propagate to a significant extent.

A second case was attempted, with a weakened element placed in the centre of the mesh. Two diagonal localisation bands were seen to emanate from the weakened element (Figure 3-29). Additional diagonal regions of plastic strain also appeared to have been initiated in the latter part of the loading.

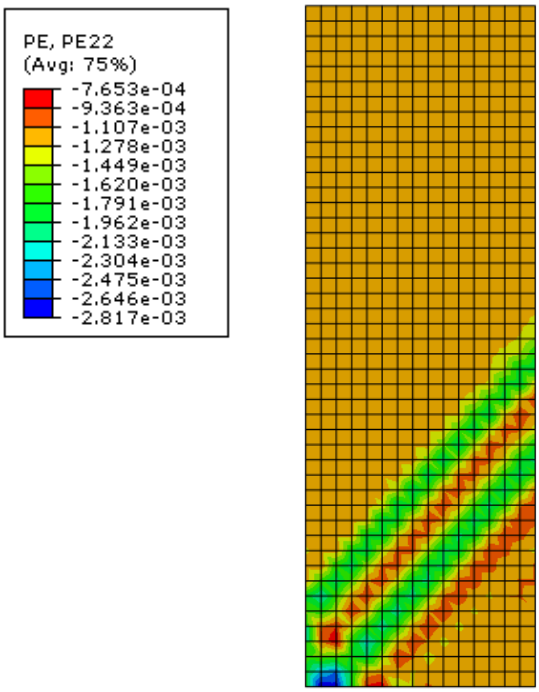

Figure 3-27: Plastic strain in a cylinder under uniaxial compression when an overlay layer of elements is included, and element 46 is weakened (left hand side row 4 from the base). The overlay elements are not plotted here, only the normal elements beneath.

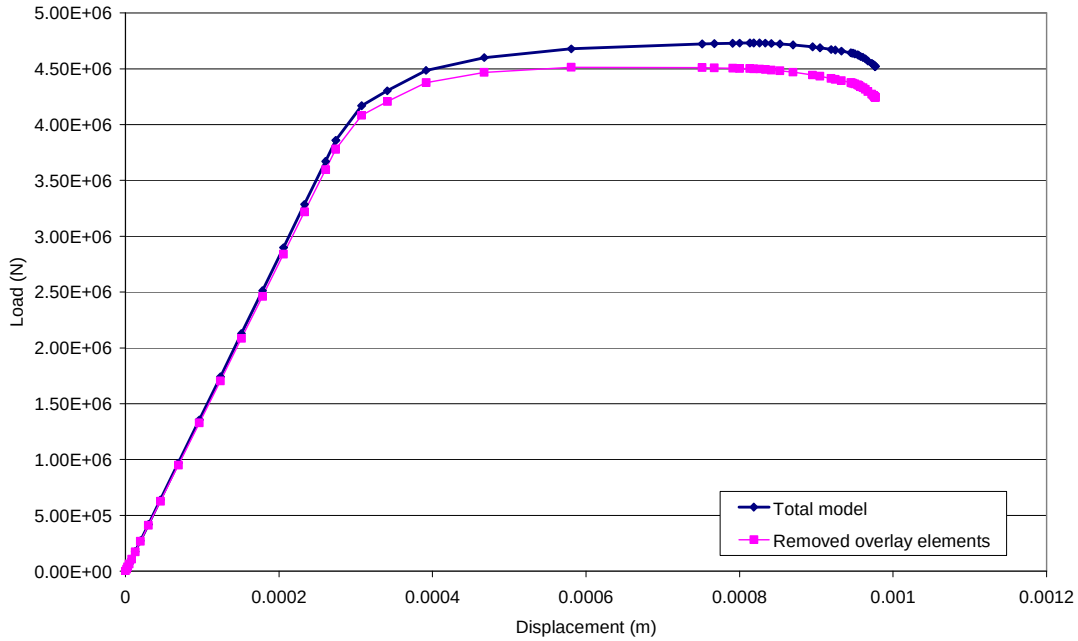

Figure 3-28: Vertical load-vertical displacement for a cylinder under uniaxial compression when an overlay layer of elements is included, and element 46 is weakened (left hand side row 4 from the base). As the band of localised yield develops the load carried by the cylinder remains constant before some softening occurs.

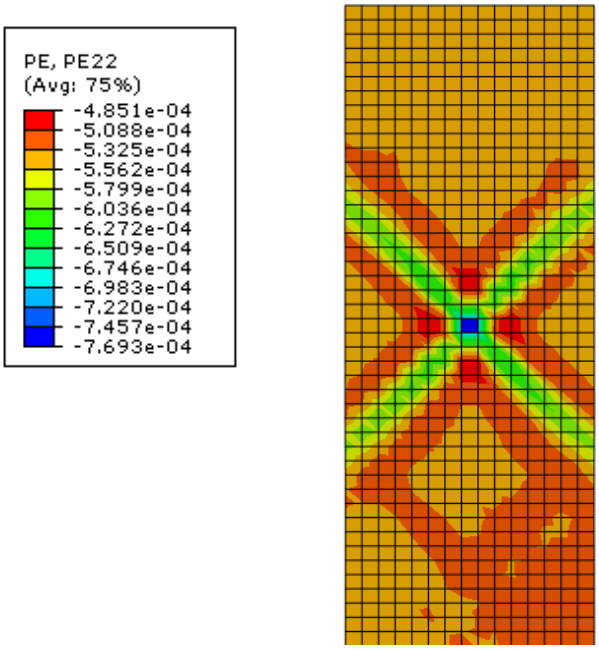

Figure 3-29: Plastic strain in a cylinder under uniaxial compression when an overlay layer of elements is included, and an element in the centre of the model is weakened

3.4.6 Localisation under compression – Example 6

In section 3.2.2, it was shown that when using the concrete damaged plasticity model with the material properties described there, under uniaxial compression yield would be localised in a band at 47^o from the horizontal. Previous studies have shown that localisation bands tend to follow element boundaries (Pankaj 1990; de Borst et al. 2004).

In order to force localisation in a band, a mesh of triangular plane strain elements was generated, and all the elements within the band were made slightly weaker. Three different meshes with varying mesh densities were considered. Upon application of uniaxial compressive strain, the elements within the band were found to enter the plastic regime as shown in Figures 3-30 to 3-32. However, in each case, the plastic strains were seen to spread outside the band, i.e. localisation remained uncaptured. This could be due to a variety of reasons including changing localisation directions with continued plastic deformation due to the non-associated flow rule used in concrete damaged plasticity. This study evaluated the localisation band direction at the onset of plasticity. The damage – plasticity model uses a non-associated flow rule with a curvilinear surface in the principal space. The continuous change of plastic strain direction may cause a shift in the localisation direction.

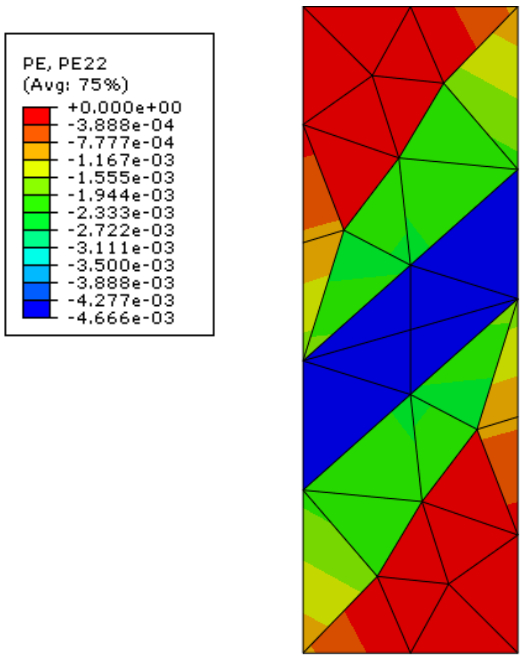

Figure 3-30: Plastic strain localised in a weakened band of elements at 47º to the horizontal

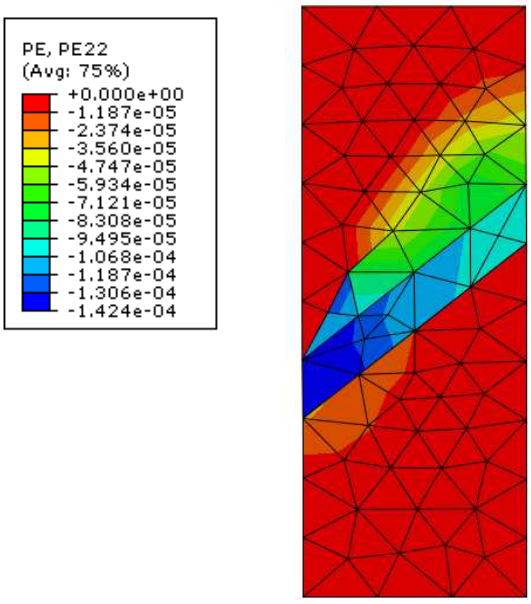

Figure 3-31: Plastic strain localised in a weakened band of elements at 47º to the horizontal

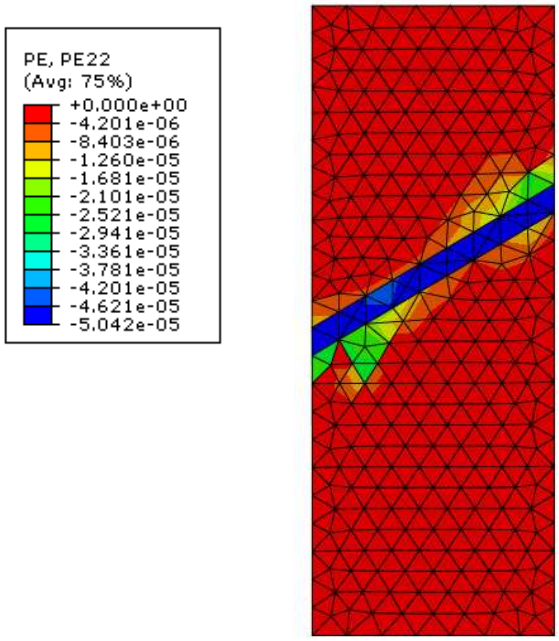

Figure 3-32: Plastic strain localised in a weakened band of elements at 47° to the horizontal

3.5 References

Abaqus (2008). Abaqus Analysis User's Manual. Providence, Dassault Systemes Simulia Corp.

Abrams, M. (1971). Compressive Strength of Concrete at Temperatures to 1600 deg F. ACI. **SP-25**.

ACI216R (2007). Guide for determining the fire endurance of concrete elements. Farmington Hills, MI, American Concrete Institute.

Anderberg, Y. and S. Thelandersson (1976). Stress and Deformation Characteristics of Concrete, 2 - experimental investigation and material behaviour model. Sweden, University of Lund. **Bulletin 54**.

ASCE (1992). Structural Fire Protection. ASCE Manuals and Reports on Engineering Practice No.78. New York, American Society of Civil Engineers.

Cartensen, J. (2011). Material Modelling of Reinforced Concrete at Elevated Temperatures. Department of Civil Engineering, The Technical University of Denmark. **Masters Thesis**.

Castillo, C. and A. J. Durani (1990). "Effect of Transient High Temperatures on High-Strength Concrete." ACI Materials Journam **87**(1): 47-53.

Cheng, F. P., V. K. R. Kodur, et al. (2004). "Stress-Strain Curves for High Strength Concrete at Elevated Temperatures." Journal of Materials in Civil Engineering **16**(1): 84-90.

de Borst, R., J. J. C. Remmers, et al. (2004). "Discrete vs smeared crack models for concrete fracture: bridging the gap." International Journal for Numerical and Analytical Methods in Geomechanics **28**: 583-607.

EN1992-1-1 (2004). Eurocode 2: Design of Concrete Structures - Part 1-1: General Rules and Rules for Buildings.

EN1992-1-2 (2004). Eurocode2: Design of Concrete Structures - Part 1-2: General Rules - Structural Fire Design.

Feenstra, P. H. and R. de Borst (1995). "Constitutive Model for Reinforced Concrete." Journal of Engineering Mechanics **121**(5): 587.

Harmathy, T. Z. and J. E. Berndt (1966). "Hydrated Portland Cement and Lightweight Concrete at Elevated Temperatures." Journal of the American Concrete Institute **63**(1): 93-112.

Hertz, K. D. (2005). "Concrete strength for fire safety design." Magazine of Concrete Research **57**(8): 445-453.

Khoury, G. A., B. N. Grainger, et al. (1985). "Transient Thermal Strain of Concrete - Literature-Review, Conditions within Specimen and Behavior of Individual Constituents." Magazine of Concrete Research **37**(132): 131-144.

Knaack, A. M., Y. C. Kurama, et al. (2009). Stress-Strain Properties of Concrete at Elevated Temperatures. Structural Engineering Research Report, Department of Civil Engineering and Geological Sciences, University of Notre Dame.

Kodur, V. K., M. M. Dwaikat, et al. (2008). "High-Temperature Properties of Concrete for Fire-Resistance Modeling of Structures." ACI Materials Journal **105**(5): 517-527.

Law, A. and M. Gillie (2008). Load Induced Thermal Strain: Implications for Structural Behaviour. Proceedings of the Fifth International Conference on Structures in Fire (SiF'08).

Li, L. Y. and J. Purkiss (2005). "Stress-strain constitutive equations of concrete material at elevated temperatures." Fire Safety Journal **40**(7): 669-686.

Nakamura, H. and T. Higai, Eds. (2001). Compressive Fracture Energy and Fracture Zone Length of Concrete. Modeling of Inelastic Behavior of RC Structures under Seismic Loads, ASCE.

Pankaj, P. (1990). Finite Element Analysis in Strain Softening and Localisation Problems, University of Wales. **PhD thesis**.

Shi, X., T. H. Tan, et al. (2002). "Concrete constitutive relationships under different stress-temperature paths." Journal of Structural Engineering **128**(12): 1511-1518.

Terro, M. J. (1998). "Numerical Modelling of the Behaviour of Concrete Structures in Fire." ACI Structural Journal **95**(2): 183-193.

Vonk, R. (1992). Softening of Concrete Loaded in Compression, Eindhoven University of Technology. **Ph.D. Thesis**.

4

Modelling reinforced concrete at elevated temperatures

4.1 Introduction

Plain concrete has a high compressive strength; however it is much weaker in tension. As a result, in structural applications concrete is invariably used with reinforcing steel bars. These are strong and ductile under tensile loading, and

can bond with the concrete mix to make a composite material which is strong in both tension and compression.

The behaviour of plain concrete has been discussed in previous chapters, and this information is used to determine the behaviour of reinforced concrete. Steel reinforcing bars are generally characterised by their yield strength, and the Eurocode assumes that for design purposes they behave in an entirely elastic-perfectly plastic manner (EN1992-1-1 2004). At elevated temperatures the reinforcement's behaviour is characterised by a decreasing yield stress and a decreasing elastic modulus (EN1992-1-2 2004).

While the behaviour of plain concrete and steel bars can be determined separately, it is the interaction of the two that is most relevant here. It is important that the bond between the concrete matrix and the reinforcing bar is modelled accurately as it can have a huge effect on the resultant composite material behaviour. When the material cracks under tensile loading, the cracked concrete maintains some of its load-carrying ability next to the reinforcing steel bars. Hence the cracked reinforced concrete bar is stronger under tensile loading than the lone reinforcing bar would have been. This interaction behaviour is termed tension stiffening (Hofstetter and Mang 1996). Different methods used to include tension stiffening in computational material models are discussed in the following section.

4.2 Behaviour of reinforcement

As has been stated previously, the Eurocodes (EN1992-1-1 2004) characterise the behaviour of reinforcing steel very clearly. They give curves which incorporate ductility and strain hardening behaviour, however accept that simplified assumptions can be made in design. The following stress-strain graph is given for use in design (Figure 4-1).

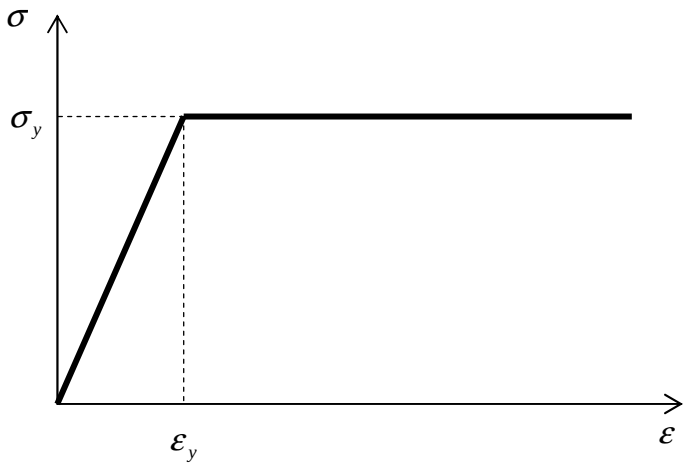

Figure 4-1: Idealised design stress-strain graph for reinforcing steel (EN1992-1-1 2004)

The behaviour of reinforcing steel at elevated temperatures is also defined (EN1992-1-2 2004). The yield strength decreases from a maximum at ambient temperature, to zero at 1200^{o}C, while the elastic modulus also decreases as the temperature increases. The parameters used to define the change in these values are given in Table 4-1. Material properties for steel with ambient yield strength of 500 MPa is shown in Figure 4-2.

Table 4-1: Values for the parameters of the stress-strain relationship of steel at elevated temperatures – taken for cold worked reinforcing steel – where $f_{sp,\theta}/f_{yk}$ is the ratio of tensile strength at temperature θ to tensile strength at ambient temperature, and $E_{s,\theta}/E_s$ is the ratio of the elastic modulus at temperature θ to the elastic modulus at ambient temperature.

Steel temperature θ (°C)	$f_{sp,\theta}/f_{yk}$	$E_{s,\theta}/E_s$
20	1.00	1.00
100	0.96	1.00
200	0.92	0.87
300	0.81	0.72
400	0.63	0.56
500	0.44	0.40
600	0.26	0.24
700	0.08	0.08
800	0.06	0.06
900	0.05	0.05
1000	0.03	0.03
1100	0.02	0.02
1200	0.00	0.00

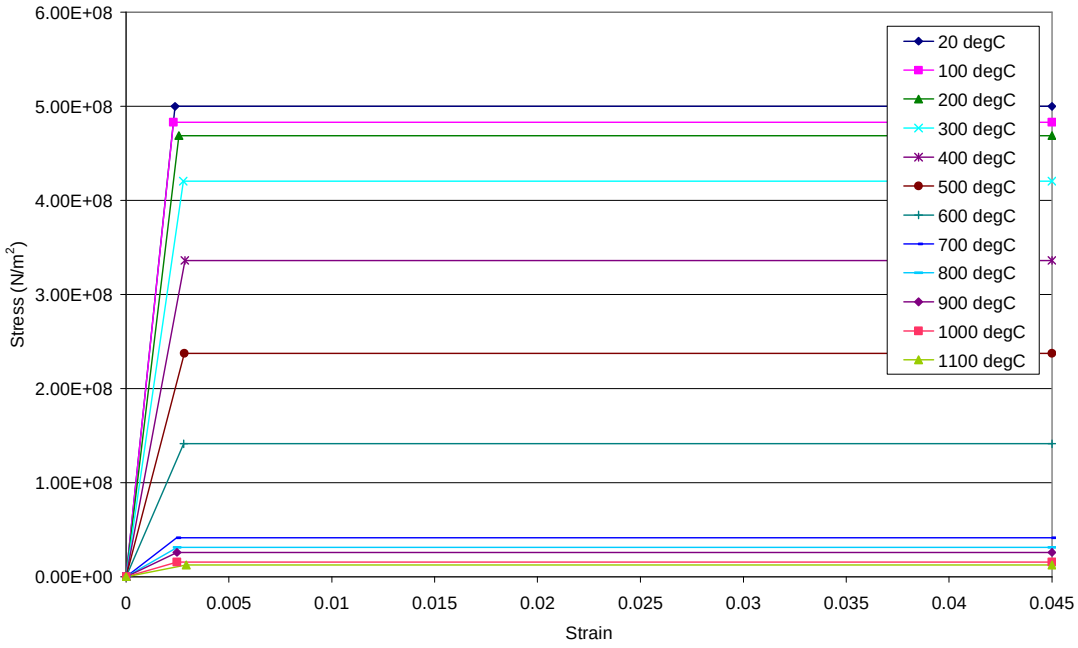

Figure 4-2: Reinforcement stress-strain material properties at elevated temperatures, for reinforcing bars of yield strength 500 MPa

4.3 Modelling the reinforced concrete composite at ambient temperatures

Generally it is assumed that the concrete matrix and steel reinforcement work together to create a composite which behaves as a singular material under loading. Under compression it is assumed that the bond between concrete and reinforcement is relatively unimportant, and hence reinforced concrete is normally just modelled as plain concrete with embedded steel reinforcing bars (Gilbert and Warner 1978), in other words, the behaviour of the composite in compression is assumed to be the combined individual behaviour of plain concrete and reinforcement.

However under tension the material behaves quite differently. As has been mentioned previously, concrete is relatively weak in tension, while steel reinforcement is strong and ductile. In the post-elastic regime the reinforced concrete composite is stronger and can carry more tensile load than the sum of its parts. This is due to the concrete being able to carry tensile loading across the

cracked concrete matrix (Feenstra and de Borst 1995). This additional strength is called tension stiffening, and it is important to include its behaviour in material models of reinforced concrete under tension. This is normally done by altering the concrete strain softening curve, to give it additional strength, particularly in the descending branch.

Several authors have discussed varying ways of modelling reinforced concrete computationally, and three main strands have emerged: (a) ignoring any tension stiffening behaviour present but incorporating tensile fracture energy in the concrete material; (b) including tension stiffening behaviour by altering the concrete material model but ignoring tensile fracture energy and its effects on mesh sensitivity; and (c) including both tension stiffening behaviour and tensile fracture energy in the concrete material model.

Hofstetter and Mang (1996) follow this first type of model. They assume that reinforced concrete behaviour in tension can be represented by combined individual behaviours of reinforcement and concrete.

Stramandinoli and La Rovere (2008) and Gupta and Maestrini (1990) follow the second approach, modifying the constitutive equation for concrete by changing the descending branch of the stress-strain curve to include tension stiffening and reflect reinforced concrete's increased load-carrying ability post-peak. Stramandinoli and La Rovere assume that concrete is linear-elastic until peak stress under tension is reached, after which the stress present decreases exponentially until the reinforcement present starts yielding. Hence this model is affected by the reinforcement ratio present in the composite. Gupta and Maestrini also produce simplified stress-strain curves for concrete in tension. In a slight variation to this, Gilbert and Warner (1978) also include the tension stiffening effect post-peak, but do so by altering the steel constitutive equation as opposed to the concrete one.

Feenstra and de Borst (1995), He et al. (2008), Barros et al. (2001) and Cervenka and Pukl (1990) use the third approach which includes both tension stiffening and fracture energy in their material models. Feenstra and de Borst state that the

total stress can be divided up into individual components carried by the plain concrete, the reinforcement and the interaction between the concrete and reinforcement as shown in Figure 4-3.

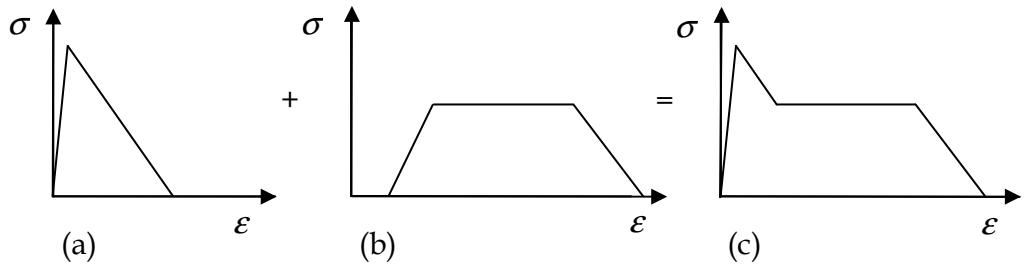

Figure 4-3: Constitutive model for concrete when modelling it as a constituent of reinforced concrete: (a) plain concrete; (b) tension stiffening contribution; and (c) combined response

As can be seen in Figure 4-3, the reinforcement is represented by a standard elastic-plastic relationship, and a trilinear function is used to define the interaction between concrete and reinforcement. In this model the fracture energy can be used with Figure 4-3 (a) to minimise mesh sensitivity. He et al. (2008) look at reinforced concrete under cyclic loading and show that it is important to include damage under this loading, by using nonlinear unloading curves and a degraded value for the reloading stiffness.

A typical graph developed from Gupta and Maestrini's work is shown in Figure 4-4. The figure was plotted for $n = E_S/E_C$ = 11.667, $\rho = A_S/A_C$ = 0.01, f_t' = 1.45x10^6 Pa, f_y = 5x10^8 Pa and $\varepsilon_y = f_y/E_S$ = 0.00238 at ambient temperature. Comparing figures 4-3 and 4-4, it can be seen that the fracture energy contribution only affects the initial drop of strength after first yield. The subsequent behaviour is primarily governed by tension stiffening, whose contribution is in the form of a descending branch in Figure 4-4 and a flat portion in Figure 4-3.

Recent studies have indicated that fracture energy does not play an important role in obtaining mesh insensitive solutions for reinforced concrete (Kingston

and Pankaj 2012). Syroka et al. (2011) carried out finite element analysis of reinforced concrete samples looking at various parameters including characteristic length and tensile and compressive fracture energy. They found that tensile fracture energy G_f was not significant in affecting how the reinforced concrete samples behaved, and so in our modelling of reinforced concrete any change in tensile fracture energy can be ignored.

With this in view, the model by Gupta and Maestrini was extended for elevated temperatures. In this the post-peak behaviour of concrete was taken as a material property. Using the parameters from the Eurocode (EN1992-1-2 2004) at elevated temperatures, in conjunction with the formulation of Gupta and Maestrini, the developed stress-strain model for concrete is shown in Figure 4-5.

In this study the model from Gupta and Maestrini (1990) will be used, as it is simple to calculate, is not affected by bond slip values, and it is clear and easy to plot the concrete stress-strain curves using its values. Typical stress-strain properties for concrete at ambient temperature (Figure 4-4) and at elevated temperatures (Figure 4-5) are seen below.

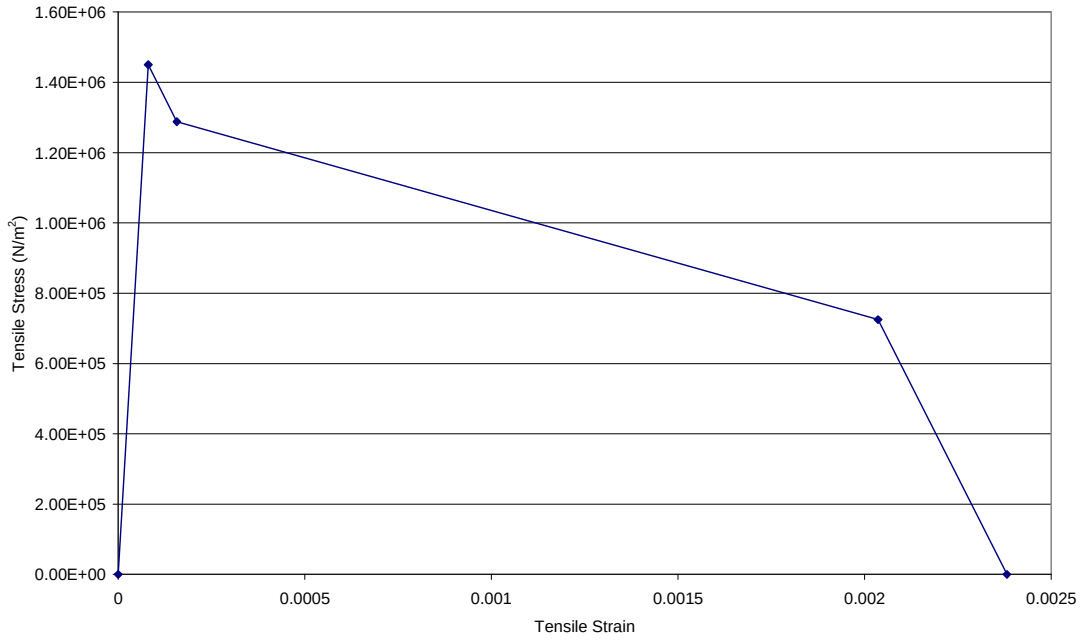

Figure 4-4: Stress-strain material properties for concrete under tension at ambient temperature when tension stiffening is included (Gupta and Maestrini 1990)

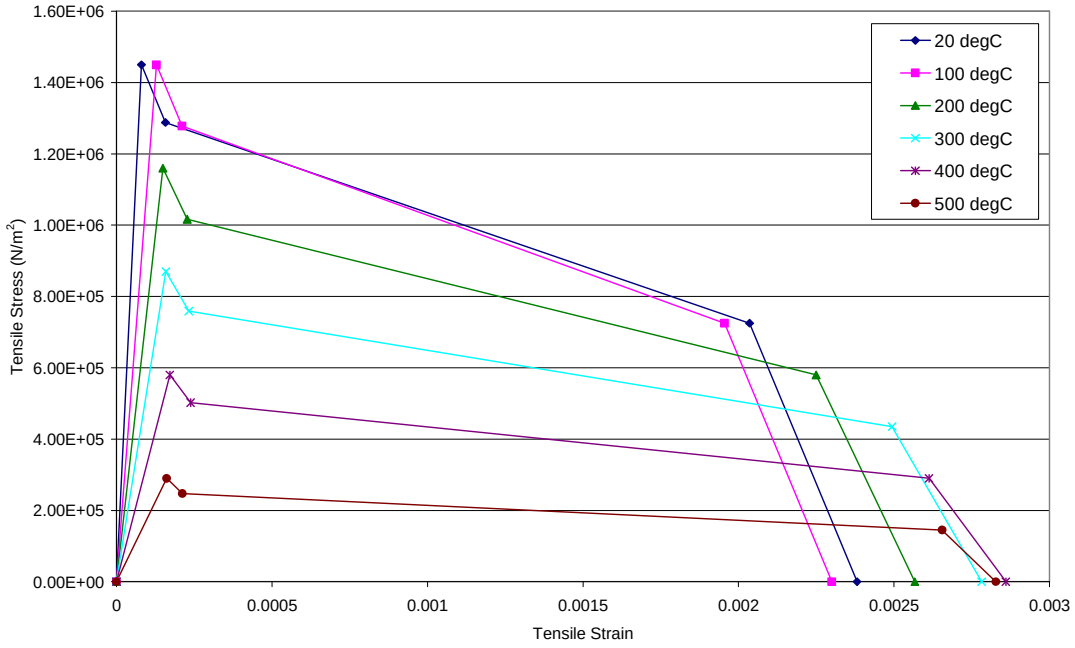

Figure 4-5: Stress-strain material properties for concrete under tension at elevated temperatures when tension stiffening is included (Gupta and Maestrini 1990)

4.4 Extending reinforced concrete models to elevated temperatures

4.4.1 Behaviour of reinforced concrete at elevated temperatures under compression

A square one-element plane stress model was used to investigate how reinforced concrete behaves in computational models at elevated temperatures. Displacement controls applied as boundary conditions were used to simulate loading. The model is shown in Figure 4-6. The reinforcement was modelled as an embedded truss element, and had cross-sectional area 0.0001 m^2, giving the entire element a reinforcement ratio of 1%. There was assumed to be no slip in the bond between the concrete and the reinforcement present – modelled computationally by embedding the truss element into the plane stress concrete element so that its ends were tied to the surfaces of the plane stress element. The material properties used included concrete compressive strength σ_c = 30 MPa,

concrete tensile strength σ_t = 1.45 MPa, concrete elastic modulus E_c = 1.8x10^{10} Pa, reinforcing steel strength σ_s = 500 MPa and reinforcing steel elastic modulus E_s = 2.1x10^{10} Pa. Concrete's tensile properties were as described previously in Figure 4-5, while the reinforcing steel stress-strain material property curves were as shown in Figure 4-2. The material properties of concrete in compression are shown in Figure 4-7, and are based on the Eurocode (EN1992-1-2 2004), and described in the last chapter.

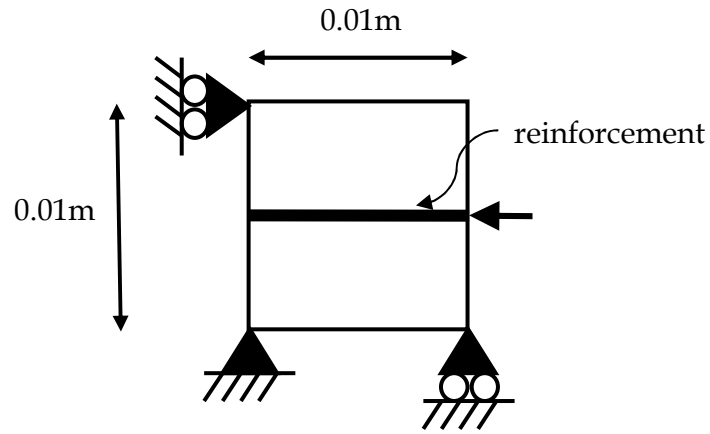

Figure 4-6: Diagram of one element plane stress concrete model with one bar of reinforcement through its centre

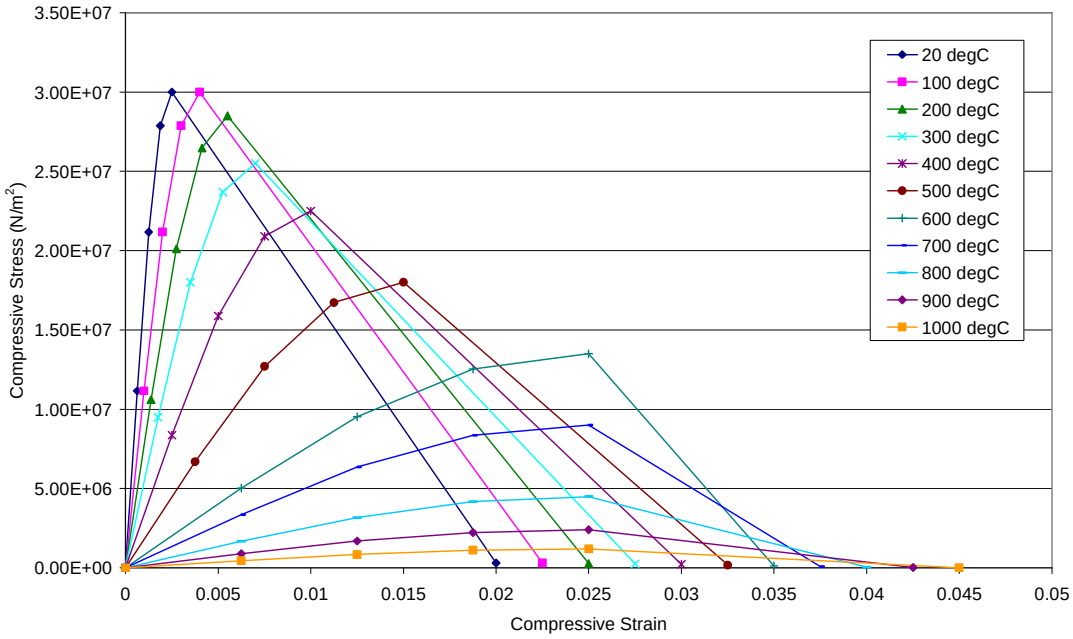

Figure 4-7: Compressive stress-strain material properties for concrete at elevated temperatures, based on the Eurocode (EN1992-1-2 2004)

In the first analysis the model was loaded under uniaxial compression and then heated to 200°C by applying increasing temperatures directly to all nodes. In the second analysis the model was heated to 200°C throughout before being loaded under compression. The stress-strain response within the concrete part of the model from both of these analyses is shown in Figure 4-8. The response corresponding to the reinforcement is shown in Figure 4-9. The complete load-displacement response is shown in Figure 4-10.

When the model was loaded first and then heated, the stress-strain curve first follows the ambient temperature material properties curve, as expected. This is seen to happen both within concrete (Figure 4-8) and reinforcement (Figure 4-9). When the model was then heated, the concrete and reinforcement were unable to expand due to restrained boundary conditions, causing an increasing compressive stress in both concrete and steel. It can be seen in Figure 4-8 that the response in concrete to increasing temperature is a vertical line of increasing stress at constant strain due to this boundary condition. However, Figure 4-9

shows that the stress present in reinforcement on heating decreases while at constant strain. This is because the increase in compressive stress caused by heating is overridden by the change in material properties with increasing temperature. At 200°C reinforcing steel has a lower elastic modulus than its ambient value and, since the material must have constant strain due to the boundary condition, the compressive stress must decrease due to the reduction in elastic modulus. The load-displacement curve for this first analysis matches this behaviour (Figure 4-10), with the compressive load increasing and then decreasing as the compressive displacement increases. When heating occurs, the load increases and the displacement remains constant. This is due to the restrained boundary condition not permitting expansion of the model.

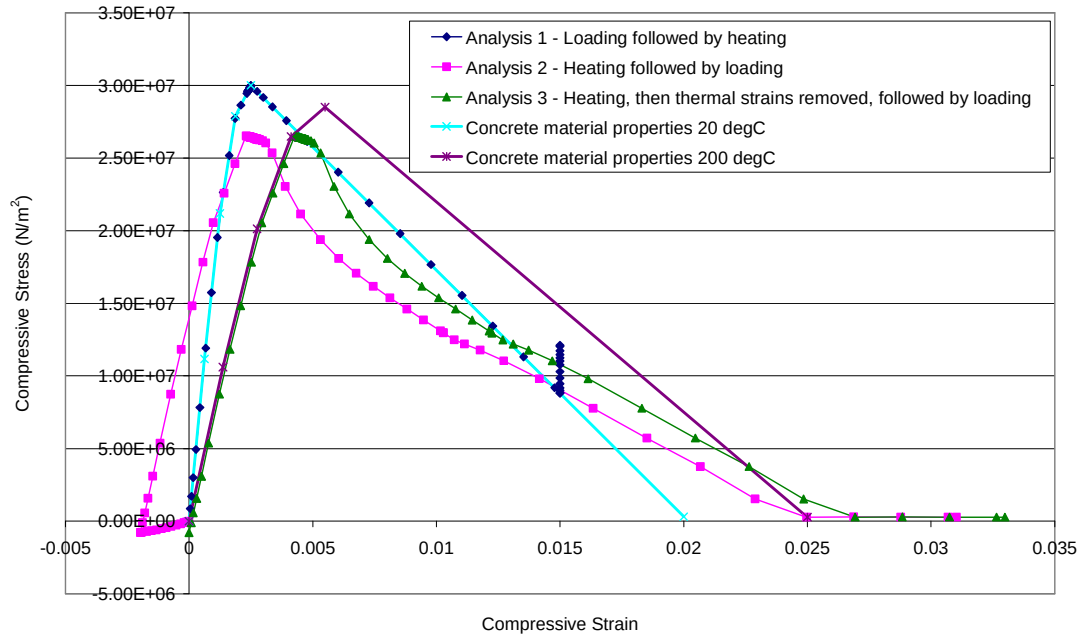

Figure 4-8: Stress-strain for concrete in a one-element RC model with thermal expansion included under compression, compared with concrete material properties, with: (1) The element loaded in compression using a displacement-controlled boundary condition and then heated to 200°C. The model follows the ambient material properties curve during loading, while on being heated the compressive stress increases as expansion is not permitted due to the boundary condition. (2) The element is heated to 200°C with free expansion permitted and then loaded under compression at elevated temperature. This model shows initial tensile stress and strain on heating due to compromise between the differing thermal expansions of concrete and reinforcement – reinforcing steel has a higher coefficient of thermal expansion and expands more than concrete, forcing the concrete into tension. On loading the model follows the shape of the loading branch of concrete's 200°C material properties curve, with strain softening occurring post-peak. (3) The element is heated to 200°C, strains due to thermal expansion are removed, and then the element is loaded under compression. This model follows the 200°C material properties curve up to peak stress, without the offset seen previously caused by thermal strains.

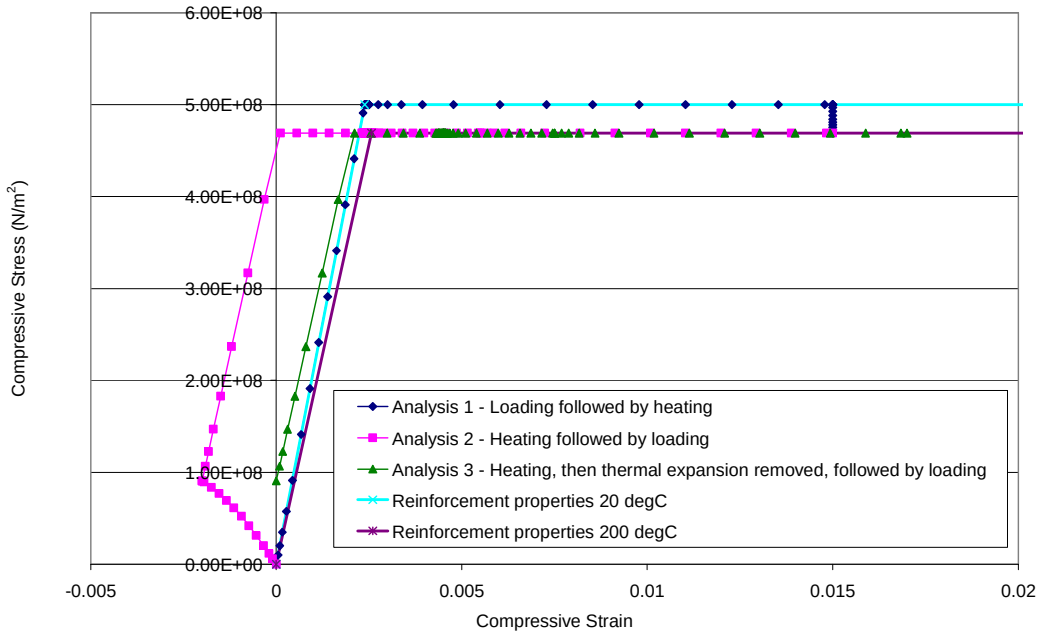

Figure 4-9: Stress-strain for reinforcement in a one-element RC model with thermal expansion included under compression, compared with material properties, with: (1) The element loaded in compression using a displacement-controlled boundary condition and then heated to 200°C. The model follows the ambient material properties curve during loading, while on being heated the compressive stress decreases as the elastic modulus of steel reduces with increasing temperature. (2) The element is heated to 200°C with free expansion permitted and then loaded under compression at elevated temperature. This model shows initial compressive stress and tensile strain on heating due to compromise between the differing thermal expansions of concrete and reinforcement – concrete has a lower coefficient of thermal expansion and expands less than reinforcing steel, forcing the reinforcement into compression. On loading the model follows the shape of the loading branch of steel's 200°C material properties curve. (3) The element is heated to 200°C, strains due to thermal expansion are removed, and then the element is loaded under compression. This model follows the 200°C material properties with a smaller offset than seen previously, but does not follow the curve exactly due to the strains which are removed at the end of the heating phase being a mix of thermal and mechanical (caused by the compromise in expansion between concrete and reinforcement on heating), and not being pure thermal strains.

When the model was heated first (with unrestrained boundary conditions) before being loaded (Figures 4-8, 4-9 and 4-10) it was seen that with increasing

temperature, tensile strains and stresses occur in concrete. In reinforcement, tensile strains are accompanied by compressive stresses. In the heating phase, due to the unrestrained boundary conditions, both steel and concrete experience thermal strains which are tensile in nature. With free expansion permitted, unrestrained heating of plain concrete or steel bars does not cause any stresses, however this is not the case with reinforced concrete. Since concrete has a lower coefficient of thermal expansion than steel it expands less. Due to the bond between concrete and reinforcement, this single element model was forced to have uniform overall expansion. Hence the concrete and reinforcement 'compromised' while expanding, causing tension in the concrete (due to concrete being strained further than it had expanded) and compression in the reinforcement (due to its expansion being restricted by the concrete) at the end of the heating step. Once loading began the concrete experienced compressive stresses and strains as usual. However, during the heating step, the element as a complete model exhibits zero total load while tensile displacement (thermal expansion) occurs, as seen in Figure 4-10. The resultant of the tensile stresses in the concrete and the compressive stresses in the reinforcement is zero. Softening is shown in the load-displacement curve during the loading step, when the load carried reduces with increasing displacement.

In the previous chapters on plain concrete, thermal strains could be directly removed at the end of the heating step. A similar process was attempted in this case, and the strains at the end of the heating step were removed from the stress-strain curves for both steel and concrete. It can be seen from Figures 4-8 and 4-9 that the curves after this strain removal do not match up with the material property curves. The reason for this becomes apparent when one considers that although the strains in steel and concrete at the end of the heating step are caused by thermal expansion, they are not purely thermal strains; the variable expansion between concrete and steel induces mechanical strains as well. It is apparent that this mismatch will be dependent on the reinforcement ratio and other material property parameters.

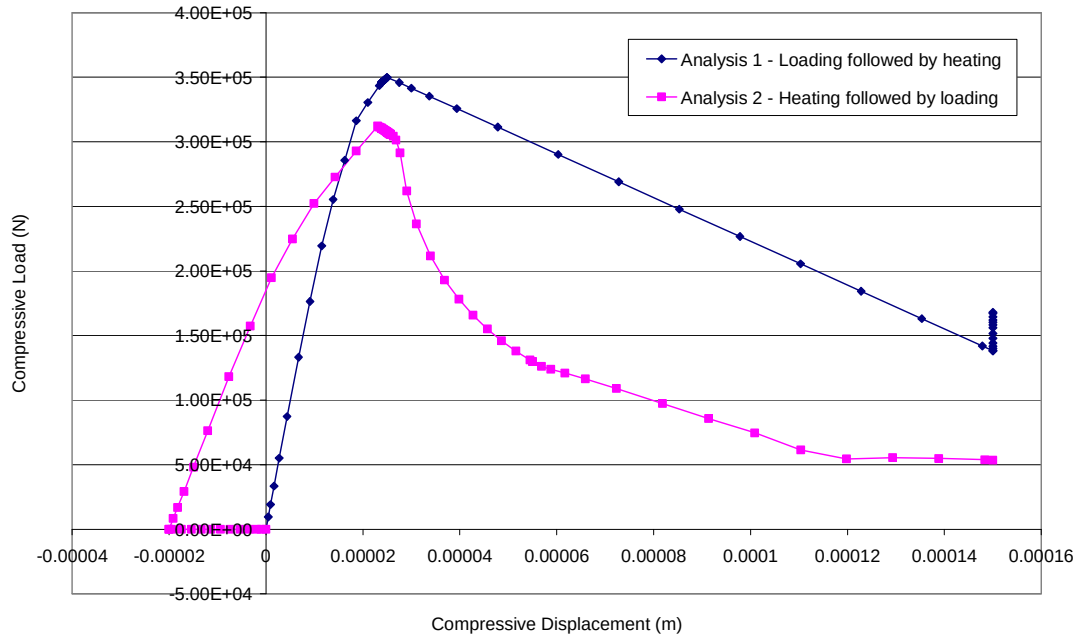

Figure 4-10: Load-displacement for a one-element RC model, with thermal expansion included, under compression when: (1) The element is loaded in compression using a displacement-controlled boundary condition and then heated to 200°C. The model shows typical load-displacement behaviour on loading, while on heating the displacement remains constant due to the boundary condition and the compressive load present increases – thermal stresses due to expansion not being permitted. (2) The element is heated to 200°C while allowed to expand freely and then loaded in compression. Although tensile stresses are seen in the concrete and compressive stresses in the reinforcement during the heating phase, the total load experienced by the model is zero throughout heating while expansion (tensile displacement) occurs.

4.4.2 Behaviour of reinforced concrete at elevated temperatures in tension – tension stiffening ignored

Next the same model was used, but this time the loading applied was tensile. Tension stiffening, discussed previously, was ignored in this analysis and the behaviour of reinforced concrete was assumed to be represented by the plain concrete behaviour with embedded steel reinforcing bars. Once again two analyses were conducted: application of tensile strain followed by heating to 200°C; and heating to 200°C followed by tensile straining. The stresses and

strains found within the concrete and the reinforcement are plotted against the material properties at ambient and 200°C. Figures 4-11 and 4-12 show the stress-strain response for concrete and Figure 4-13 shows the response for reinforcement.

It is seen that the model behaves as expected with the stress-strain of the first analysis following the ambient material properties under loading. Heating the model under restrained conditions causes the stress in the concrete to decrease or become less tensile, and is seen in the graph as a vertical line at constant strain. If heated to high enough temperatures, eventually the stresses present would become zero and then compressive. Similar behaviour is seen in steel as well, in Figure 4-13. The load-displacement response for this analysis (Figure 4-14 and 4-15) shows very clearly the point at which concrete yields. There is then further strain hardening as the load carried by the unyielded reinforcement increases with increasing displacement. The tensile load present decreases and becomes compressive on heating for the same reason as discussed previously.

In the second analysis the unrestrained model was heated first by applying uniformly increasing temperatures up to 200°C to the nodes of the model. Tensile stress and strain in concrete is seen to increase with increasing temperature, while the reinforcement shows an increase in compressive stress and tensile strain. This is due to the differential thermal expansion in concrete and reinforcement, and comes about from the compromise which occurs as described in the previous section. It is interesting to note that the stress-strain response for both steel and concrete is non-linear in the heating phase. This is due to the material properties constantly changing, and the varying levels of compromise. On subsequent loading, an initial elastic response is followed by both constituent materials entering the plastic regime.

During the heating step of this analysis, the load in the element remains zero (Figures 4-14 and 4-15) while the tensile displacement increases due to expansion. In the loading part of the curve, there is again a clear distinction between the first part of the curve when both materials are elastic, and the

second part when concrete has yielded (shown in Figure 4-15). It is noted that this second analysis shows a steeper gradient in the load-displacement graph in comparison to the first analysis. This is due to the concrete having a less steep softening slope at elevated temperature, which dominates the reduced elastic modulus of steel.

Strains at the end of the heating step were removed from the total strains, and compared with the material property curve at 200^{o}C. Once again it can be seen that these lines do not match up. Figure 4-12 shows the elastic behaviour for concrete in greater detail. The reason for this mismatch is, once again, the variable expansion between concrete and steel, which not only induces thermal strains, but also mechanical strains, i.e. the strains at the end of the heating step are not purely thermal.

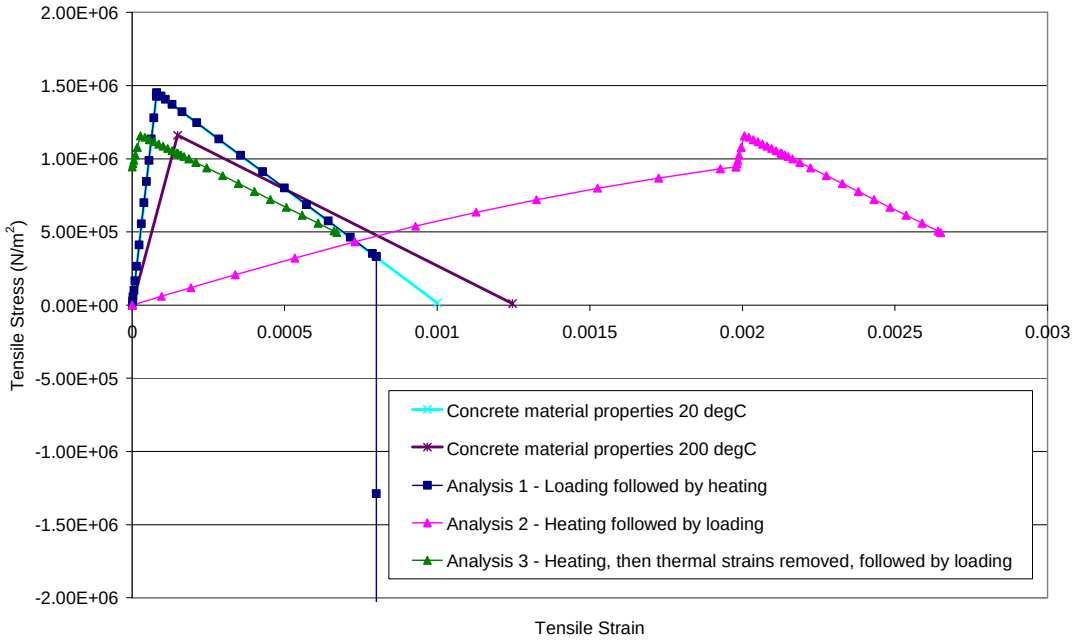

Figure 4-11: Stress-strain for concrete in a one-element RC model with thermal expansion included under tension, compared with concrete material properties, with: (1) The element loaded in tension using a displacement-controlled boundary condition and then heated to 200°C. The model follows the ambient material properties curve during loading, while on being heated the tensile stress decreases (becomes more compressive) as expansion is not permitted due to the boundary condition. (2) The element is heated to 200°C with free expansion permitted and then loaded under tension at elevated temperature. This model shows initial tensile stress and strain on heating as before, due to compromise between the differing thermal expansions of concrete and reinforcement – reinforcing steel has a higher coefficient of thermal expansion and expands more than concrete, forcing the concrete into tension. On loading the model follows the shape of the loading branch of concrete's 200°C material properties curve, with strain softening occurring post-peak. (3) The element is heated to 200°C, strains due to thermal expansion are removed, and then the element is loaded under tension. This model follows the 200°C material properties with less of an offset than was seen previously, but does not follow the curve exactly due to the strains which are removed at the end of the heating phase being a mix of thermal and mechanical (caused by the compromise in expansion between concrete and reinforcement on heating), and not being pure thermal strains.

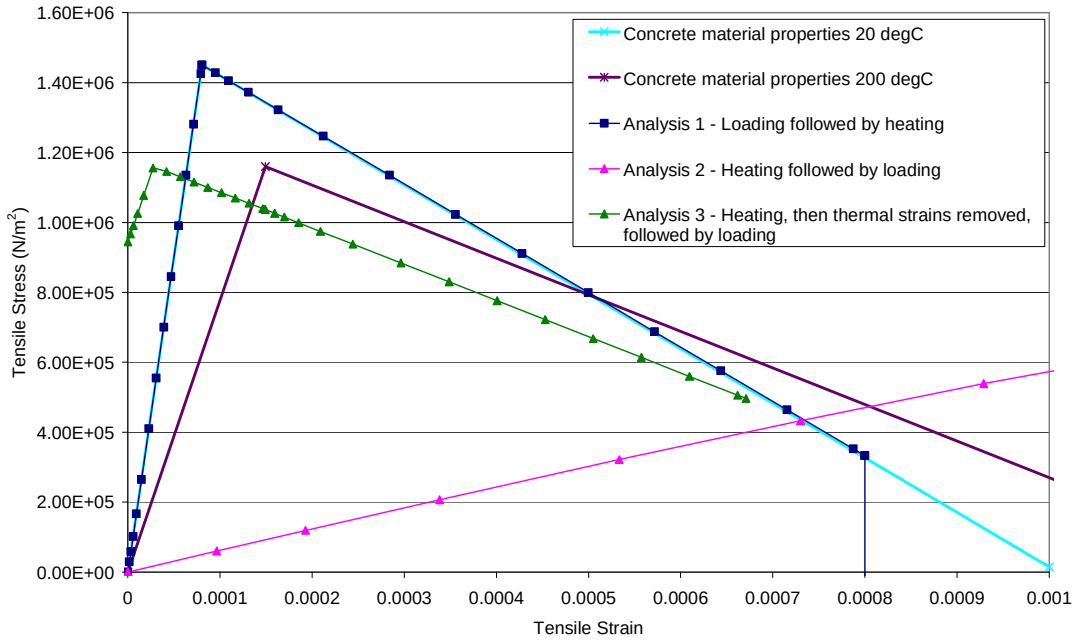

Figure 4-12: Stress-strain for concrete in a one-element model, with thermal expansion included, under tension, compared with material properties of concrete, showing the elastic regime in greater detail.

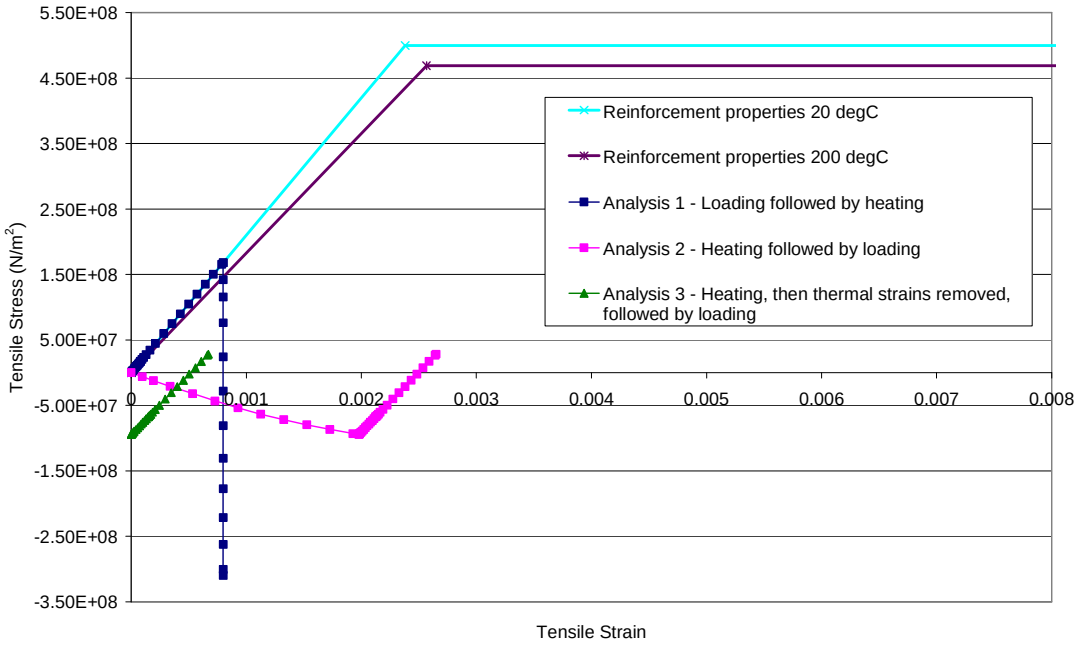

Figure 4-13: Stress-strain for reinforcement in a one-element RC model with thermal expansion included under tension, compared with material properties, with: (1) The element loaded in tension using a displacement-controlled boundary condition and then heated to 200°C. The model follows the ambient material properties curve during loading, while on being heated the tensile stress decreases as the elastic modulus of steel reduces with increasing temperature. Note that the reinforcement remains in the elastic regime throughout the analysis. (2) The element is heated to 200°C with free expansion permitted and then loaded under tension at elevated temperature. This model shows initial compressive stress and tensile strain on heating due to compromise between the differing thermal expansions of concrete and reinforcement – concrete has a lower coefficient of thermal expansion and expands less than reinforcing steel, forcing the reinforcement into compression. On loading the model follows the shape of the loading branch of steel's 200°C material properties curve. (3) The element is heated to 200°C, strains due to thermal expansion are removed, and then the element is loaded under tension. This model follows the 200°C material properties with a smaller offset than seen previously, but does not follow the curve exactly due to the strains which are removed at the end of the heating phase being a mix of thermal and mechanical (caused by the compromise in expansion between concrete and reinforcement on heating), and not being pure thermal strains.

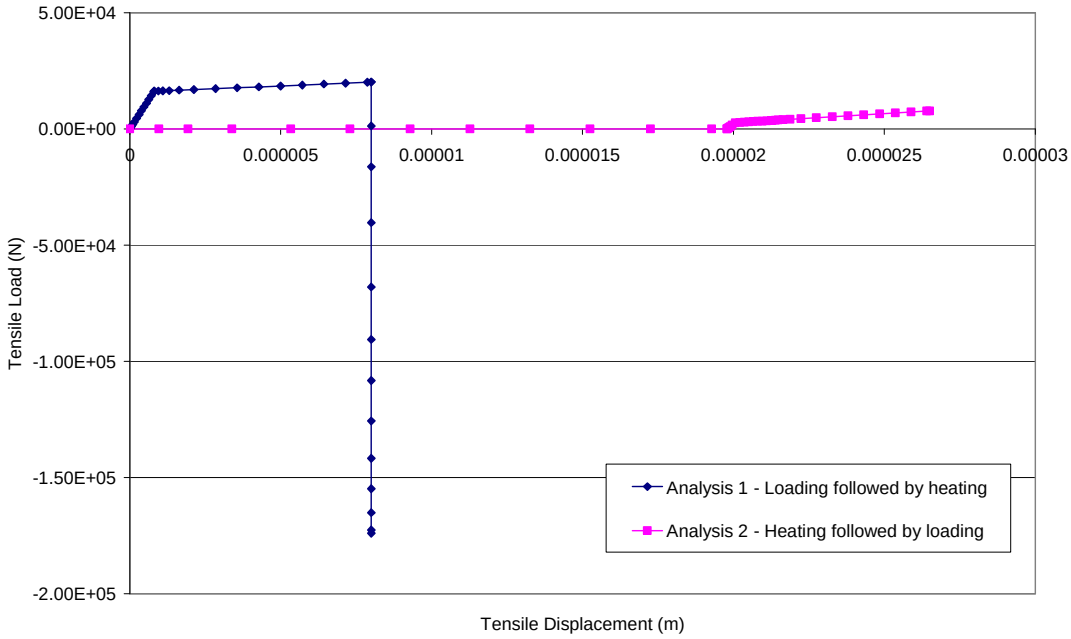

Figure 4-14: Load-displacement for a one-element RC model, with thermal expansion included, under tension when (1) the element is loaded in tension using a displacement-controlled boundary condition and then heated to 200°C, and (2) the element is heated to 200°C with free expansion permitted and then loaded in tension at elevated temperature. The point at which concrete yields is seen very clearly in this graph, with further strain hardening caused by additional load being carried by the unyielded reinforcement.

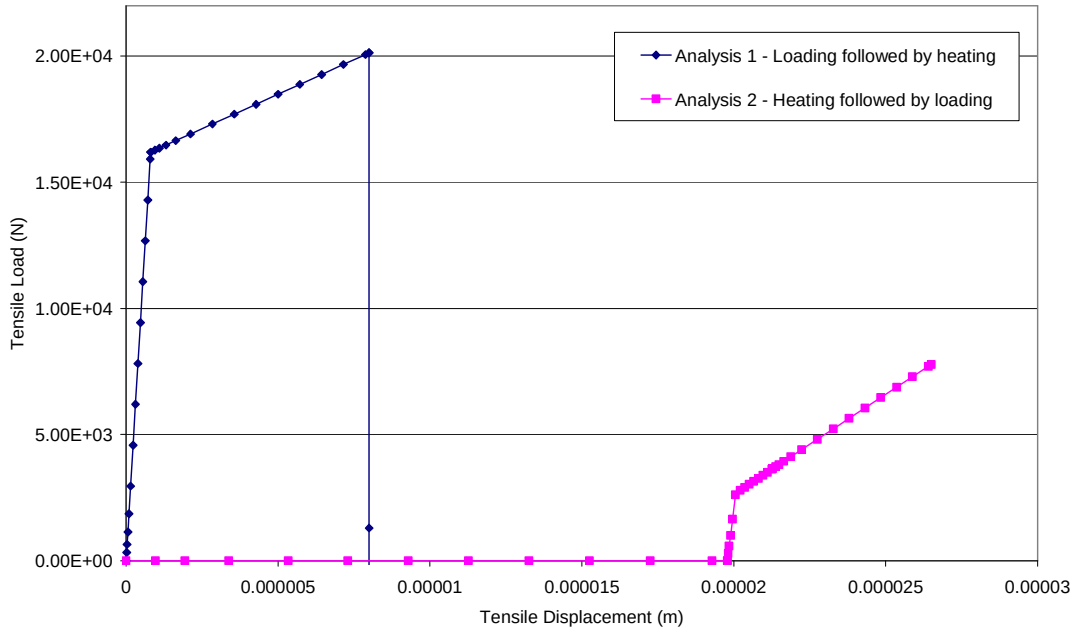

Figure 4-15: Load-displacement for a one-element RC model, with thermal expansion included, under tension when (1) the element is loaded in tension using a displacement-controlled boundary condition and then heated to 200°C, and (2) the element is heated to 200°C with free expansion permitted and then loaded in tension at elevated temperature; with the tensile load section shown in more detail.

4.4.3 Behaviour of reinforced concrete at elevated temperatures in tension – tension stiffening included

Lastly, the same model and analyses as in the previous subsection were used with material properties of concrete altered to include tension stiffening effects.

The model was first tested with the coefficient of thermal expansion set to zero. This ensured that the stress and strain in each material should follow its material properties, and indeed this is what is seen in Figures 4-16 and 4-17.

It is seen that when the model is loaded first, both concrete and reinforcement follow the ambient material properties curves, and then when the loaded model is heated the stress in both materials decreases (or becomes less tensile) at constant strain. This is not due to thermal expansion (or the model being restrained against expansion due to boundary conditions), as the expansion

coefficient here is zero. Instead it is due to the elastic modulus of the material decreasing as the temperature increases. Hence, if the strain is to remain constant (as it must, due to the loading being a displacement-controlled boundary condition) the stress must decrease due to decreasing elastic modulus at elevated temperature. It is noted that at the tensile strains applied, the reinforcement remains elastic throughout these analyses.

Meanwhile, if the model is heated to 200^{o}C first and then loaded, the material follows the 200^{o}C material properties, as expected. As there is no thermal expansion there are no thermal strains present in the model, and the stress and strain in the material remain zero throughout the heating step and there is no offset of the stress-strain curve from the 200^{o}C material properties.

The load-displacement response for these two analyses is seen in Figure 4-18 and 4-19. The tensile load carried increases throughout the analysis, with a change in gradient at the point where the concrete yields. When heating occurs in the first analysis the tensile load present decreases. This is due to the reduction in elastic modulus of both the concrete and reinforcement at elevated temperatures. The second analysis provides a similar curve, as no load or displacement occurs during the heating step, as thermal expansion is zero. The gradient of the curve and the load values reached are lower, due to the reduced elastic modulus and strength of the materials at elevated temperatures.

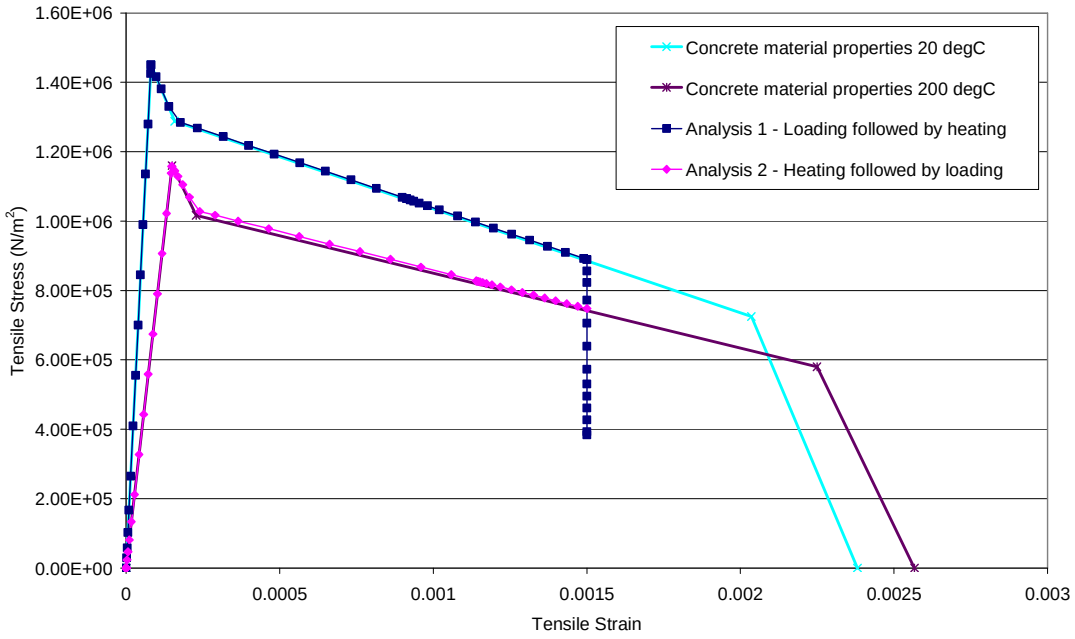

Figure 4-16: Stress-strain for concrete in a one-element RC model with no thermal expansion present, tension stiffening included, under tension, compared with tension stiffening material properties of the concrete material, with: (1) The element loaded in tension using a displacement-controlled boundary condition and then heated to 200°C. The model follows the ambient material properties curve during loading, while on being heated the tensile stress decreases due to the reduction in the elastic modulus with increasing temperature. (2) The element is heated to 200°C with free expansion permitted and then loaded under tension at elevated temperature. As there is no thermal expansion included in this model the stress and strain present remain zero throughout the heating phase. On loading the model follows the shape of the concrete's 200°C material properties curve.

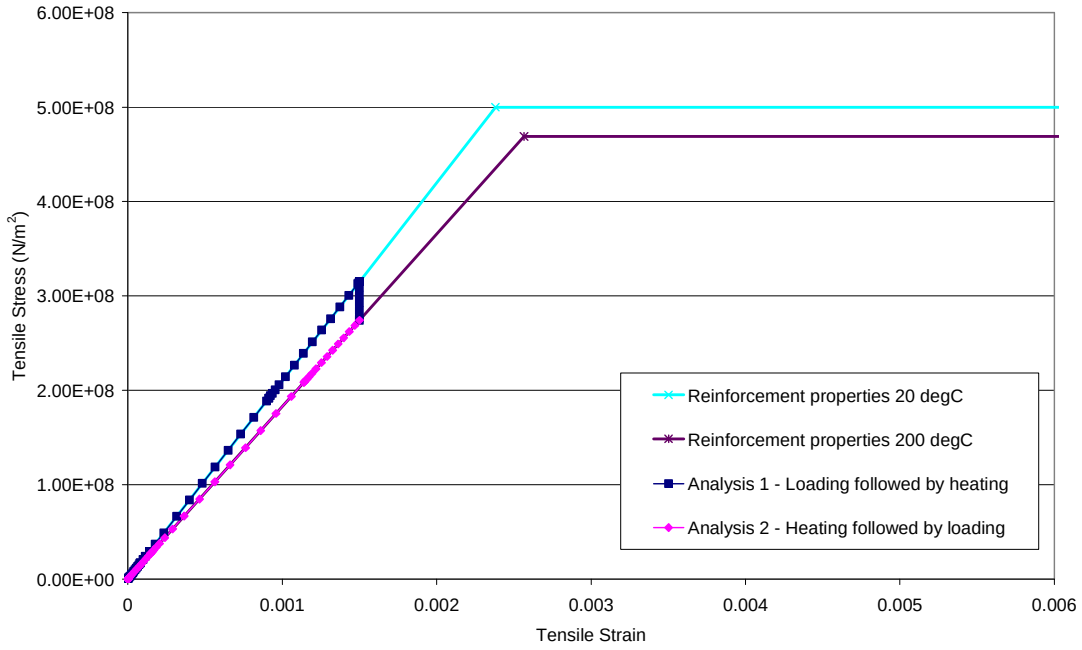

Figure 4-17: Stress-strain for reinforcement in a one-element RC model with no thermal expansion present, tension stiffening included, under tension, compared with steel material properties, with (1) The element loaded in tension using a displacement-controlled boundary condition and then heated to 200°C. The model follows the ambient material properties curve during loading, while on being heated the tensile stress decreases due to the reduction in the elastic modulus with increasing temperature. (2) The element is heated to 200°C with free expansion permitted and then loaded under tension at elevated temperature. As there is no thermal expansion included in this model the stress and strain present remain zero throughout the heating phase. On loading the model follows the shape of the steel's 200°C material properties curve.

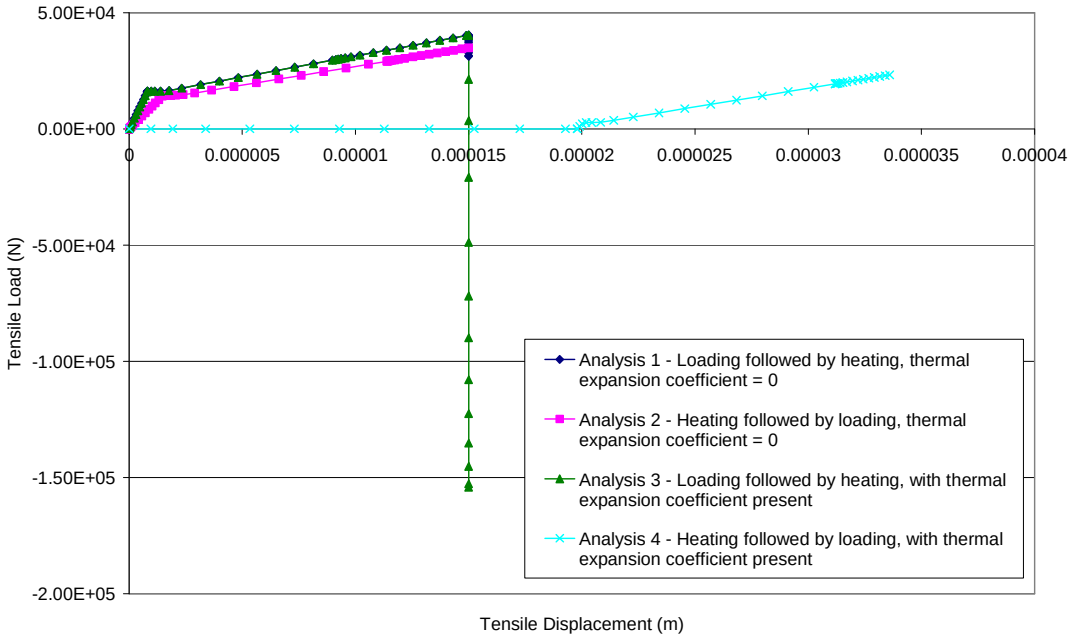

Figure 4-18: Load-displacement for a one-element RC model with tension stiffening included, under tension when (1) The element is loaded in tension using a displacement-controlled boundary condition and then heated to 200°C. There is a change in gradient at the point where the concrete yields, the tensile load carried increases throughout the loading phase as the unyielded reinforcement carries increasing load. On heating, the tensile load present decreases as the elastic modulus of both materials decreases at elevated temperatures. (2) The element is heated to 200°C with free expansion permitted and then loaded under tension at elevated temperature. As there is no thermal expansion included in this model the load and displacement remain zero throughout the heating phase. The gradient of the curve and load values reached on loading are lower here due to the reduced elastic modulus and strength of the materials at elevated temperatures. (3) With thermal expansion included, the element is loaded in tension and then heated to 200°C. This curve follows that seen in analysis (1) throughout loading, however on heating the tensile load carried reduces dramatically and becomes compressive, due to both a reducing elastic modulus and thermal stresses caused by expansion not being permitted. (4) With thermal expansion included, the element is heated to 200°C and then loaded under tension. Throughout the heating phase the load present remains zero while the tensile displacement increases, this is due to the balance between the concrete and reinforcement stresses which appear on heating in a RC element. During loading, the gradient of the curve and the load values reached are lower than in analysis (3), due to the reduced elastic modulus and strength of the materials at elevated temperatures.

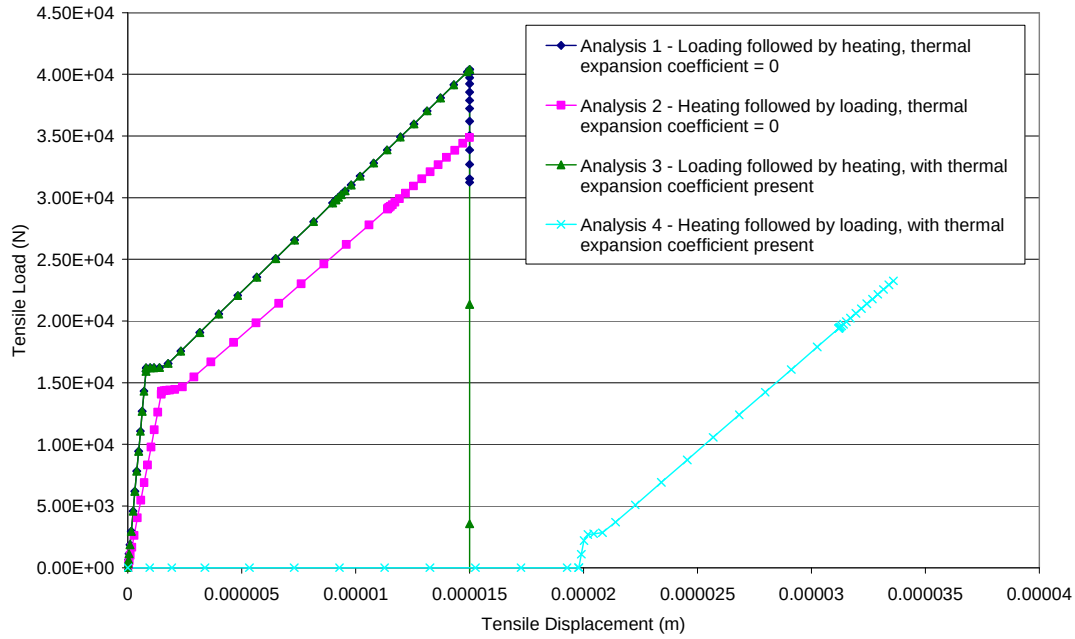

Figure 4-19: Load-displacement for a one-element RC model with tension stiffening included, under tension when: (1) The element is loaded in tension using a displacement-controlled boundary condition and then heated to 200°C; (2) The element is heated to 200°C with free expansion permitted and then loaded under tension at elevated temperature; (3) With thermal expansion included, the element is loaded in tension and then heated to 200°C; (4) With thermal expansion included, the element is heated to 200°C and then loaded under tension; showing the tensile region in more detail.

Finally, the same analyses are carried out with thermal expansion included. The results are seen in Figures 4-20 and 4-21. Similar behaviour to that discussed in the previous section is observed. When the model is loaded before being heated, the stress-strain curve follows the ambient material properties. During heating, expansion is not permitted due to the displacement controlled boundary condition, and hence in both concrete and reinforcement the tensile stress present reduces and becomes compressive with increasing temperature while the strain remains constant. The compression seen in this case is due to two different reasons: firstly, thermal expansion; and secondly, due to lower elastic modulus at elevated temperatures, as was seen in the case with zero thermal expansion.

Meanwhile, when the model is heated first to 200^{o}C, an increase in tensile stress and strain is seen in concrete, while reinforcement shows an increase in compressive stress and tensile strain. This is due to the differential thermal expansion in concrete and reinforcement. Once loading begins, both the concrete and reinforcement stress-strain curves appear to have a shape similar to the 200^{o}C material properties curves. However, on removal of strains at the end of the heating step, it can be seen that the two curves do not match up. The reason, once again, is that at the end of the heating step the strains within the constituent materials are not purely thermal.

The load-displacement response for the analyses which include thermal expansion is seen in Figure 4-18 and 4-19. The third analysis (load then heat, with thermal expansion included) matches the first analysis throughout the loading step, and also shows decreasing tensile load on heating. However when thermal expansion is included the load decreases much more dramatically on heating, becoming compressive. This is due to two factors: the reduction of the elastic modulus at elevated temperatures; and the thermal stresses caused by the boundary condition during heating. The final analysis shows increasing tensile displacement at zero load throughout the heating step. As discussed previously, this is due to the balance between the concrete and reinforcement stresses. During the loading step, the gradient of the curve and the load values reached are lower than in the previous analysis, due to the reduced elastic modulus and strength of the materials at elevated temperatures. It may be recalled that the gradient increased when tension stiffening was ignored (Figure 4-15), but since the softening slope of concrete does not play a major role with the inclusion of tension stiffening, the gradient decreases here.

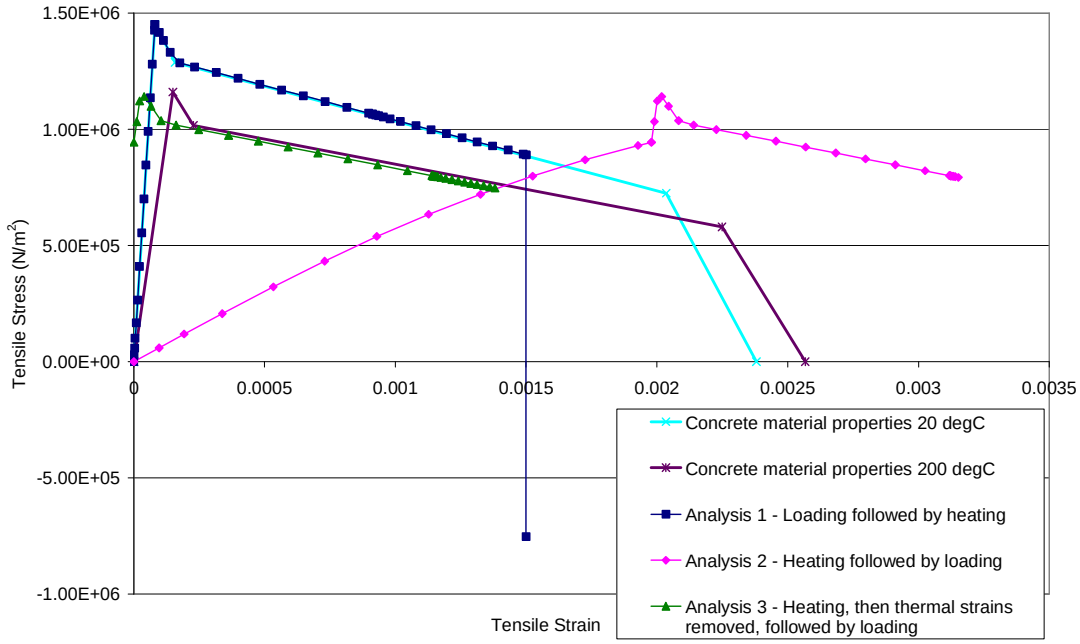

Figure 4-20: Stress-strain for concrete in a one-element RC model, with thermal expansion and tension stiffening included, under tension, compared with tension stiffening material properties of the concrete material, with: (1) The element loaded in tension using a displacement-controlled boundary condition and then heated to 200°C. The model follows the ambient material properties curve during loading, while on being heated the tensile stress decreases due to both the reduction in elastic modulus with increasing temperature, and the thermal stresses caused by expansion not being permitted due to the boundary condition. (2) The element is heated to 200°C with free expansion permitted and then loaded under tension at elevated temperature. This model shows initial tensile stress and strain on heating, due to compromise between the differing thermal expansions of concrete and reinforcement – reinforcing steel has a higher coefficient of thermal expansion and expands more than concrete, forcing the concrete into tension. On loading the model follows the shape of concrete's 200°C material properties curve. (3) The element is heated to 200°C, strains due to thermal expansion are removed, and then the element is loaded under tension. This model follows the 200°C material properties with less of an offset than was seen previously, but does not follow the curve exactly due to the strains which are removed at the end of the heating phase being a mix of thermal and mechanical (caused by the compromise in expansion between concrete and reinforcement on heating), and not being pure thermal strains.

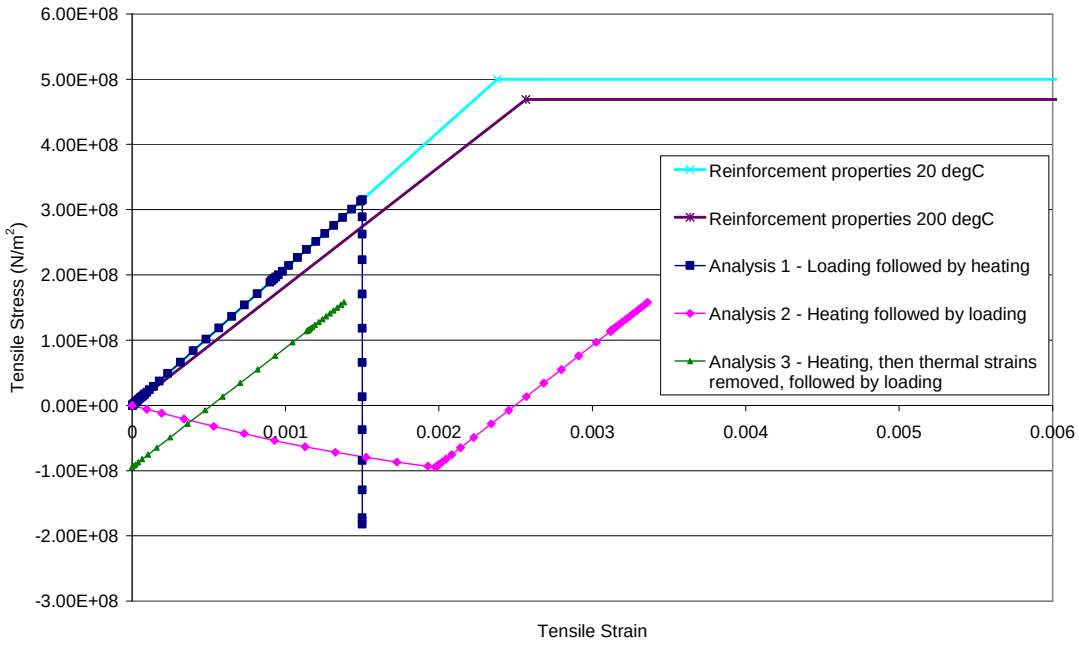

Figure 4-21: Stress-strain for reinforcement in a one-element RC model, with thermal expansion and tension stiffening included, under tension, compared with steel material properties, with (1) The element loaded in tension using a displacement-controlled boundary condition and then heated to 200°C. The model follows the ambient material properties curve during loading, while on being heated the tensile stress decreases as the elastic modulus of steel reduces with increasing temperature and thermal stresses occur due to expansion not being permitted by the boundary condition. Note that the reinforcement remains in the elastic regime throughout the analysis. (2) The element is heated to 200°C with free expansion permitted and then loaded under tension at elevated temperature. This model shows initial compressive stress and tensile strain on heating due to compromise between the differing thermal expansions of concrete and reinforcement – concrete has a lower coefficient of thermal expansion and expands less than reinforcing steel, forcing the reinforcement into compression. On loading the model follows the gradient of the loading branch of steel's 200°C material properties curve. (3) The element is heated to 200°C, strains due to thermal expansion are removed, and then the element is loaded under tension. This model follows the 200°C material properties with a smaller offset than seen previously, but does not follow the curve exactly due to the strains which are removed at the end of the heating phase being a mix of thermal and mechanical (caused by the compromise in expansion between concrete and reinforcement on heating), and not being pure thermal strains.

4.5 References

Barros, M., R. A. F. Martins, et al. (2001). "Tension stiffening model with increasing damage for reinforced concrete." Engineering Computations **18**(5-6): 759-785.

Cervenka, V. and R. Pukl (1990). Computer simulation of anchoring technique in reinforced concrete beams. Computer aided analysis and design of concrete structures. Swansea, Pineridge Press**:** 1-21.

EN1992-1-1 (2004). Eurocode 2: Design of Concrete Structures - Part 1-1: General Rules and Rules for Buildings.

EN1992-1-2 (2004). Eurocode2: Design of Concrete Structures - Part 1-2: General Rules - Structural Fire Design.

Feenstra, P. H. and R. de Borst (1995). "Constitutive Model for Reinforced Concrete." Journal of Engineering Mechanics **121**(5): 587.

Gilbert, R. I. and R. F. Warner (1978). "Tension stiffening in reinforced concrete slabs." Journal of the Structural Division ASCE **104**(2): 1885-1900.

Gupta, A. K. and S. R. Maestrini (1990). "Tension-Stiffness Model for Reinforced Concrete Bars." Journal of Structural Engineering **116**(3): 769-790.

He, W., Y. F. Wu, et al. (2008). "A fracture energy based constitutive model for the analysis of reinforced concrete structures under cyclic loading." Computer Methods in Applied Mechanics and Engineering **197**(51–52): 4745-4762.

Hofstetter, G. and H. A. Mang (1996). "Computational plasticity of reinforced and prestressed concrete structures." Computational Mechanics **17**(4): 242-254.

Kingston, W. G. and P. Pankaj (2012). "Is fracture energy important for finite element modelling of reinforced concrete behaviour in tension." Journal of Engineering Mechanics ASCE **submitted**.

Stramandinoli, R. S. B. and H. L. La Rovere (2008). "An efficient tension-stiffening model for nonlinear analysis of reinforced concrete members." Engineering Structures **30**(7): 2069-2080.

Syroka, E., J. Bobiński, et al. (2011). "FE analysis of reinforced concrete corbels with enhanced continuum models." Finite Elements in Analysis and Design **47**(9): 1066-1078.

5

Residual behaviour of preheated plain and reinforced concrete

5.1 Introduction

It has been established that concrete's material properties alter at elevated temperatures, with its tensile and compressive strength reducing, its elastic modulus decreasing, and its ultimate strain and strain at peak stress increasing

with increasing temperature. However if concrete is heated and then cooled, for example in a fire, does it regain any of its original strength and stiffness? These properties of concrete post-heating and cooling are called 'residual properties.'

Several sets of tests have been carried out in order to characterise these residual properties (Chan et al. 1999; Luo et al. 2000; Nassif 2002; Nassif 2006; Ghandehari et al. 2010). These are mainly compression tests, with only a few involving tensile loading (Chan et al. 1999; Ghandehari et al. 2010). All the samples were heated in electric furnaces, and the peak temperatures tested varied between 217^{o}C and 1200^{o}C. Some tests (Chan et al. 1999; Luo et al. 2000) kept the samples at the maximum test temperature for a specific time – 2 hours, while others (Nassif 2002; Nassif 2006) use the point at which the core of the specimen reaches the same temperature as its surface as the end point of heating. Different cooling regimes are considered – both natural air cooling and quenching water cooling.

Both Chan et al. (1999) and Ghandehari et al. (2010) tested plain concrete samples under compression and tensile loading, after they had been heated and cooled naturally. They provide information on how concrete's compressive and tensile splitting strengths decrease with increasing exposure temperature.

Luo et al. (2000) tested plain concrete cubes under compression only, however they investigated two different cooling methods – cooling naturally at ambient temperatures, and quenching the cubes by cooling them in water. They state that the cooling method does have an effect on the material properties, with water-cooled samples deteriorating more than air-cooled ones. However this effect was less pronounced at higher exposure temperatures.

Nassif (2002; 2006) aimed to capture the complete stress-strain response of plain concrete samples by measuring both the compressive strength and the ultimate strain after heating and cooling cycles. The difference between air-cooled and quenched samples (Nassif 2006) and the effect that a series of five loading and unloading cycles had (Nassif 2002) were considered. It was found that a long

heat exposure (2 hours) caused greater strength and stiffness degradation, while brief water exposure of the heated concrete (5 minutes) also caused large reductions in the stiffness. The ultimate strain was found to increase as the exposure temperature increased, significantly so after 320^{o}C, while the compressive strength decreased with increasing temperature.

Numerical work has been carried out by Hsu and Lin (2008), with a material model for residual properties of concrete and reinforcing steel being given. The finite difference method was used to calculate and model heat transfer through the beam, and the lumped method for the mechanical structural analysis of the element. The model calculated the residual bending moment, shear strength and elastic modulus of the temperature-damaged material. These three values were all found to decrease as the length of time the material was exposed to high temperatures increased.

Finally, some recent experimental tests were carried out by Zaidi et al. (2012) at IIT Roorkee, India as part of the joint UKIERI project between IIT Roorkee and the University of Edinburgh. These were cylindrical compression tests on both plain and reinforced concrete. The data from the tests was used as the basis for comparison with modelling work later in this chapter.

The studies described previously give some indication as to why concrete's material properties change on heating and cooling cycles. Chan et al. (1999) and Nassif (2002) suggest that most strength loss occurs between 400 and 800^{o}C, and is caused by the dehydration of the calcium hydroxide gel in concrete, especially under prolonged thermal exposure. Chan et al. also report that concrete loses its tensile splitting strength more sharply than its compressive strength. Below 600^{o}C they suggest that a 'microstructure coarsening effect' which causes changes to the pore structure of concrete causes most strength loss.

An increase in porosity leads to strength degradation, according to Luo et al. (2000), with water cooling affecting porosity more than furnace cooling. Nassif

(2002) agrees with this, suggesting that quenching with water causes a sudden reversed thermal profile, which causes damage to concrete.

This study considers a simple hypothesis: the strength degradation of concrete under heating is caused solely by thermal gradients which cause differential expansion and occur in the material during the heating regime. It is further hypothesised that during heating and cooling phases irreversible damage occurs in concrete specimens which leads to strength degradation. This damage is caused by the stress fields associated with large thermal gradients - due to the low conductivity of concrete, thermal gradients will always exist. Differential expansion of concrete and steel due to their differing thermal expansion coefficients also causes large variations in stress, and damage to the concrete-reinforcement bond. The effect of differential thermal expansion and subsequent differential thermal contraction can only be minimised if the rate of heating / cooling is extremely slow.

A series of computational models were created and analysed to test these hypotheses against experimental tests.

5.2 Experimental tests

Results were made available from the experimental tests carried out at IIT Roorkee as part of a joint research initiative (Zaidi et al. 2012). Forty-two short concrete columns were cast and tested, 21 of which were plain concrete (CAN series of tests) and 21 of which were reinforced concrete (CBN series of tests). They were all cylindrical columns, with diameter 150mm and height 450mm. The cylinders were tested in groups of three after 90 days of ageing (which includes 28 days of curing), and underwent a single heating and cooling cycle. Each group was heated to a prescribed temperature in a furnace with the furnace temperature rising at a rate of 5^{o}C/min. The maximum furnace temperature was held constant for 4.5 hours before cooling occurred. Each cylinder was tested under monotonic compression. Thermocouples cast into the

cylinders recorded the temperature at the surface, at the depth of the reinforcement (if present), and at the centre of each cylinder for the full duration of the experiment including cooling. There was no difference in the testing regime used for unreinforced (CAN) and reinforced (CBN) specimens. The details of the samples tested are shown in Figure 5-1. The thermocouple data was used to plot temperatures with time throughout the experiment. A sample set of temperature data is shown in Figure 5-2.

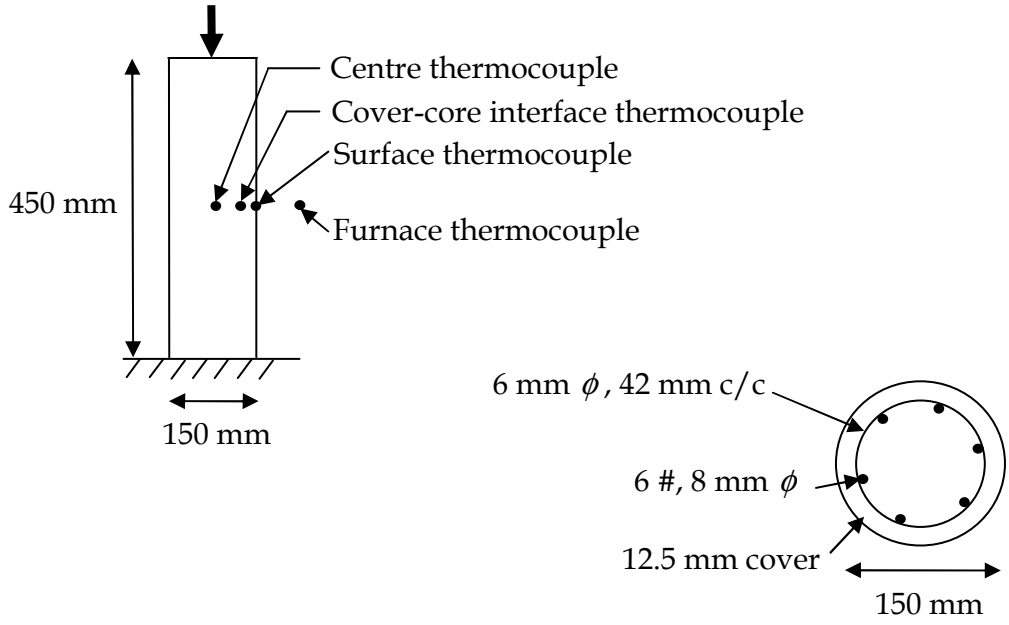

Figure 5-1: Information of the cylinders tested, with location of thermocouples and reinforcement in reinforced concrete specimens

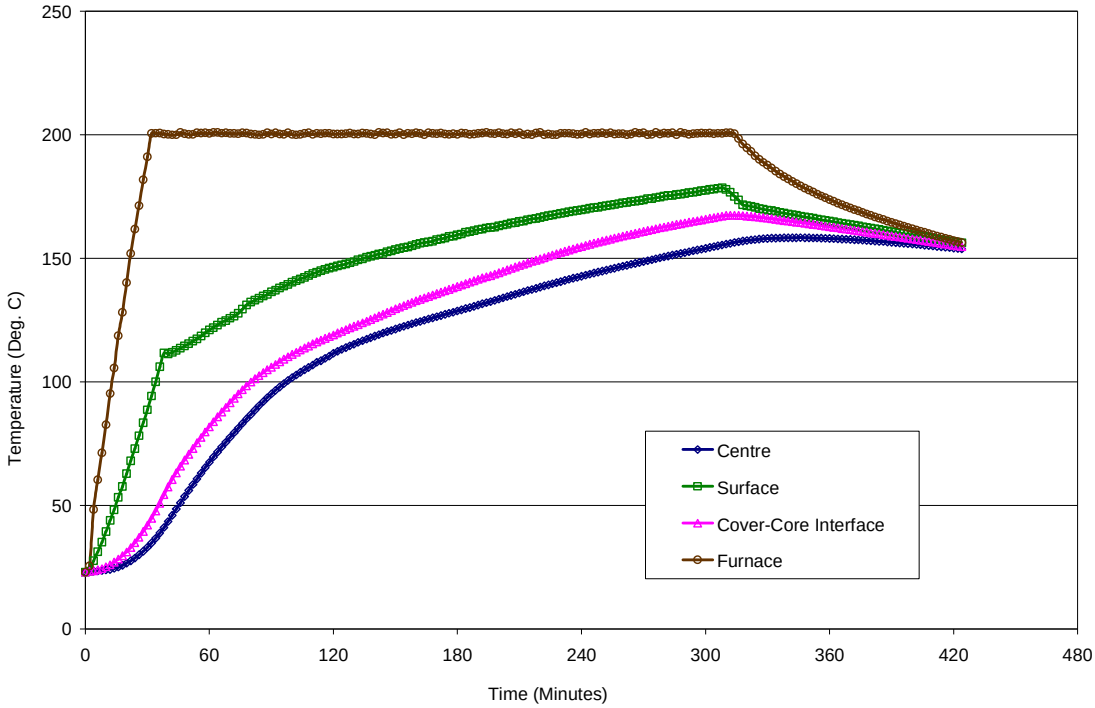

Figure 5-2: Temperature readings from thermocouples located in a sample heated to 200°C

The vertical displacement of the cylinders when loaded in compression was measured by taking the average of two linear variable displacement transducers (LVDTs), placed with gauge length of 200mm on either side of the cylinders. Specimen nomenclature and the key results from both plain and reinforced concrete specimens are given in Table 5-1. The stress-strain behaviour for plain concrete cylinders is shown in Figure 5-3 and that for reinforced concrete in Figure 5-4. It can be seen that the residual response is somewhat akin to the response at elevated temperatures, as it shows a reduced elastic modulus, reduced peak stress, increased peak strain and increased ultimate strain, even after the samples have been cooled.

Table 5-1: Results of unreinforced (CAN) and reinforced (CBN) concrete specimens

Specimen Name	Exposed Temperatures (°C)	Peak Load (kN)	Strain at Peak Stress
CAN	Ambient	694	0.00215
CA2N	200	721	0.00203
CA3N	300	723	0.00253
CA4N	400	689	0.0033
CA5N	500	599	0.0049
CA6N	600	323	0.0080
CBN	Ambient	906	0.0101
CB2N	200	929	0.0101
CB3N	300	912	0.0102
CB4N	400	865	0.0101
CB5N	500	821	0.0138
CB6N	600	668	0.0210
CB8N	800	401	0.0259

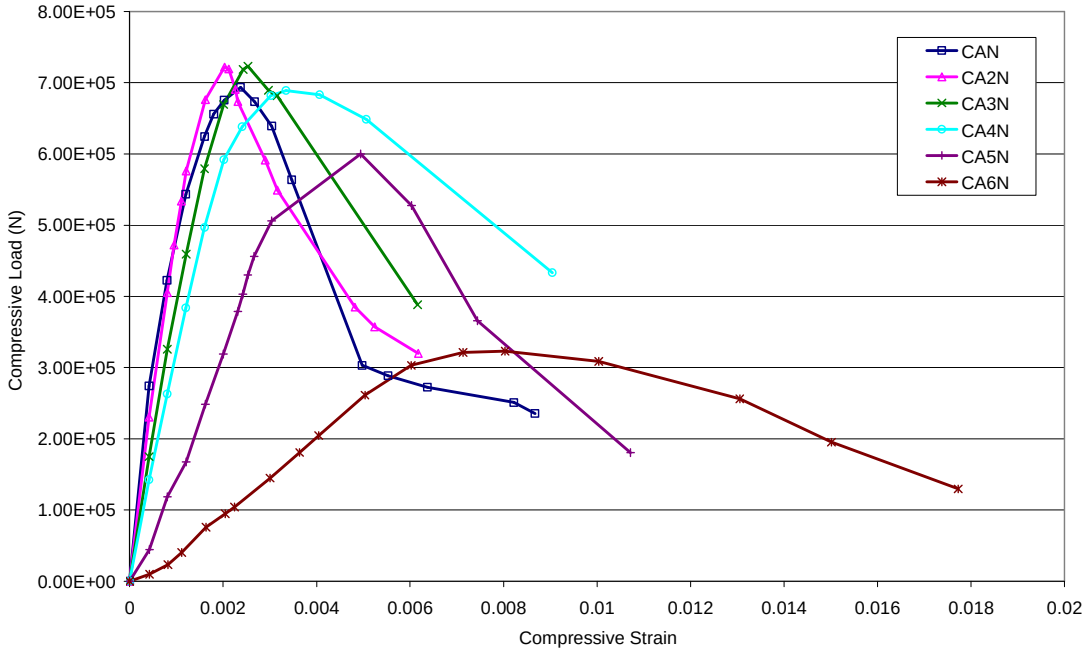

Figure 5-3: Test data for plain concrete cylinders which are heated to various exposure temperatures before being subjected to compression loading

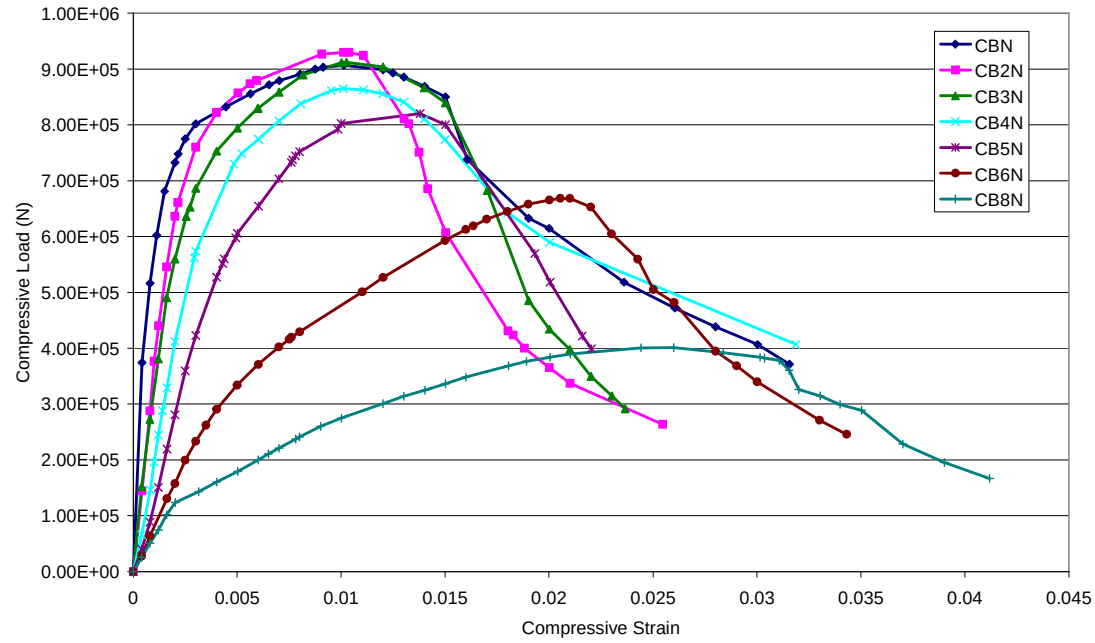

Figure 5-4: Test data for reinforced concrete cylinders which are heated to various exposure temperatures before being subjected to compression loading

5.3 Finite element modelling

The experimental tests discussed in the previous section were computationally simulated using an axisymmetric analysis (Figure 5-5). Only half the height of the cylinder was modelled (225 mm), with a boundary condition at the model's base being used to replicate the presence of the other half. Loading was applied by using a displacement controlled boundary condition on the nodes of the top surface.

Throughout these analyses, the concrete damaged plasticity model was used. An elastic-perfectly plastic anisotropic material model was used for the reinforcing steel, and tension stiffening properties were included in the concrete material model. More information on the material models used is given in the following sections.

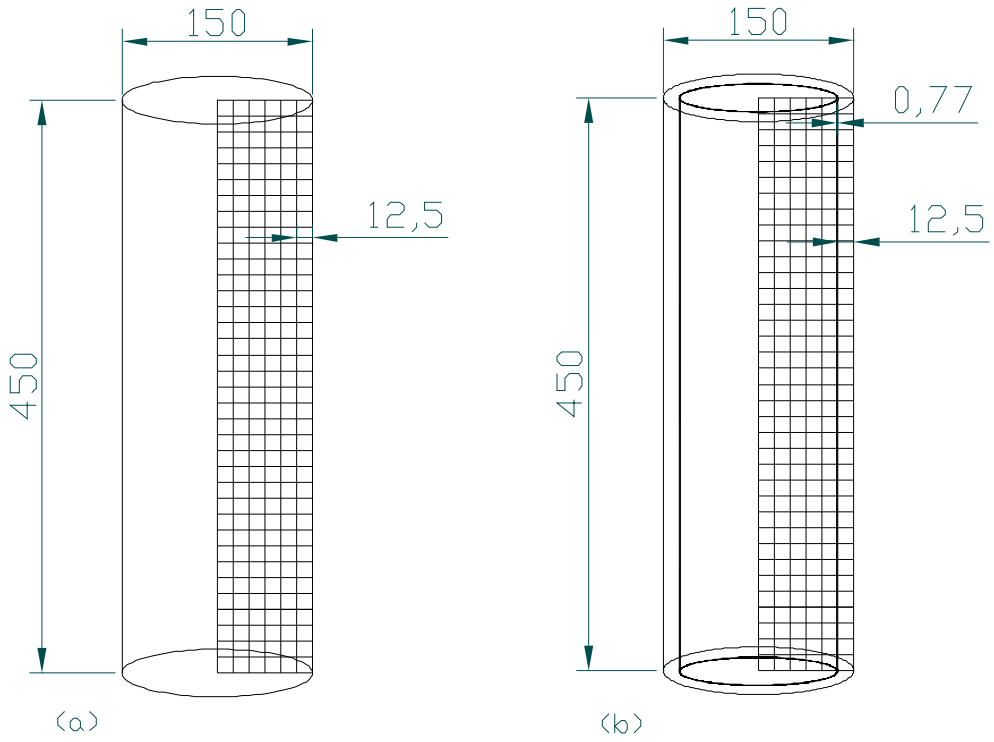

Figure 5-5: Diagram of the concrete cylinders tested, dimensions given in mm, and the FE mesh used to model them showing (a) the plain concrete cylinder, and (b) the reinforced concrete cylinder

In the experimental tests the cylinders were exposed to elevated temperatures in a furnace for at least 5 hours (for the 200°C test). Thermocouples gave the temperature at three points within the samples (at the surface, at the cover-core interface and at the centre); this data was used to subject the models to elevated temperatures. It was also used for the subsequent cooling phase. The surface temperatures and cover-core temperatures were used for the external and internal nodes of the column of elements at the cylinder's surface. The centre temperatures were applied to the row of nodes at the cylinder's centre, and the values for the centre and cover-core thermocouples were linearly interpolated to determine the temperature of each column of nodes within the cylinder (nodes at a similar distance from the surface of the model). The temperatures were then applied directly to the nodes of the model in steps (see Figure 5-6), with each step representing a 50 minute interval, i.e. Step 1 represents the ramping up of temperature from the beginning of the test to 50 minutes into the test, and so on. This number of steps keeps the thermal gradient realistic (much larger in the outer layer of elements than within the cylinder's core) while also keeping the number of steps needed in the analysis reasonable.

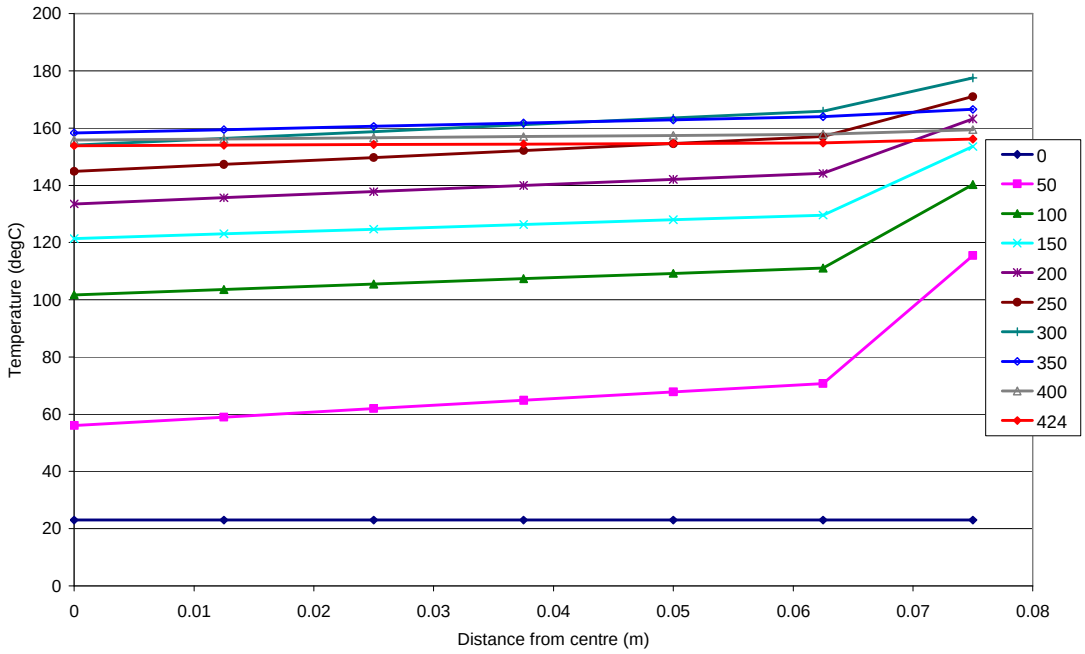

Figure 5-6: Temperatures applied to the nodes of the FE model at various times throughout the 200°C analysis, the legend shows the time elapsed in the test in minutes

It was shown in chapter 2 that square elements are preferable in finite element models, and so a mesh made up of 36 by 6 elements, of side length 12.5mm, were used for the plain concrete analyses. The mesh is shown in Figure 5-5. When the reinforced concrete specimens were modelled the reinforcing bars needed to be included. As axisymmetric elements were being used to model a plane within the cylinder, the reinforcing bars could not be included discretely. Either a full 3D solid model would be required, or the reinforcement would have to be represented in the plane modelled. The second method was used, and carried out by including a thin hollow cylinder of steel material at the level of reinforcement in the model. The hollow cylinder had the same volume as the total volume of reinforcing bars used in the tests. The steel was assigned anisotropic material properties to replicate the vertical and hoop reinforcement bars present in the specimens tested, and to ensure that in the radial direction the steel did not provide a confining behaviour to the concrete that was not present in the experiments.

The thermal expansion coefficient in both concrete and reinforcing steel was assumed to remain constant at elevated temperatures, with the coefficient for concrete α_c = 9.288x10^{-6} /^{o}C, and the coefficient for steel α_s = 1.248x10^{-5} /^{o}C.

5.3.1 Plain concrete

Generalised Eurocode properties (EN1992-1-1 2004; EN1992-1-2 2004) are used as the basis of the concrete material model in the plain concrete analyses. Considering the plain concrete experimental data (Table 5-1 and Figure 5-3), it was seen that the stress-strain constitutive curve was similar for cylinders exposed to ambient, 200 and 300^{o}C temperatures. Therefore all three of these curves were used to determine the initial, ambient concrete material properties. It was seen that the concrete used was of approximate compressive strength of 40.8 MPa, and hence the Eurocode material curve was altered to give a maximum compressive strength of 40.8 MPa at ambient temperatures. Peak stress was seen at an average strain of 0.0025, and hence this value was used in the material's ascending branch (this value is the same as the one used by the Eurocodes, and hence the Eurocode criteria was used to shape the ascending branch). Interpolation of the descending branches of these three curves was used to estimate the ultimate strain of the concrete. A value of 0.01 was used, and again this was inserted into the modified Eurocode material curve to give complete stress-strain behaviour (the original Eurocode value was 0.02, and this value needed to be halved to give material properties matching the test data). The resulting ambient stress-strain curve can be seen in Figure 5-7.

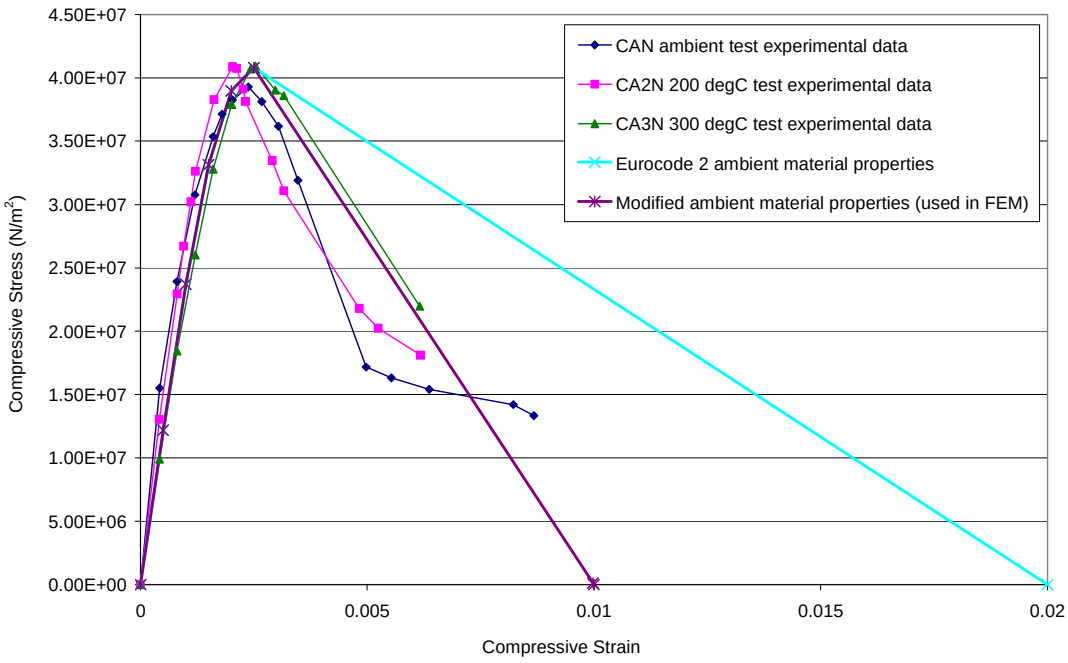

Figure 5-7: Stress-strain data for ambient, 200 and 300°C experimental tests on plain concrete (CAN, CA2N, CA3N), a stress-strain curve at ambient temperature based on the Eurocode properties (EN1992-1-2 2004), and the resulting changed ambient temperature material properties used in FE modelling

It was assumed that the concrete material properties changed and decayed with increasing temperatures in the same way that has been remarked upon in earlier chapters (generally based on Eurocode assumptions). From this behaviour, a full set of stress-strain curves at increasing temperatures was developed and used in computational modelling (Figure 5-8).

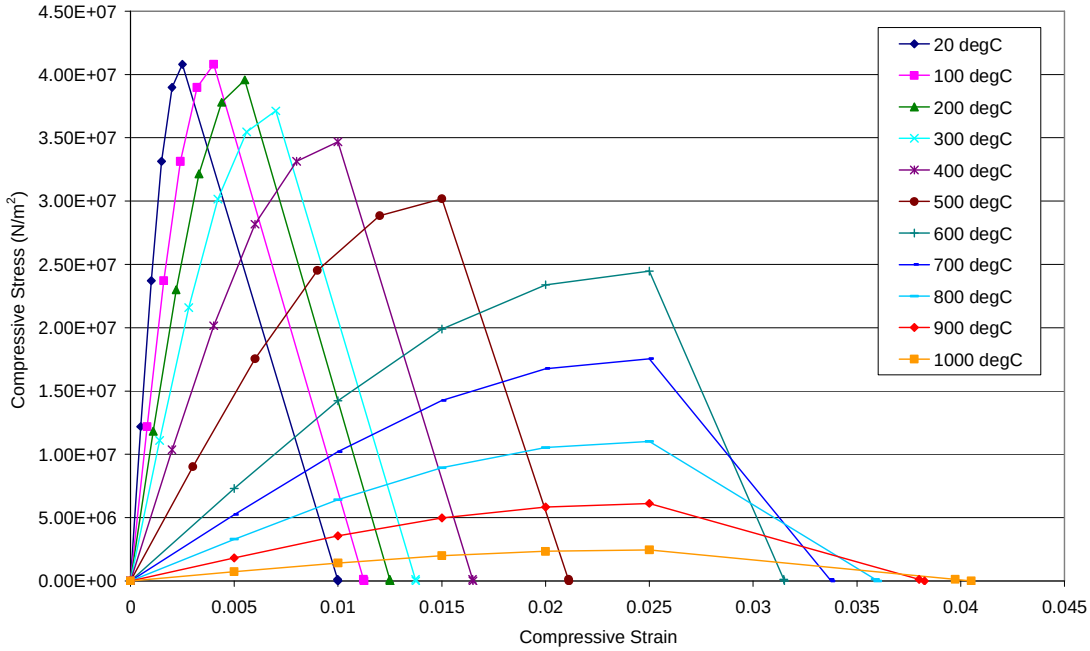

Figure 5-8: Compressive material properties used for plain concrete in FE modelling at elevated temperatures

As no direct tension experimental tests were carried out on the cylinders, there were no results on which to base the tensile material properties to be used for plain concrete in these models. A standard linearly increasing and decreasing model with a fracture energy of 100 N/m and an ambient tensile strength of 1.45 MPa similar to that used in previous modelling work was used, and stress-strain properties calculated using an element size of 225 mm (half of the cylinder height). The tensile strength was assumed to decrease at elevated temperatures, in line with the Eurocodes, while the fracture energy used was constant throughout. Stress-strain curves for these properties can be seen in Figure 5-9.

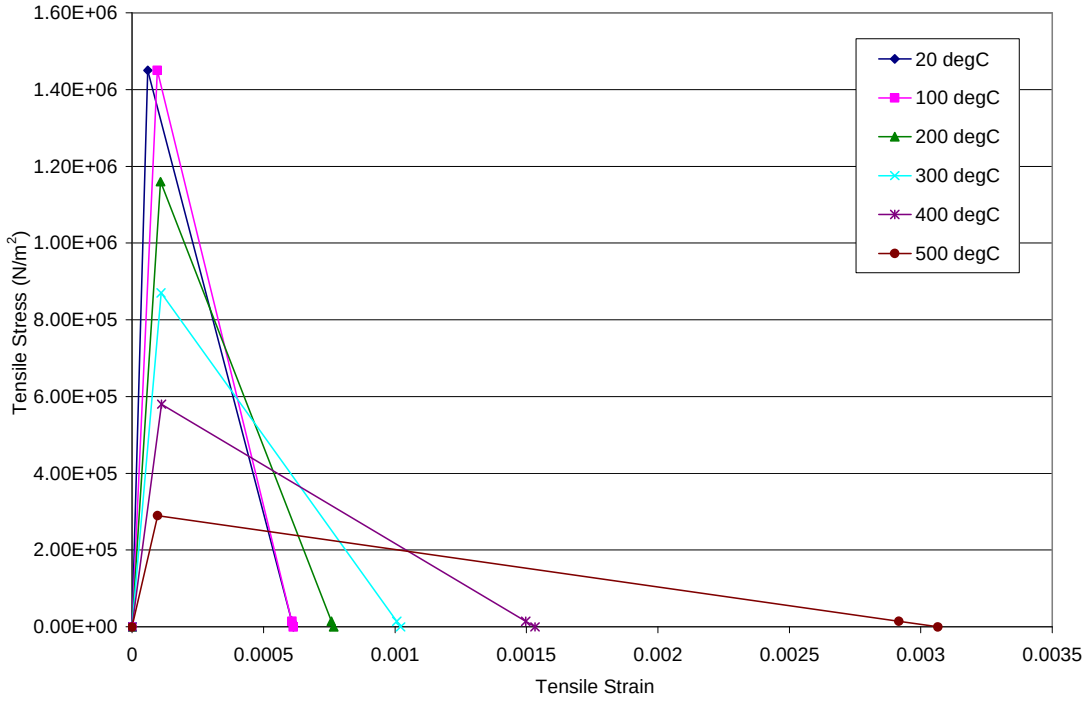

Figure 5-9: Tensile material properties for plain concrete, tensile strength decreases with increasing temperature, while the fracture energy used is a constant 100 Nm throughout

An important aspect to consider was how much of the material's strength and stiffness was recovered on being cooled after heating. Stiffness degradation was considered through damage variable d_t in tension $(0 \le d_t \le 1)$, and d_c in compression $(0 \le d_c \le 1)$. In these a value of 1 indicates complete loss of stiffness, while zero indicates no stiffness loss.

Upon unloading, some of this stiffness degradation can be recovered (e.g. due to crack closure). Two variables which can be used within these damage parameters are tension recovery w_t and compression recovery w_c. They define the stiffness recovery value in both tension and compression, and range from 1.0 (full stiffness recovery) to 0.0 (no stiffness recovery).

The damage and recovery variables determine the proportion of the stiffness which is recovered by the material on unloading, leading to material properties becoming dependent on the amount of load applied prior to unloading. Upon

heating, the loading or unloading may occur due to differential thermal expansion within concrete.

The damage variables in this study are assumed to be zero at zero plastic strain (i.e. no degradation of the material properties), 0.9 at ultimate plastic strain (i.e. the material has only 10% of its original stiffness), and linearly increasing between these values. Given that the stress-strain relationships are defined up to ultimate strain values at zero stress, these damage variables are among the most extreme that could be used. They were chosen to give a worst-case scenario for the concrete material in the models. An example plot of the stress-strain curves for concrete in compression at 600°C is shown in Figure 5-10 for different values of compression damage d_c. With respect to the damage recovery variables, w_c and w_t, a range of values was considered and are discussed alongside the problems analysed.

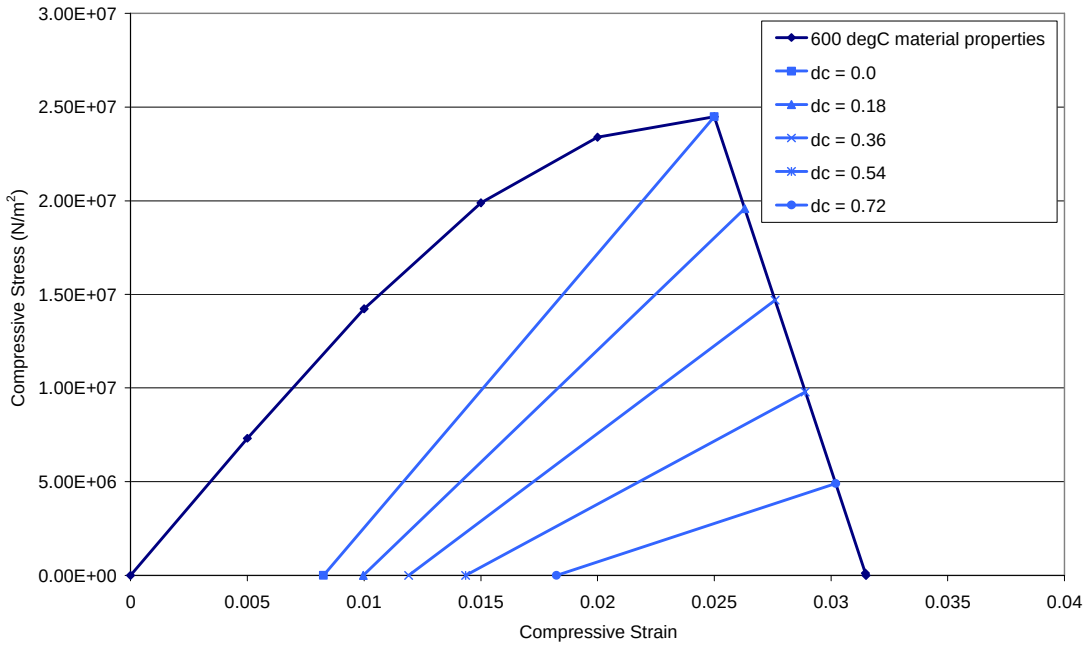

Figure 5-10: Stress-strain curve for concrete under compression at 600°C, incorporating linearly increasing damage variables present after peak-stress

5.3.2 Reinforced concrete

For the reinforced concrete analyses the concrete material model used was modified in tension to include tension stiffening behaviour, discussed in the last chapter. Even though the samples were tested only under compressive loading, tensile forces will arise within concrete due to differential thermal expansion (within concrete and between reinforcement and concrete). Tension stiffening was incorporated using the model described by Gupta and Maestrini (1990). Typical tensile concrete properties including tension stiffening are shown in Figure 5-11 for temperatures from 0°C to 500°C.

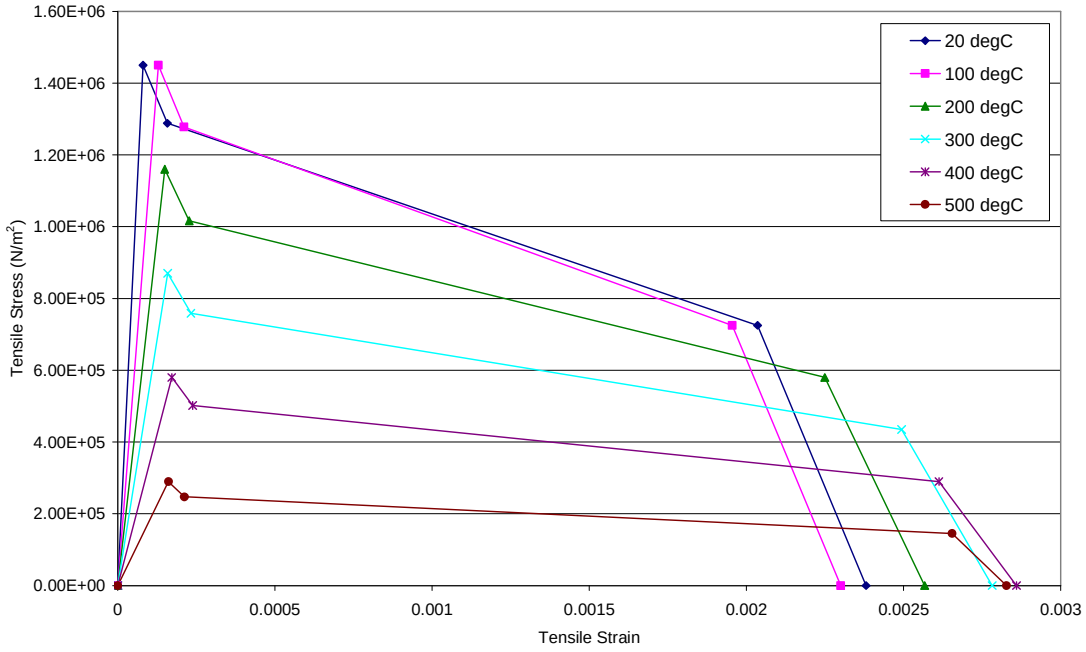

Figure 5-11: Concrete material properties incorporating the effects of tension stiffening

An elastic-perfectly plastic material model was used for the reinforcing steel included in the model. The strength of steel used in the experimental tests was 650 MPa. The strength and stiffness of reinforcement was assumed to decrease with increasing temperature at the same rate as discussed in the last chapter. Complete stress-strain graphs for reinforcement are seen in Figure 5-12.

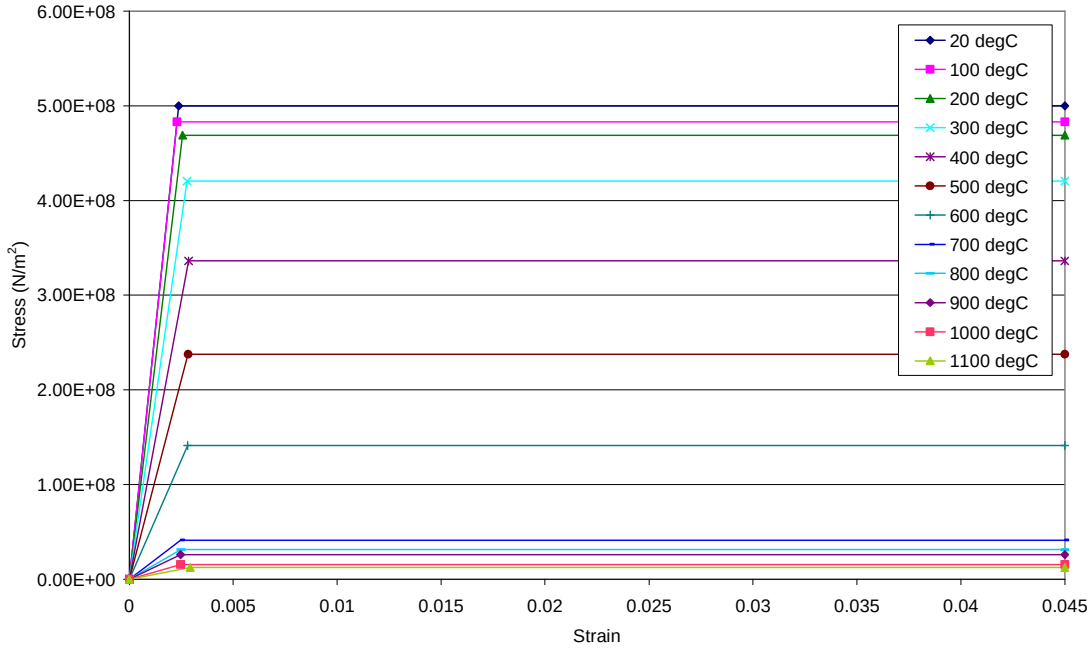

Figure 5-12: Reinforcing steel material properties at elevated temperatures

5.4 Comparison of numerical and experimental results

5.4.1 Plain concrete

As stated previously the plain concrete cylinders were modelled in Abaqus using axisymmetric elements, with mesh size of 10 x 10 mm. The concrete damaged plasticity model was used for the concrete, and the cylinder was heated by applying temperatures directly to the nodes of the elements. The cylinder was heated to the temperatures measured in the test, then cooled to ambient temperatures (following the temperatures from the thermocouple data) and finally tested under compression by using displacement controlled loading.

Initially the cylinder model was used to verify the concrete material properties and to ensure that the model was working as predicted. First the cylinder was heated to 600^{o}C uniformly and, while at that temperature, tested under compression. The cylinder was then unloaded, while still at the test temperature. It was seen that the model followed the stress-strain curve exactly when the damage variables were set to zero. However once damage was included (the

material's stiffness changed on unloading) the stress-strain curve deviated from the material properties after the ultimate compressive stress had been reached (see Figure 5-13). This deviation is due to decreased stiffness which, in conjunction with the elastic strain, defines the stress at the post-yield state. Post-peak stiffness degradation leads to considerably increased elastic strains, which in turn implies higher stresses.

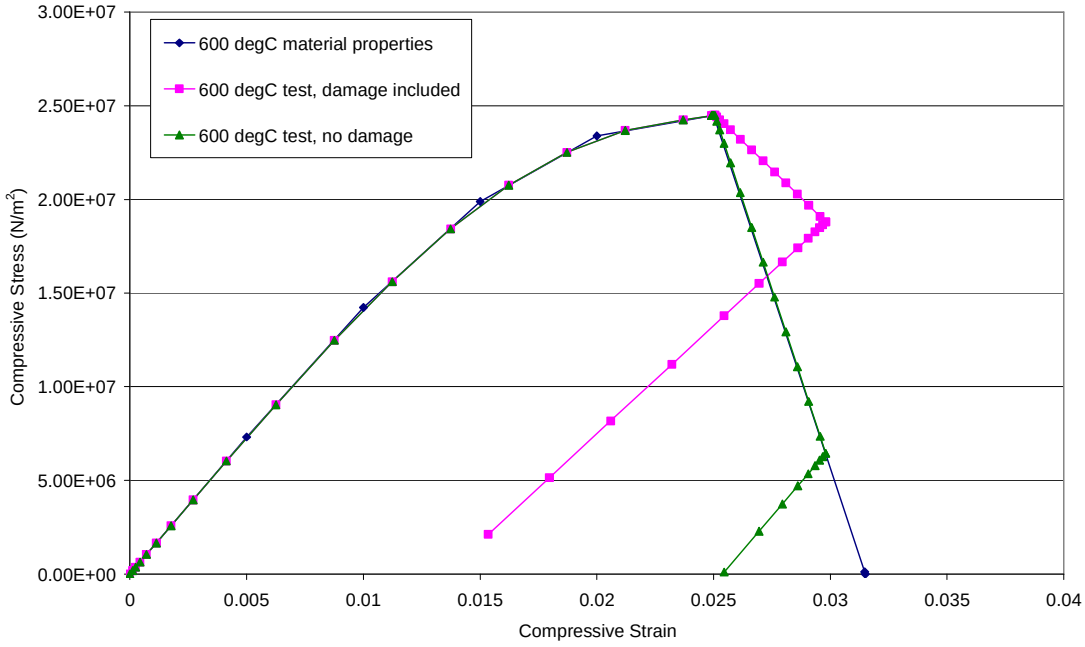

Figure 5-13: Concrete compressive material properties at 600°C, compared with the plain concrete cylinder under compressive loading at 600°C when damage variables are included and not included. The model follows the material properties when no damage is present, however it deviates in the post-peak regime when damage is included. It is seen that the unloading branch of the damage included model has a less steep gradient than the loading branch, due to the damage variables having reduced the elastic modulus.

However, if the stress was plotted against the plastic strains, then both models (with and without damage) followed the stress-inelastic strain curve throughout. At equal total strain, the plastic strain was lower in the damaged model (as expected), and hence it followed the material's descending branch exactly (see Figure 5-14).

Similar behaviour was seen under tensile loading, as demonstrated in Figure 5-15.

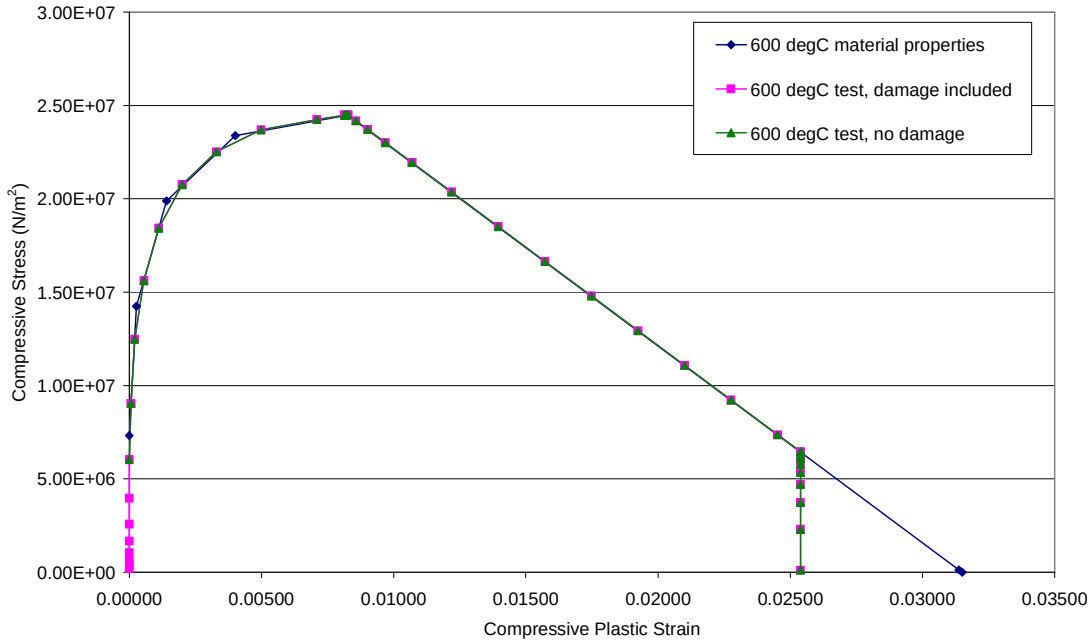

Figure 5-14: Inelastic compressive material properties at 600°C, compared with results for the plain concrete cylinder when damage variables are both included and not included. Both models follow the material properties curve.

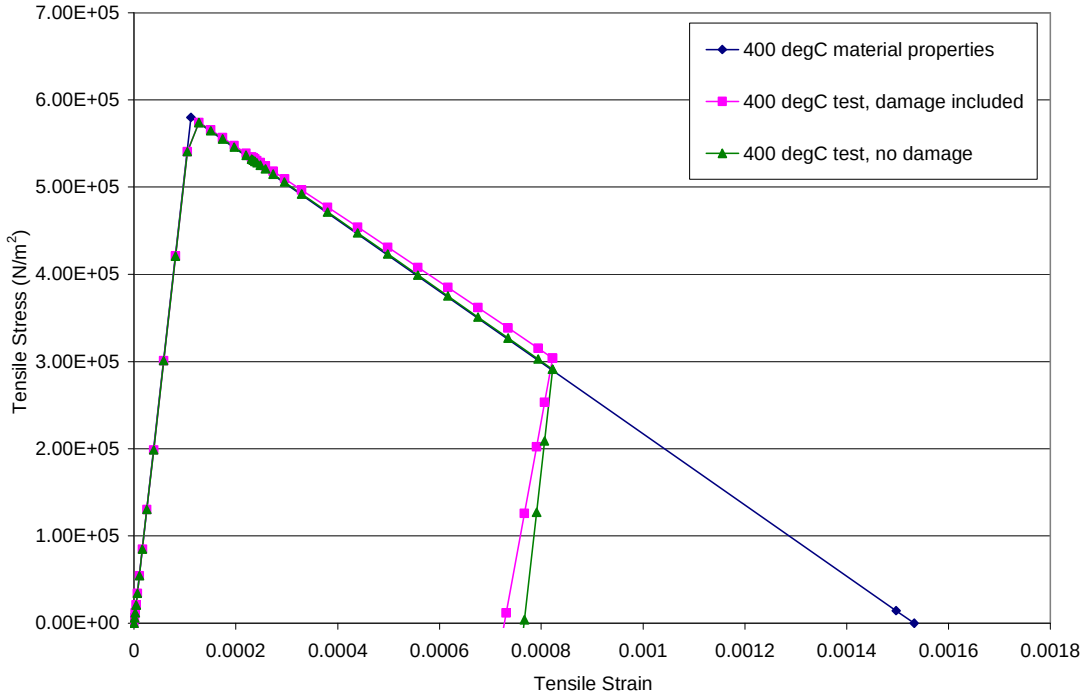

Figure 5-15: Concrete tensile material properties at 600°C, compared with the plain concrete cylinder under tensile loading at 600°C when damage variables are included and not included. Similar behaviour to that seen in compression is observed.

Once the material models were tested individually the cylinder was heated and cooled before being loaded, as in the experimental tests. The simulation for the CA6N test which was heated to 600°C is shown in Figure 5-16, along with the experimental data. As with the tests, the stress represents the total load applied divided by the cross-sectional area of the cylinder, and the strain represents deformation divided by the height of the cylinder.

Two simulations were considered, the first with no damage recovery and the second with full damage recovery (achieved by varying the damage recovery variables). No damage recovery represents the case where no crack closure is expected on unloading or load reversal, and hence the full loss of stiffness due to the damage variables will be seen. Full damage recovery occurs when complete crack closure and recovery of the material's stiffness on unloading or load reversal is modelled. A situation in between these two extremes is normally

expected, but both are used here to consider the effect of the damage and damage recovery variables on the model. It can be seen that the peak strength for both the simulation with full damage recovery and the one with no damage recovery is significantly lower than that for the virgin ambient temperature model.

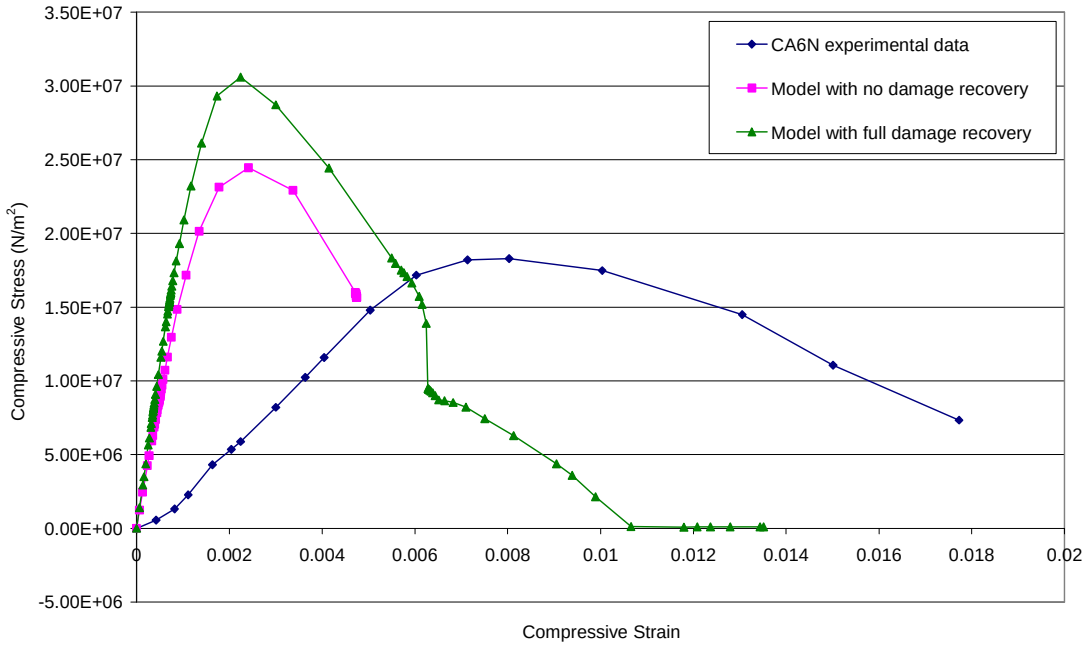

Figure 5-16: Graph comparing experimental data for the CA6N (unreinforced 600°C) test with FE model data for analyses with damage parameters included, and either full or no damage recovery permitted. The peak strength for both simulations is lower than that for an ambient temperature model; however they are both still significantly higher than the experimental data given. Damage, and damage recovery, is seen to have an effect on the peak strength – the peak strength is reduced when no damage recovery is present. The elastic stiffness of the model is slightly affected by damage recovery, with the model with no damage recovery having a slightly lower stiffness. Both models show a much higher elastic stiffness than the experimental data. This model, with its damage caused solely by thermal gradients within the material, does not capture the loss of elastic stiffness on heating and cooling cycles.

Furthermore the results are dependent on the compression and tension recovery variables, with the ultimate compressive strength lower when recovery is set to

zero. It can also be seen that the elastic stiffness is slightly different for the two models with different damage recoveries. Both the simulations indicate loss of stiffness and strength due to heating and subsequent cooling. However, neither of the two models was found to match up with experimental tests – both the finite element models have a higher stiffness and a lower ultimate strain value than the experiments. This model, with its damage caused solely by thermal gradients within the material, does not capture the loss of elastic stiffness seen experimentally on heating and cooling cycles.

From the experimental results it was seen that concrete does not regain its full strength and stiffness on cooling following heating. The simulations indicate that part of this loss of stiffness and strength is because of the damage that occurs due to differential thermal expansion and contraction in the heating/cooling phases. This phenomenon needs to be included alongside other factors which are known to reduce residual strength – dehydration of calcium hydroxide, microstructure coarsening, and change in porosity. Since damage depends on thermal gradients, which in turn depend on the rate of heating, these phenomena are not purely temperature based; a uniform increase and decrease in temperature will cause no damage and no loss of strength. Damage occurs in the form of inelastic/non-recoverable deformations.

The variation of damage throughout each cylinder can be represented by plotting the plastic strain present at the end of the cooling phase of the test. Figure 5-17 shows contour plots of the vertical plastic strain in two simulations – one that had full damage recovery and one that had no damage recovery. The largest plastic deformation is at the axis of axisymmetry, which will be cooler than the rest of the cylinder during the heating phase, and is therefore subject to large tensile stresses.

It was seen that the CA6N (unreinforced) test data had an initial elastic stiffness somewhere between that for ambient and 600^{o}C concrete, and hence some of the concrete's stiffness had been recovered on cooling from 600^{o}C to ambient temperatures. However the ultimate compressive strength seen in the

experiments was lower than both that of the ambient and 600°C material properties curves, so it appears that further strength degradation of the material occurred on cooling.

While differential thermal expansion and consequent damage can be seen to contribute to stiffness and strength degradation, the exact quantification of this was not possible. The reason is that while the material properties under compression were calibrated against the experimental tests at ambient temperatures, this could not be done at elevated temperatures. The elevated temperature parameters were extrapolated on the basis of Eurocodes (EN1992-1-2 2004).

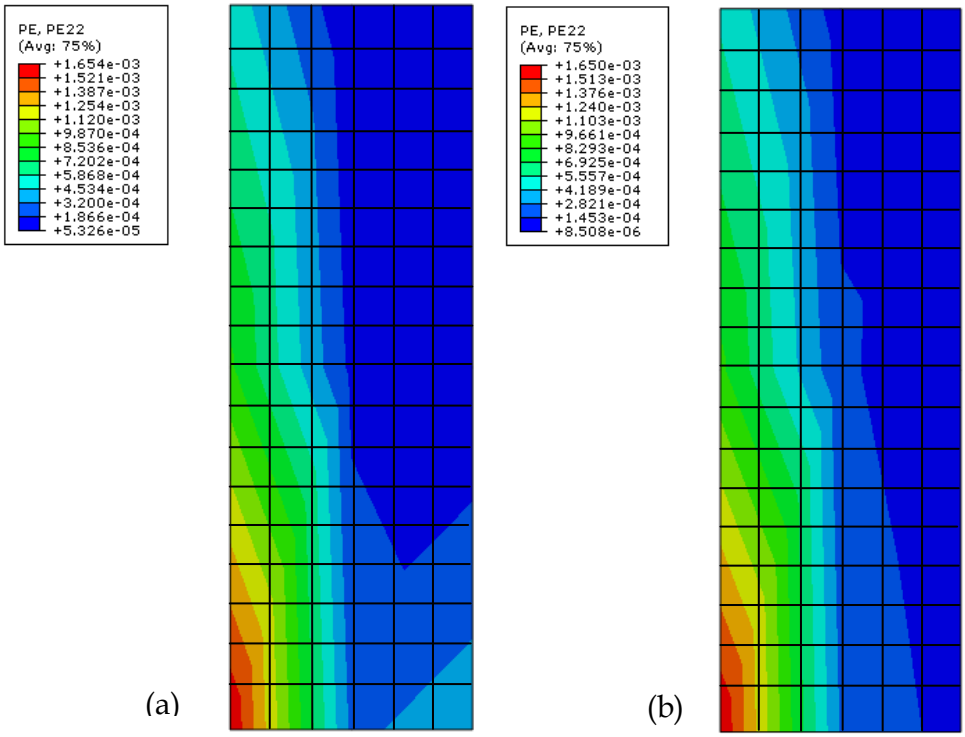

Figure 5-17: Contour plots for a plain concrete cylinder showing plastic strain in the vertical direction after the heating and cooling cycle, using CB6N (600°C) test temperatures and (a) full damage recovery, and (b) no damage recovery

5.4.2 Reinforced concrete

A number of numerical tests were conducted on the reinforced concrete cylinder described earlier. The first set of tests considered uniform heating followed by compression (cooling was not included). Three tests were conducted – one at ambient temperature, and the other two at 200 and 600°C. Damage parameters were not included in these simulations.

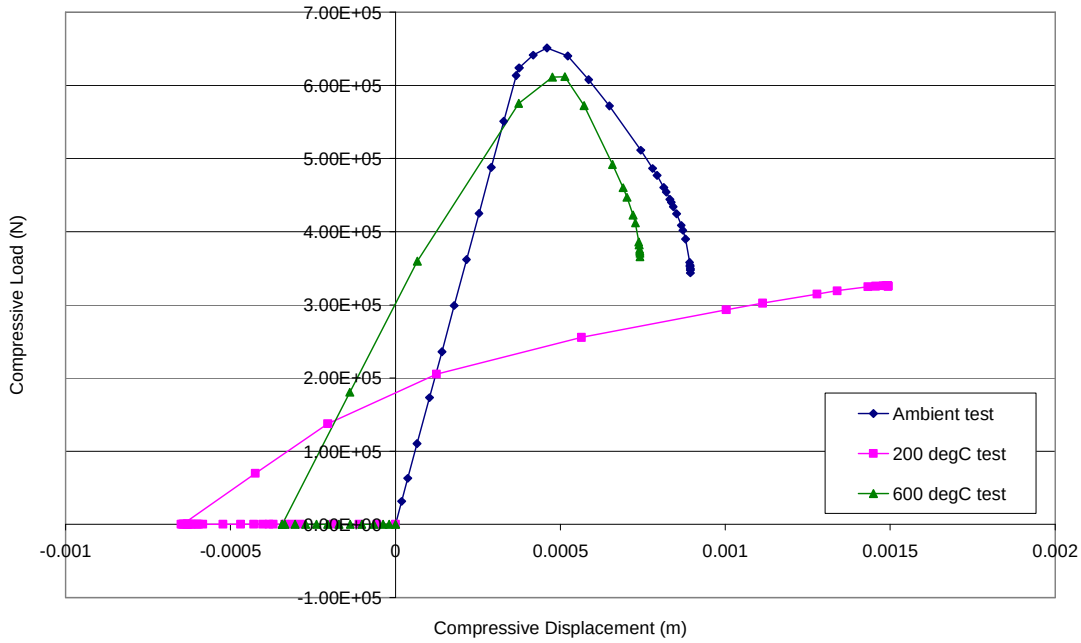

Figure 5-18: Vertical load-vertical displacement results from a FE reinforced concrete cylinder loaded in compression at ambient temperature, 200°C and 600°C. The elevated temperature curves are offset to the left due to the expansion of the cylinder (tensile displacement), while the gradient of the loading part of the curve decreases with increasing temperature. This is due to the reduction in elastic moduli and peak strength of both concrete and reinforcing steel.

The resulting load-displacement curves are shown in Figure 5-18. Compared with the ambient temperature test, the elevated temperature curves are offset to the left due to the expansion of the cylinder. As expected, the gradient of the ascending part of the graph is less steep at elevated temperatures due to the reduction in elastic moduli of both concrete and reinforcing steel. The peak loads also reduce at elevated temperatures.

Next, a test was conducted in which the cylinder was restrained from expanding vertically during the heating step. After heating to 200°C, additional compression was applied using displacement boundary conditions. The vertical load-vertical displacement of this cylinder is shown in Figure 5-19. The results are compared with the case in which thermal expansion was permitted. It can be seen that the displacement of the cylinder remains zero throughout the heating step while the compressive load increases, as the cylinder is heated but not permitted to expand. However, the rest of the curve follows the free-expansion behaviour almost exactly.

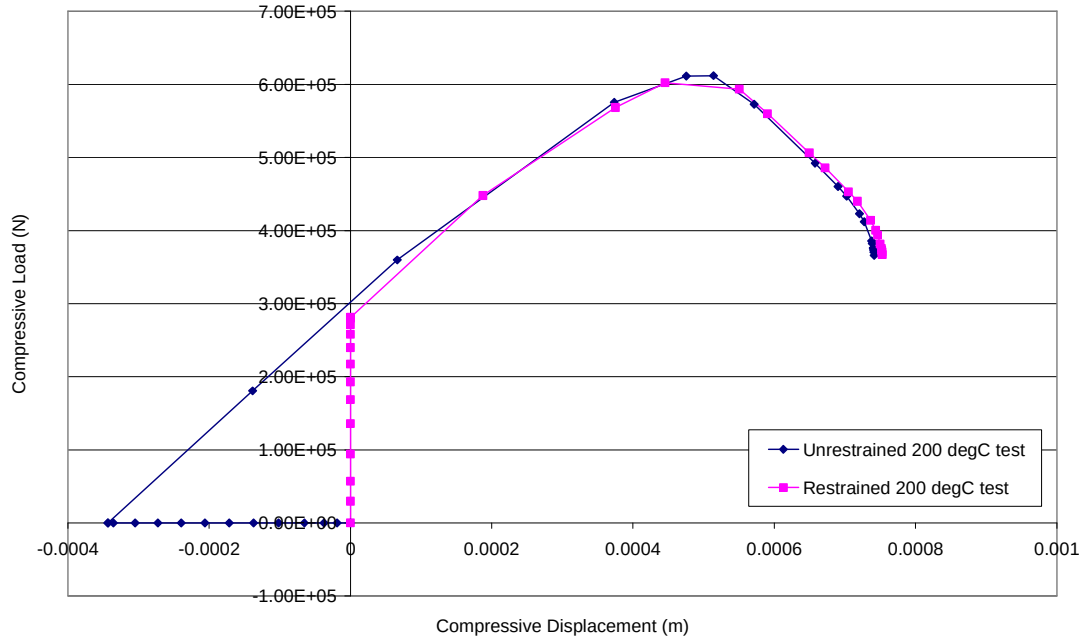

Figure 5-19: Vertical load-vertical displacement for a reinforced concrete cylinder heated to 200°C under either restrained or unrestrained boundary conditions, and then loaded in compression. The unrestrained cylinder shows thermal expansion through tensile displacement on heating, while the displacement of the restrained cylinder remains zero throughout heating. The loading part of the restrained curve follows the free-expansion example almost exactly.

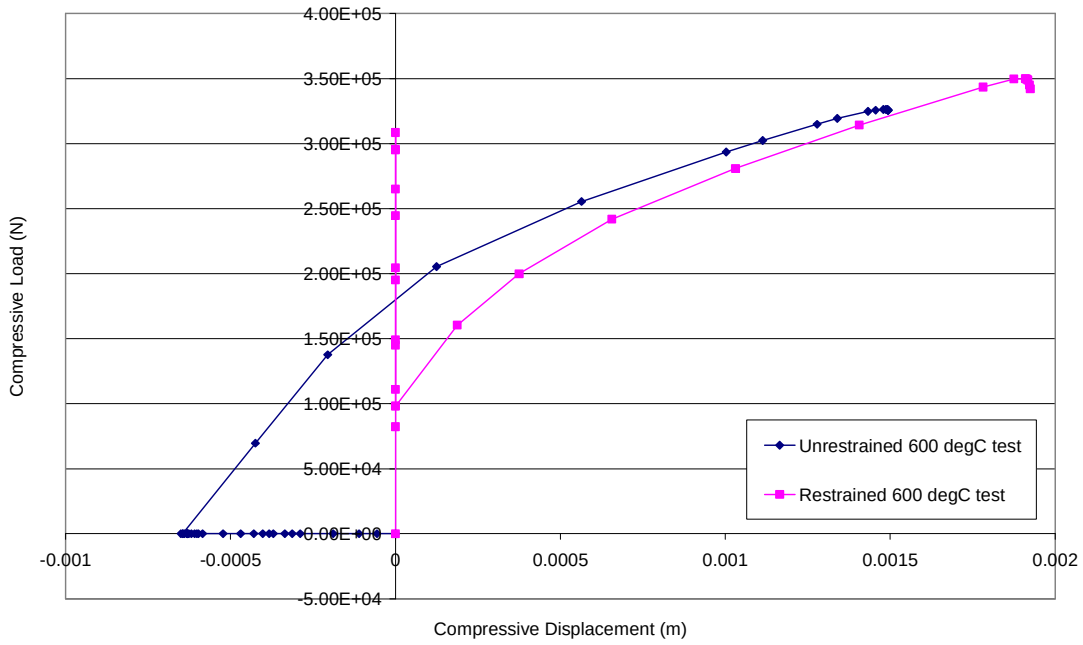

Figure 5-20: Vertical load-vertical displacement for a reinforced concrete cylinder heated to 600°C under either restrained or unrestrained boundary conditions, and then loaded in compression. The unrestrained cylinder shows thermal expansion through tensile displacement on heating, while the displacement of the restrained cylinder remains zero throughout heating. However, the compressive load present in the restrained cylinder increased and then decreased during heating, before increasing again on loading. This is caused by the slow heating under restraint – yielding and stiffness degradation occurs due to the restrained boundary conditions, with the peak strength reducing with increasing temperature. At 600°C the material can carry additional loads, as the strain at peak stress has not been reached through heating, resulting in an increased load response on compression.

When the same analysis (restrained heating followed by compression) was carried out by heating the reinforced cylinder to 600°C (Figure 5-20), it was seen that the compressive load during the heating step increased and then decreased while the displacement remained zero. Subsequent loading resulted in an ascending branch of the load-displacement curve. An initial increase followed by decrease of load during the heating phase, followed by an increase during the loading phase appears unexpected. However this phenomenon can be explained

with the help of material property curves in Figures 5-8 and 5-12. As temperature is slowly increased from zero to 600^{o}C, the restrained heating will cause yielding and stiffness degradation of concrete. Since the peak strength reduces with increasing temperature, an initial increase in load is followed by a decrease in the heating phase. At 600^{o}C however, the composite is capable of carrying additional loads, as strain at peak stress has not been reached, resulting in an increased load response on compression.

In order to investigate the residual response of the cylinder, two tests were carried out. The cylinder was uniformly heated to either 200^{o}C or 600^{o}C and then cooled back to ambient temperature, all while free to expand. After this the cylinders were tested under compression. The resulting compressive load-compressive displacement graph is shown in Figure 5-21. In this simulation no damage variables were included in the model. In the 200^{o}C test, it can be seen that the cylinder regains all of its strength and stiffness when cooled, and hence when loaded matches the ambient temperature simulation almost exactly. Clearly the differential thermal expansion between concrete and steel does not affect the response. However, in the 600^{o}C case, the heating is of great enough magnitude that there is a significant difference in the expansion of concrete and steel. As the concrete expands less than the reinforcement, this causes damage within the model and hence, on compressive loading, there is a slight difference in the response. On residual heating to uniform temperature, the stiffness of the 600^{o}C model has been reduced slightly, the peak load reached is slightly lower, and the displacement is larger than for the 200^{o}C model.

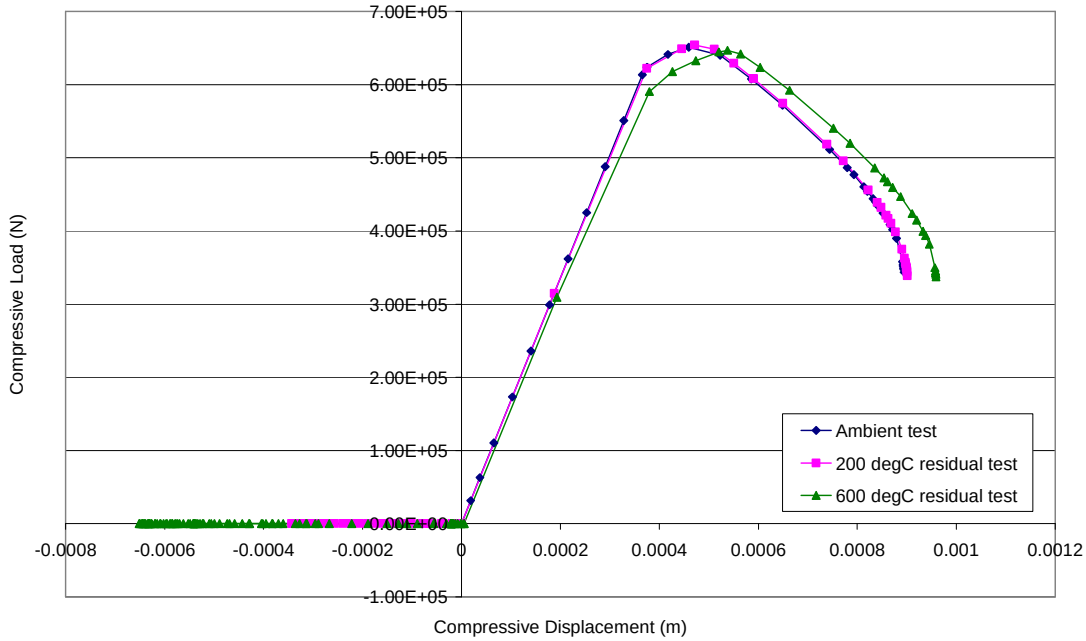

Figure 5-21: Vertical load-vertical displacement for a reinforced concrete cylinder: 1. loaded in compression at ambient temperature; 2. heated to 200°C while free to expand, cooled to ambient temperature, then tested in compression (200°C residual test) ; and 3. heated to 600°C while free to expand, cooled to ambient temperature and tested in compression (600°C residual test). No damage variables were included in these materials and it is seen that the model in the 200°C test regains all of its stiffness and strength when cooled, behaving exactly like an unheated model when tested under compression. However in the 600°C test, the peak load and gradient of the loading curve (stiffness of the material) are seen to be slightly lower than the ambient test values, while the displacement is larger. When heating to 600°C there is a significant enough difference between the expansion of concrete and of reinforcing steel to affect the response of the model.

Finally the issue of thermal gradients, as seen in the experiments, was explored using the temperature data available. First the cylinder was heated and then cooled back to ambient temperature using the variation seen in the CB2N (reinforced 200°C) test. The cylinder was then loaded in compression and the vertical load-vertical displacement response is shown in Figures 5-22 and 5-23. This is compared with the CB2N test data discussed previously. It is seen that

the residual peak load is lower than that seen in the experimental test, however, the finite element model retains more of its stiffness and shows much lower displacements throughout the loading.

The compression and tension recovery variables were varied to investigate their effect on the response. It is seen in Figures 5-22 and 5-23 that the recovery variables have no effect on this test, possibly due to the temperature gradients not being high enough to cause significant damage to the cylinder. It is interesting to note that with thermal gradients, peak strength in simulations was higher than the experimental values for plain concrete (Figure 5-16). However for reinforced concrete the peak strengths in simulation were found to be lower than that for experiments. This cannot be readily explained, but could be due to the assumptions in material properties at elevated temperatures.

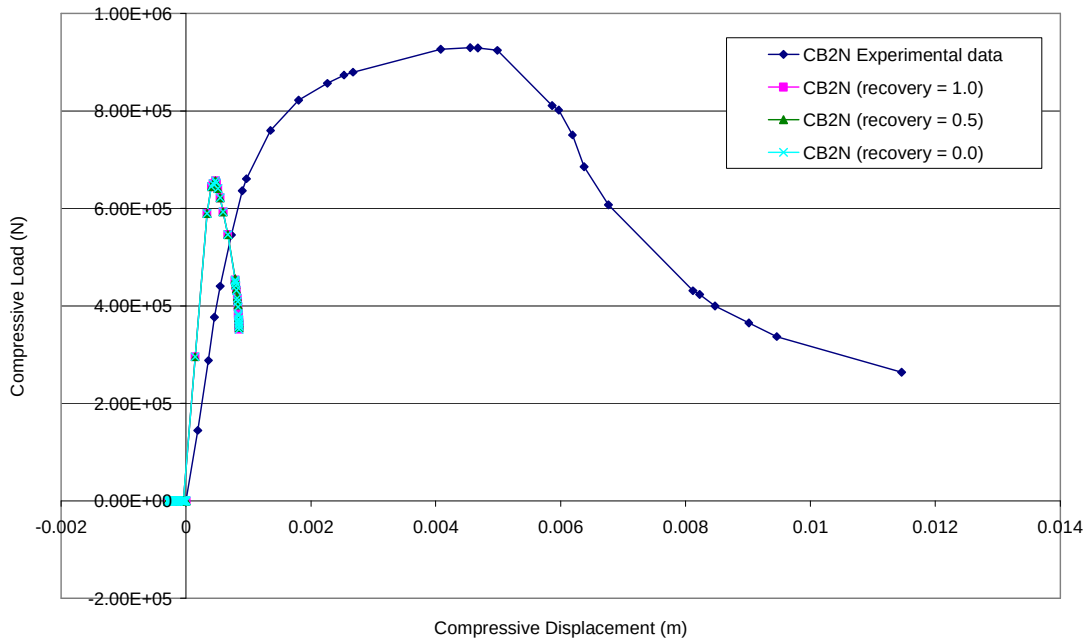

Figure 5-22: Graph comparing experimental data for the CB2N (reinforced 200°C) test with FE model data for analyses with damage parameters included, and either full (recovery = 1.0), 50% (recovery = 0.5) or no (recovery = 0.0) damage recovery permitted. The residual peak load is lower for the model than that seen in the experimental data, however the model regains more stiffness and has a greater stiffness and smaller displacement throughout loading than the experimental data. The difference in peak strength is difficult to explain but may be due to the assumptions made about the concrete and reinforcement material properties at elevated temperature. The regaining of stiffness upon cooling may be because, on heating to 200°C, the thermal gradient present in the model is not high enough to cause significant damage to the material. For the same reason it is seen that the recovery variable used has no effect on the results.

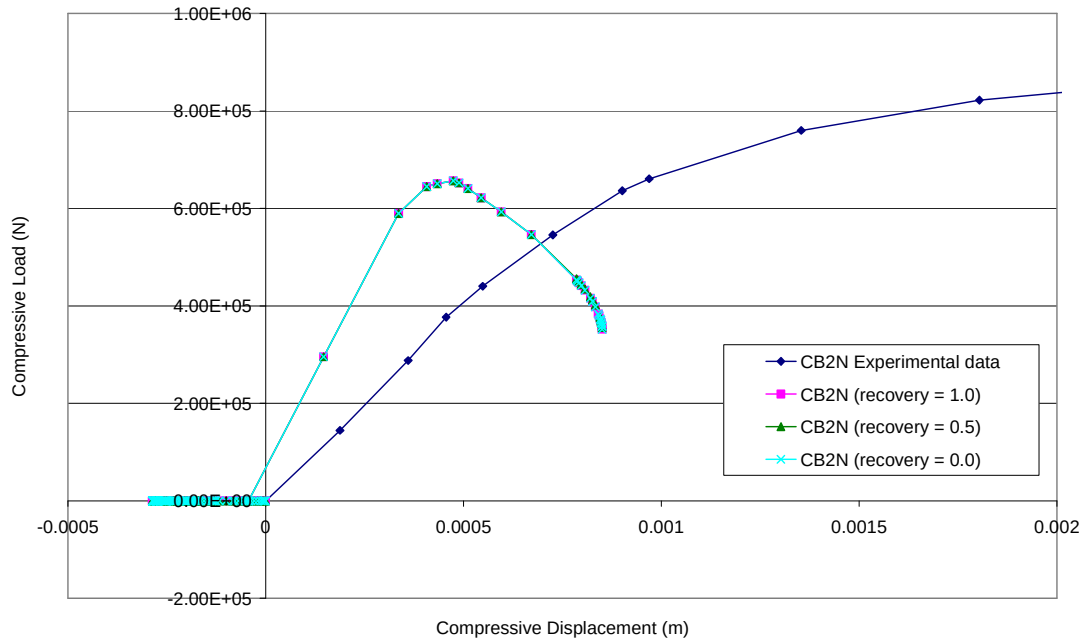

Figure 5-23: Magnification of the graph comparing experimental data for the CB2N (reinforced 200°C) test with FE model data for analyses with damage parameters included, and either full (recovery = 1.0), 50% (recovery = 0.5) or no (recovery = 0.0) damage recovery permitted, showing the model data in greater detail.

Contour plots of the vertical normal plastic strain after the heating and cooling phases of the simulation are shown in Figure 5-17. For a plain concrete cylinder, the largest plastic deformation was at the cylinder's core which remains at the lowest temperature while the rest of the cylinder expands during the heating phase. Unlike this, in the case of reinforced concrete, damage occurs due to the differential thermal expansion between steel and concrete. The largest variation is near the reinforcement and at the top of the cylinder – this is where localisation is seen, and where plastic deformation is largest. The distribution of damage after the heating and cooling phase, throughout the reinforced concrete cylinder, is seen in Figure 5-24, where plastic strain in the vertical direction is plotted for two simulations – full damage recovery, and no damage recovery.

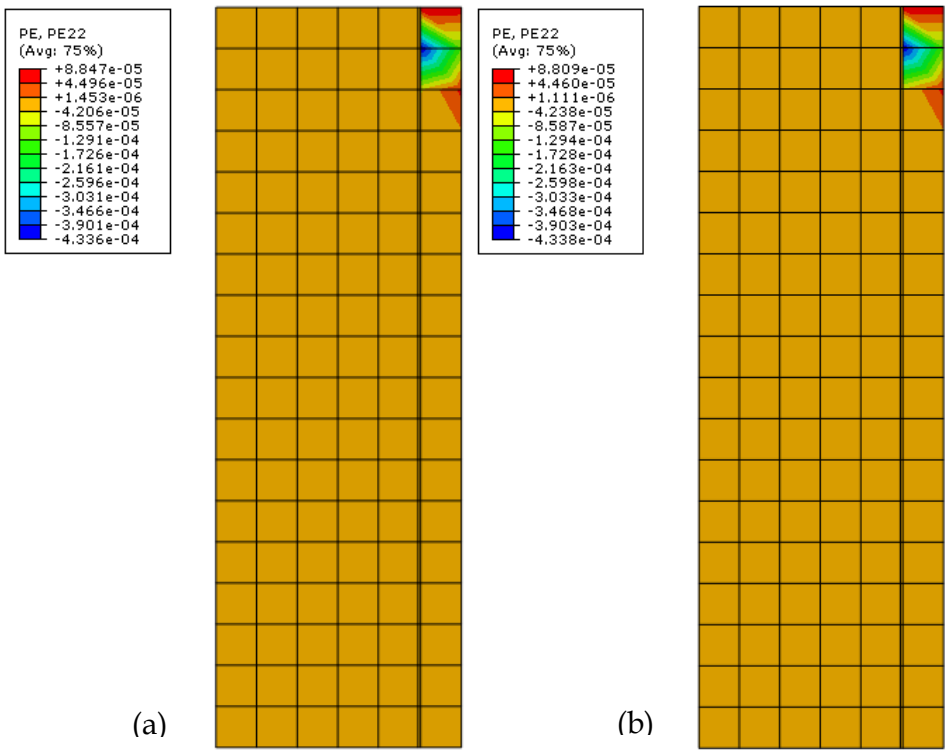

Figure 5-24: Contour plots for a reinforced concrete cylinder showing plastic strain in the vertical direction after the heating and cooling cycle, using CB2N (reinforced 200°C) test temperatures and (a) full damage recovery, and (b) no damage recovery. The largest plastic strains and deformations are concentrated in the outer column of elements, near the reinforcement and at the top of the cylinder. This deformation, caused by differential thermal expansion between concrete and reinforcement, causes tensile stresses in the model.

As damage was seen to be concentrated near the reinforcement at the top of the cylinder, and as this damage causes tensile stresses in the model, the effect of tension stiffening on the simulation was considered. As discussed at the beginning of this chapter, tension stiffening allows concrete to have a more ductile tensile response to loading through the interaction between concrete and reinforcement. Furthermore, reinforcement provides confinement to the expanding concrete during the heating phase and also during the compression phase, resulting in increased strength of concrete inside the reinforcement cage.

The same simulation was carried out (heating and cooling as in the CB2N 200°C test, followed by compressive loading) on a cylinder with compressive concrete properties and reinforcement properties as before, but with plain concrete tensile properties with a fracture energy of 100 N/m. As with plain concrete, where no localisation occurred or was assumed, the stress-strain curve employed corresponded to an element length of 225 mm which is the full height of the semi-cylinder. This simulation did not converge, and failed part way through the heating phase. The reason perhaps was localisation in elements adjacent to the reinforcement; the characteristic length corresponding to the full cylinder height perhaps resulted in a snap-back kind of situation.

Next, the characteristic length was changed to a single element size of 12.5 mm. This element length was chosen as damage is confined to one element's width of material at the edge of the model. This simulation did converge and complete, and the load-displacement graph is shown in Figure 5-25. It follows the original graph which includes tension stiffening properties exactly.

Lastly, the cylinder was modelled with the original plain concrete tensile properties (an element length of 225 mm), but with tension stiffening concrete properties in the concrete elements adjacent to the reinforcement. Again, this model converges, and gives an identical response to the original tension stiffening simulation (Figure 5-25). This demonstrates the localisation of damage in the concrete elements surrounding the reinforcement, and shows the dominance of their response in determining the overall response of the cylinder.

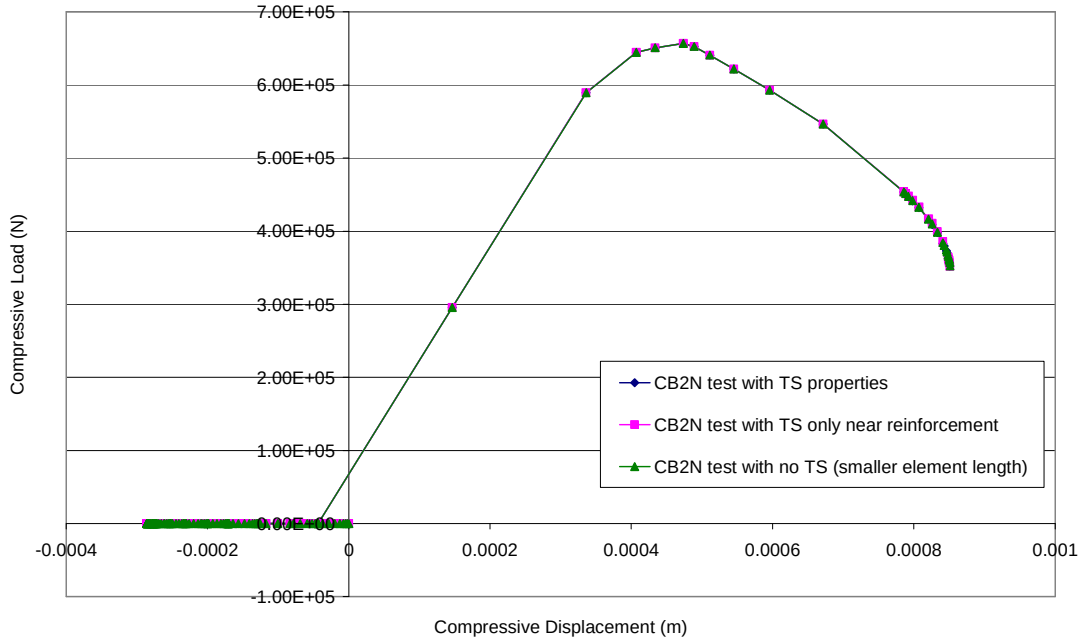

Figure 5-25: FE data for the CB2N (reinforced 200°C) test with: (1) full tension stiffening material properties for concrete included; (2) tension stiffening properties only present in concrete element adjacent to reinforcement; and (3) no tension stiffening properties for concrete, but a smaller characteristic length used with concrete tensile fracture energy. As all three models give identical results, the localisation of damage and deformation near to the reinforcement is shown. These elements dominate the overall behaviour of the cylinder.

Lastly the cylinder was heated to 600°C and then cooled back to ambient temperature using the variation seen in the CB6N test. Once again, the cylinder was subjected to axial compression after cooling, and three damage recovery values were considered. The vertical load-vertical displacement response is seen in Figures 5-26 and 5-27. This is compared with the CB6N test data discussed previously. It is seen that the residual peak load is similar to that seen in the experimental test, however, the finite element model retains more of its stiffness and shows much lower displacements throughout the loading, which is consistent with the lower temperature test.

Like plain concrete, the ascending branch of the simulations is identical for different damage variables, as is the peak strength. Damage due to differential thermal expansion is likely to be predominantly due to induced tensile stresses

in concrete. The inclusion of tension stiffening, for the concrete model, apparently makes damage less likely. As a result, unlike plain concrete, little difference is seen by varying damage recovery variables.

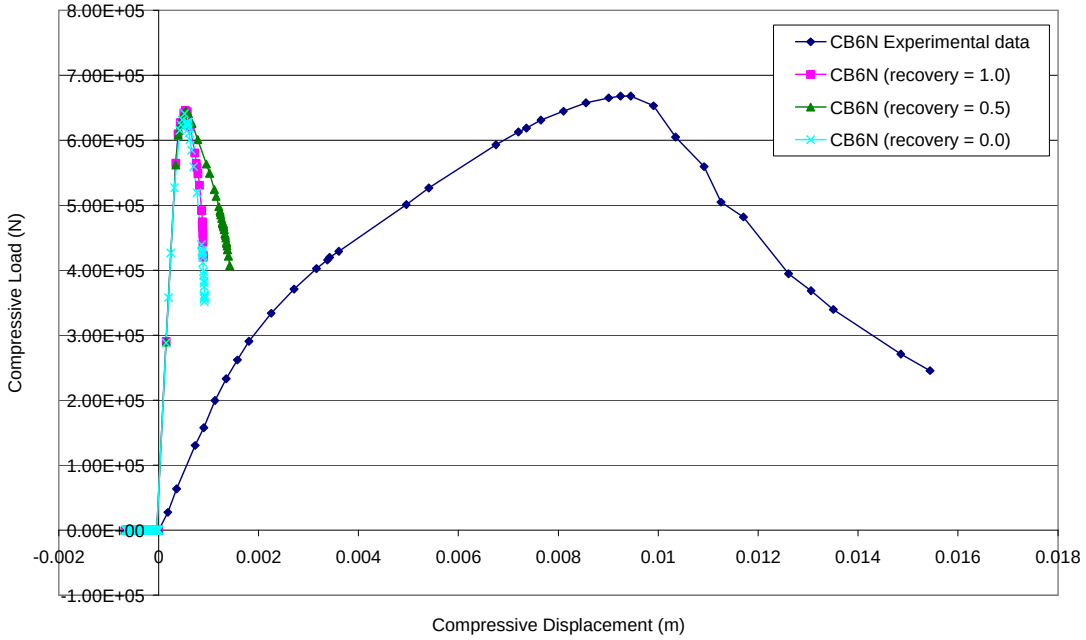

Figure 5-26: Graph comparing experimental data for the CB6N (reinforced 600°C) test with FE model data for analyses with damage parameters included, and either full (recovery = 1.0), 50% (recovery = 0.5) or no (recovery = 0.0) damage recovery permitted. The residual peak load is approximately the same for the model as that seen in the experimental data, however the model regains more stiffness and has a greater stiffness and smaller displacement throughout loading than the experimental data. The similarity in peak strength is good and may be due to greater damage and a greater reduction in the peak load of the experimental data, bringing it into line with the material model used in FEM. The regaining of stiffness upon cooling may be because, damage due to differential thermal expansion on heating to 600°C occurs mainly due to tensile stresses in concrete. Including tension stiffening in the concrete model makes this damage less likely, and so damage recovery variables again have little effect on the overall response.

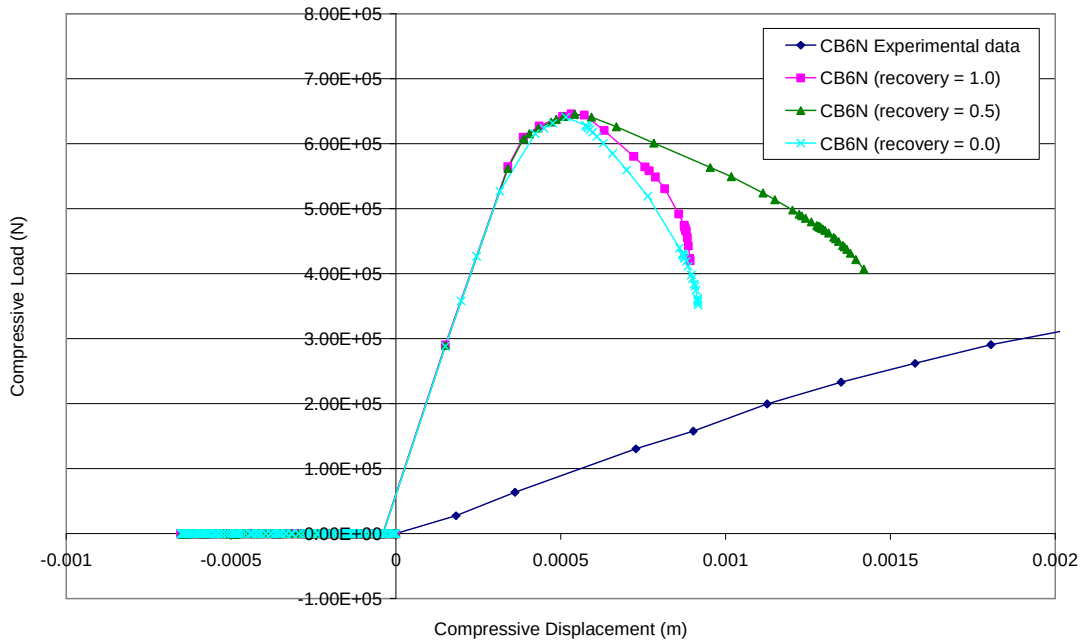

Figure 5-27 : Magnification of the graph comparing experimental data for the CB6N (reinforced 600°C) test with FE model data for analyses with damage parameters included, and either full (recovery = 1.0), 50% (recovery = 0.5) or no (recovery = 0.0) damage recovery permitted, showing the model data in greater detail.

Contour plots of the vertical plastic strain after the heating and cooling phases of the simulation are shown in Figure 5-28, and are very similar to those seen in the 200°C test simulation (Figure 5-24). They show localisation at the top of the cylinder, near the reinforcement. The damage is caused by the disparity in thermal expansion between steel and concrete in the simulation.

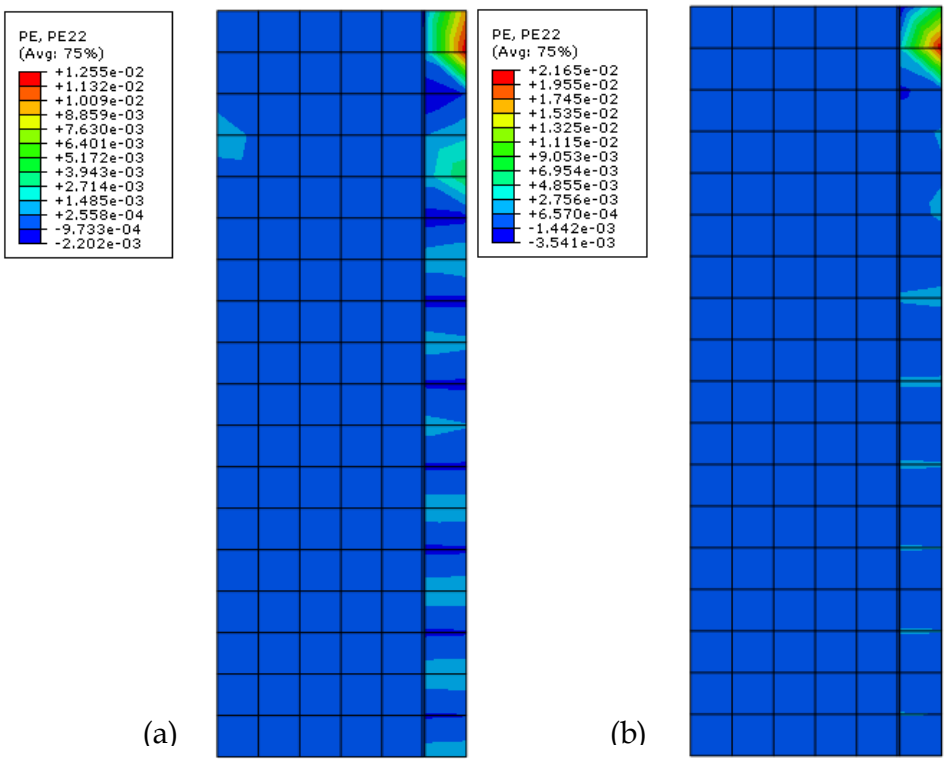

Figure 5-28: Contour plots for a reinforced concrete cylinder showing plastic strain in the vertical direction after the heating and cooling cycle, using CB6N (600°C) test temperatures and (a) full damage recovery, and (b) no damage recovery. Localisation of damage is seen in the outer elements of the cylinder, near to the reinforcement, and especially towards the top of the cylinder. This is caused by differential expansion of concrete and reinforcement, particularly under high thermal gradients.

As in the previous test example, the effect of tension stiffening on the simulation was considered. Again the same three simulations were carried out: heating and cooling as in the CB6N 600°C test, followed by compressive loading on a cylinder with compressive concrete properties and reinforcement properties as before, but with plain concrete tensile properties (i.e. a fracture energy of 100 N/m and characteristic length of 225 mm); heating, cooling and compressive loading on a cylinder with a characteristic length of 12.5 mm; and heating, cooling and compressive loading on a cylinder modelled with tension stiffening material properties in concrete adjacent to the reinforcement but plain concrete tensile properties (based on a 225 mm element length) elsewhere. The results

throughout were similar to those seen in the 200°C test, with the first simulation not converging, but the other two giving very similar vertical load-vertical displacement graphs to the original simulation which included tension stiffening concrete material properties (Figure 5-29). Again, these models can be said to demonstrate the localisation of damage in the concrete elements surrounding the reinforcement, and to show the dominance of their response in determining the overall response of the cylinder.

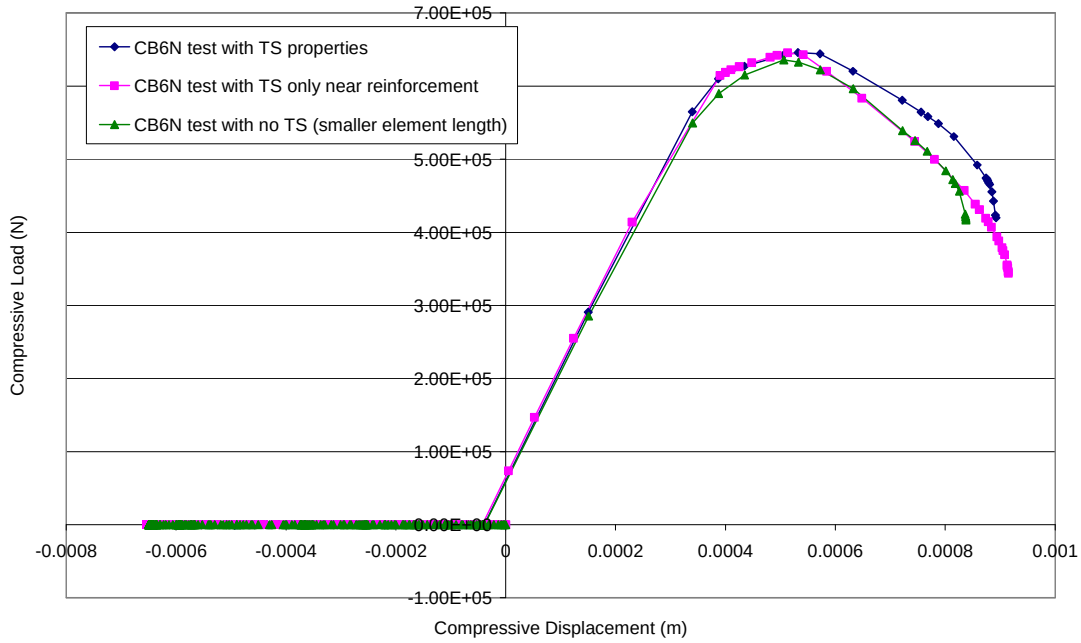

Figure 5-29: FE data for the CB6N (reinforced 600°C) test with: (1) full tension stiffening material properties for concrete included; (2) tension stiffening properties only present in concrete elements adjacent to reinforcement; and (3) no tension stiffening properties for concrete, but a smaller characteristic length used with concrete tensile fracture energy. As all three models give similar results, the localisation of damage and deformation near to the reinforcement is shown. These elements dominate the overall behaviour of the cylinder. However the slight difference in response between having full tension stiffening for concrete and tension stiffening only in elements adjacent to reinforcement suggests that as the heating regime becomes more extreme, yield starts to become affected by the whole of the cylinder.

5.5 References

Chan, Y. N., G. F. Peng, et al. (1999). "Residual strength and pore structure of high-strength concrete and normal strength concrete after exposure to high temperatures." Cement and Concrete Composites **21**(1): 23-27.

EN1992-1-1 (2004). Eurocode 2: Design of Concrete Structures - Part 1-1: General Rules and Rules for Buildings.

EN1992-1-2 (2004). Eurocode2: Design of Concrete Structures - Part 1-2: General Rules - Structural Fire Design.

Ghandehari, M., A. Behnood, et al. (2010). "Residual Mechanical Properties of High-Strength Concretes after Exposure to Elevated Temperatures." Journal of Materials in Civil Engineering **22**(1): 59-64.

Gupta, A. K. and S. R. Maestrini (1990). "Tension-Stiffness Model for Reinforced Concrete Bars." Journal of Structural Engineering **116**(3): 769-790.

Hsu, J.-H. and C.-S. Lin (2008). "Effect of Fire on the Residual Mechanical Properties and Structural Performance of Reinforced Concrete Beams." Journal of Fire Protection Engineering **18**(4): 245-274.

Luo, X., W. Sun, et al. (2000). "Effect of heating and cooling regimes on residual strength and microstructure of normal strength and high-performance concrete." Cement and Concrete Research **30**(3): 379-383.

Nassif, A. (2006). "Postfire full stress–strain response of fire-damaged concrete." Fire and Materials **30**(5): 323-332.

Nassif, A. Y. (2002). "Postfiring stress-strain hysteresis of concrete subjected to various heating and cooling regimes." Fire and Materials **26**(3): 103-109.

Zaidi, K. A., U. K. Sharma, et al. (2012). "Effect of temperature on uni-axial compressive behavior of confined concrete." Fire Safety Journal **48**(0): 58-68.

6

Modelling beams at elevated temperature

6.1 Introduction

Previous chapters have looked at the material properties of concrete in tension and compression at ambient and elevated temperatures. Benchmark problems have been used to demonstrate the material properties – one element plane

stress models and axisymmetric cylinder models, where the loading is uniaxial in compression or tension.

However, the majority of structural elements in construction are not like this – they do not solely experience uniaxial loading, but are loaded in tension, compression, shear, bending or several of these at once. A homogenous beam and a reinforced concrete beam are modelled, and the effects of elevated temperatures investigated.

6.2 Simply supported beam

In this section, issues associated with strain softening were investigated using a simply supported beam for elevated temperature conditions. To aid understanding of the analyses, the material was assumed to be homogenous and have linear elasticity, followed by a linear strain softening branch (Figure 6-1). Changes in peak strength and elastic modulus at elevated temperatures were not incorporated. As a result, these analyses focus on the mechanical response of the beam due to thermal expansions, elastic and softening properties, and thermal gradients. All modelling in this section was done using beam elements.

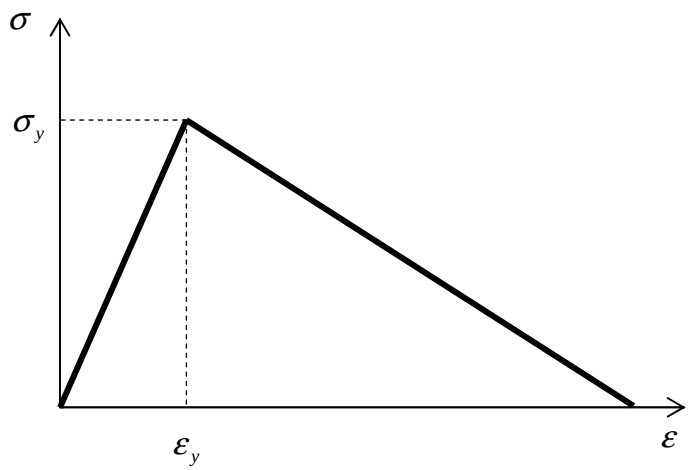

Figure 6-1: Stress-strain behaviour which shows linear elasticity and linear strain softening

The beam was given pinned end supports (Figure 6-2); it had a span L = 6000 mm, depth d = 100mm and width w = 50 mm; Young's modulus E = 2.05x10^5 N/mm^2; yield stress σ_y = 300 N/mm^2; and coefficient of thermal expansion α = 12x10^{-6} / ^{o}C. These properties are close to those for steel, though this is not important for the purpose of the investigation in this section.

Figure 6-2: Concrete beam with pinned end supports

It should be noted that throughout this section, positive values in graphs indicate compression, while negative values indicate tensile stresses or strains.

6.2.1 Uniform temperature increase

Consider a beam with pinned end supports as shown in Figure 6-2. If the beam is subjected to uniform temperature increase, the thermal expansion is cancelled out by equal and opposite contraction caused by the forces at the restrained ends.

It is easy to see that in the elastic regime the compressive stress in the beam will be uniform and given by:

$$\sigma = E\alpha\Delta T \tag{6.1}$$

where σ is the compressive stress, E is the elastic modulus, α is the coefficient of thermal expansion and ΔT is the temperature increase.

If the temperature continues increasing, and the beam is stocky (i.e. the possibility of buckling is ignored), the compressive stress will at a certain temperature reach the yield stress σ_y. With continued increase in temperature, strain softening will cause the stress to decrease. It is apparent that the decrease in stress results from some kind of crushing which will be localised, i.e. failure will not be distributed over the entire span. With increasing temperature the

crushed zone will get crushed further, and to maintain force compatibility the remainder of the beam will undergo elastic unloading. In order to numerically simulate this consider the beam idealised using 25 and 50 element discretisations. Localisation is forced by making one element fractionally weaker than the rest. With increase in temperature, localisation does occur in the weaker element, with elastic unloading in the others. As a result the reaction force at each of the pinned ends decreases with an increase in temperature, as shown in Figure 6-3.

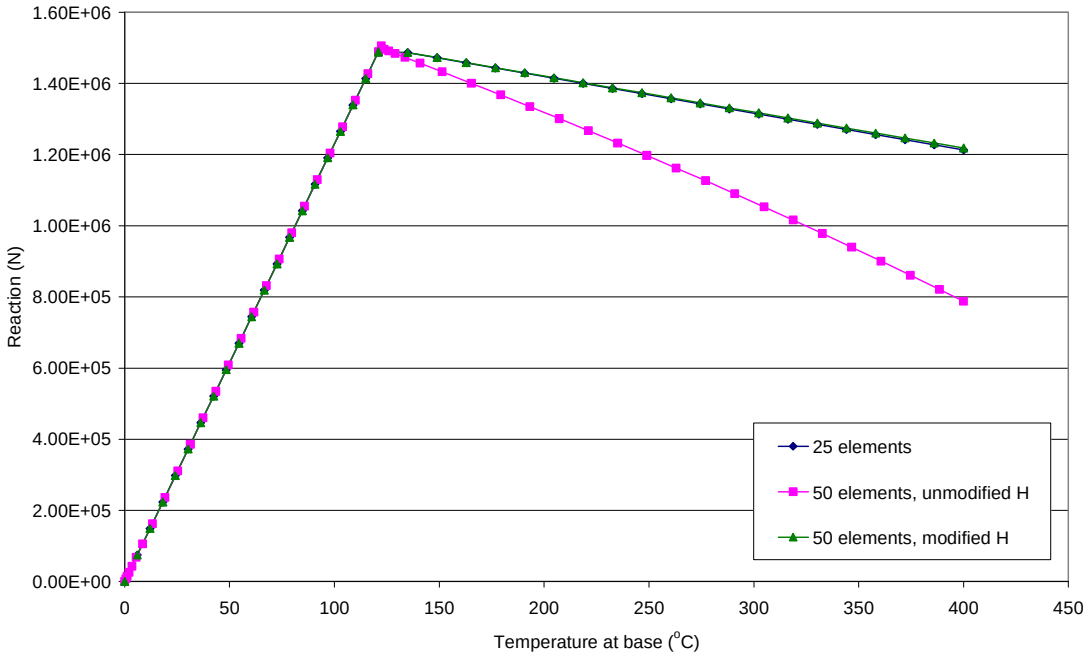

Figure 6-3: Horizontal reaction force due to uniform temperature increase with different mesh discretisations and softening modulus H

If the softening modulus is treated as a material property (in this case it was assumed H = -635 N/mm^2) then the post-peak response is different for the two idealisations. If, however, the softening modulus for the 50 element discretisation is reduced to half its previous value, an identical post-peak response is obtained as shown in Figure 6-3. This illustrates that treating the softening modulus as a material property can lead to mesh sensitive results. Another obvious feature of high temperature analysis is that this problem is akin

to a displacement controlled static analysis, i.e. there is no problem in convergence necessitating any form of indirect displacement control.

6.2.2 Constant thermal gradient, elastic material properties

The beam was subjected to a constant thermal gradient across the depth with the largest increase in temperature at the bottom, and the largest decrease in temperature at the top surface. The neutral axis remained at a constant temperature. This caused thermal bowing throughout the beam, resulting in uniform curvature along its length. If one of the beam supports was a roller, then due to the curvature of the beam, the horizontal distance between the ends of the beam would reduce. In computational simulation this feature can only be included through a geometrically nonlinear analysis, that is, one that includes large-displacement effects. In fact if geometrical nonlinearity is ignored (if a 'small-displacement' analysis is carried out), then the results for a beam with restrained pin supports and one with a roller support would be identical and no stresses would be induced in the beam in either of the two cases.

The beam in Figure 6-2, which has pinned end supports, with entirely elastic material properties has two analyses carried out. A uniform thermal gradient is applied across the depth of the beam, with and without the inclusion of geometric nonlinearity in the analysis. Results from these analyses are shown in Figures 6-4 and 6-5. Figure 6-4 shows the central deflection of the beam when geometric nonlinearity is included (NLGEOM) and when it is not (no NLGEOM). It can be seen that inclusion of nonlinear geometry, that is, performing a large-displacement analysis where elements are permitted to distort from their original shapes, causes axial forces which limit the central deflection; whereas when this is excluded the deflection goes on increasing linearly. When the thermal gradient is first applied pure bending stresses are generated. If the geometry of the beam is not updated to include deflection (the analysis does not include geometric nonlinearity) then the stresses remain pure bending stresses and the central deflection of the beams continues increasing with increasing thermal gradient. However, if a nonlinear geometric analysis is

carried out, the geometry of the beam is updated to include any deformation at each increment, and so axial forces are caused which limit the central deflection of the beam. Figure 6-5 shows the increase in horizontal reaction with temperature when nonlinear geometry is present. The horizontal reaction remains zero when nonlinear geometry is excluded, as the stresses present in the beam remain pure bending stresses, passing through the neutral axis of the beam, due to the geometry of the beam not being updated as it deflects.

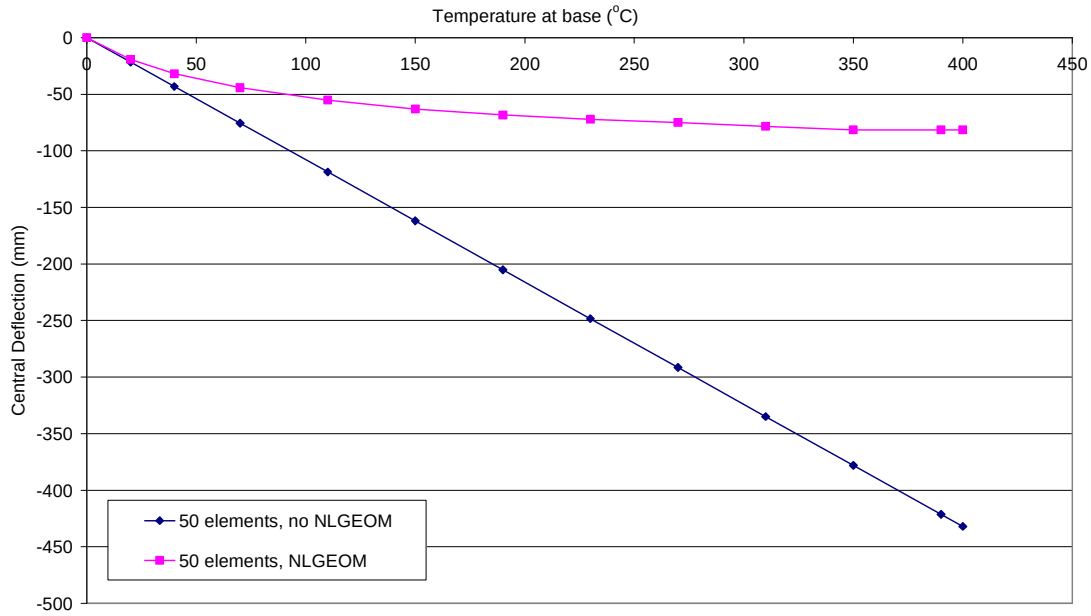

Figure 6-4: Deflection in an elastic beam with and without nonlinear geometry; temperature refers to the temperature at the bottom face of the beam when a pure thermal gradient is applied (i.e. the temperature at the neutral axis remains constant). When nonlinear geometry is absent, a 'small-displacement' analysis is carried out which does not take change of geometry of the beam during the analysis into account. This means that the thermal gradient causes the central deflection of the beam to increase linearly throughout the analysis. When nonlinear geometry is included, the large-displacement analysis updates the geometry of the beam as it deflects, causing an increasing axial force at the supports which limits central deflection.

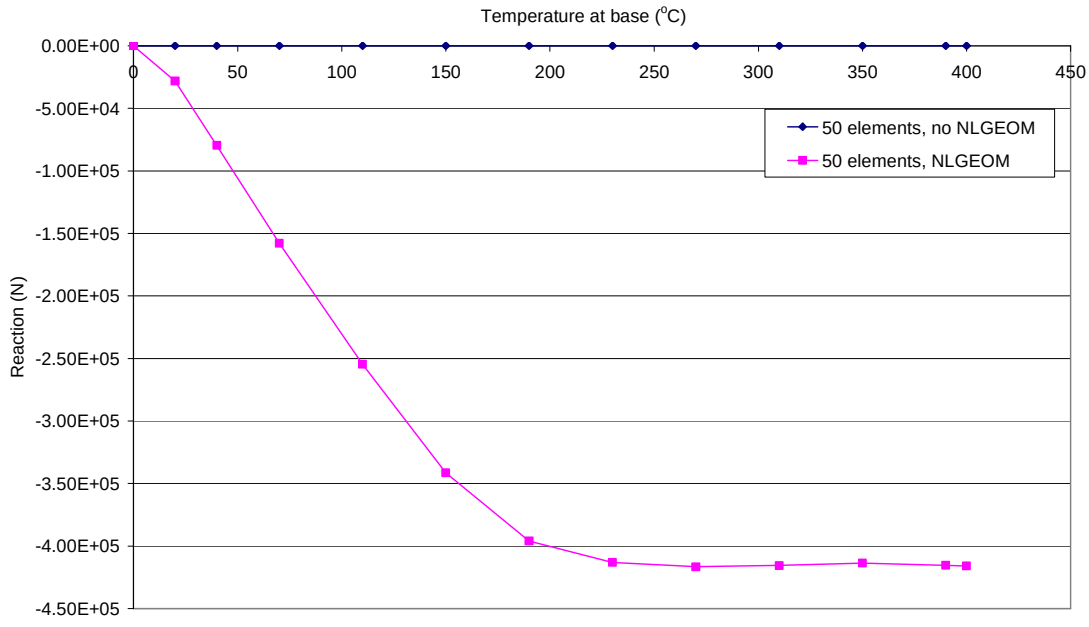

Figure 6-5: Horizontal reaction force in an elastic beam with and without nonlinear geometry; temperature refers to the temperature at the bottom face of the beam when a pure thermal gradient is applied (i.e. the temperature at the neutral axis remains constant). When nonlinear geometry is absent, a 'small-displacement' analysis is carried out which does not take change of geometry of the beam during the analysis into account. This means that the thermal gradient causes pure bowing in the beam, and no horizontal reaction force is generated. When nonlinear geometry is included, the large-displacement analysis updates the geometry of the beam as it deflects, causing an increasing horizontal reaction force at the supports which then limits central deflection.

6.2.3 Constant thermal gradient, strain softening material properties

Next, strain softening was included in the material properties of the beam, and nonlinear geometry was made part of every analysis. Once again a constant thermal gradient without an average increase in temperature was applied. It is apparent that, in addition to axial forces, bending moments were induced in the beam and the largest moment was at the centre of the span. As a result, with increasing temperature, the central region underwent inelastic deformation accompanied by strain softening. The question arises whether with continued increase in temperature the remainder of the beam (away from the central

region) would elastically unload with strain localisation in the centre. Interestingly this does not occur in this case, and the strain softened region spreads outwards. To explain this phenomenon, consider the beam to have two different materials: a small central region with an elasto-strain softening material; and remainder of the beam comprising a purely elastic material. With increasing temperature gradient the central region becomes inelastic, and with continued increase of temperature the thermal bowing proceeds in the form of two elastic beams with a hinge in the middle as shown in Figure 6-6 (a). It is apparent from this configuration that the stresses in some of the elastic regions will be higher than the central region to maintain equilibrium. The consequence of the above discussion is that for a uniform beam (with no variation in properties) softening will start in the centre and extend outwards with deflected shapes as shown in Figure 6-6 (b).

(a) (b)

Figure 6-6: (a) Deflected shape of the beam with softening limited to the central region; (b) Progressive deflection with increasing thermal loading

This indicates that for the "thermal gradient only" problem strain softening does not result in strain localisation. So numerically results would not be mesh sensitive if the softening modulus were taken to be a material property. This is found to be the case and Figures 6-7 and 6-8 show central deflections and horizontal reactions with different mesh discretisations. It can be seen that the results are almost identical.

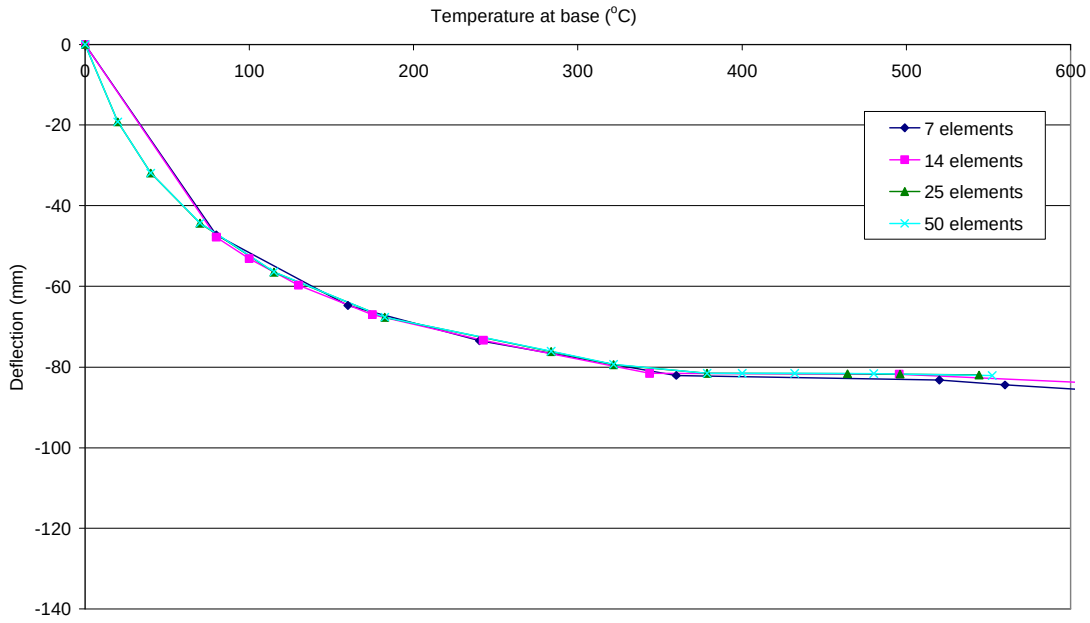

Figure 6-7: Mid-span deflection in an elasto-strain softening beam, when thermal gradient is applied; several mesh sizes are shown

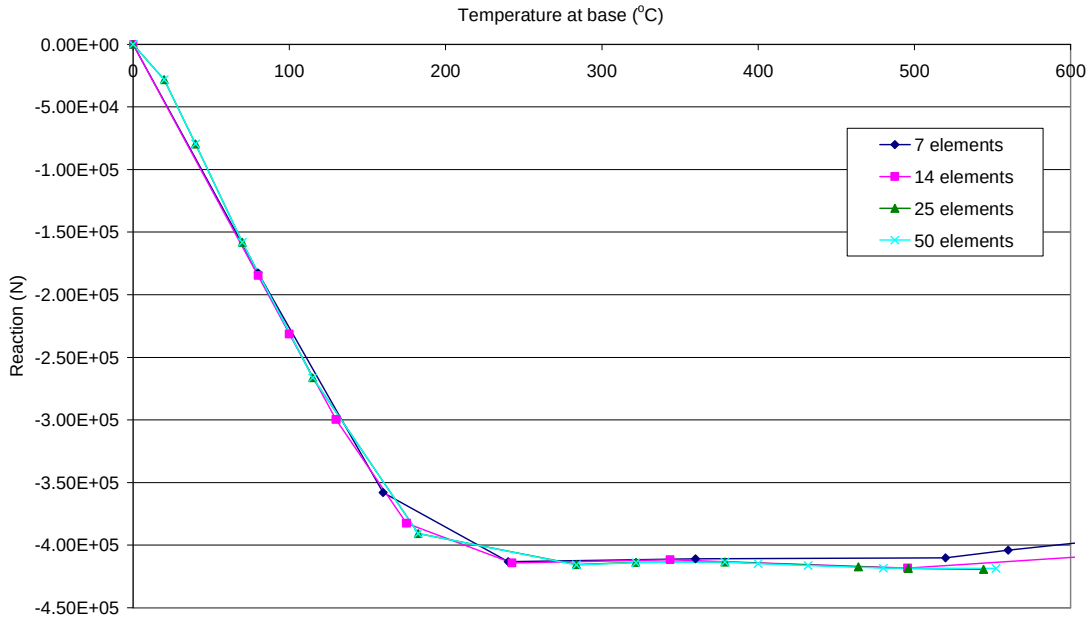

Figure 6-8: Horizontal reaction force in an elasto-strain softening beam when thermal gradient is applied; several mesh sizes are shown

6.2.4 Temperature increase and constant thermal gradient, elastic material properties

In the event of a fire, structural elements experience both an average temperature increase and a thermal gradient (the hottest being the surface exposed to fire). The beam in Figure 6-2, with entirely elastic material properties present, was subjected to an average temperature increase and a constant thermal gradient applied through its depth. The deflection at mid-span is shown in Figure 6-9.

The exclusion of nonlinear geometry causes the central deflection to increase linearly due to thermal gradient only, as when nonlinear geometry is not present a pure thermal expansion does not induce any deflection in the beam at all. As before, the inclusion of nonlinear geometry limits central deflection. Initially deflection is larger when nonlinear geometry is present, due to thermal expansion of the beam dominating its behaviour; however as the thermal gradient applied increases, thermal bowing is induced and the overall deflections are limited by the restraint at the supports.

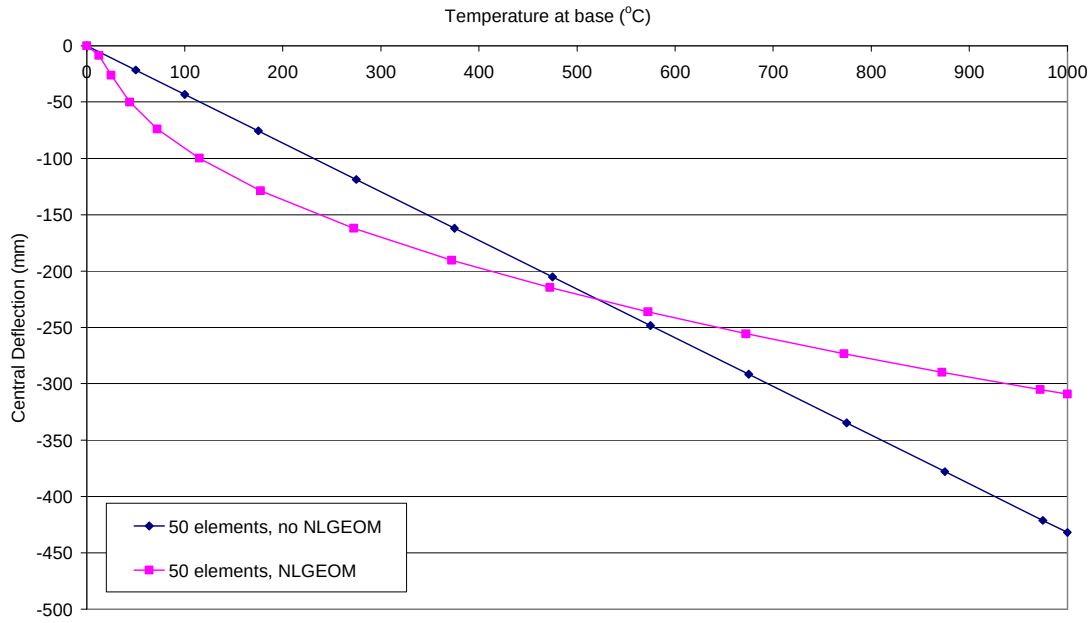

Figure 6-9: Deflection in an elastic beam with and without nonlinear geometry when a constant temperature increase and constant thermal gradient are applied

6.2.5 Temperature increase and constant thermal gradient, strain softening material properties

The above simple examples show that while average temperature increase causes strain localisation accompanied by elastic unloading, thermal gradient does not.

The beam in Figure 6-2, with strain softening properties as in Figure 6-1, was subjected to an average temperature increase and a constant thermal gradient applied along its length. The deflection at mid-span and the pinned end horizontal reaction forces are shown in Figures 6-10 and 6-11. In these the beam was discretised using 25 and 50 beam elements, and the softening modulus was treated as a material property. As discussed earlier, nonlinear geometry was included.

It is seen that the analysis is not mesh sensitive, that is, varying the mesh size does not affect the results shown in Figures 6-10 and 6-11. The evolution of deflected shapes is shown in Figure 6-12. It can be seen that the central region tends to become flatter with temperature increase, indicating distributed damage. From Figure 6-10 it can be seen that the central deflection increases rapidly in the initial phase of heating, before becoming almost constant due to thermal bowing and spread of plasticity.

Figure 6-11 shows the reaction force at the ends of the beam. Initially the reaction force is compressive, caused by expansion of the beam under average temperature increase. However as the temperature increases, the thermal gradient applied starts to dominate the response, with the reaction force decreasing and becoming tensile. A reduction in the tensile reaction force starts to be seen towards the end of this analysis, when strain softening begins to occur in the material.

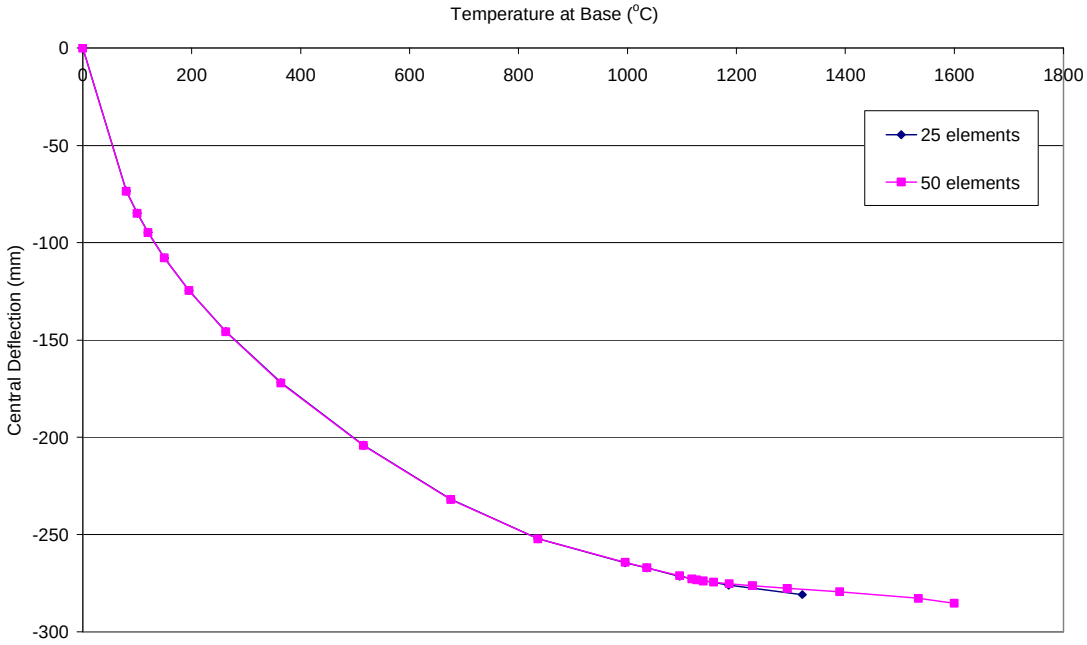

Figure 6-10: Deflection in a materially nonlinear beam when both a uniform thermal expansion and a constant temperature gradient are applied with different mesh discretisations

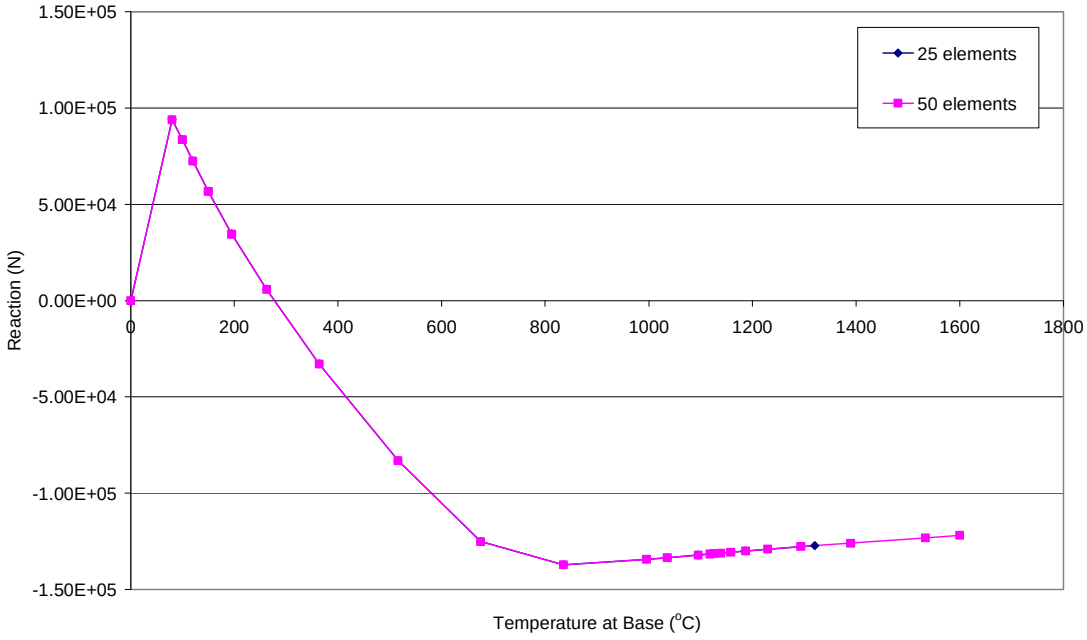

Figure 6-11: Horizontal reaction force in a materially nonlinear beam when both a uniform thermal expansion and a constant temperature gradient are applied with different mesh discretisations

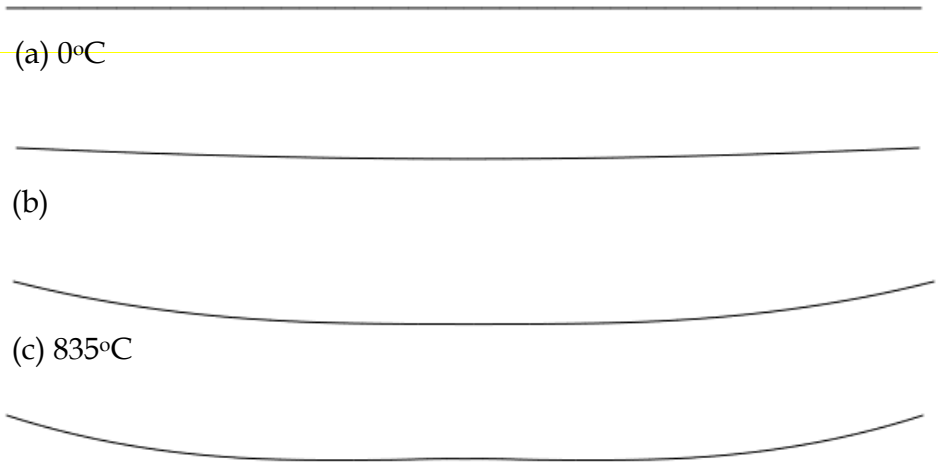

Figure 6-12: Evolution of the deflected shape of the beam throughout the analysis, the temperature given being the temperature at the base of the beam at that point

The above simple examples showed that while temperature increase caused strain localisation accompanied by elastic unloading, pure thermal gradient did not – yield was distributed throughout the beam, and hence the strain softening branch could be treated as a material property. When both temperature increase and thermal gradient were applied to the beam the same behaviour, with no strain localisation, was seen. Hence, in this situation, softening behaviour can be considered as a material property also.

6.3 Reinforced concrete plane strain analysis

A plane strain reinforced concrete model is created in Abaqus with a span L = 4000 mm, depth d = 150 mm, and was provided with both tension and compression reinforcement. In a 1 m wide section of the model, the cross-sectional area of reinforcing steel present was 160 mm^2 in compression (at the top) and 330 mm^2 in tension (at the bottom of the model). Plane strain elements were used and there were 6 elements present through the model's depth. The reinforcement was modelled using embedded truss elements. No shear

reinforcement was included in the model. It was assumed to be clamped at both ends (all nodes at the two ends were assumed to be restrained in both horizontal and vertical directions).

The concrete and reinforcement material properties used were varied throughout the simulations to investigate the effect that temperature dependency had on them.

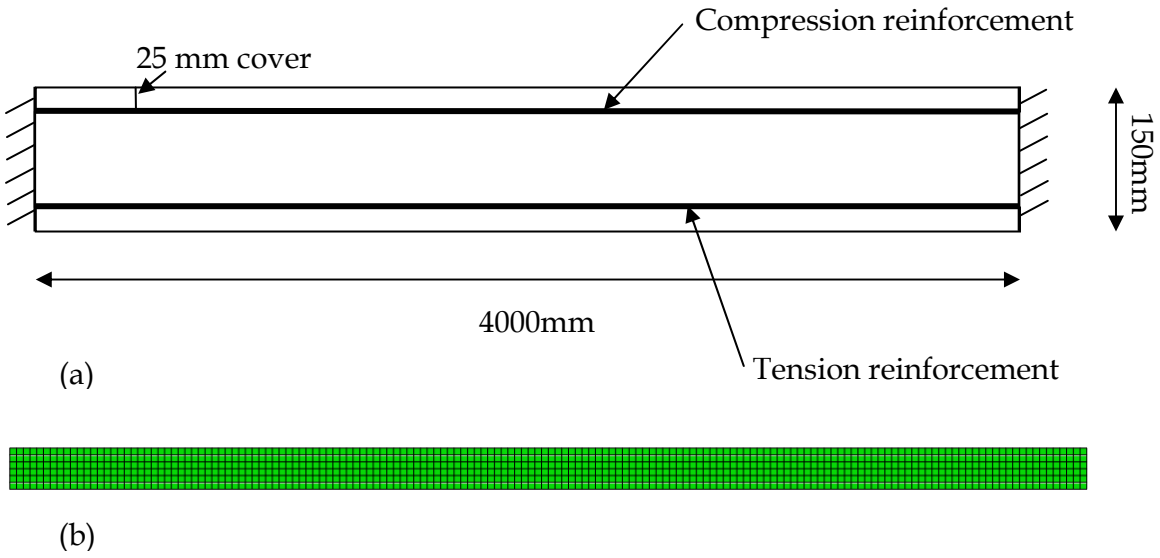

Figure 6-13: The reinforced concrete model: (a) dimensioned sketch (not to scale); and (b) finite element mesh

A uniformly distributed load based on a slab for typical office design and self-weight (approximately 11 kN/m^2) was applied in step 1 of the analysis. The results corresponding to this step are designated as 0s to 1s in figures. In the second step of the analysis, all elements were heated in accordance with a 900^{o}C, 60 min exponential fire curve by applying linearly increasing temperatures directly to the nodes of the elements. From the base to the top of the model, the final temperatures in the seven layers of nodes were: 715^{o}C, 388^{o}C, 196^{o}C, 137^{o}C, 101^{o}C, 72^{o}C, and 50^{o}C. The results of this step are designated as 1s to 2s in the figures.

Again, it is noted that throughout the rest of this chapter, positive stress and strain values indicate tension, while negative values indicate compression.

6.3.1 Perfect elastic-plastic material properties, not temperature dependant

In the first set of analyses, the material properties were kept constant with temperature. Furthermore, while the yield strengths of concrete and steel were input as their ambient values, they were assumed to be perfectly plastic.

The longitudinal stress and strain plots at integration points along the depth of the model, at the integration points closest to the support are shown in Figures 6-14 and 6-15. Incremental application of load in step 1 (0s to 1s) results in concrete exceeding its tensile strength in the longitudinal direction in the top-most element adjacent to the support (Figure 6-14). Compressive stresses of the same order are seen at the base, indicating that the material has not yielded in compression yet. Tensile strains at the top and compressive strains at the bottom are also seen (Figure 6-15).

As the model is heated (1s to 2s), it experiences differential thermal expansion due to the large thermal gradient applied over the model depth. This causes the all elements to move into compression, with maximum values occurring at the base of the model where temperatures are highest. Integration points in the two bottom-most elements adjacent to the support exceed the yield strength in compression. The integration points in concrete close to the embedded reinforcement are seen to carry lower stresses.

The uniformly distributed load induces tensile strain at the top and compressive strain at the bottom of the model in step 1. On heating, generally an average temperature increase would induce compressive strains all through the depth at the support, however, in this case, thermal bowing dominates the response and causes the total strains to be tensile in nature almost in the entire depth, and more so in the bottom region.

Figure 6-16 shows contour plots of the longitudinal plastic strain variation near the restraint throughout the analysis. Figure 6-16 (a) shows tensile plastic strain at the top and compressive at the base, at the end of the loading step (1s). Figure 6-16 (b), (c) and (d) show that the longitudinal plastic strains are tensile almost right through the depth of the beam at the support, and these tensile plastic strains continue to increase with heating. This is similar to the total strain response, seen in Figure 6-15. It is interesting to note that while stresses are compressive, both longitudinal total strains and longitudinal plastic strains at the support are tensile. Figure 6-16 (d) shows that the tension at the top and compression at the bottom type of plastic strain behaviour happens at some distance away from the support. This can be explained by the fact that the total strain present (as seen in Figure 6-15) is tensile, while the elastic strain is compressive (due to the compressive stress present, see Figure 6-14), and the thermal strain is tensile (Figure 6-17). When the elastic and thermal strains are removed from the total strain, plastic strain is what is left – and in this case it is tensile, as seen in Figure 6-16.

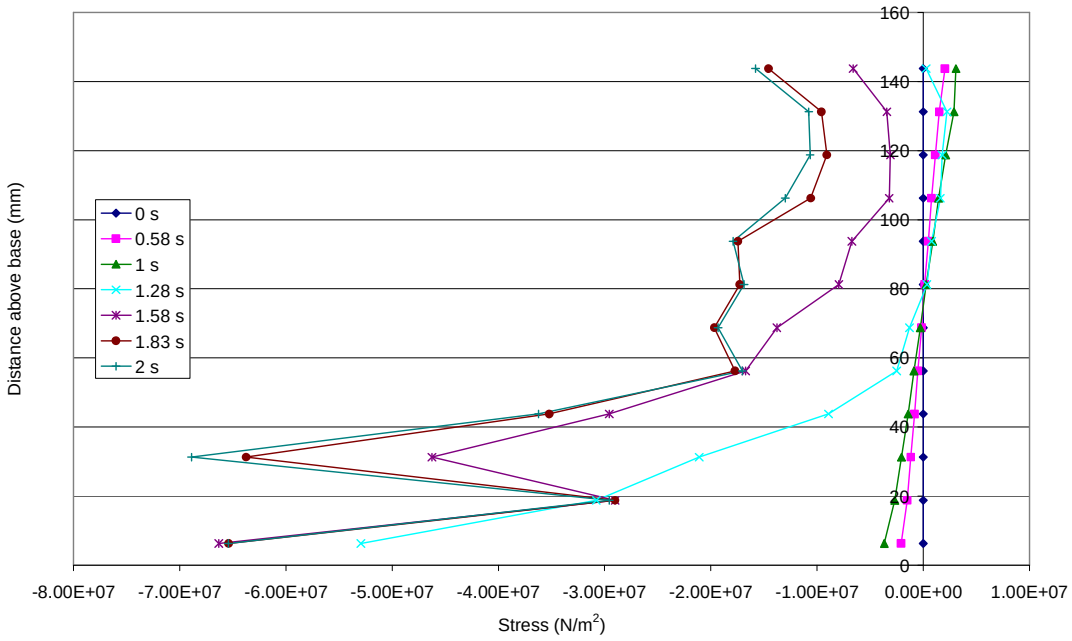

Figure 6-14: Stress in the longitudinal direction, plotted for integration points next to the restraint, at various times throughout the analysis in the loading (0s – 1s) and the heating step (1s – 2s). On loading, tensile stress is seen at the top of the model, while compression is seen at the base. The concrete has yielded in tension at the topmost integration points by the end of the loading step. As heating occurs, thermal expansion causes all integration points to move into compression, with maximum values at the base where temperatures are highest. Integration points at the base have yielded in compression, while the integration points nearest to the embedded reinforcement carry lower stresses.

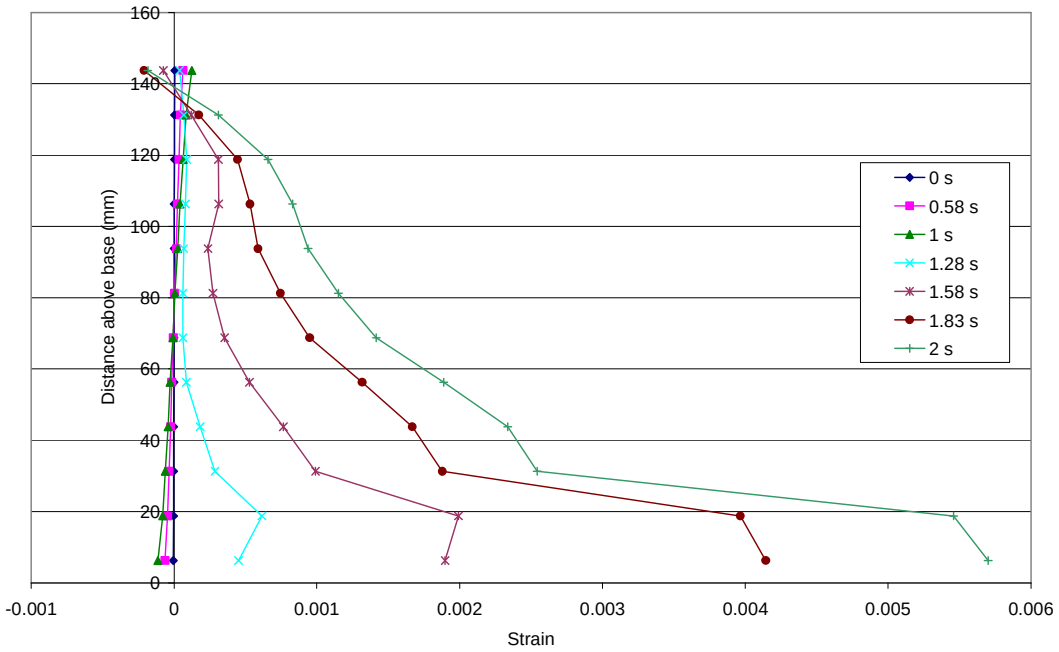

Figure 6-15: Total strain in the longitudinal direction, plotted for integration points next to the restraint, at various times throughout the analysis in the loading step (0s – 1s) and the heating step (1s – 2s). During application of the load, tensile strains develop at the top of the model while compression strains are present at the base. On heating, thermal bowing dominates the response and causes the total strains present to be tensile throughout almost the entire depth. The top experiences compressive strains due to thermal expansion from the temperatures applied.

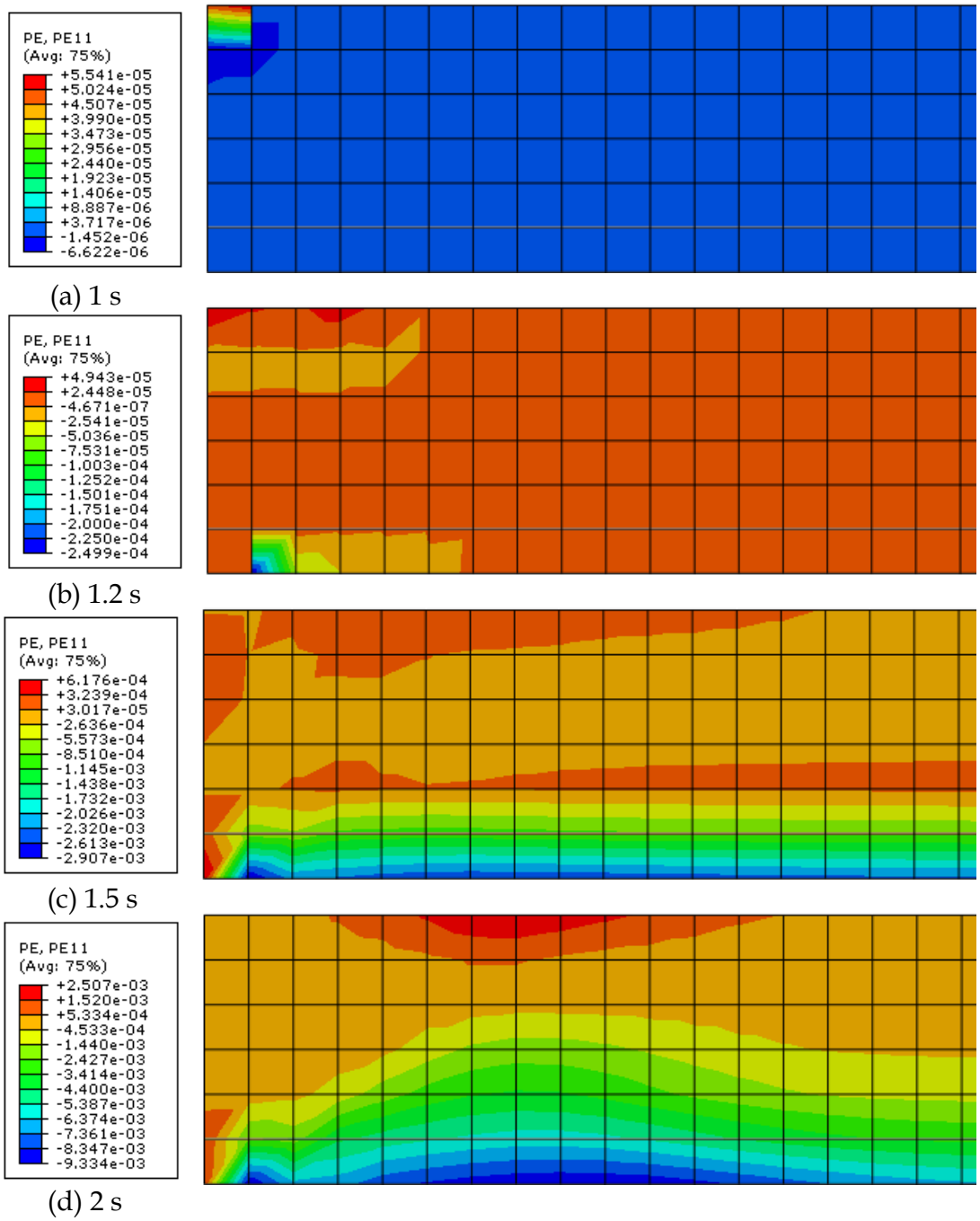

Figure 6-16: Contour plots of plastic strain in the longitudinal direction, magnified on the restraint at the left hand side of the model, at various times throughout the analysis: (a) at the end of loading; (b) and (c) mid-way through heating; and (d) at the end of the heating step. The top of the model has tensile plastic strain and the base compressive plastic strain at the end of loading, while during heating the plastic strain throughout the depth of the model becomes tensile. While stresses are compressive throughout the model, both the total strains and plastic strains are tensile at the support. Compressive plastic strains are seen at the base of the model, further away from the support – here the more typical tension at the top and compression at the base behaviour is seen.

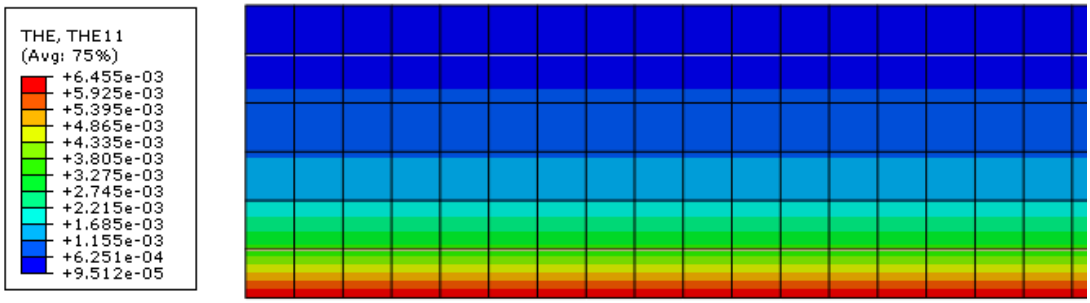

Figure 6-17: Contour plot of thermal strain in the longitudinal direction, magnified on the restraint at the left hand side of the model, at the end of the analysis. The thermal strain is tensile throughout, and largest at the base where temperatures are highest.

6.3.2 Perfect elastic-plastic material properties with temperature dependant yield strength

The analysis considered in the previous subsection was again conducted, in which both concrete and steel were assumed to lose peak strength at elevated temperatures. The elastic modulus, however, was assumed to remain unchanged, and both materials remain perfectly plastic. The results are shown in Figures 6-18 to 6-20.

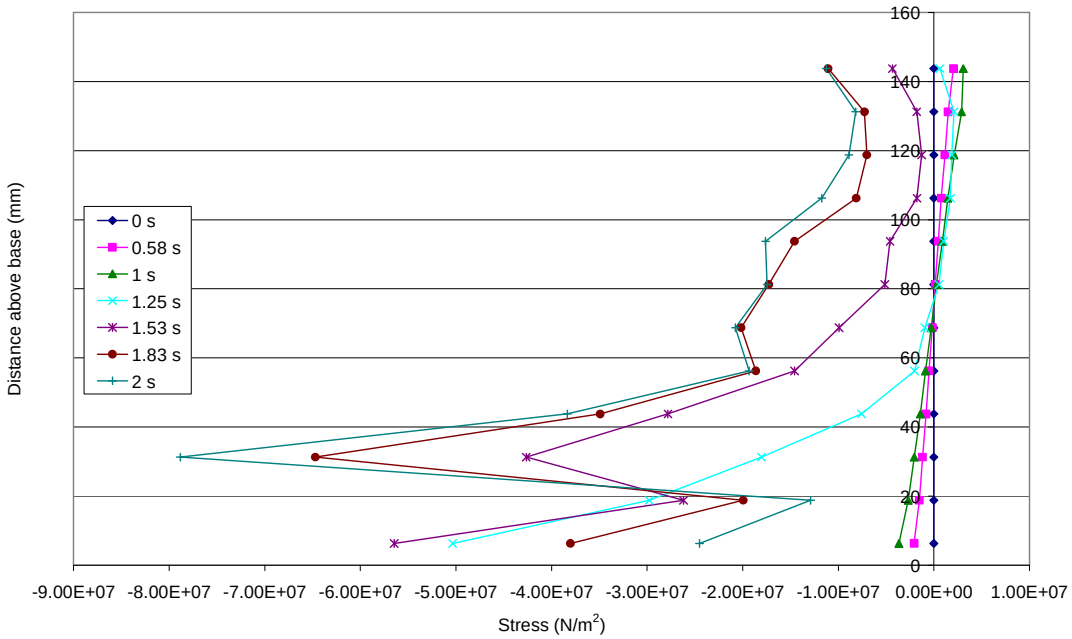

Figure 6-18: Stress in the longitudinal direction, plotted for integration points next to the restraint, at various times throughout the analysis in the loading (0s – 1s) and the heating step (1s – 2s). On loading, tensile stress is seen at the top of the model, while compression is seen at the base. As heating occurs, thermal expansion causes all integration points to move into compression. Partway though the heating step the stress values present become limited by the decreasing yield strength of concrete at elevated temperatures, hence in the last increments the stress at the base decreases.

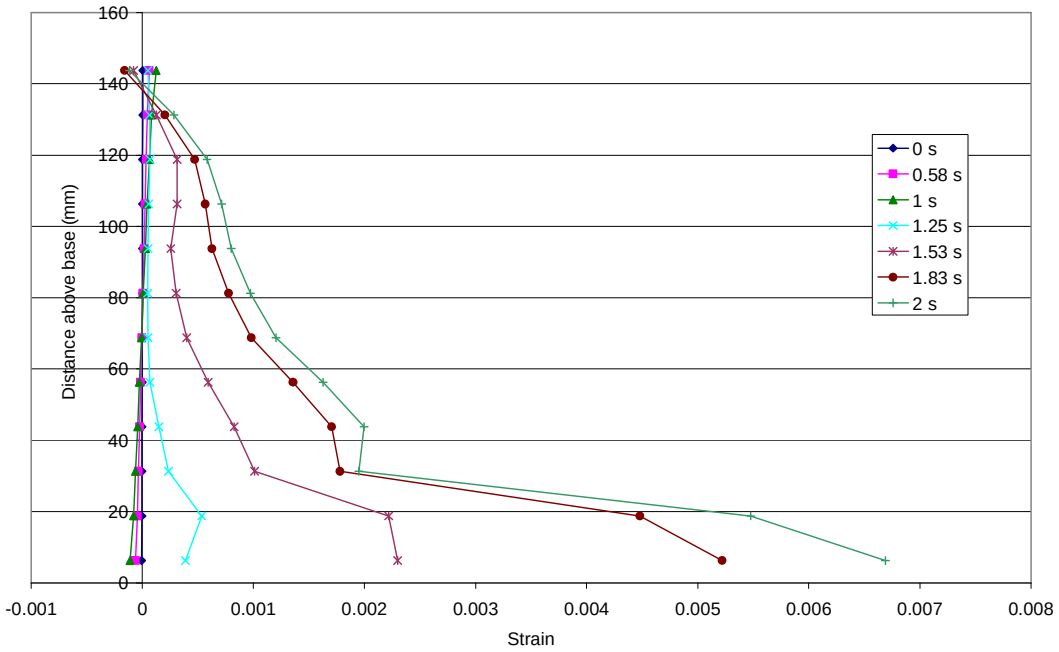

Figure 6-19: Total strain in the longitudinal direction, plotted for integration points next to the restraint, at various times throughout the analysis in the loading step (0s – 1s) and the heating step (1s – 2s). During application of the load, tensile strains develop at the top of the model while compression strains are present at the base. On heating, thermal bowing dominates the response and causes the total strains present to be tensile throughout almost the entire depth. The top experiences compressive strains due to thermal expansion from the temperatures applied. In this case the total strains present are higher than in the previous example, due to the smaller stresses present at elevated temperatures.

Generally the results are similar to those seen in the previous example, with tensile stress at the top during the loading step converting to compressive stress on heating. Compressive stress at the base increases throughout the analysis, until part-way through the heating step, when the stress values present become limited by the decreasing yield strength of concrete at elevated temperatures. Hence, in the last increments, the compressive stress present at the base decreases. Lower stresses are seen at the concrete integration points adjacent to the embedded reinforcement.

The total strain response is similar to that observed when strength degradation was ignored, with initial tensile and compressive total strains converting to mainly tensile strains after the heating step. Again, this is due to the dominance of thermal bowing in the model's response. In this case though, the strains are relatively higher than in the previous example, due to the slight increase in stresses present at various points, and the elastic modulus constant at increasing temperature.

Contour plots of plastic strain show the same overall behaviour as in the previous example. It is noted that larger plastic strains (both tensile and compressive) are present at the end of the analysis, due to strength degradation of concrete and reinforcement at elevated temperatures.

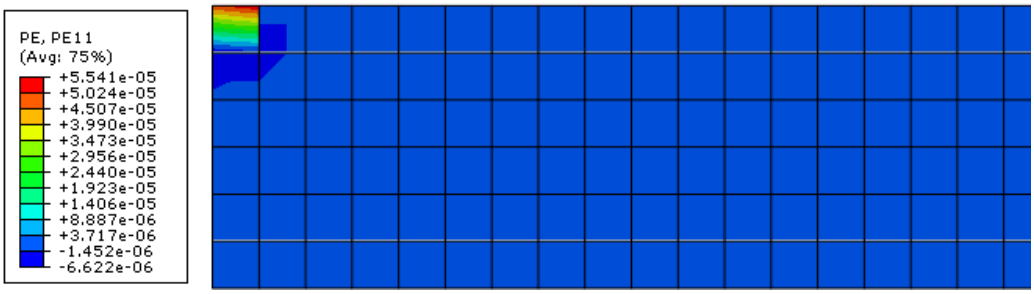

(a) 1 s

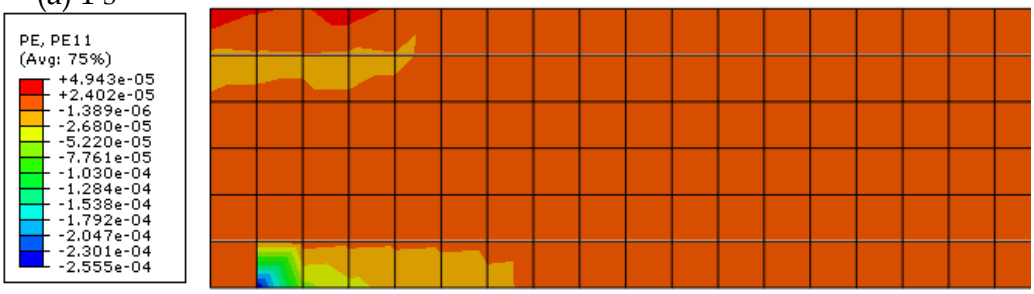

(b) 1.2 s

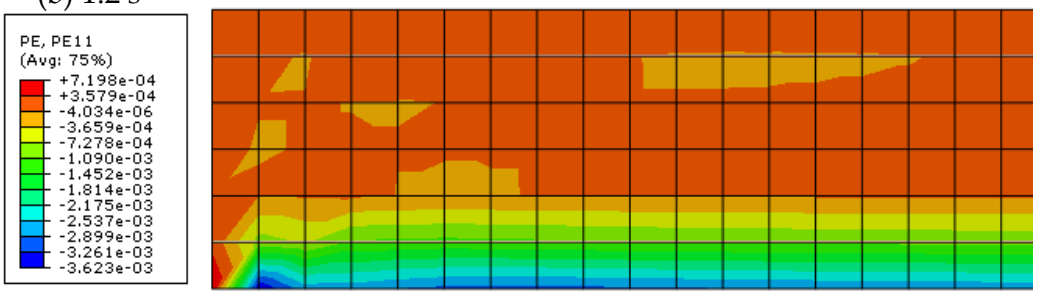

(c) 1.5 s

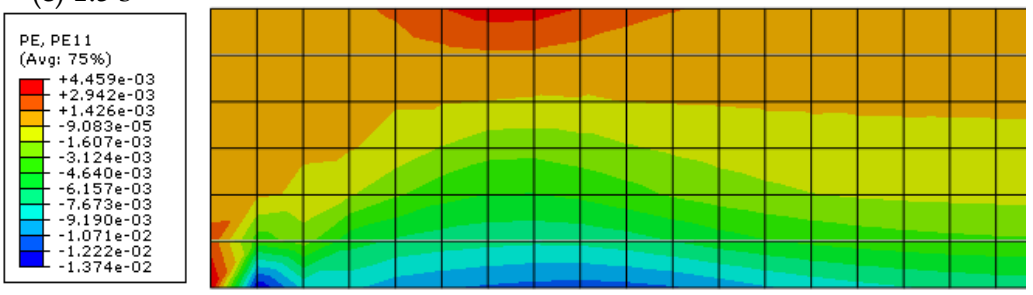

(d) 2 s

Figure 6-20: Contour plots of plastic strain in the longitudinal direction, magnified on the restraint at the left hand side of the model, at various times throughout the analysis: (a) at the end of loading; (b) and (c) mid-way through heating; and (d) at the end of the heating step. The top of the model has tensile plastic strain and the base compressive plastic strain at the end of loading, while during heating the plastic strain throughout the depth of the model becomes tensile. Larger plastic strains (both tensile and compressive) are seen in this example than in the previous one, due to the strength degradation of concrete and reinforcement at elevated temperatures.

6.3.3 Perfect elastic-plastic material properties with temperature dependant yield strength and elastic modulus

Lastly, the same analysis was carried out, but with both yield strength and elastic modulus decreasing as temperature of steel and concrete increases. Results from this are shown in Figures 6-21 to 6-23.

Results from the loading step (0s – 1s) are as seen previously, however the changing material properties at elevated temperatures affect results from the heating step (1s – 2s).

Figure 6-21 shows the stress in the longitudinal direction throughout the analysis. Smaller stress values are seen here at elevated temperatures than in the previous examples, and the stress at the base of the model is seen to decrease on increasing heating (as described in the last example). This is due to the reduced yield stress and elastic modulus of concrete at elevated temperatures.

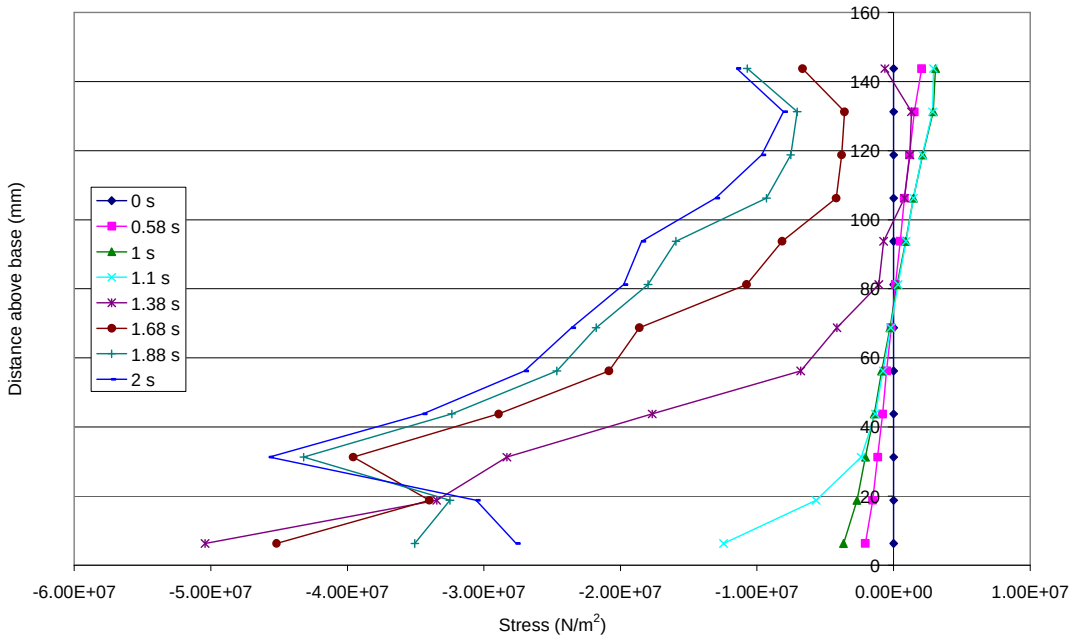

Figure 6-21: Stress in the longitudinal direction, plotted for integration points next to the restraint, at various times throughout the analysis in the loading (0s – 1s) and the heating step (1s – 2s). On loading, tensile stress is seen at the top of the model, while compression is seen at the base. As heating occurs, thermal expansion causes all integration points to move into compression. Partway though the heating step the stress values present become limited by the decreasing yield strength and elastic modulus of concrete at elevated temperatures, hence in the last increments the stress at the base decreases.

The total longitudinal strain at the support is also seen to be smaller (Figure 6-22). A smaller elastic modulus results in lower stresses. Since yielding is based on stresses, the plastic strains are smaller as well, resulting in smaller total strains in comparison to previous examples.

Once again, contour plots of plastic strain show the same overall behaviour as in the previous example (Figure 6-23). Smaller plastic strains (both tensile and compressive) are present at the end of the analysis than in the example where only yield stress was temperature dependent. It is evident that the reduction in elastic modulus with increasing temperature causes a reduction in plastic strain too.

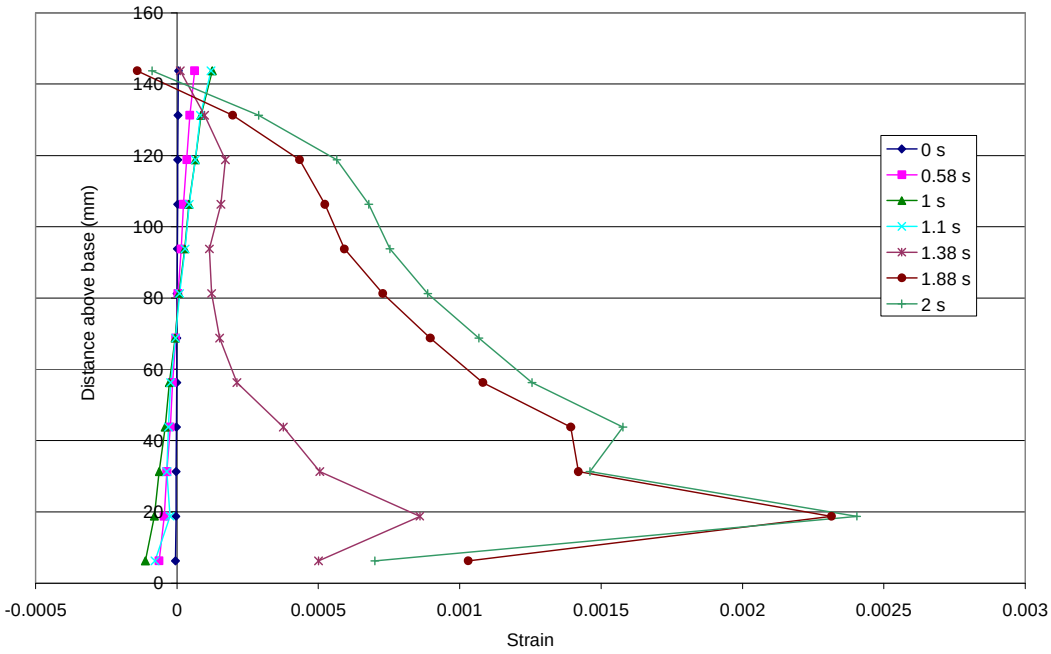

Figure 6-22: Total strain in the longitudinal direction, plotted for integration points next to the restraint, at various times throughout the analysis in the loading step (0s – 1s) and the heating step (1s – 2s). During application of the load, tensile strains develop at the top of the model while compression strains are present at the base. On heating, thermal bowing dominates the response and causes the total strains present to be tensile throughout almost the entire depth. The top experiences compressive strains due to thermal expansion from the temperatures applied. In this case the total strains present are lower than in the previous examples, due to the smaller stresses present at elevated temperatures and the reduction in elastic modulus at elevated temperatures.

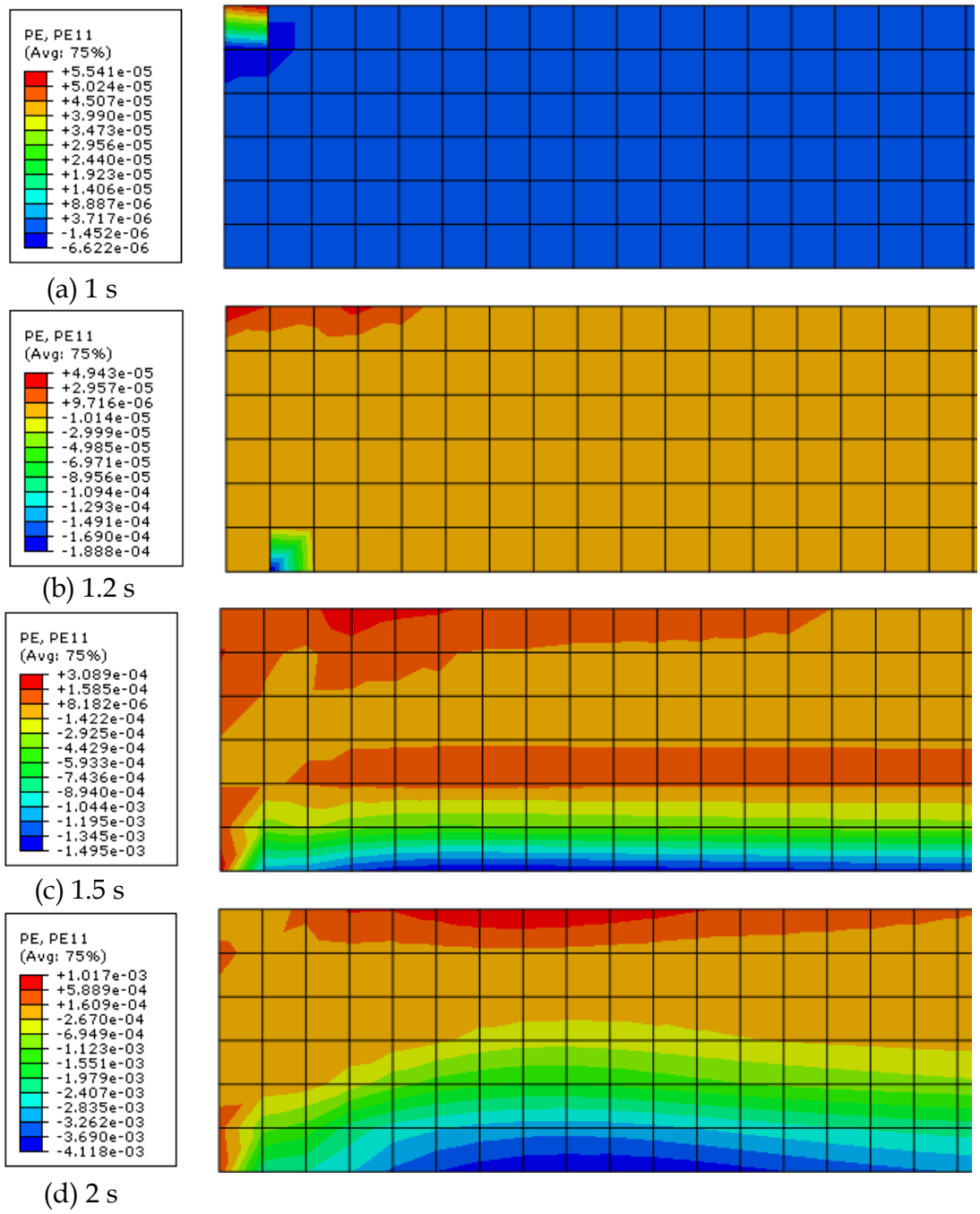

Figure 6-23: Contour plots of plastic strain in the longitudinal direction, magnified on the restraint at the left hand side of the model, at various times: (a) at the end of loading; (b) and (c) mid-way through heating; and (d) at the end of the heating step. The top of the model has tensile plastic strain and the base compressive plastic strain at the end of loading, while during heating the plastic strain throughout the depth of the model becomes tensile. Smaller plastic strains (both tensile and compressive) are seen in this example than in the previous one, due to the reduction in elastic modulus of concrete and reinforcement at elevated temperatures causing a reduction in the plastic strains present.

.

6.4 Reinforced concrete model, considering tension stiffening

The examples of the last section did not incorporate strain softening, and were meant to examine the effect of the change of different parameters at temperature on the response. In this section the same model geometry as described in the previous section was used, with the same magnitude of loading, and the same heating pattern of average temperature increase and constant thermal gradient. The material properties of concrete used, however, were based on the previous chapter for reinforced concrete cylindrical specimens. The material properties for reinforcement were assumed to be as shown in Figure 6-24, and the uniaxial compressive strength of concrete was assumed to be as shown in Figure 6-25. Further, the concrete was modelled with tension stiffening, using properties as shown in Figure 6-26.

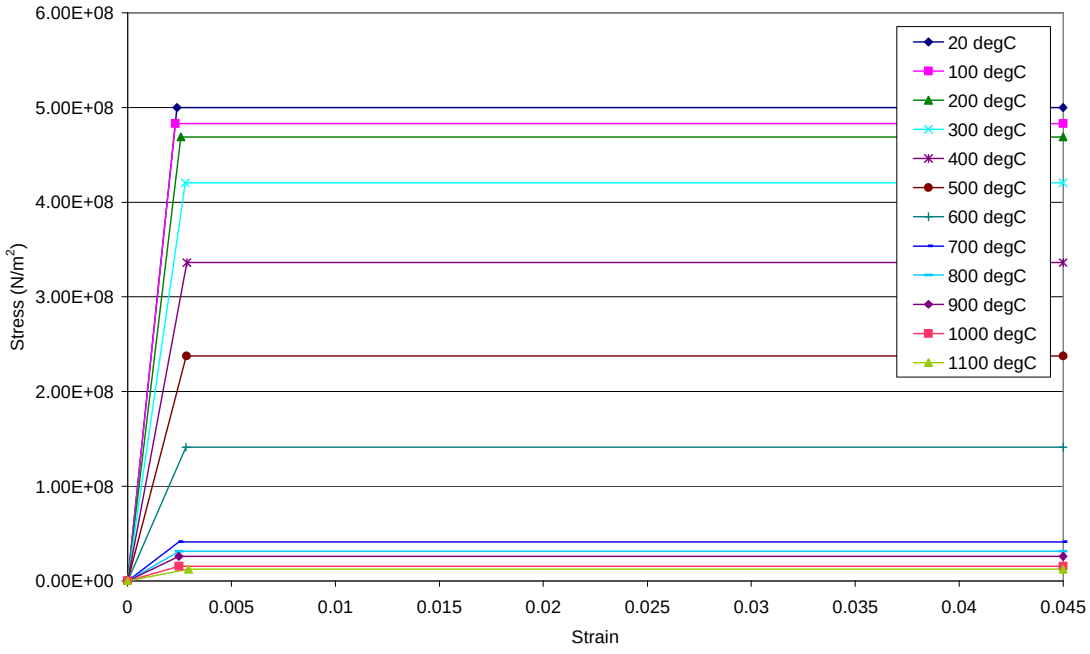

Figure 6-24: Reinforcing steel material properties at elevated temperatures

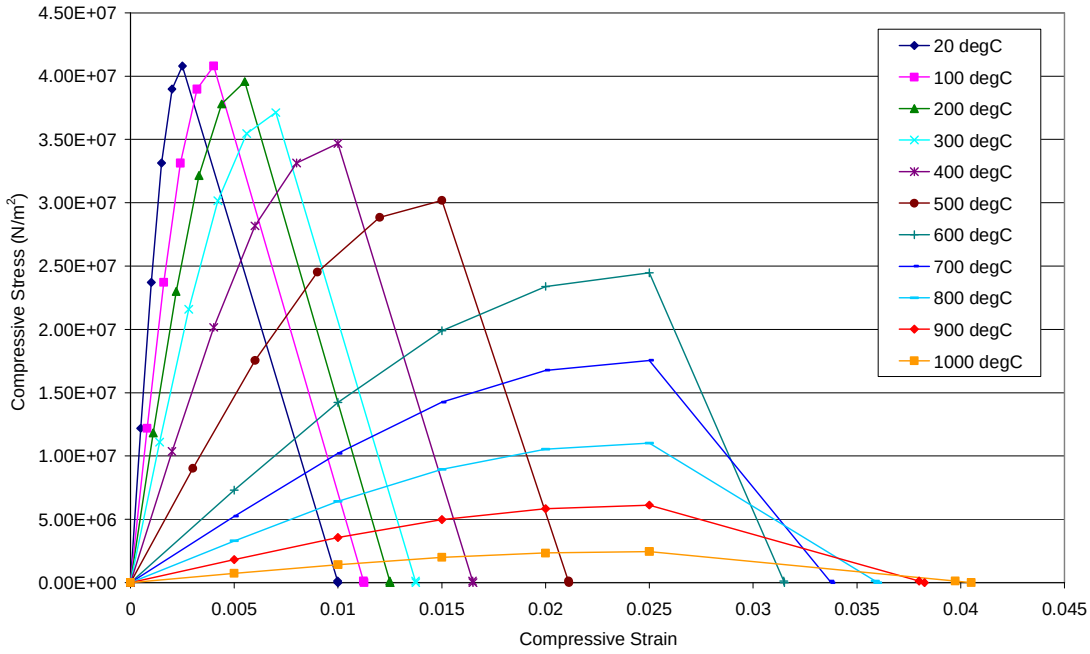

Figure 6-25: Compressive material properties used for plain concrete in FE modelling at elevated temperatures

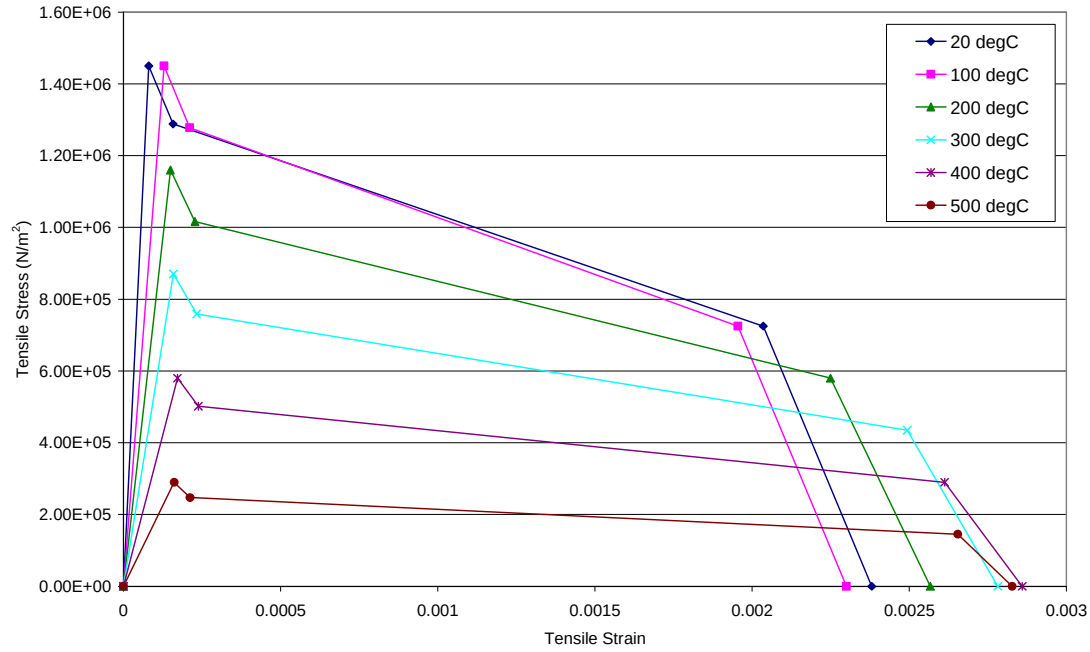

Figure 6-26: Concrete material properties incorporating the effects of tension stiffening

6.4.1 Inclusion of tension stiffening, but no damage

In the first analysis no damage parameters were included. The results from this analysis are shown in Figures 6-27 and 6-28.

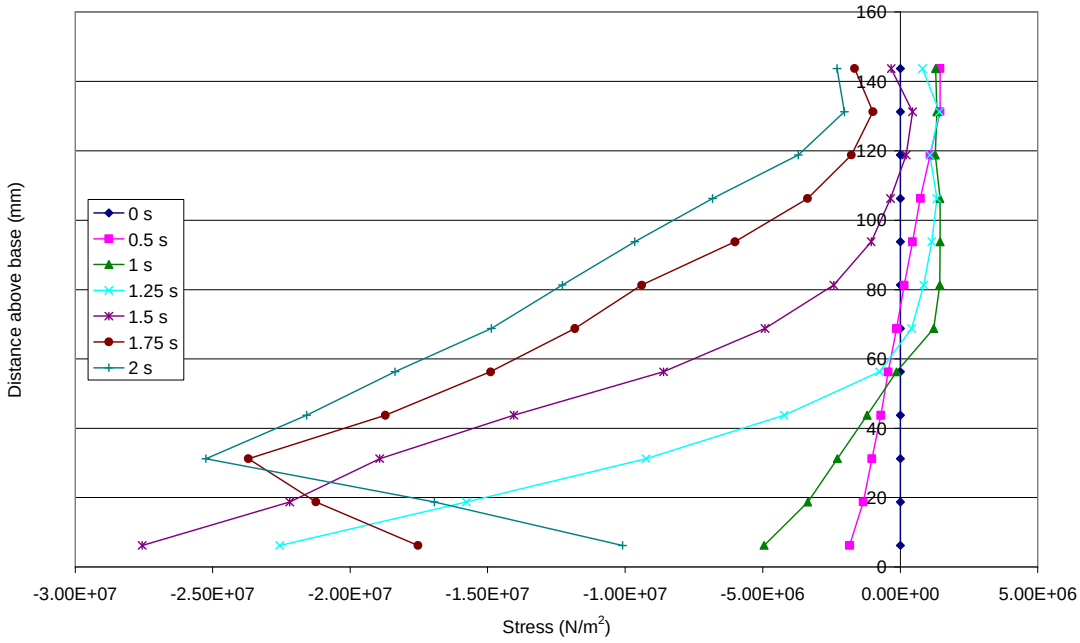

Figure 6-27: Stress in the longitudinal direction, plotted for integration points next to the restraint, at various times throughout the analysis in the loading (0s – 1s) and the heating step (1s – 2s). On loading, tensile stress is seen at the top of the model, while compression is seen at the base. The top of the model has yielded in tension by the end of the loading step. As heating occurs, thermal expansion causes all integration points to move into compression. Partway though the heating step the stress values present become limited by the decreasing yield strength and elastic modulus of concrete at elevated temperatures, hence in the last increments the stress at the base decreases.

Figure 6-27 shows the stress in the longitudinal direction in concrete adjacent to the restraint throughout the analysis. Initially tensile stress at the top and compressive stress at the base of the model occur, due to the UDL applied. It is seen that concrete has yielded plastically in tension at the top of the model, having reached its tensile yield stress there. On heating, thermal expansion occurs, and the model moves into compression throughout. On further heating,

and the reduction of yield stress at elevated temperatures, the stress at the base of the model reduces significantly.

Figure 6-28 shows contour plots of longitudinal plastic strain at various times throughout the analysis, concentrating on the area of the model next to the restraint on the left. Initially, on loading, tensile plastic strain occurs at the top of the model, while compressive plastic strain is present at the base. As heating occurs, thermal expansion causes the compressive plastic strains to increase. However, as heating continues, thermal bowing starts to dominate the response, and the tensile plastic strain increases through the depth of the model, though it is localised at the top some distance away from the support. Plastic strains throughout the depth are seen to be tensile.

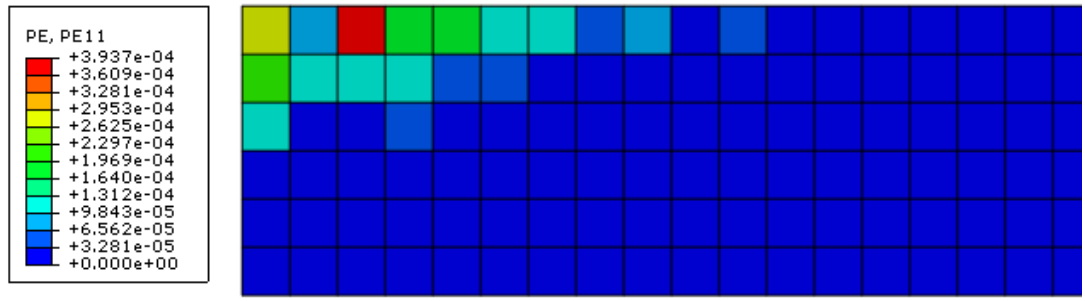

(a) 1 s

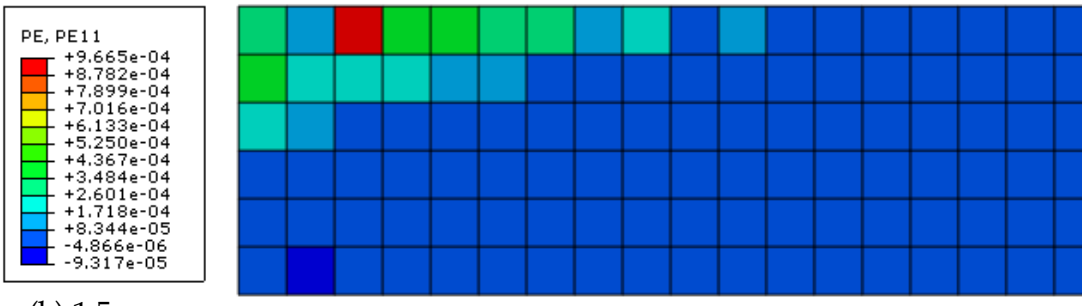

(b) 1.5 s

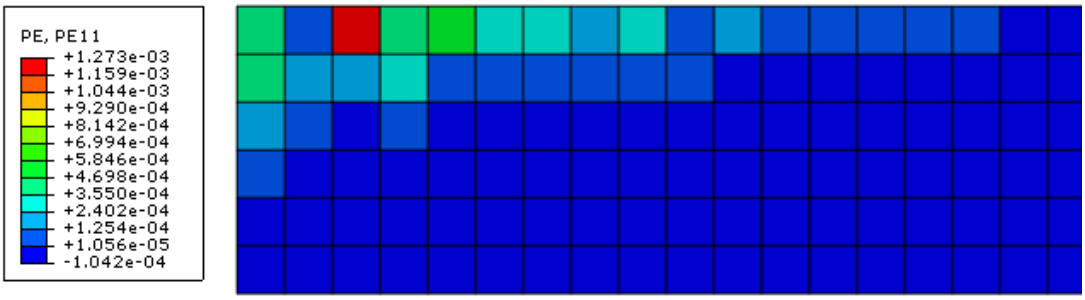

(c) 1.8 s

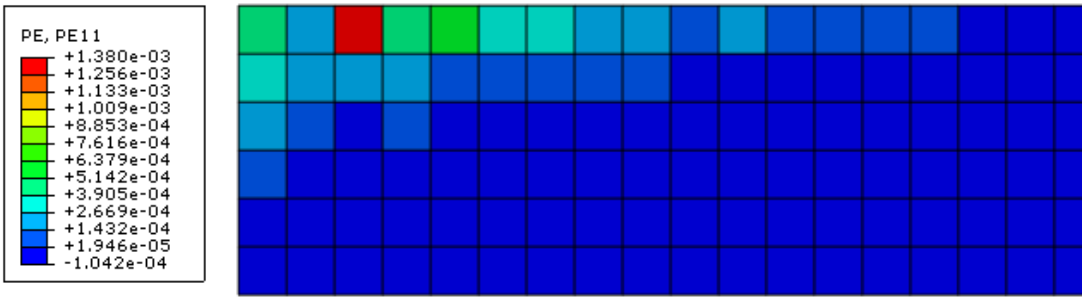

(d) 2 s

Figure 6-28: Quilt contour plots of plastic strain in the longitudinal direction, magnified on the restraint at the left hand side of the model, at various times throughout the analysis: (a) at the end of loading; (b) and (c) mid-way through heating; and (d) at the end of the heating step. The top of the model has tensile plastic strain and the base compressive plastic strain at the end of loading, while during heating, initially, the compressive strains present increase due to thermal expansion. However by the end of the heating step, thermal bowing has dominated the response of the model and the plastic strain present becomes tensile. The tensile plastic strain is localised at the top of the model, a small distance from the support.

6.4.2 Inclusion of tension stiffening and damage

The analysis of the previous subsection was again conducted, with damage and recovery parameters included. The values used for these are shown in Figure 6-29, and damage recovery was set to zero in both tension and compression. The results of the analysis are shown in Figures 6-30 and 6-31. It can be seen that the variation of the longitudinal stress in Figure 6-30 is almost identical to that seen in Figure 6-27 where damage was not included. Similarly, the evolution of longitudinal plastic strains in Figure 6-31 is also almost identical to that seen in Figure 6-28.

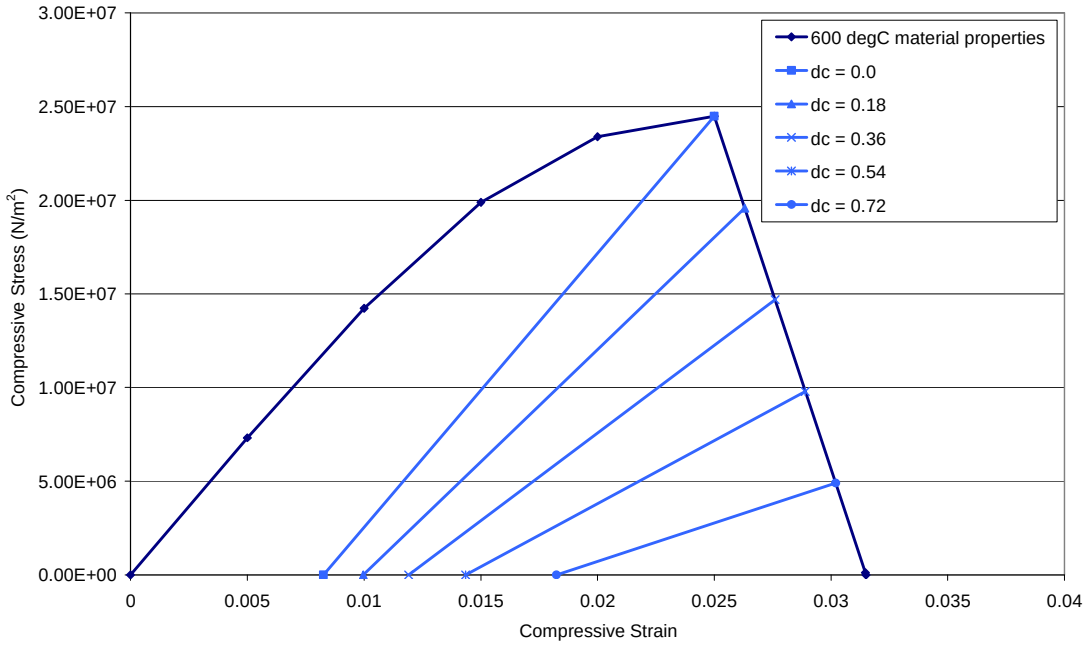

Figure 6-29: Stress-strain curve for concrete under compression at 600°C, incorporating linearly increasing damage variables present after peak-stress

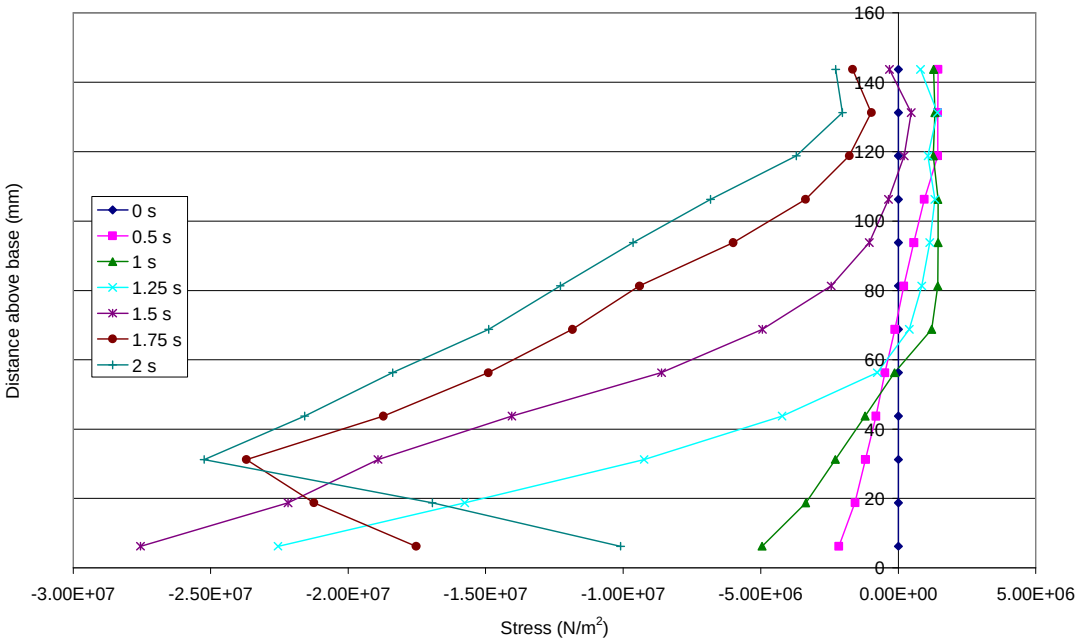

Figure 6-30: Stress in the longitudinal direction, plotted for integration points next to the restraint, at various times throughout the analysis in the loading (0s – 1s) and the heating step (1s – 2s). On loading, tensile stress is seen at the top of the model, while compression is seen at the base. As heating occurs, thermal expansion causes all integration points to move into compression. Partway though the heating step the stress values present become limited by the decreasing yield strength and elastic modulus of concrete at elevated temperatures, hence in the last increments the stress at the base decreases. The variation seen here is almost identical to that seen in the previous example, showing that damage and recovery variables have little effect on this model.

It can be seen that damage and recovery parameters have a negligible effect on the response of the model. This is consistent with the results obtained in the previous chapter. It may be recalled that the behaviour of the plain concrete cylinder heated and subjected to compression showed considerable difference in response with and without inclusion of damage variables. Similarly, the simulation after cooling the plain concrete cylinder showed significant difference due to inclusion of damage parameters. However, for reinforced concrete cylinders, damage parameters were found to have negligible effect on the response. Once again, here for the model, inclusion of reinforcement and consequent tension stiffening makes inclusion of damage parameters inconsequential.

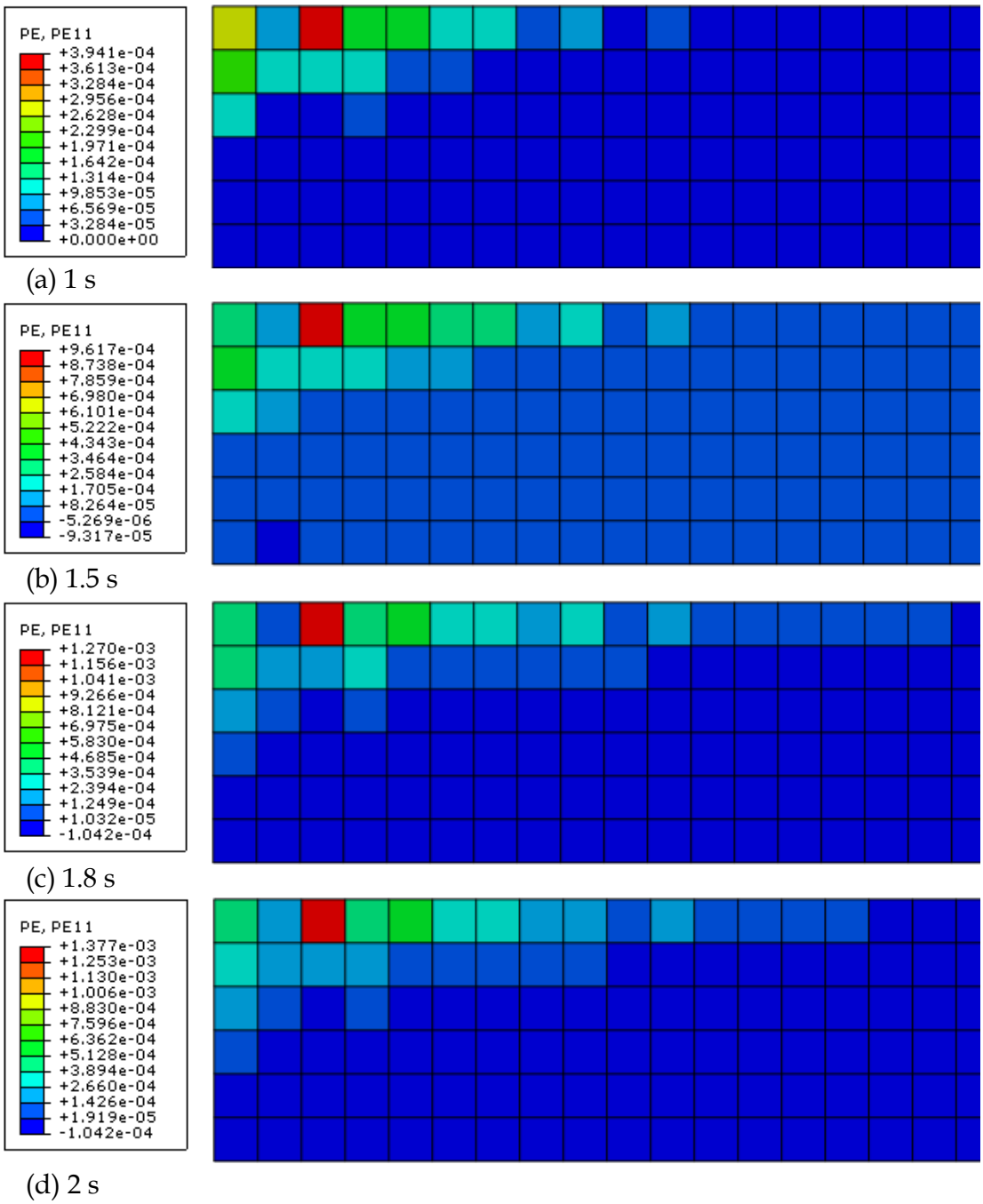

Figure 6-31: Quilt contour plots of plastic strain in the longitudinal direction, magnified on the restraint at the left hand side of the model: (a) at the end of loading; (b) and (c) mid-way through heating; and (d) at the end of the heating step. The evolution of plastic strains here is very similar to that seen in the previous example, suggesting that damage and recovery variables have a negligible effect on the response of this model.

7

Pre-damaged reinforced concrete structural systems in fire

7.1 Introduction

Earthquake and fire are two extreme events in which the former is very likely to be followed by the latter. There have been a plethora of studies to examine the

response of structures subjected to earthquake loading or fire loading. This study considers the response of a simple structural system subjected to an earthquake followed by fire. A single storey reinforced concrete portal frame is used for analytical demonstration. The analysis is conducted using the finite element package Abaqus. Both material and geometric nonlinearities are included in the models. Continuum plasticity is used to model post-elastic behaviour and damage. Damage due to earthquake is induced using static procedures. Fire loading is modelled by applying a temperature increase directly to the nodes of the model and both a constant temperature increase and a thermal gradient are included to more realistically model what occurs in concrete structures in fire. The aim of the study is to examine the response qualitatively rather than seek quantitative answers.

7.2 The test structure and material model

The test structure used is shown in Figure 7-1. The frame has a bay width of 5m and a height of 3m, while the columns have cross-section dimensions of 0.4m by 0.4m and the beam at the top is 0.3m deep and 0.2m wide. The columns were assumed fixed at the base. The finite element model used 2-noded linear beam elements. Each column is meshed using two elements, while the beam contains four elements along its span. The main reinforcement in the columns comprises 4 bars of 16mm diameter. The tension and compression reinforcement in the beam comprises 2 bars of 25mm diameter and 2 bars of 16mm diameter respectively. Steel and concrete are included explicitly in the model. Concrete is modelled using the concrete damaged plasticity model available in Abaqus. The yield criterion is pressure sensitive and based on the work by Lubliner et al. (1989) and Lee and Fenves (1998). For modelling reinforcement the von Mises yield criterion is employed. For concrete it is assumed that the uniaxial tensile strength is one tenth the uniaxial compressive strength, and the post yield behaviour is perfectly plastic at any given temperature. Reinforcement is assumed to be perfectly plastic as well. In order to partly conform to Eurocode 2

(EN1992-1-2 2004) on structural fire design both Young's modulus and yield stress are assumed to decrease with increasing temperature.

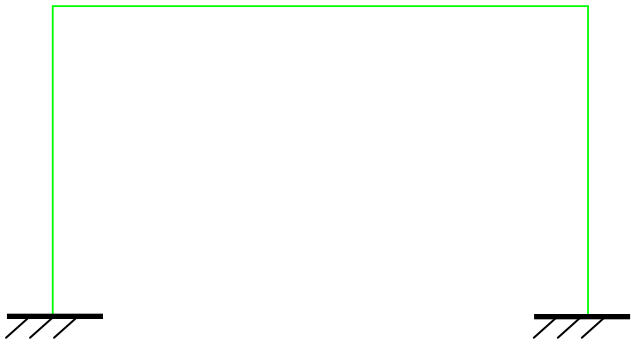

Figure 7-1: The test structure

7.3 Applied loadings

Two forms of extreme loadings are considered. The first is earthquake loading, in the form of a lateral displacement controlled push of 0.15m applied at the beam level. This loading is considered in two forms: a push in one direction and its removal, and a push in one direction followed by load reversal and then load removal.

The second form of loading is fire loading, which is applied only to the nodes of the beam in this study. A constant temperature increase of 365.5°C is applied at mid-depth, and a temperature gradient of -2.3°C/mm is applied across the beam's depth. An exponential fire curve given by the equation

$$T_f = 20.0 + (T_{\max} - 20.0) \times (1 - \exp(t \times q)) \tag{7.1}$$

was used to find the concrete temperatures for the base and top of the beam in a 900°C fire after 60 minutes. In the above equation T_f is the fire temperature at the current time, $T_{\max}$ is the maximum fire temperature achieved, t is the current time and q is the cooling rate of the fire. These temperatures were then used to calculate the linear thermal gradient over the depth of the beam.

Realistically the temperature gradient would not be constant over the depth of the beam due to concrete's low thermal conductivity – the temperature would decrease rapidly on moving away from the surface at the base of the beam.

7.4 Fire loading only

Consider the frame being subjected to the fire loading alone, as described above. If static loads (dead and imposed) are ignored then the deflected shape of the test structure is obtained as shown in Figure 7-2.

Figure 7-2: Deformed shape under fire loading only (magnification x200)

It can be seen that in spite of the temperature gradient which should cause bowing downwards in the beam, joint rotation due to the constant temperature increase causes upward bowing. This thermal loading is sufficient to cause inelastic deformation in the structure. Plastic strain is almost constant along the beam span and decreases to zero at the fixed ends of the columns. The beam is in compression along its length, caused by the constant temperature increase at its mid-depth.

A realistic uniformly distributed load (which is included in all subsequent analyses) was then included, and fire loading was applied to the structure. The

resulting deformed shape and consequent plastic strains are shown in Figure 7-3. It is noted that upward bowing is not apparent here and that the UDL has confined the largest plastic strains to the central elements of the beam. Both the UDL and the thermal gradient cause tension at the base of the beam; whereas a constant temperature increase induces compression and causes joint rotation at the ends of the beam. This reduces the amount of thermal bowing downwards. It is important to note that for reinforced concrete structures thermal gradient is likely to dominate the response of the structure, particularly in short, hot fires, due to the poor thermal conductivity of concrete.

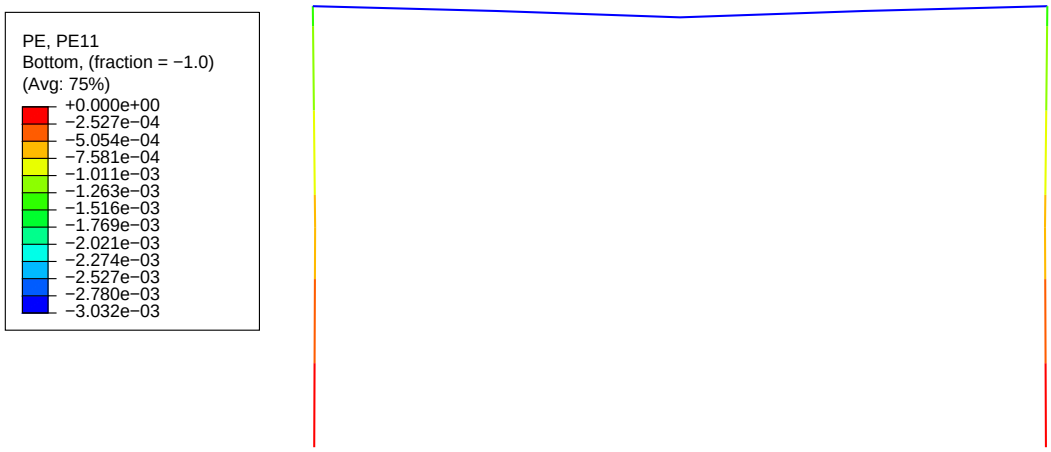

Figure 7-3: Deformed shape under UDL and fire loading (magnification x200)

7.5 Earthquake and fire loading

Consider the application of earthquake loading (in the form of a push) in one direction, its removal and application of fire loading as discussed above. The load – horizontal deformation (at the point of load application) graph is shown in Figure 7-4. The resulting deformed shapes with plastic strains are shown in Figure 7-5.

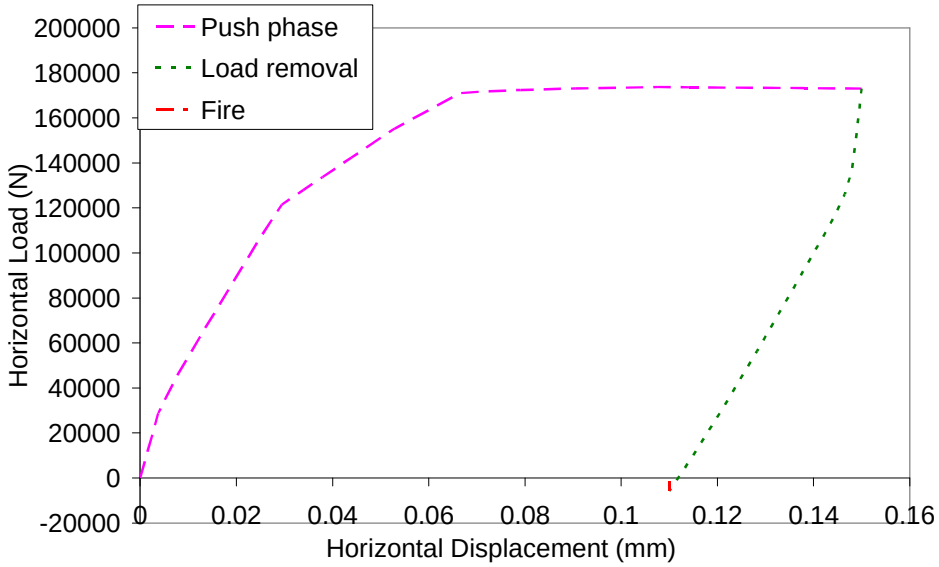

Figure 7-4: Load – horizontal deformation (at the point of load application)

It can be seen that the lateral load causes the largest compressive plastic strains to occur at the right end of the beam and the largest tensile plastic strains at the bottom end of the right column (see Figure 7-5 (a)). The tensile plastic strain at the left end of the beam is larger in magnitude than the compression found at the right; this is due to lower tensile yield strength. Load removal causes the structure to displace leftwards (Figure 7-5 (b)); this can also be seen in Figure 7-4. However, the plastic strain profile and the deformed shape are not significantly altered.

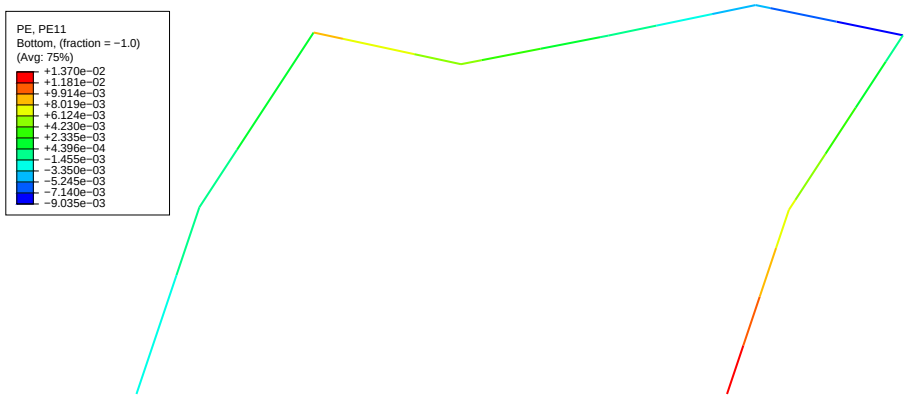

(a)

continued

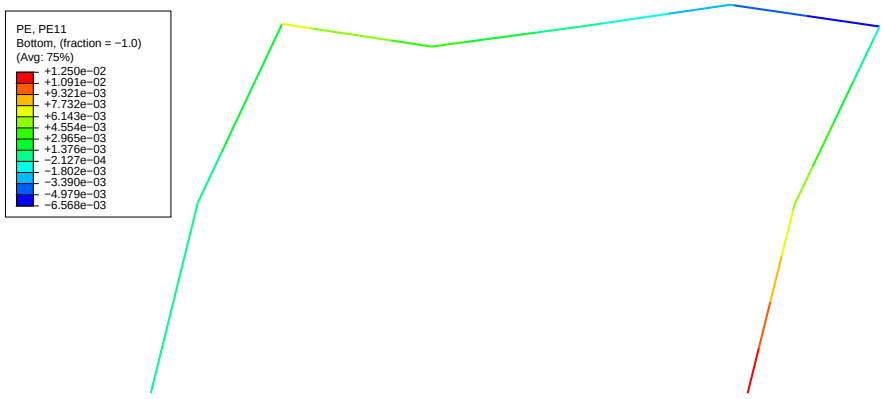

(b)

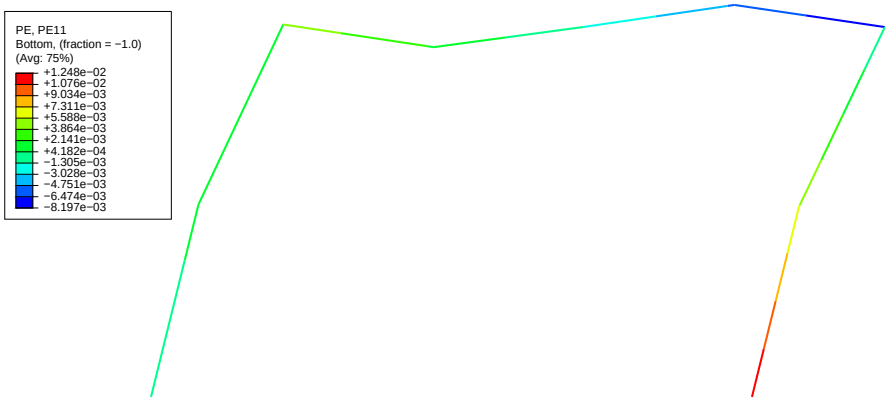

(c)

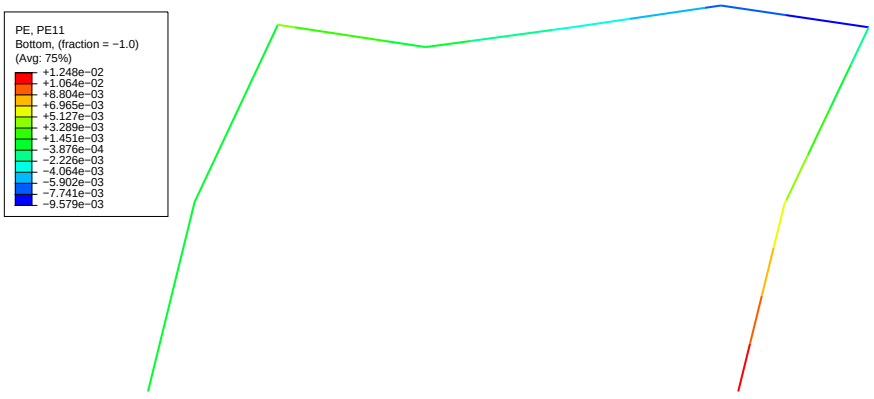

(d)

Figure 7-5: Deformed shape (magnification x 10) after: (a) Push to the right, (b) Load removal, (c) 60% of fire loading, (d) End of fire step

Figure 7-5 (c) and (d) are for the fire application step. Figure 7-5 (c) shows the structure after 60% of fire load has been applied and Figure 7-5 (d) is the response after complete application of the fire loading. From these figures it is seen that there is no change in the maximum tensile plastic strains found at the base of the right column. Meanwhile, in the beam, the compressive strains (at the right side) increase over the fire step, while the tensile strains (at the left side) decrease. This is due to expansion of the beam, due to the constant temperature increase, causing compression. There is little change to the deformed shape of the frame on being heated, it remains very similar to the shape seen on first loading occurring.

Now consider the application of loading as: push in one direction, followed by load reversal, load removal and finally application of fire load. The load-deformation plot is shown in Figure 7-6.

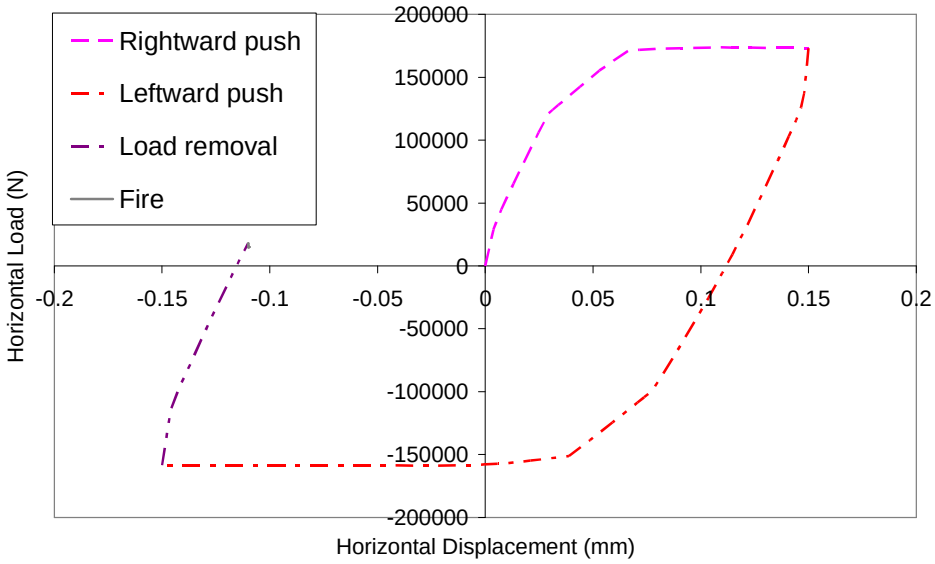

Figure 7-6: Load – horizontal deformation (at the point of load application)

The development of deformation and principal plastic strains is shown in Figure 7-7. Figure 7-7 (a) is identical to Figure 7-5 (b) and shows the response when the load applied rightwards is removed. Figure 7-7 (b) is the response when load has been applied in the leftward direction. It can be seen that load reversal leads

to all plastic deformation becoming tensile. Figure 7-7 (c) is of deformation after load removal, when it is seen that all plastic strains remain tensile. Once again this causes elastic recovery, but overall deformation now is towards the left. Figure 7-7 (d) and (e) show the development of the fire loading response. As in Figure 7-5 there is no change in the tensile strains found at the base of the left column (where maximum tension occurs). Throughout the beam, the value of tensile plastic strains present decreases as fire loading increases, both where the value is relatively large (the right side) and where it is smaller (the left side). Again, this is due to the expansion of the beam with constant temperature increase, causing compression. As in the previous example, the deformed shape of the frame changes little on heating, with it remaining very similar to that seen at the end of the loading steps.

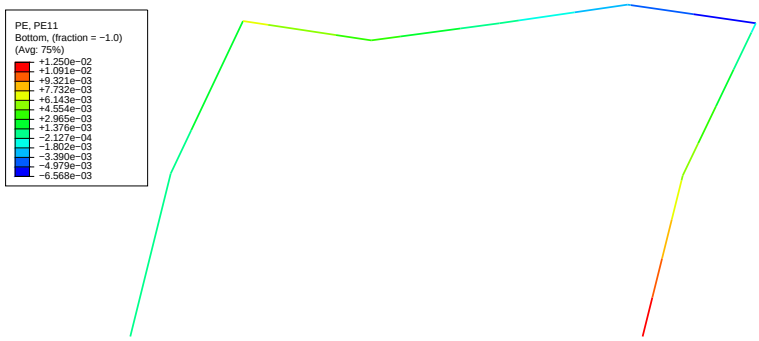

(a)

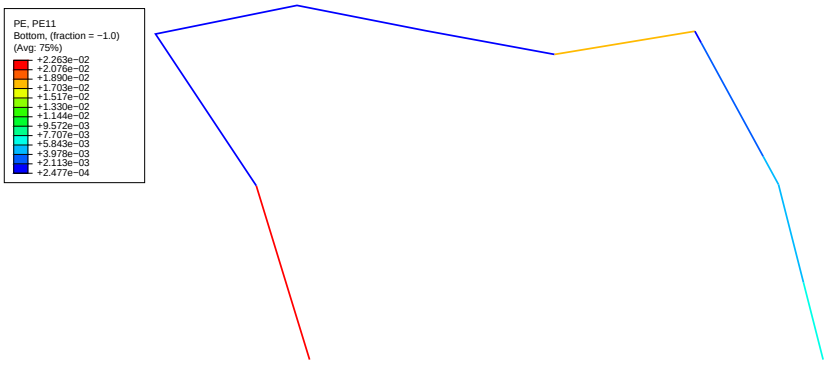

(b)

continued

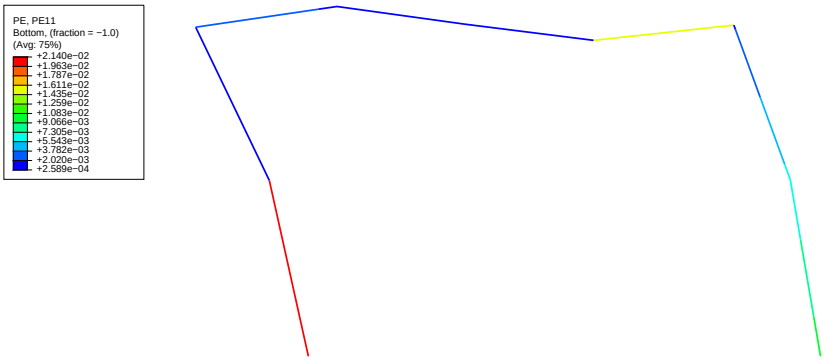

(c)

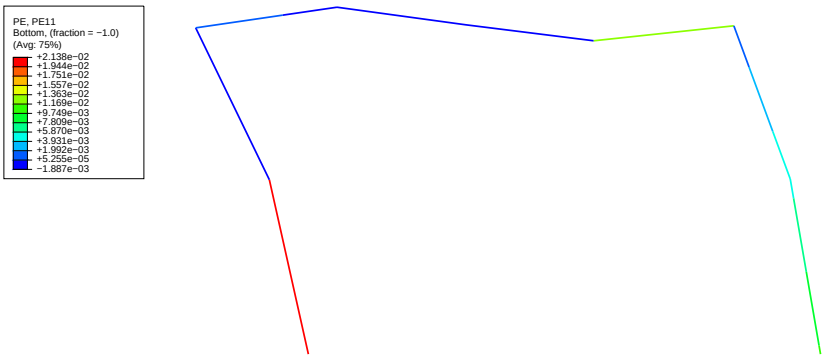

(d)

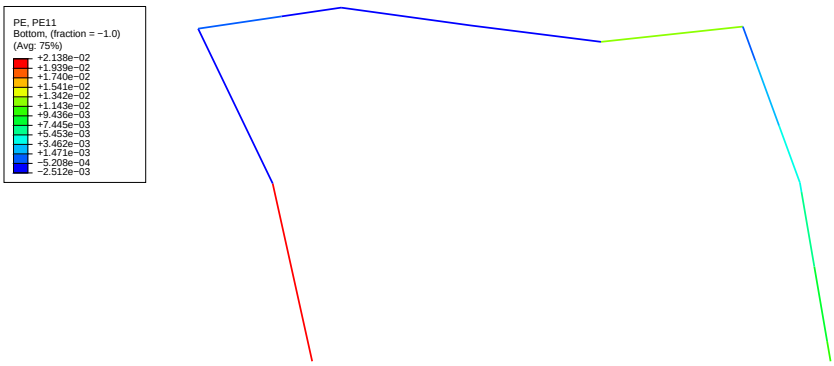

(e)

Figure 7-7: Deformed shape (magnification x10) after: (a) Removal of rightward push, (b) Leftward push, (c) Load removal, (d) 80% of fire loading, (e) End of fire step

In these cases the static displacement (causing pre-damage) influences the shape and deflection of the frame much more than the heating step that occurs afterwards. It is also seen that with the heating regime used here, thermal

expansion due to temperature increase has a larger effect on the plastic strains found in the frame than thermal bowing due to the temperature gradient present. This may not always be the case when more realistic non-uniform thermal gradients are applied within the concrete.

7.6 References

EN1992-1-2 (2004). Eurocode2: Design of Concrete Structures - Part 1-2: General Rules - Structural Fire Design.

Lee, J. H. and G. L. Fenves (1998). "Plastic-damage model for cyclic loading of concrete structures." Journal of Engineering Mechanics-Asce **124**(8): 892-900.

Lubliner, J., J. Oliver, et al. (1989). "A Plastic-Damage Model for Concrete." International Journal of Solids and Structures **25**(3): 299-326.

8

Conclusions

8.1 Introduction

This thesis has discussed the behaviour of concrete at elevated temperatures, through considering plain concrete in both tension and compression; reinforced concrete in both tension and compression at uniform temperatures; and finally, through looking at the residual strength of plain and reinforced concrete after it has been heated variably and cooled. It also considered simple reinforced concrete components (beam/portal frame) subjected to elevated temperatures.

This final chapter collates the specific conclusions drawn in each of the previous chapters, and then discusses more general findings.

8.2 Plain concrete in tension

It is recognised that for problems involving tensile localisation the softening branch of the stress-strain curve needs to be element size dependent or be based on fracture energy. Finite element codes' approximate element sizes and large aspect ratios distort the characteristic length calculation, and a mesh sensitive response is seen.

At elevated temperatures, reduction in concrete's tensile strength and its elastic modulus are commonly made assumptions. However post-peak softening behaviour at elevated temperatures is not well defined.

It was found that, even for a simple one-element test, heating and loading concrete under uniaxial tension is strongly path-dependent, with loading prior to heating giving very different results to heating followed by loading.

8.3 Plain concrete in compression

Concrete in uniaxial compression at ambient temperature is well characterised, with lots of experimental testing having been carried out. However, its elevated temperature behaviour is less well known. On investigation, it was concluded that generally concrete's compressive peak strength decreases with increasing temperature, its elastic modulus also decreases, the strain at peak stress increases with increasing temperature, as does the ultimate strain.

If there are no weaknesses in the material, yield under compression can be diffused over the entire model making the descending branch of the stress-strain relationship material model dependent (as opposed to element size dependent).

If a weakened element is introduced then a localisation band can occur. This localisation causes compression strain softening and consequent mesh

sensitivity. However, fracture energy type concepts are not used in compression, with material models having to be altered according to element size individually.

As seen in tension, it was found that the stress-strain behaviour of concrete in compression was strongly dependent on the order of loading and heating when subjected to both regimes.

8.4 Modelling reinforced concrete

Reinforced concrete cannot be modelled solely from the sum of its parts - interaction between the concrete and reinforcement results in increased load-carrying capacity. This is represented by tension stiffening properties for concrete in a reinforced concrete material model. Tension stiffening behaviour at elevated temperatures can, however, be defined on the basis of the behaviour of constitutive materials at elevated temperatures. Even simple reinforced concrete samples subjected to heating and loading demonstrate a complex response, due to changing material properties at elevated temperatures for each of the two materials and differential thermal expansion. This causes mechanical strains during heating when free expansion is permitted and only thermal strains are expected.

Inclusion of tension stiffening increases the load carrying capacity at all temperatures, and changes the gradient of the load-displacement response as the sharing of loads between concrete and reinforcement is altered. Differential thermal expansion at elevated temperatures induces a complex load-sharing arrangement between steel and concrete, resulting in a non-linear load-displacement response, even when all material properties comprise of multi-linear curves.

Again, the stress-strain behaviour of reinforced concrete is strongly path dependent with loading prior to heating, and heating followed by loading giving quite different results.

8.5 Residual behaviour of plain and reinforced concrete

The hypothesis: variation of temperatures in heating and cooling phases will cause damage in plain and reinforced concrete through thermal gradients and differential thermal expansion, resulting in a deteriorated mechanical response, is considered. It is found that this does result in inferior residual mechanical response for plain concrete. However, on comparison with experiments, it is seen that damage due to differential thermal expansion/contraction cannot fully explain the significantly higher reduction in the elastic load-displacement slope seen in experiments. It is also unable to fully explain the reduction in peak strength. Therefore damage due to these thermal gradients and differential expansions is not the sole cause of strength and stiffness degradation in residual tests, and other causes should be investigated and included e.g. changes in porosity, dehydration of calcium hydroxide and microstructure coarsening.

For reinforced concrete samples, with tension stiffening included, damage due to differential thermal expansion/contraction was found to induce negligible difference in residual response in the pre-peak regime.

8.6 Modelling beams at elevated temperature

A simple beam was used to investigate the effect of average temperature increase and thermal gradient on elastic and post-elastic behaviour. For a simply supported beam it was found that pure thermal expansion from average temperature increase causes localisation, and hence a mesh sensitive response. However, when a pure thermal gradient was applied across the depth of the beam, yielding is distributed, resulting in no mesh sensitivity, even when softening is treated as a material property. For the example considered, when both average temperature increase and a thermal gradient were applied yielding was once again distributed, and therefore it was not necessary to use softening as a non-local material property.

A plane strain model with fixed ends was examined under realistic loading and temperature variations. It was found that the heating step causes increased compressive stresses throughout the depth of the model at the supports. This, however, is accompanied by the longitudinal total strains, as well as the longitudinal plastic strains, in the same region being tensile.

Damage variables and compression or tension recovery were found to have no effect on the response of the plane strain model.

8.7 Pre-damaged reinforced concrete structural systems in fire

It was shown that fire loading causes plastic strains to be distributed in the beam of a portal frame when it is exposed to heating. Column rotation acts against temperature gradient and uniformly distributed load, preventing or limiting downward thermal bowing. Further research needs to consider more realistic thermal gradients and the effect when temperature loading is applied to columns as well as to the beam.

Heating of the beam after application of displacement loading appears to have little effect on the columns. It induces compressive strains in the beam, thereby increasing compressive or reducing tensile plastic strains present after the loading steps.

Application of displacement loading causing plastic damage changes the behaviour of the structure under heating – instead of symmetrical compressive plastic strains being induced, areas of varying tensile and compressive strain are caused within the beam. In the cases simulated, the static displacement (causing pre-damage) influenced the shape and deflection of the frame much more than the heating step that occurred afterwards. It was also seen that with the heating regime used, thermal expansion due to temperature increase had a larger effect on the plastic strains found in the frame than thermal bowing due to the

temperature gradient present. This may not always be the case when more realistic non-uniform thermal gradients are applied within the concrete.

8.8 Suggestions for further work

There are lots of areas mentioned throughout this thesis where further research and investigation would be beneficial. Briefly, this work may include:

(a) Additional experiments at elevated temperatures, with different rates of heating. Both plain and reinforced concrete experiments are particularly important in tension as this may be important for critical facilities such as nuclear power plants.

(b) Investigation into the behaviour of concrete under triaxial loading regimes.

(c) Computational modelling, to include the changing pore pressure, the hydrothermal aspects of concrete, and microstructure coarsening of concrete at elevated temperatures. In this regard, novel imaging technologies may be able to help.

(d) The manner in which load induced thermal strains are currently considered in simulations are either too approximate or too complicated, and simpler methods of their inclusion in numerical simulations need to be created.

(e) It is unclear how tension stiffening is affected at elevated temperatures. This needs to be investigated.